# Model order reduction methods for data assimilation; state estimation and structural health monitoring

by

Tommaso Taddei

Submitted to the Department of Mechanical Engineering and to the Center for Computational Engineering
in partial fulfillment of the requirements for the degree of

Doctor of Philosophy

at the

MASSACHUSETTS INSTITUTE OF TECHNOLOGY

February 2017





Author . Signature redacted .....
Department of Mechanical Engineering
Center for Computational Engineering
September 13th, 2016

Certified by..... Signature redacted .....
Anthony T. Patera
Professor of Mechanical Engineering
Thesis Supervisor

Accepted by ..... Signature redacted .....
Rohan Abeyaratne
Chairman, Department Committee on Graduate Theses
Department of Mechanical Engineering

Accepted by ... Signature redacted .....
Youssef Marzouk
Chairman, Department Committee on Graduate Theses
Center for Computational Engineering

To Sofia

*E poi saran le ultime, oramai*

**Model order reduction methods for data assimilation; state estimation and structural health monitoring**

by

Tommaso Taddei

Submitted to the Department of Mechanical Engineering
Center for Computational Engineering
on September 13th, 2016, in partial fulfillment of the
requirements for the degree of
Doctor of Philosophy

## Abstract

The objective of this thesis is to develop and analyze model order reduction approaches for the efficient integration of parametrized mathematical models and experimental measurements. Model Order Reduction (MOR) techniques for parameterized Partial Differential Equations (PDEs) offer new opportunities for the integration of models and experimental data. First, MOR techniques speed up computations allowing better explorations of the parameter space. Second, MOR provides actionable tools to compress our prior knowledge about the system coming from the parameterized best-knowledge model into low-dimensional and more manageable forms. In this thesis, we demonstrate how to take advantage of MOR to design computational methods for two classes of problems in data assimilation.

In the first part of the thesis, we discuss and extend the Parametrized-Background Data-Weak (PBDW) approach for state estimation. PBDW combines a parameterized best-knowledge mathematical model and experimental data to rapidly estimate the system state over the domain of interest using a small number of local measurements. The approach relies on projection-by-data, and exploits model reduction techniques to encode the knowledge of the parametrized model into a linear space appropriate for real-time evaluation.

In this work, we extend the PBDW formulation in three ways. First, we develop an experimental *a posteriori* estimator for the error in the state. Second, we develop computational procedures to construct local approximation spaces in subregions of the computational domain in which the best-knowledge model is defined. Third, we present an adaptive strategy to handle experimental noise in the observations. We apply our approach to a companion[1] heat transfer experiment to prove the effectiveness of our technique.

In the second part of the thesis, we present a model-order reduction approach to simulation-based classification, with particular application to Structural Health Monitoring (SHM). The approach exploits (i) synthetic results obtained by repeated solution of a parametrized PDE for different values of the parameters, (ii) machine-learning algorithms to generate a classifier that monitors the state of damage of the system, and (iii) a reduced basis method to reduce the computational burden associated with the model evaluations. The approach is based on an offline/online computational decomposition. In the offline stage, the fields associated with many different system configurations, corresponding to different states of damage, are computed and then employed to teach a classifier. Model reduction techniques, ideal for this many-query context, are employed to reduce the computational burden associated with

[1]The experiments are performed by Dr. James D. Penn (MIT).

the parameter exploration. In the online stage, the classifier is used to associate measured data to the relevant diagnostic class.

In developing our approach for SHM, we focus on two specific aspects. First, we develop a mathematical formulation which properly integrates the parameterized PDE model within the classification problem. Second, we present a sensitivity analysis to take into account the error in the model. We illustrate our method and we demonstrate its effectiveness through the vehicle of a particular companion experiment, a harmonically excited microtruss[1].

Thesis Supervisor: Anthony T. Patera
Title: Professor of Mechanical Engineering

## Acknowledgments

I would like to thank my advisor, Professor A.T. Patera, for giving me the opportunity to work with him, and for his extraordinary guidance and support throughout my graduate studies. In addition, I would like to thank my committee members, Professors J.J. Leonard, P.F.J. Lermusiaux, and J. Peraire, for their comments and insights that led to many improvements in my PhD work. I would also like to thank Professors S. Perotto, A. Quarteroni, and S. Salsa, who introduced me to the field of (numerical analysis of) PDEs, and helped me be admitted to MIT.

I would also like to thank my former colleagues in the group of Professor Patera, James D. Penn, Kathrin Smetana, and Masayuki Yano. I am indebted to them for the numerous contributions to this work and for the many insightful discussions on (and off) the topics of this thesis. In particular, I would like to acknowledge James, for the design and the implementation of the experimental apparata considered in this work; Kathrin, for many fruitful discussions about the topic of localised state estimation; and Masayuki, for his active contributions to almost all the different topics covered in this thesis, and for the high-order Finite Element code used in all numerical simulations. Last, but not least, I am very grateful to Debra R. Blanchard for her invaluable help and her sense of humour.

I would also like to thank the friends that I found at MIT throughout these three years: my MechE mates — Andrew, Claudio, Connor, Janille, João, Joseph, Katie, Mustafa, Robert, Sara and Uyanga — the former and present members of MITaly — Andrea, Federico, Giovanni, Giulia, Mariapaola and Stefano — and my roommates Aleksey, Augustus and Seth. I am grateful to all of them for having made MIT a better place for me.

I would like to thank my parents, Laura and Marzio, for their continuous and unconditional support during the last twenty-eight years of my life. Finally, I would like to thank Sofia for having been by my side for all these years. To her, this thesis is dedicated.

Finally, I would like to acknowledge the financial support provided by OSD/AFOSR/MURI Grant FA9550-09-1-0613, ONR Grant N00014-11-1-0713, by the MIT-Singapore International Design Center, and by MIT through the MIT Presidential fellowship.

# Contents

# List of Figures

# List of Tables

# Chapter 1

# Introduction

## 1.1 Motivation

In many applications, integration of mathematical models and experimental observations is needed to perform accurate predictions. Mathematical models of physical systems are often deficient due to the uncertainty in the value of the parameters representing material properties and input forces, and might also neglect important aspects of the system's behavior. On the other hand, experimental measurements are often scarce, corrupted by random and systematic noise, and they might also provide indirect measurements of the quantity we wish to predict.

Data Assimilation (DA) refers to the process of integrating information coming from a mathematical model with experimental observations for prediction. In Numerical Weather Prediction (NWP), DA refers to the process of combining mathematical models with data to estimate the state of atmospheric or oceanic flow. In other fields such as control or Structural Health Monitoring, the output of the procedure might be either a real-valued or a discrete-valued function of the state.

DA tasks present several challenges for applied mathematicians and engineers. Mathematical models often consist of (systems of) Partial Differential Equations (PDEs) that are typically extremely expensive to evaluate: since state-of-the-art DA procedures are cast as optimization problems, which hence involve many model evaluations, the computational burden might be unsustainable for real-time and in situ applications. This challenge becomes even more severe when the available mathematical model is affected by substantial parametric uncertainty: in this case, current research focuses on the development of nu-

merical techniques that (i) are designed to appropriately take into account the parametric uncertainty in the model, (ii) are directly informed by the specific DA task at hand, and (iii) meet the computational (time and memory) constraints.

Recent advances in Model Order Reduction (MOR) for parameterized systems offer new opportunities for the integration of models and experimental data. First, MOR techniques speed up computations allowing better explorations of the parameter space at an acceptable computational cost. Second, MOR provides actionable tools to compress our prior knowledge about the system coming from the parameterized mathematical model into low-dimensional and more manageable forms. *This thesis presents work toward the development of efficient model reduction strategies for DA problems for systems modeled by PDEs. In more detail, we shall focus on two distinct DA tasks: state estimation for stationary problems, and damage identification for Structural Health Monitoring applications.*

## 1.2 Model order reduction for parameterized PDEs

Parametric Model Order Reduction (pMOR) is a mathematical and computational field of study that aims to systematically reduce the *marginal* computational cost of the solution to a parametrized mathematical model. pMOR is part of the broader field of Model Order Reduction (MOR), and is mainly motivated by real-time applications (control, parameter estimation) and many-query applications (design and optimization, uncertainty quantification). In real-time applications, the goal is to provide rapid responses with little or no communication with extensive offline resources; in many-query applications, the goal is to speed up the computational cost associated with the evaluation of a given quantity of interest in the limit of many model evaluations. We observe that in both these contexts the *premium* is on marginal cost (or perhaps asymptotic average cost) per input-output evaluation; we can thus accept increased pre-processing or "Offline" costs, which are not tolerable for a single or few evaluations. In this section, we shall discuss the general problem of parametric model reduction, and we shall introduce the particular pMOR technique employed in this work, the Reduced Basis method. We refer to the recent surveys [23, 53] for a thorough introduction to pMOR. We further refer to [180, 106, 188] for a complete introduction to the Reduced Basis method.

We define the best-knowledge (bk) mathematical model corresponding to the (stationary)

phenomenon of interest as follows: given $\mu \in \mathcal{P}^{\text{bk}} \subset \mathbb{R}^P$, find $u^{\text{bk}}(\mu) \in \mathcal{V}^{\text{bk}}$ such that

$$\mathcal{G}^{\text{bk},\mu}(u^{\text{bk}}(\mu), v) = 0 \qquad \forall\, v \in \mathcal{W}^{\text{bk}}. \tag{1.2.1}$$

The form $\mathcal{G}^{\text{bk},\mu} : \mathcal{V}^{\text{bk}} \times \mathcal{W}^{\text{bk}} \to \mathbb{R}$ denotes the mathematical model associated with the particular physical system of interest; the model depends on a set of $P$ parameters, $\mu \in \mathcal{P}^{\text{bk}} \subset \mathbb{R}^P$, where the region $\mathcal{P}^{\text{bk}}$ corresponds to the expected parameter range. Here, $\mathcal{V}^{\text{bk}}, \mathcal{W}^{\text{bk}}$ are two suitable Hilbert spaces defined over a $d$-dimensional domain $\Omega^{\text{bk}} \subset \mathbb{R}^d$. Finally, $u^{\text{bk}}(\mu)$ denotes the bk approximation of the system's state over $\Omega^{\text{bk}}$ for a given value of $\mu$ in $\mathcal{P}^{\text{bk}}$. We further define the bk solution manifold associated with the solution to (1.2.1) for each value of $\mu \in \mathcal{P}^{\text{bk}}$:

$$\widehat{\mathcal{M}}^{\text{bk}} := \{u^{\text{bk}}(\mu) : \mu \in \mathcal{P}^{\text{bk}}\} \subset \mathcal{V}^{\text{bk}}. \tag{1.2.2}$$

Given the bk map $\mu \in \mathcal{P}^{\text{bk}} \mapsto u^{\text{bk}}(\mu) \in \mathcal{V}^{\text{bk}}$, we introduce the rank-$N$ approximation ([56]) to $u^{\text{bk}}$, $\mu \mapsto u_N^{\text{bk}}(\mu) \in \mathcal{V}^{\text{bk}}$ such that

$$u_N^{\text{bk}}(x;\, \mu) = \sum_{n=1}^{N} \phi_n(\mu)\, \zeta_n^{\text{bk}}(x), \qquad x \in \Omega^{\text{bk}},\ \mu \in \mathcal{P}^{\text{bk}}, \tag{1.2.3}$$

where $\phi_1, \ldots, \phi_N : \mathcal{P}^{\text{bk}} \to \mathbb{R}$, and $\mathcal{Z}_N^{\text{bk}} := \text{span}\{\zeta_n^{\text{bk}}\}_{n=1}^N \subset \mathcal{V}^{\text{bk}}$. Based on this decomposition, we can view the problem of parametric model reduction as the combination of two distinct tasks: (i) the determination of the reduced space $\mathcal{Z}_N^{\text{bk}} := \text{span}\{\zeta_n^{\text{bk}}\}_{n=1}^N$, and (ii) the estimation of the coefficients $\{\phi_n(\mu)\}_{n=1}^N$ for any value of $\mu$ in $\mathcal{P}^{\text{bk}}$. If we denote by $\|\cdot\|_{\mathcal{V}^{\text{bk}}}$ the norm over $\mathcal{V}^{\text{bk}}$, the space $\mathcal{Z}_N^{\text{bk}}$ should be chosen such that $\inf_{z \in \mathcal{Z}_N^{\text{bk}}} \|u^{\text{bk}}(\mu) - z\|_{\mathcal{V}^{\text{bk}}} \leq tol$ for any $\mu \in \mathcal{P}^{\text{bk}}$ and for a given tolerance $tol > 0$. On the other hand, the coefficients $\{\phi_n(\mu)\}_{n=1}^N$ should be chosen such that $\inf_{z \in \mathcal{Z}_N^{\text{bk}}} \|u^{\text{bk}}(\mu) - z\|_{\mathcal{V}^{\text{bk}}} \approx \|u^{\text{bk}}(\mu) - u_N^{\text{bk}}(\mu)\|_{\mathcal{V}^{\text{bk}}}$, and such that the maps $\mu \mapsto \phi_n(\mu)$ can be evaluated in a cost-efficient way in the limit of many queries.

Reduced Basis (RB) method represents a very efficient approach to the problem of parametric model reduction. The method was first proposed in the late 1970s ([3, 159, 162, 82]) to address linear and nonlinear structural analysis problems, and was then extended to fluid dynamics in the late 1980s ([170, 98]). Starting with the works of Maday, Patera and coauthors in the early 2000s ([176, 223]), RB method was set on a more general mathemat-

ical ground with special emphasis on (i) efficient sampling strategies for the construction of the hierarchical reduced spaces $\{\mathcal{Z}_N^{\rm bk}\}_N$, (ii) rigorous *a posteriori* error estimation procedures, and (iii) offline-online computational procedures for the efficient construction of the coefficients $\{\phi_n(\mu)\}_{n=1}^N$ in the limit of many queries.

In the RB literature, several approaches have been considered for the construction of the reduced space. In the early works, non-adaptive Taylor and Lagrange ([175]) and Hermite ([118]) spaces have been considered. More recent approaches rely on Proper Orthogonal Decomposition (POD, [28, 130, 122]), and Greedy methods ([176, 177]). Both these techniques have been applied to several classes of PDEs and have also been studied theoretically. We refer to [173] for an overview of the several applications of POD in model reduction, and to [28] for the mathematical analysis. On the other hand, Greedy algorithms have been first applied to stationary problems, and then extended to time-dependent problems in a space-time setting ([219, 240]), or in combination with POD ([101]); we refer to [40, 32, 66, 56] for a rigorous analysis of the convergence properties of Greedy algorithms.

Efficient offline/online strategies for the rapid computation of the RB state estimate $u_N^{\rm bk}(\mu)$ for a given $\mu \in \mathcal{P}^{\rm bk}$ rely on (Petrov-) Galerkin projection. In more detail, following the standard idea of Galerkin methods for PDEs, we seek $u_N^{\rm bk}(\mu) \in \mathcal{Z}_N^{\rm bk}$ that solves:

$$\mathcal{G}^{{\rm bk},\mu}(u_N^{\rm bk}(\mu), v) = 0 \qquad \forall\, v \in \mathcal{W}_N^{\rm bk}, \tag{1.2.4}$$

where $\mathcal{W}_N^{\rm bk} \subset \mathcal{W}^{\rm bk}$ is a suitable $N$-dimensional space, which is equal to $\mathcal{Z}_N^{\rm bk}$ in the Galerkin case. During the offline stage, we construct the spaces $\mathcal{Z}_N^{\rm bk}$ and $\mathcal{W}_N^{\rm bk}$ and we assemble and store suitable parameter-independent quantities; during the online stage, we assemble and solve the parameter-dependent reduced order model (1.2.4) to compute the coefficients $\{\phi_n(\mu)\}_{n=1}^N$. We note that the offline stage is computationally expensive and is performed once, while the online stage is in general extremely inexpensive and is performed for each model query. Since the cost of a single online evaluation is significantly less expensive than the corresponding high-fidelity evaluation (based on a Finite Element or a Finite Volume discretization), we can amortize the offline computational cost in the limit of many queries. For parametric-affine linear problems (see, e.g., [188, 168]), it is easy to estimate the coefficients $\{\phi_n(\mu)\}_{n=1}^N$ at an online cost of $\mathcal{O}(N^3)$; for nonlinear and/or non-parametrically-affine problems Empirical Interpolation Method (EIM, [12, 97], see also [48]) can be employed to

guarantee online efficiency.

Before concluding, we remark that RB method is still the subject of active research. In particular, several recent proposals combine RB with domain decomposition strategies to tackle large-scale problems ([145, 117, 171, 72, 203]) and multi-scale problems ([126, 2]). In this thesis, we rely on the more standard RB method for linear elliptic PDEs as presented in [188], and we refer to the above-mentioned literature for further details.

## 1.3 Thesis objective

The objective of this work is to develop model reduction approaches for the efficient integration of parameterized mathematical models and experimental measurements. In developing our techniques, we focus on three aspects.

- **Real-time and in situ predictions:** we wish to develop algorithms that provide rapid responses with little or no communication with extensive computational resources.

- **Reliability:** we wish to quantify the level of uncertainty in our estimate, and thus the degree of confidence the user should have in the prediction.

- **Generality:** we wish to develop techniques that can be applied to a broad range of applications in continuum mechanics.

We shall focus here on two problems in data assimilation: state estimation and damage identification (Structural Health Monitoring). The former deals with the reconstruction of the true state associated with the system in a given region of interest. The latter, in its most basic form, deals with the assessment of the state of damage (properly defined according to the system specifications) of a given structure. In the next two sections, we discuss in detail the mathematical formulation of these two classes of problems, and we provide definitions used throughout the thesis.

### 1.3.1 Mathematical description of the objective: state estimation

The objective of state estimation is to approximate the state $u^{\text{true}}$ associated with physical systems of interest over the domain of interest $\Omega \subset \mathbb{R}^d$. We shall here assume that $u^{\text{true}}$ is

deterministic and stationary (or time-harmonic). We shall further assume that $u^{\text{true}}$ belongs to a suitable functional space $\mathcal{U}$ defined over $\Omega$.

We shall afford two sources of information: a bk mathematical model of the form (1.2.1) (here, stated in compact form),

$$G^{\text{bk},\mu}(u^{\text{bk}}(\mu)) = 0, \qquad \mu \in \mathcal{P}^{\text{bk}}, \tag{1.3.1}$$

defined over a domain $\Omega^{\text{bk}}$ which contains $\Omega$, and $M$ experimental observations $\ell_1^{\text{obs}}, \ldots, \ell_M^{\text{obs}}$ such that

$$\ell_m^{\text{obs}} = \ell_m^o(u^{\text{true}}) + \epsilon_m. \tag{1.3.2}$$

Here, the mathematical model (1.3.1) should be interpreted as the best-knowledge representation of the physical phenomenon, while $\mathcal{P}^{\text{bk}} \subset \mathbb{R}^P$ is a confidence region for the true values of the parameters of the model. The functionals $\ell_1^o, \ldots, \ell_M^o$ are associated to the particular transducers employed, and are assumed to be linear: we anticipate that in this thesis we consider observations associated to local averages of the state (e.g., local measurements of the acoustic pressure obtained using an acoustic microphone, local measurements of the thermal field based on local thermal probes). Finally, $\{\epsilon_m\}_{m=1}^M$ are unknown disturbances caused by either systematic error in the data acquisition system, or experimental noise.

We summarise the state estimation task considered in this thesis in the next box.

**State estimation:** given the parametrized mathematical model $G^{\text{bk},\mu}$ (1.3.1) and the $M$ functionals $\ell_1^o, \ldots, \ell_M^o$, develop a computational algorithm $A$ that takes as input $M$ measurements $\ell_1^{\text{obs}}, \ldots, \ell_M^{\text{obs}}$ and returns

- an estimate $u^\star = A(\ell_1^{\text{obs}}, \ldots, \ell_M^{\text{obs}}) \in \mathcal{U}$ of the state $u^{\text{true}}$ over the domain $\Omega$, and
- an estimate of the error $\|u^\star - u^{\text{true}}\|_\star$ in a suitable metric of interest.

The computational time should be independent of the high-fidelity solver used to discretize (1.3.1).

We observe that our definition of the task is consistent with the requirements discussed at the beginning of section 1.3. The metric $\|\cdot\|_\star$ might be associated with a norm over $\Omega$ (e.g. the $L^2$ error over $\Omega$), or with the error in a given quantity of interest that depends on the

state (e.g. the error in the output $\mathcal{L}^{\text{true}} = \mathcal{L}(u^{\text{true}})$ where $\mathcal{L} : \mathcal{U} \to \mathbb{R}$ is a given functional). We anticipate that pMOR is here crucial to develop algorithms that are directly informed by the parametrized best-knowledge model (1.3.1). We further discuss this point in section 1.4.1.

### 1.3.2 Mathematical description of the objective: Structural Health Monitoring

Structural Health Monitoring (SHM) refers to any automated monitoring procedure designed to assess the state of damage of a given aerospace, civil, or mechanical structure of interest. In the context of SHM, damage is formally defined as intentional or unintentional changes to the system which adversely affect its current or future performance ([79]). The ultimate objective of SHM is to identify (in an automated fashion) damage before failure occurs. For civil engineering applications, SHM must provide real-time reliable assessment information regarding the integrity of a structure ([64]). In the aerospace industry, monitoring systems are required to assess the health of aircraft components during reconditioning or during the mission. In these contexts, SHM is very similar in objective to Operational Loads Monitoring (OLM, [236, 206]) and Integrated Vehicle Health Management (IVHM, [21, 166]).

Following [190, 238], we can formalize the objective of SHM into five levels of increasing difficulty: (i) detection (is the system damaged?); (ii) localization (where is the damage in the structure?); (iii) classification (which is the type of damage present in the structure?); (iv) assessment (how severe is the damage?); and (v) prediction (how much residual life remains?). In this thesis, we shall focus on the first two levels: as observed independently by Farrar et al. in [78], and by Hurtado in [114], both these levels can be formulated as classification problems. In the remainder of this section, we shall provide an abstract formulation of the classification problem, which will be used to develop our approach. We refer to Chapter 7 for the instantiation of the definitions below for a particular companion experiment.

We denote by $\mathcal{C} \in \mathbb{R}^{P+D}$ a set of parameters that uniquely identifies a system configuration. To provide a concrete point of reference, $\mathcal{C}$ might include information related to the geometry of the system, to the material properties, and to the boundary conditions. We then characterize our system by a finite number $K$ of exhaustive states of damage. In the simplest case (Level 1), we have $K = 2$ states: the label $y = 1$ corresponds to undamaged

systems, and the label $y = 2$ corresponds to damaged systems. We denote by $y = y(\mathcal{C})$ the state of damage associated with the configuration $\mathcal{C}$. We further introduce the raw measurements $\mathbf{q}^{\text{exp}} \in \mathbb{R}^{\mathcal{Q}}$ obtained experimentally. For reasons that will become clear soon, we also introduce the set of $Q_{\text{feat}}$ functions (features) of $\mathbf{q}^{\text{exp}}$, $\mathbf{z}^{\text{exp}} = \mathcal{F}(\mathbf{q}^{\text{exp}}) \in \mathbb{R}^{Q_{\text{feat}}}$; we refer to the application $\mathcal{F} : \mathbf{q}^{\text{exp}} \mapsto \mathbf{z}^{\text{exp}}(\mathbf{q}^{\text{exp}})$ as *feature map.*

In view of the definition of the mathematical model, we introduce the incomplete (bk) configuration vector $\mu \in \mathbb{R}^P$, and the hidden vector $\xi \in \mathbb{R}^D$ such that $\mathcal{C} = (\mu, \xi)$. We further introduce the anticipated configuration set $\mathcal{P}^{\text{bk}} \subset \mathbb{R}^P$, and the configuration set $\mathcal{P}^{\text{exp}} = \mathcal{P}^{\text{bk}} \times \mathcal{V} \subset \mathbb{R}^{P+D}$. We here postulate that there exists a function $f^{\text{dam}} : \mathcal{P}^{\text{bk}} \rightarrow \{1, \ldots, K\}$ such that

$$y(\mathcal{C} = (\mu, \xi)) = f^{\text{dam}}(\mu), \qquad \forall\, (\mu, \xi) \in \mathcal{P}^{\text{exp}}. \tag{1.3.3}$$

We observe that this implies that the state of damage associated with any configuration $\mathcal{C}$ is uniquely determined by the subset of parameters included in $\mu$.

Assuming that the raw measurements $\mathbf{q}^{\text{exp}}$ are based on a set of $Q_{\text{exp}}$ experiments, we introduce $Q_{\text{exp}}$ bk models

$$G_q^{\text{bk},\mu}(u_q^{\text{bk}}(\mu)) = 0, \qquad q = 1, \ldots, Q_{\text{exp}}, \tag{1.3.4a}$$

and the (non-necessarily linear) functional $\mathcal{L}$ such that

$$\mathbf{z}^{\text{bk}}(\mu) = \mathcal{L}(u_1^{\text{bk}}(\mu), \ldots, u_{Q_{\text{exp}}}^{\text{bk}}(\mu)), \qquad \mathcal{L} : \underbrace{\mathcal{U} \times \ldots \times \mathcal{U}}_{Q_{\text{exp}}} \rightarrow \mathbb{R}^{Q_{\text{feat}}}, \tag{1.3.4b}$$

approximates the features $\mathbf{z}^{\text{exp}}(\mathcal{C})$ for any $\mu \in \mathcal{P}^{\text{bk}}$ and $\xi \in \mathcal{V}$. We observe that the bk models are intended to approximate the features $\mathbf{z}^{\text{exp}}$ rather than the raw data $\mathbf{q}^{\text{exp}}$.

We summarise the damage identification task in the next box. Some comments are in order. We observe that the damage identification task depends on a fair amount of quantities: the raw data $\mathbf{q}^{\text{exp}}$, the feature map $\mathcal{F} : \mathbb{R}^{\mathcal{Q}} \rightarrow \mathbb{R}^{Q_{\text{feat}}}$, the damage function $f^{\text{dam}} : \mathcal{P}^{\text{bk}} \rightarrow \{1, \ldots, K\}$, and the mathematical model $(\{G_q^{\text{bk},\mu}\}_{q=1}^{Q_{\text{exp}}}, \mathcal{L})$ (1.3.4). Since the objective of this thesis is the development of a general computational procedures that maps experimental measurements to the corresponding state of damage, in this section, we have implicitly assumed that all these quantities are given *a priori.* In section 1.4.2, we

provide a general overview of a general Structural Health Monitoring procedure, and we provide further details about each of these quantities. We further observe that although we tailored the discussion to Structural Health Monitoring the task can be generalized to a wide spectrum of inverse problems, which aim to estimate a discrete-valued QOI based on experimental data. As an example, we mention Acoustic Pulse Reflectometry (APR, [4, 200]): as SHM, APR can be recast as a classification problem.

**Damage identification:** given the parametrized mathematical models $\{G_q^{\mathrm{bk},\mu}\}_{q=1}^{Q_{\mathrm{exp}}}$ (1.3.4a), the functional $\mathcal{L}$ (1.3.4b), and the feature map $\mathcal{F} : \mathbf{q}^{\mathrm{exp}} \mapsto \mathbf{z}^{\mathrm{exp}}(\mathbf{q}^{\mathrm{exp}})$, develop a computational algorithm $A$ that, for any configuration $\mathcal{C}$, takes as input the raw measurements $\mathbf{q}^{\mathrm{exp}} = \mathbf{q}^{\mathrm{exp}}(\mathcal{C}) \in \mathbb{R}^{\mathcal{Q}}$ and returns

- an estimate $\hat{y} = A(\mathbf{q}^{\mathrm{exp}})$ of the state of damage $y(\mathcal{C}) \in \{1, \ldots, K\}$, and
- a measure of the confidence in the estimate.

The computational time should be independent of the high-fidelity solver used to discretize (1.3.4).

## 1.4 Background

### 1.4.1 Variational approaches to state estimation

We present an overview of state-of-the-art techniques that have been proposed to tackle the problem of state estimation; we here place special emphasis on the treatment of parametrized mathematical models, and on the application of model reduction techniques. Since in this work we only consider stationary problems, we do not explore in this section methods for sequential data assimilation. We refer to [24, 63, 217, 216] for a thorough introduction to data assimilation from the perspective of ocean and atmospheric sciences. We further refer to [233] for a survey about Bayesian methods for data assimilation. Finally, we refer to [222, 44] and to the works by Navon and coauthors ([207, 208, 239]) for an application of model reduction techniques to unsteady data assimilation (state estimation) tasks in the framework of 4D-VAR ([59]).

We shall first consider the case of non-parametric background ($\mathcal{P}^{\mathrm{bk}} = \{\bar{\mu}\}$, $u^{\mathrm{bk}} = u^{\mathrm{bk}}(\bar{\mu})$). In this case, if we assume that disturbances are uncorrelated, with zero mean and variance

$\sigma^2$, the most popular approach is the so-called 3D-VAR:

$$u_\xi^\star := \arg\min_{u\in\mathcal{U}} \xi\|u - u^{\mathrm{bk}}\|^2 + \frac{1}{M}\sum_{m=1}^{M}\left(\ell_m^o(u) - \ell_m^{\mathrm{obs}}\right)^2. \tag{1.4.1}$$

Here, $(\mathcal{U}, \|\cdot\|)$ is a suitable Hilbert space defined over $\Omega$ endowed with the inner product $(\cdot,\cdot)$ and the induced norm $\|\cdot\| = \sqrt{(\cdot,\cdot)}$; $u^{\mathrm{bk}}$ is either referred to as *background*, or *first guess*, or *forecast*, while the state estimate $u_\xi^\star$ is referred to as *analysis*. The parameter $\xi > 0$ regulates the relative importance of the background compared to the experimental data. From a statistical perspective, the approach corresponds to a variational form of least-squares statistical linear estimation ([216]), and can be interpreted as the application of the Bayes' rule for linear Gaussian systems ([182]). We recall that 3D-VAR was first proposed by Lorenc in [138]: Lorenc further developed a Bayesian framework to link 3D-VAR to a number of other proposals including optimal interpolation ([73, 22, 90, 139]), kriging ([149, 209]) successive corrections ([60, 37]), constrained inizialization ([22]), Kalman-Bucy filter ([123, 134] ) and adjoint model data assimilation ([70]). Similarly, in [26], Bennett and McIntosh proposed the so-called generalized inverse method, which has been later proved to be equivalent to optimal interpolation ( [25]) and thus to 3D-VAR.

The analysis $u_\xi^\star$ can be written as the sum of the background $u^{\mathrm{bk}}$ and a correction term associated with experiments. More precisely, if we introduce the Riesz representations of the observation functionals in $\mathcal{U}$ — $(R_{\mathcal{U}}\ell_m^o, v) = \ell_m^o(v)$ for all $v \in \mathcal{U}$ and $m = 1, \ldots, M$ — and we define the $M$-dimensional space $\mathcal{U}_M = \mathrm{span}\{R_{\mathcal{U}}\ell_m^o\}_{m=1}^M$, there exists a basis of $\mathcal{U}_M$ $\psi_1, \ldots, \psi_M$ (referred to as *array modes* in [25]) such that

$$u_\xi^\star = u^{\mathrm{bk}} + \eta_\xi^\star, \qquad \eta_\xi^\star = \sum_{m=1}^{M}\left(\ell_m^{\mathrm{obs}} - \ell_m^o(u^{\mathrm{bk}})\right)\psi_m. \tag{1.4.2}$$

We can consider two different strategies to extend (1.4.1) to parametrized backgrounds. First, we can substitute $u^{\mathrm{bk}}$ with $u^{\mathrm{bk}}(\mu)$ in (1.4.1), and then minimize with respect to $\mu$ and $u$ at the same time:

$$(\mu_\xi^\star, u_\xi^\star) := \arg\min_{(\mu,u)\in\mathcal{P}^{\mathrm{bk}}\times\mathcal{U}} \xi\|u - u^{\mathrm{bk}}(\mu)\|^2 + \frac{1}{M}\sum_{m=1}^{M}\left(\ell_m^o(u) - \ell_m^{\mathrm{obs}}\right)^2. \tag{1.4.3}$$

Statement (1.4.3) corresponds to the partial-spline model (see, e.g., [226, Chapter 9]). As for

3D-VAR, we can show that the solution is of the form (1.4.2), that is $u_\xi^\star = u^{\text{bk}}(\mu_\xi^\star) + \eta_\xi^\star$ with $\eta_\xi^\star = \sum_{m=1}^M \left(\ell_m^{\text{obs}} - \ell_m^o(u^{\text{bk}}(\mu_\xi^\star))\right)\psi_m$. However, statement (1.4.3) requires the solution to a nonlinear, non-convex minimization statement, which is likely to be ill-posed, and requires multiple evaluations of the bk map $\mu \mapsto u^{\text{bk}}(\mu)$. Second, we might neglect the correction term $\eta^\star$, and thus simply optimize with respect to $\mu$:

$$\mu^\star := \arg\min_{\mu \in \mathcal{P}^{\text{bk}}} \frac{1}{M} \sum_{m=1}^M \left(\ell_m^o(u^{\text{bk}}(\mu)) - \ell_m^{\text{obs}}\right)^2. \tag{1.4.4}$$

We can then estimate the system's state using $u^\star = u^{\text{bk}}(\mu^\star)$. We observe that (1.4.4) corresponds to a deterministic inverse problem for the values of the parameters $\mu \in \mathcal{P}^{\text{bk}}$, and can be interpreted as a (nonlinear) projection onto the manifold $\mathcal{M}^{\text{bk}} = \{u^{\text{bk}}(\mu)|_\Omega : \mu \in \mathcal{P}^{\text{bk}}\}$. As observed by multiple authors, problem (1.4.4) might also be ill-posed, and thus requires some form of regularization. In this respect, we observe that the Bayesian framework provides a rigorous mathematical ground for addressing this problem. We refer to [211] for a discussion about Bayesian approaches for inverse problems of the form (1.4.4). We further observe that, due to the absence of a correction mechanism, our estimate might be inaccurate if the bk model is not sufficiently accurate. In the remainder of this section, we discuss how to exploit model reduction techniques to tackle problem (1.4.4).

A first application of model reduction to problem (1.4.4) is based on substituting in (1.4.4) the high-fidelity map $\mu \mapsto u^{\text{bk}}(\mu)$ with the Reduced Order Model, $\mu \mapsto u_N^{\text{bk}}(\mu)$ (1.2.3). By doing so, we can reduce the computational cost of the evaluation of the model, and thus reduce the overall cost associated with the application of an iterative scheme for (1.4.4). In this respect, we recall [88, 135, 84], in which model reduction strategies are exploited in a Bayesian setting to speed up computations associated with a MCMC procedure, and [131], in which the authors apply reduced basis techniques to reduce the computational burden associated with the application of deterministic and statistical approaches for solving an inverse problem of the form (1.4.4).

A second strategy is based on the relaxation of problem (1.4.4). In more detail, if we substitute $u_N^{\text{bk}}(\mu)$ in (1.4.4), we obtain

$$\mu^\star := \arg\min_{\mu \in \mathcal{P}^{\text{bk}}} \frac{1}{M} \sum_{m=1}^M \left(\sum_{n=1}^N \phi_n(\mu)\ell_m^o(\zeta_n) - \ell_m^{\text{obs}}\right)^2, \tag{1.4.5}$$

where $\zeta_n := \zeta_n^{\text{bk}}|_\Omega \in \mathcal{U}$ is the restriction of the $n$-th basis of $\mathcal{Z}_N^{\text{bk}}$ to $\Omega$. If we now assume that $N \leq M$, we can relax (1.4.5) as $\boldsymbol{\phi}^\star = \arg\min_{\boldsymbol{\phi}\in\mathbb{R}^N} \frac{1}{M}\sum_{m=1}^{M}\left(\sum_{n=1}^{N}\phi_n \ell_m^o(\zeta_n) - \ell_m^{\text{obs}}\right)^2$, which can also be written as

$$u^\star := \arg\min_{z\in\mathcal{Z}_N} \sum_{m=1}^{M}\left(\ell_m^o(z) - \ell_m^{\text{obs}}\right)^2, \tag{1.4.6}$$

where $\mathcal{Z}_N$ is the restriction of $\mathcal{Z}_N^{\text{bk}}$ to $\Omega$, $\mathcal{Z}_N = \{z|_\Omega : z \in \mathcal{Z}_N^{\text{bk}}\}$. We observe that for $N = M$, (1.4.6) corresponds to the Generalized Empirical Interpolation method (GEIM, [140, 141]); while for $N < M$ and $\mathcal{Z}_N$ built using POD, (1.4.6) corresponds to Gappy-POD ([75, 234]). Both these approaches rely on pMOR techniques to generate background spaces $\mathcal{Z}_N$ informed by an underlying parametrized mathematical model. We observe that by appealing to this approach we are no longer in position to estimate the parameters $\mu$ of the model; on the other hand, we greatly reduce the computational complexity of the state-estimation procedure.

### 1.4.2 A general paradigm for damage identification

We shall here discuss a general paradigm for the development of a Structural Health Monitoring procedure. This will clarify the definition of the damage identification task presented in section 1.3.2. The paradigm was originally proposed by Farrar and collaborators in[78], and is defined through the integration of four sequential procedures: operational evaluation, data acquisition, feature extraction, and statistical inference. We anticipate that in this thesis we focus on the last stage of the paradigm, the statistical inference. As in the previous section, we place special emphasis on the application of model reduction techniques.

*Operational evaluation* sets the limitations on what will be monitored and how the monitoring will be accomplished. During this stage, a formal definition of the potential states of damage is given. From a mathematical perspective, during this stage we define the damage function $f^{\text{dam}}$ (1.3.3).

*Data acquisition* deals with the implementation of the sensing system. The sensing system can be based on static responses (in terms of strain ([193]) or displacement ([194, 195])) or on dynamic (such as frequency) responses ([46, 191]). Furthermore, sensing systems are referred to as *passive* if they rely on the ambient loading environment as an excitation source, and *active* if they can provide a local excitation tailored to the damage detection

process (see, e.g., [79, Chapter 4.11]).

*Feature extraction* identifies the vector-valued functions $\mathbf{z}^{\text{exp}}$ of the acquired raw data $\mathbf{q}^{\text{exp}}$. Modal analysis ([231]) is the most widely-used feature-extraction technique; monitoring systems that rely on modal features are referred to as *vibration-based SHM* ([78, 77, 79]). Features based on modal properties are used for both passive and active sensing systems: Operational Modal Analysis (OMA, [6]) deals with the identification of modal properties of structures based on vibration data collected when the structure is in operation. Other popular techniques rely on Principal Component Analysis (PCA,[243]), or equivalently on Proper Orthogonal Decomposition (POD,[15, 147]).

Finally, *statistical inference* deals with the development of a decision rule which serves to monitor the system. There are two competing approaches to accomplish the inference step: the "inverse-problem" or "model-based" approach, and the "data-based" approach. Both approaches are based on an offline-online decomposition of the monitoring process: the *offline stage* is performed before the structure of interest starts to operate, while the *online stage* corresponds to the normal operations of the structure. We emphasize that mathematical models do play a role in both approaches: the "model-based" vs "data-based" taxonomy refers to the online stage of the process.

In the *model-based approach* ([85]), a physics-based model (typically consisting of a set of differential equations) of the structure of interest is built and properly calibrated during the offline stage. During the online stage, this model is updated on the basis of the new measured data from the real structure. The solution to the updated model is then used to assess the state of damage of the system. From a mathematical perspective, during the online stage, given the measurements $\mathbf{q}^{\text{exp}} = \mathbf{q}^{\text{exp}}(\mathcal{C})$, and the features $\mathbf{z}^{\text{exp}} = \mathcal{F}(\mathbf{q}^{\text{exp}})$, we first solve an inverse problem of the form[1]

$$\mu^\star := \arg\min_{\mu \in \mathcal{P}^{\text{bk}}} \|\mathbf{z}^{\text{bk}}(\mu) - \mathbf{z}^{\text{exp}}\|_2, \tag{1.4.7a}$$

where the map $\mu \mapsto \mathbf{z}^{\text{bk}}(\mu)$ is defined implicitly in (1.3.4). Then, we return the estimate of the state of damage as follows:

$$\hat{y} = f^{\text{dam}}(\mu^\star). \tag{1.4.7b}$$

[1]The choice of the Euclidean norm is completely arbitrary and other options can be considered.

We note that (1.4.7a) is of the same form as (1.4.4) although here we potentially consider the case of multiple mathematical models, which correspond to the different physical experiments performed on the structure. Since (1.4.7a) is likely to be ill-posed, a form of (either statistical or deterministic) regularization is needed. We refer to the works of Friswell, Mottershead and coauthors ([87, 86, 154]) for further details. We observe that these approaches were not originally developed for the estimation of discrete-valued quantities of interest (the state of damage), and so they do not directly address the engineering task at hand.

Instead of proceeding from a law-based model, the *data-based approach* ([78, 79]) is based on the collection of a dataset of offline training data from all the possible healthy and damaged states of interest. The dataset can be collected (i) by performing experiments on the structure itself or on similar structures (see, e.g., [79]), or (ii) by performing synthetic experiments based on a (possibly parametrized) mathematical model of the structure of interest (see, e.g., [115, 114, 132]). Given the dataset, machine learning algorithms are used to train a classifier that assigns measured data from the monitoring phase to the relevant diagnostic class label. This classifier is then employed to monitor the structure during the online stage. We denote by Simulation-Based Classification (SBC) the particular procedural choices "data-based" and "synthetic experiments". Exploiting the definitions in section 1.3.2, in SBC, we first consider $M$ different parameters $\mu^1, \ldots, \mu^M \in \mathcal{P}^{\text{bk}}$, and we assemble the dataset

$$\mathcal{D}_M^{\text{bk}} := \{(\mathbf{z}^{\text{bk}}(\mu^m), f^{\text{dam}}(\mu^m))\}_{m=1}^M. \tag{1.4.8a}$$

Then, we appeal to a supervised learning (SL) algorithm for classification (see, e.g., [104, 157, 120]) that takes as input the dataset $\mathcal{D}_M^{\text{bk}}$ and returns the classifier $g_M^\star : \mathbb{R}^{Q_{\text{feat}}} \to \{1, \ldots, K\}$

$$[g_M^\star] = \texttt{SL-algorithm}(\mathcal{D}_M^{\text{bk}}). \tag{1.4.8b}$$

During the online stage, we simply acquire the new measurements, we compute the features $\mathbf{z}^{\text{exp}}$ and we evaluate the classifier:

$$\hat{y} = g_M^\star(\mathbf{z}^{\text{exp}}). \tag{1.4.8c}$$

The main challenge associated with the application of the data-based (or simulation-based)

approach is the construction of the offline dataset used to train the classifier $g$. Since classification performance strongly depends on the amount of offline training data, the offline dataset should be representative of all possible system configurations (characterized by different geometries, and operational and environmental conditions) that can potentially occur online.

While several authors applied model reduction techniques to speed up computations within the model-based framework, the use of parametric model reduction in a simulation-based setting has yet to be fully explored. As regards the model-based framework, there is a large body of literature that exploits parametric model reduction techniques to reduce the overall cost associated with the solution to (1.4.7) (see [158, 137, 110] and [62, Chapter 9]). These techniques are similar in objective to the techniques presented in section 1.4.1 for solving problem (1.4.4). As regards the simulation-based framework, most of the early literature ([105, 155]) resort to surrogate models to speed up computations of the dataset, while more recent works focus on adaptive sampling schemes ([14, 17, 16]) to reduce the number $M$ of datapoints in (1.4.8a) without affecting classification performances. A notable exception is provided by the work of Lecerf, Allaire and Willcox [132], which already incorporate important aspects of model order reduction to accelerate the dataset construction. However, the reduction approach employed in [132] is based on a reduction of the dimension of the underlying PDE, and it does not exploit the parametric nature of the mathematical model.

## 1.5 Thesis overview

This thesis consists of two separate parts.

**Part 1** deals with the development of a model reduction procedure for state estimation, the Parametrized-Background Data-Weak (PBDW) approach. PBDW was first presented in [142, 143] for stationary problems and perfect measurements (i.e., $\ell_m^{\text{obs}} = \ell_m^o(u^{\text{true}})$, $m = 1, \dots, M$). The key idea of the PBDW formulation is to seek an approximation $u^\star = z^\star + \eta^\star$ to the true field $u^{\text{true}}$ employing projection-by-data. The first contribution to $u^\star$, $z^\star \in \mathcal{Z}_N$, is the "deduced background estimate". The linear $N$-dimensional space $\mathcal{Z}_N \subset \mathcal{U}$ is informed by the bk manifold $\mathcal{M}^{\text{bk}} = \{u^{\text{bk}}(\mu)|_\Omega : \mu \in \mathcal{P}^{\text{bk}}\}$, which we hope is close to the true field. The second contribution to $u^\star$, $\eta^\star \in \mathcal{U}_M$, is the "update estimate". The linear

$M$-dimensional space $\mathcal{U}_M$ is the span of the Riesz representations $\{R_{\mathcal{U}}\ell_m^o\}_{m=1}^M$ of the $M$ observation functionals $\{\ell_m^o\}_{m=1}^M$. While the background estimate incorporates our *a priori* knowledge of the state, the update addresses the deficiencies of the bk model by improving the approximation properties of the search space.

In this thesis, we extend the PBDW formulation in three directions. Some of the results have been first presented in the papers [213, 212].

- We propose an experimental *a posteriori* estimation procedure for the $L^2(\Omega)$ state-estimation error $\|u^{\text{true}} - u^\star\|_{L^2(\Omega)}$, and for the error in output $\mathcal{L}(u^{\text{true}}) - \mathcal{L}(u^\star)$, where $\mathcal{L} : L^2(\Omega) \to \mathbb{R}$. The procedure allows us to quantify the uncertainty in the state estimate.

- We propose a computational procedure for the construction of the background space $\mathcal{Z}_N$ when $\Omega \subset \Omega^{\text{bk}}$. We remark that traditional model reduction strategies aim to generate linear approximation spaces for the manifold $\widehat{\mathcal{M}}^{\text{bk}} = \{u^{\text{bk}}(\mu) : \mu \in \mathcal{P}^{\text{bk}}\}$ over $\Omega^{\text{bk}}$. If $\Omega$ is strictly contained in $\Omega^{\text{bk}}$, these strategies might either be unfeasible or might lead to inaccurate approximation spaces for the restricted manifold $\mathcal{M}^{\text{bk}}$.

- We consider the case of pointwise noisy measurements ($\ell_m^{\text{obs}} = u^{\text{true}}(x_m^{\text{obs}}) + \epsilon_m$). In more detail, we rely on the theory of Reproducing Kernel Hilbert Spaces (RKHS) that allows us to consider spaces $\mathcal{U}$ for which the Riesz representers $\{K_{x_m} = R_{\mathcal{U}}\ell_m^o\}_m$ associated with the observation functionals $\{\ell_m^o = \delta_{x_m}\}_m$ are explicitly known. We demonstrate that explicit expressions for the representers greatly improve the flexibility of the approach; in addition, we find much faster convergence with respect to the number of measurements $M$ than in the approach presented in [142, 143].

**Part 2** deals with the development of a model reduction procedure for Simulation-Based Classification with application to Structural Health Monitoring. As explained in section 1.4.2, we generate a dataset $\mathcal{D}_M^{\text{bk}} = \{(\mathbf{z}^{\text{bk}}(\mu^m), f^{\text{dam}}(\mu^m))\}_{m=1}^M$ by repeated solution of a parametrized mathematical model for $M$ different parameters $\mu^1, \ldots, \mu^M \in \mathcal{P}^{\text{bk}}$. Then, we appeal to a supervised learning algorithm to compute a classifier $g_M^\star$ to map features (and thus experimental observations) to the corresponding configuration label.

We demonstrate that the use of pMOR techniques, which is enabled by the parametrized description of damage, is crucial to reduce the computational burden associated with the

construction of the dataset without sacrifying the accuracy of the approximation. We present a rigorous mathematical formulation which integrates the PDE model within the classification framework, and we provide a framework for error analysis, which takes into account non-parametric model error. We illustrate the procedure and motivate the use of model reduction techniques through a cradle-to-grave example: a physical harmonically-excited microtruss system. Some of the results have been first presented in the paper [214].

We resort to a 2D-3D high-order continuous-Galerkin Finite Element solver. Our implementation is based on a suite of Matlab codes ([150]) that has been developed by Professor Masayuki Yano (University of Toronto) during his stay at MIT. We refer to [107, Appendix A] for details related to the implementation. Experimental apparata have been designed and implemented by Doctor James D Penn (MIT).

# Part I

# Parametrized-Background Data-Weak approach to state estimation

# Chapter 2

# The PBDW approach: formulation and analysis

In this chapter, we introduce the PBDW formulation. First, in section 2.1, we derive the problem statement, and we highlight the role of model order reduction. Then, in section 2.2, we study the well-posedness of the PBDW statement, we derive an important representation formula for the PBDW state estimate, and we discuss the connection with the problem of optimal recovery. In section 2.3, we exploit the representation formula proved in section 2.2.1 to derive an algebraic formulation that permits rapid computations. In section 2.4 we summarize the computational procedure, and in section 2.5 we relate our approach to other data assimilation formulations presented in the literature. Finally, in section 2.6, we summarise the main contribution of the PBDW formulation, and we present and motivate the research goals addressed in the next chapters. We state upfront that in this chapter we only consider real-valued problems. The formulation and the mathematical analysis can be trivially extended to complex-valued problems.

## 2.1 Formulation

### 2.1.1 Problem statement

We aim to estimate the deterministic state $u^{\text{true}} \in \mathcal{U}$ over the domain of interest $\Omega \subset \mathbb{R}^d$. As explained in the introduction, we shall afford ourselves two sources of information: a bk

mathematical model

$$G^{\mathrm{bk},\mu}(u^{\mathrm{bk}}(\mu)) = 0, \quad \mu \in \mathcal{P}^{\mathrm{bk}}$$

defined over a domain $\Omega^{\mathrm{bk}}$ that contains $\Omega$; and $M$ experimental observations $\ell_1^{\mathrm{obs}}, \ldots, \ell_M^{\mathrm{obs}}$ such that

$$\ell_m^{\mathrm{obs}} = \ell_m^o(u^{\mathrm{true}}) + \epsilon_m, \qquad m = 1, \ldots, M,$$

where $\ell_1^o, \ldots, \ell_M^o \in \mathcal{U}'$ are suitable observation functionals, $\mathcal{P}^{\mathrm{bk}} \subset \mathbb{R}^P$ is a confidence region for the true values of the parameters of the model, and $\{\epsilon_m\}_{m=1}^M$ are unknown disturbances caused by either systematic error in the data acquisition system or experimental random noise. We further introduce the bk manifold $\mathcal{M}^{\mathrm{bk}} = \{u^{\mathrm{bk}}(\mu) : \mu \in \mathcal{P}^{\mathrm{bk}}\}$ associated with the solution to the parametrized model.

If $\mathcal{P}^{\mathrm{bk}} = \{\bar{\mu}\}$, we propose to estimate the state $u^{\mathrm{true}}$ as follows:

$$u_\xi^\star := \arg\min_{u \in \mathcal{U}} \xi \|u - u^{\mathrm{bk}}\|^2 + \frac{1}{M} \sum_{m=1}^{M} \left(\ell_m^o(u) - \ell_m^{\mathrm{obs}}\right)^2, \tag{2.1.1}$$

where $\xi > 0$ regulates the relative importance of the background $u^{\mathrm{bk}}(\bar{\mu})$ compared to the data. We observe that if $\epsilon_1, \ldots, \epsilon_M$ are independent identically distributed random disturbances such that $\mathbb{E}[\epsilon_m] = 0$, $\mathbb{E}[\epsilon_m \epsilon_{m'}] = \sigma^2 \delta_{m,m'}$ then (2.1.1) corresponds to the 3D-VAR statement ([24, Chapter 2],[138]).

If $\mathcal{P}^{\mathrm{bk}} \neq \{\bar{\mu}\}$, we can generalize (2.1.1) as follows:

$$(\mu_\xi^\star, u_\xi^\star) := \arg \min_{(\mu,u) \in \mathcal{P}^{\mathrm{bk}} \times \mathcal{U}} \xi \|u - u^{\mathrm{bk}}(\mu)\|^2 + \frac{1}{M} \sum_{m=1}^{M} \left(\ell_m^o(u) - \ell_m^{\mathrm{obs}}\right)^2. \tag{2.1.2}$$

Formulation (2.1.2) is known as partial spline model ([226, Chapter 9]), and can also be restated in terms of the update $\eta_\xi^\star = u_\xi^\star - u^{\mathrm{bk}}(\mu_\xi^\star)$:

$$(\mu_\xi^\star, \eta_\xi^\star) := \arg \min_{(\mu,\eta) \in \mathcal{P}^{\mathrm{bk}} \times \mathcal{U}} \xi \|\eta\|^2 + \frac{1}{M} \sum_{m=1}^{M} \left(\ell_m^o(u^{\mathrm{bk}}(\mu) + \eta) - \ell_m^{\mathrm{obs}}\right)^2. \tag{2.1.3}$$

We observe that (2.1.2) (and equivalently (2.1.3)) is non-convex in $\mu$; furthermore, evaluations of the map $\mu \mapsto u^{\mathrm{bk}}(\mu)$ involve the solution to the bk model. Therefore, it is not suitable for real-time computations.

If we introduce the rank-$N$ approximation ([56]) of the bk field $u^{\text{bk}}(\mu)$,

$$u_N^{\text{bk}}|_\Omega(x,\mu) = \sum_{n=1}^{N} \phi_n(\mu)\,\zeta_n(x), \qquad x \in \Omega,\ \ \mu \in \mathcal{P}^{\text{bk}},$$

we can approximate statement (2.1.3) as

$$(\mu_\xi^\star, \eta_\xi^\star) := \arg \min_{(\mu,\eta)\in\mathcal{P}^{\text{bk}}\times\mathcal{U}} \xi\|\eta\|^2 + \frac{1}{M}\sum_{m=1}^{M}\left(\ell_m^o\left(\sum_{n=1}^{N}\phi_n(\mu)\zeta_n\right) + \ell_m^o(\eta) - \ell_m^{\text{obs}}\right)^2. \quad (2.1.4)$$

Then, we can relax (2.1.4) as follows:

$$(\boldsymbol{\phi}_\xi^\star, \eta_\xi^\star) = \arg \min_{(\boldsymbol{\phi},\eta)\in\mathbb{R}^N\times\mathcal{U}} \xi\|\eta\|^2 + \frac{1}{M}\sum_{m=1}^{M}\left(\ell_m^o\left(\sum_{n=1}^{N}\phi_n\,\zeta_n\right) + \ell_m^o(\eta) - \ell_m^{\text{obs}}\right)^2,$$

which can also be rewritten as

$$(z_\xi^\star, \eta_\xi^\star) := \arg \inf_{(z,\eta)\in\mathcal{Z}_N\times\mathcal{U}} J_\xi(z,\eta) := \xi\|\eta\|^2 + \frac{1}{M}\sum_{m=1}^{M}\left(\ell_m^o(z+\eta) - \ell_m^{\text{obs}}\right)^2, \quad (2.1.5)$$

where $\mathcal{Z}_N = \text{span}\{\zeta_n\}_{n=1}^N \subset \mathcal{U}$ is the $N$-dimensional linear space induced by $\{\zeta_n\}_{n=1}^N$. We further denote by $u_\xi^\star = z_\xi^\star + \eta_\xi^\star$ the corresponding state estimate.

Statement (2.1.5) is the Parametrized-Background Data-Weak (PBDW) formulation, and $u_\xi^\star = z_\xi^\star + \eta_\xi^\star$ is the PBDW state estimate. We observe that PBDW is a (convex) relaxation of the partial spline model for a parametric affine background: instead of penalizing the distance between the state estimate and the manifold $\mathcal{M}^{\text{bk}} = \{u^{\text{bk}}(\mu) : \mu \in \mathcal{P}^{\text{bk}}\}$, we penalize the distance from the linear space $\mathcal{Z}_N$. The parameter $\xi$ should be chosen based on the accuracy of the background space — hence on the accuracy of the bk mathematical model — and on the magnitude of the disturbances $\epsilon_1, \ldots, \epsilon_M$, and might be typically set adaptively. Our derivation allows us to interpret $z_\xi^\star$ as the *deduced background*: $z_\xi^\star$ is the component of the state informed by the prior knowledge of the system, and represents anticipated uncertainty in the mathematical model. Similarly, we can interpret $\eta_\xi^\star$ as the *update*, the component of the state that accomodates unanticipated or non-parametric uncertainty. Consistently, we refer to $\mathcal{Z}_N$ as the *background space.*

Before concluding, we investigate the noise-free case (i.e., $\ell_m^{\text{obs}} = \ell_m^o(u^{\text{true}})$, $m = 1, \ldots, M$) corresponding to the limit $\xi \to 0^+$. Proceeding formally, we obtain the noise-free PBDW

formulation:

$$(z^\star, \eta^\star) := \arg \inf_{(z,\eta)\in\mathcal{Z}_N\times\mathcal{U}} \|\eta\| \quad \text{subject to} \quad \ell_m^o(z+\eta) = \ell_m^{\text{obs}}, \quad m = 1, \dots, M. \quad (2.1.6)$$

We denote by $u^\star = z^\star + \eta^\star$ the corresponding state estimate. Formulation (2.1.6) corresponds to the PBDW formulation first proposed in [142]. In section 2.5, we rigorously show that $\|u_\xi^\star - u^\star\| \to 0$ as $\xi \to 0^+$.

### The assumption of smoothness

We observe that our formulation relies on the assumption that the true field $u^{\text{true}}$ belongs to the Hilbert space $\mathcal{U}$, which corresponds to the Sobolev space $H^s(\Omega)$ for some $s \geq 1$. Although in some cases this assumption might be justified by the existence of physical laws with continuity and differentiability properties, it seems difficult to guarantee *a priori* that the true field belongs to $\mathcal{U}$.

As observed in [76, section 9.6], the assumption of smoothness corresponds to the assumption that "similar" inputs — in this case spatial locations — correspond to "similar" outputs in a proper metric. We argue that the latter, rather than being a technical assumption required by our particular formulation, is a necessary condition for the existence of accurate state estimation algorithms based on scattered data.

## 2.1.2 Role of model order reduction

If we denote by $\epsilon_{\text{mod}}^{\text{bk}} = \inf_{\mu\in\mathcal{P}^{\text{bk}}} \|u^{\text{true}} - u^{\text{bk}}(\mu)\|$ the *modeling error*, and by $\epsilon_N^{\text{bk}} = \inf_{z\in\mathcal{Z}_N} \|u^{\text{true}} - z\|$ the *best-fit error* associated with $\mathcal{Z}_N$, we aim to choose $\mathcal{Z}_N$ such that $\epsilon_{\text{mod}}^{\text{bk}} \approx \epsilon_N^{\text{bk}}$. Since the stability of the PBDW formulation strongly depends on the value of $N$, we further wish to keep $N$ small compared to the number of observations $M$. We observe that we may bound the best-fit error as follows:

$$\epsilon_N^{\text{bk}} = \inf_{z\in\mathcal{Z}_N} \|u^{\text{true}} - z\| \leq \sup_{\mu\in\mathcal{P}^{\text{bk}}} \inf_{z\in\mathcal{Z}_N} \|u^{\text{bk}}(\mu) - z\| + \inf_{\mu\in\mathcal{P}^{\text{bk}}} \|u^{\text{bk}}(\mu) - u^{\text{true}}\| = \epsilon_{\text{disc},N}^{\text{bk}} + \epsilon_{\text{mod}}^{\text{bk}}, \quad (2.1.7)$$

where $\epsilon_{\text{disc},N}^{\text{bk}} = \sup_{\mu\in\mathcal{P}^{\text{bk}}} \inf_{z\in\mathcal{Z}_N} \|u^{\text{bk}}(\mu) - z\|$ is the *discretization error*. Therefore, if $\epsilon_{\text{mod}}^{\text{bk}}$ is small, we can practically construct $\mathcal{Z}_N$ to minimise $\epsilon_{\text{disc},N}^{\text{bk}}$.

Assuming that $\Omega = \Omega^{\text{bk}}$ (i.e., the bk model is defined over the domain of interest), we observe that the task of constructing the space $\mathcal{Z}_N$ is equivalent in objective to the task of constructing the reduced trial space in parametric Model Order Reduction (pMOR) briefly outlined in the introduction. Therefore, we can resort to state-of-the-art techniques proposed in the pMOR literature to generate $\mathcal{Z}_N$, such as Proper Orthogonal Decomposition (POD, [28, 130, 122]), Proper Generalized Decomposition (PGD, [54, 52]), Taylor expansions ([80]), and Greedy algorithms.

In this work, we rely on the Weak-Greedy algorithm for the construction of the space $\mathcal{Z}_N$. The algorithm was first proposed in [223] in the context of Reduced Basis method, and has been applied to elliptic and parabolic, linear and nonlinear, differential equations. The convergence with respect to $N$ of the reduced space obtained using this Greedy procedure has been extensively studied in [40, 32, 66] and linked to the so-called Kolmogorov $N$-width [172]. We refer to [180, Chapter 7] for a thorough overview of the computational procedure; we further refer to [56, Section 8] for a review of the theoretical results.

We briefly summarise the procedure. Given the parametrized PDE $G^{\text{bk},\mu}(u^{\text{bk}}(\mu)) = 0$, $\mu \in \mathcal{P}^{\text{bk}}$, we introduce the error indicator[1]: $\Delta_N^{\text{bk}}(\mu) \approx \inf_{z \in \mathcal{Z}_N} \|u^{\text{bk}}(\mu) - z\|$, $\mu \in \mathcal{P}^{\text{bk}}$. Then, the weak-Greedy algorithm constructs a Lagrange ([175]) hierarchical approximation space $\mathcal{Z}_{N_{\max}} = \text{span}\{u^{\text{bk}}(\mu^n)\}_{n=1}^{N_{\text{train}}}$ such that $\mu^N = \arg\max_{\mu \in \Xi_{\text{train}}} \Delta_{N-1}^{\text{bk}}(\mu)$, $N = 1, \ldots, N_{\max}$, where $\Xi_{\text{train}} \subset \mathcal{P}^{\text{bk}}$ is a finite-dimensional discretization of the parameter domain $\mathcal{P}^{\text{bk}}$. Algorithm 2.1.1 summarises the computational procedure.

We briefly address the more general case $\Omega \subset \Omega^{\text{bk}}$. In this case, we might first appeal to one of the techniques presented above to build a space $\widehat{\mathcal{Z}}_N$ for the manifold $\widehat{\mathcal{M}}^{\text{bk}}$ over $\Omega^{\text{bk}}$. Then, we might define $\mathcal{Z}_N := \{z|_\Omega : z \in \widehat{\mathcal{Z}}_N\}$. If the manifold $\widehat{\mathcal{M}}^{\text{bk}}$ is low-dimensional and reducible[2], this approach should guarantee accurate reduced spaces for the bk manifold $\mathcal{M}^{\text{bk}}$. However, if $\widehat{\mathcal{M}}^{\text{bk}}$ is not reducible, and $\Omega$ is strictly contained in $\Omega^{\text{bk}}$, we envision that this approach might either be unfeasible or lead to poor approximation spaces. We address this issue in Chapter 5.

[1]The practical definition of $\Delta_N^{\text{bk}}(\mu)$ depends on the particular form of the PDE. We refer to the above-mentioned literature for further details.

[2]We refer to [180, Chapter 5] for a formal discussion about the reducibility of parametric manifolds. In Chapter 5 of the present thesis, we discuss the problem of reducibility in a special setting.

**Algorithm 2.1.1** Weak-Greedy algorithm

| | | |
|---|---|---|
| **Input** | $G^{\text{bk},\mu}$ | parametrized best-knowledge model |
| | $\mathcal{P}^{\text{bk}}$ | parameter domain |
| | $\Delta_N^{\text{bk}}$ | error estimate for $\inf_{z\in\mathcal{Z}_N} \|u^{\text{bk}}(\mu) - z\|$ |
| **Output** | $\{\mathcal{Z}_N\}_{N=1}^{N_{\max}}$ | $N$-dimensional hierarchical background space |

1: **for** $N = 1, \ldots, N_{\max}$ **do**

2: Identify the parameter associated with the largest error estimate,

$\mu^N = \arg\max_{\mu\in\Xi_{\text{train}}} \Delta_{N-1}^{\text{bk}}(\mu)$.

3: Evaluate the associated solution $\zeta_N := u^{\text{bk}}(\mu^N)$.

4: Augment the background space $\mathcal{Z}_N := \text{span}\,\{\mathcal{Z}_{N-1}, \zeta_N\}$.

5: **end for**

## 2.2 Mathematical analysis

### 2.2.1 Well-posedness analysis

In this section, we present well-posedness results for the PBDW statement together with a finite-dimensional representation formula for the state estimate, which permits efficient computations. Towards this end, we introduce the Riesz operator $R_{\mathcal{U}} : \mathcal{U}' \to \mathcal{U}$ such that $(R_{\mathcal{U}}\ell, v) = \ell(v)$ for all $v \in \mathcal{U}$ and $\ell \in \mathcal{U}'$, we further introduce the $M$-dimensional update space $\mathcal{U}_M$ as

$$\mathcal{U}_M = \text{span}\{q_m := R_{\mathcal{U}}\ell_m^o\}_{m=1}^M. \tag{2.2.1}$$

Finally, we introduce the stability constant $\beta_{N,M}$ as

$$\beta_{N,M} := \inf_{z\in\mathcal{Z}_N} \sup_{q\in\mathcal{U}_M} \frac{(z,q)}{\|z\|\|q\|}. \tag{2.2.2}$$

Some comments are in order. For perfect measurements (i.e., $\ell_m^{\text{obs}} = \ell_m^o(u^{\text{true}})$), the inner product $(u^{\text{true}}, q)$ is a weighted sum of experimental observations

$$\left(u^{\text{true}}, q = \sum_{m=1}^M \alpha_m q_m\right) = \sum_{m=1}^M \alpha_m (u^{\text{true}}, q_m) = \sum_{m=1}^M \alpha_m \ell_m^{\text{obs}}. \tag{2.2.3}$$

For this reason, we say that $\mathcal{U}_M$ is *experimentally observable*. We further observe that the stability constant $\beta_{N,M}$ is a non-increasing function of background span ($N$) and a non-decreasing function of observable span ($M$). Furthermore, $\beta_{N,M} = 0$ for $M < N$.

Next two Propositions provide the well-posedness results; for purposes of exposition, we consider the cases $\xi = 0$ and $\xi > 0$ separately.

**Proposition 2.2.1.** *Suppose that $\mathcal{Z}_N \subset \mathcal{U}$, and let $\beta_{N,M}$ be defined in* (2.2.2). *Let us further suppose that $\ell_m^{\text{obs}} = \ell_m^o(u^{\text{true}})$ for $m = 1, \ldots, M$, and that $\mathcal{U}_M$ is $M$-dimensional. Then, the following hold.*

*(i) Any solution $(z^\star, \eta^\star)$ to* (2.1.6) *belongs to $\mathcal{Z}_N \times \mathcal{Z}_N^\perp \cap \mathcal{U}_M$.*

*(ii) The pair $(z^\star, \eta^\star)$ is a solution to* (2.1.6) *if and only if $u^\star = z^\star + \eta^\star$ is a solution to the problem:*

$$u^\star := \arg\inf_{u \in \mathcal{U}} \|\Pi_{\mathcal{Z}_N^\perp} u\| \qquad \text{subject to} \quad \ell_m^o(u) = \ell_m^{\text{obs}}, \;\; m = 1, \ldots, M. \tag{2.2.4}$$

*(iii) If $\beta_{N,M} > 0$, there exists a unique solution $(z^\star, \eta^\star)$ to* (2.1.6). *Furthermore, $(z^\star, \eta^\star)$ solves the following saddle-point problem:*

$$\begin{cases} (\eta^\star, q) + (z^\star, q) &= (u^{\text{true}}, q) \quad \forall\, q \in \mathcal{U}_M; \\ (\eta^\star, p) &= 0 \qquad\quad \forall\, p \in \mathcal{Z}_N. \end{cases} \tag{2.2.5}$$

*Proof.* We first prove (i). Let $(z^\star, \eta^\star)$ be a solution to (2.1.6). We observe that $(z^\star, \Pi_{\mathcal{U}_M}\eta^\star)$ satisfies the constraints,

$$\ell_m^o(z^\star + \Pi_{\mathcal{U}_M}\eta^\star) = (z^\star + \Pi_{\mathcal{U}_M}\eta^\star, q_m) = (z^\star + \eta^\star, \underbrace{q_m}_{\in \mathcal{U}_M}) = \ell_m^o(z^\star + \eta^\star) = \ell_m^{\text{obs}}, \;\; m = 1, \ldots, M.$$

Furthermore, recalling the projection theorem, we find $\|\eta^\star\|^2 = \|\Pi_{\mathcal{U}_M}\eta^\star\|^2 + \|\Pi_{\mathcal{U}_M^\perp}\eta^\star\|^2$. Since $(z^\star, \eta^\star)$ is optimal, we must have $\Pi_{\mathcal{U}_M^\perp}\eta^\star \equiv 0$. This proves that $\eta^\star \in \mathcal{U}_M$. We now consider the pair $(z^\star + \Pi_{\mathcal{Z}_N}\eta^\star, \Pi_{\mathcal{Z}_N^\perp}\eta^\star)$. It is straightforward to verify that $(z^\star + \Pi_{\mathcal{Z}_N}\eta^\star, \Pi_{\mathcal{Z}_N^\perp}\eta^\star)$ satisfies the constraints. Therefore, appealing once again to the projection theorem, and exploiting the optimality of $(z^\star, \eta^\star)$, we must have $\Pi_{\mathcal{Z}_N}\eta^\star \equiv 0$. Thesis follows.

We now prove (ii). Recalling statement (i), we have $\eta^\star \in \mathcal{Z}_N^\perp$. This implies that we can

restate (2.1.6) as follows:

$$(z^\star, \eta^\star) := \arg \inf_{(z,\eta)\in \mathcal{Z}_N \times \mathcal{Z}_N^\perp} \|\eta\| \quad \text{subject to} \quad \ell_m^o(z+\eta) = \ell_m^{\text{obs}}, \quad m = 1, \dots, M.$$

Thesis (ii) follows by observing that $\mathcal{Z}_N \oplus \mathcal{Z}_N^\perp = \mathcal{U}$.

We finally prove (iii). Exploiting (2.2.3), we restate (2.1.6) as follows:

$$(z^\star, \eta^\star) = \arg \min_{(z,\eta)\in \mathcal{Z}_N \times \mathcal{U}} \|\eta\|, \quad \text{subject to } (z+\eta-u^{\text{true}}, q) = 0 \; \forall\, q \in \mathcal{U}_M. \tag{2.2.6}$$

We can now introduce the Lagrangian $\mathcal{L} : \mathcal{Z}_N \times \mathcal{U}_M \times \mathcal{U}_M \to \mathbb{R}$ associated with (2.2.6): $\mathcal{L}(z, \eta, \phi) = \frac{1}{2}\|\eta\|^2 + (z + \eta - u^{\text{true}}, \phi)$. By differentiating, we obtain

$$\begin{cases} \partial_\eta \mathcal{L} = 0 \Rightarrow & (\eta^\star + \phi^\star, \delta\eta) = 0 & \forall\, \delta\eta \in \mathcal{U}_M; \\ \partial_z \mathcal{L} = 0 \Rightarrow & (\phi^\star, \delta z) = 0 & \forall\, \delta z \in \mathcal{Z}_N; \\ \partial_\phi \mathcal{L} = 0 \Rightarrow & (\eta^\star + \phi^\star - u^{\text{true}}, \delta\phi) = 0 & \forall\, \delta\phi \in \mathcal{U}_M. \end{cases}$$

From the first equation, we obtain $\eta^\star = -\phi^\star$. Then, if we substitute this identity in the second equation, we obtain that any solution to (2.1.6) must solve (2.2.5). Recalling[3] [181, Theorem 7.4.1], since $\beta_{N,M} > 0$, there exists a unique solution $(z^\star, \eta^\star) \in \mathcal{Z}_N \times \mathcal{U}_M$ to (2.2.5). Thesis (iii) follows. □

**Proposition 2.2.2.** *Suppose that $\mathcal{Z}_N \subset \mathcal{U}$, and let $\beta_{N,M}$ be defined in (2.2.2). Let us further suppose that $\mathcal{U}_M$ is $M$-dimensional. Let $\xi > 0$. Then, the following hold.*

*(i) Any solution $(z_\xi^\star, \eta_\xi^\star)$ to (2.1.5) belongs to $\mathcal{Z}_N \times \mathcal{Z}_N^\perp \cap \mathcal{U}_M$.*

*(ii) The pair $(z_\xi^\star, \eta_\xi^\star)$ is a solution to (2.1.5) if and only if $u_\xi^\star = z_\xi^\star + \eta_\xi^\star$ is a solution to the problem*

$$u_\xi^\star := \arg \inf_{u\in\mathcal{U}} J_\xi^{(1)}(u) := \xi \|\Pi_{\mathcal{Z}_N^\perp} u\|^2 + \frac{1}{M} \sum_{m=1}^{M} \left(\ell_m^o(u) - \ell_m^{\text{obs}}\right)^2. \tag{2.2.7}$$

*(iii) If $\beta_{N,M} > 0$, there exists a unique solution $(z_\xi^\star, \eta_\xi^\star)$ to (2.1.5). Furthermore, $(z_\xi^\star, \eta_\xi^\star)$*

[3] We briefly present the correspondence between our notation and the notation used in [181, Theorem 7.4.1]: $M = \mathcal{Z}_N$, $X = \mathcal{U}_M$, $a(\cdot,\cdot) = (\cdot,\cdot)$, $b(\cdot,\cdot) = (\cdot,\cdot)$, $\langle \ell, v\rangle = (u^{\text{true}}, v)$ and $\sigma \equiv 0$.

*solves the following saddle-point problem:*

$$\begin{cases} 2\xi(\eta_\xi^\star, q) + \frac{2}{M}\sum_{m=1}^{M}\left(\ell_m^o(z_\xi^\star + \eta_\xi^\star) - \ell_m^{\text{obs}}\right)\ell_m^o(q) & = 0 \quad \forall q \in \mathcal{U}_M; \\ (\eta_\xi^\star, p) & = 0 \quad \forall p \in \mathcal{Z}_N. \end{cases} \tag{2.2.8}$$

In view of the proof of Proposition 2.2.2, we first present two lemmas. The first lemma is proven in [141, Proposition Appendix A.1]; we report the proof for completeness.

**Lemma 2.2.1.** *Let $\mathcal{U}_M := \text{span}\{q_m\}_{m=1}^M$ and let $\beta_{N,M}$ be defined as in (2.2.2). Then, we have that*

$$\beta_{N,M} = \inf_{\eta \in \mathcal{U}_M^\perp} \frac{\|\Pi_{\mathcal{Z}_N^\perp}\eta\|}{\|\eta\|}. \tag{2.2.9}$$

*Proof.* To simplify notation, given the linear space $\mathcal{Q}$, we define $\mathcal{Q}^{(1)} = \{q \in \mathcal{Q} : \|q\| = 1\}$. We now prove (2.2.9).

$$\begin{aligned} \beta_{N,M}^2 = & \left(\inf_{z\in\mathcal{Z}_N^{(1)}} \sup_{v\in\mathcal{U}_M^{(1)}} (z,v)\right)^2 = \inf_{z\in\mathcal{Z}_N^{(1)}} \|\Pi_{\mathcal{U}_M} z\|^2 = 1 - \sup_{z\in\mathcal{Z}_N^{(1)}} \|\Pi_{\mathcal{U}_M^\perp} z\|^2 \\ = & \ 1 - \left(\sup_{z\in\mathcal{Z}_N^{(1)}} \sup_{q\in\mathcal{U}_M^{\perp(1)}} (z,q)\right)^2 = 1 - \left(\sup_{q\in\mathcal{U}_M^{\perp(1)}} \sup_{z\in\mathcal{Z}_N^{(1)}} (z,q)\right)^2 \\ = & \ 1 - \sup_{q\in\mathcal{U}_M^{\perp(1)}} \|\Pi_{\mathcal{Z}_N} q\|^2 = \inf_{q\in\mathcal{U}_M^{\perp(1)}} \|\Pi_{\mathcal{Z}_N^\perp} q\|^2 \end{aligned}$$

Thesis follows. □

**Lemma 2.2.2.** *Let $\mathcal{U}_{M'} := span\{q_m\}_{m=1}^{M'}$, $M' \le M$. Let us introduce $\beta_{N,M'} = \inf_{z\in\mathcal{Z}_N} \sup_{v\in\mathcal{U}_{M'}} \frac{(z,v)}{\|z\|\|v\|}$, and the matrix $\mathbb{K}^{(M')} \in \mathbb{R}^{M',M'}$, $\mathbb{K}_{m,m'}^{(M')} = (q_m, q_{m'})$. Let us further define*

$$c_{N,M} := \max_{M'=1,\dots,M} \hat{c}_{N,M'}, \qquad \hat{c}_{N,M'} = \min\left(\frac{1}{2}\lambda_{\min}(\mathbb{K}^{(M')}), \frac{\lambda_{\min}(\mathbb{K}^{(M')})}{2 + \lambda_{\min}(\mathbb{K}^{(M')})}\beta_{N,M'}^2\right), \tag{2.2.10a}$$

*where $\lambda_{\min}(\mathbb{K}^{(M')})$ denotes the minimum eigenvalue of the matrix $\mathbb{K}^{(M')}$.*

*Then, the following bound holds:*

$$\widetilde{J}(u) = \|\Pi_{\mathcal{Z}_N^\perp} u\|^2 + \sum_{m=1}^{M} (\ell_m^o(u))^2 \ge c_{N,M}\|u\|^2, \qquad \forall u \in \mathcal{U}. \tag{2.2.10b}$$

*Proof.* We first claim that for any $M'$ such that $\beta_{N,M'} > 0$ we have

$$\widetilde{J}_{M'}(u) \;=\; \|\Pi_{\mathcal{Z}_N^\perp} u\|^2 + \sum_{m=1}^{M'} \left(\ell_m^o(u)\right)^2 \geq \hat{c}_{N,M'} \|u\|^2, \qquad \forall\, u \in \mathcal{U}. \tag{2.2.11}$$

Given (2.2.11), we find that

$$\widetilde{J}(u) \geq \widetilde{J}_{M'}(u) \geq \hat{c}_{N,M'} \|u\|^2 \;\; \forall\, M' \leq M \;\Rightarrow\; \widetilde{J}(u) \geq \left(\max_{M'} \hat{c}_{N,M'}\right) \|u\|^2,$$

which is the thesis.

We now show (2.2.11). Given $u \in \mathcal{U}$, we introduce $u_1 = \Pi_{\mathcal{U}_{M'}^\perp} u$, $u_2 = \Pi_{\mathcal{U}_{M'}} u = \sum_{m=1}^{M'} (\mathbf{u}_2)_m q_m$. Then, we observe that

$$u_1(x_m) = (\underbrace{q_m}_{\in \mathcal{U}_{M'}}, u_1) = 0, \qquad m = 1, \ldots, M'. \tag{2.2.12}$$

We further observe that

$$\sum_{m=1}^{M'} \left(\ell_m^o(u_2)\right)^2 = \|\mathbb{K}^{(M')} \mathbf{u}_2\|_2^2, \qquad \|u_2\|^2 = \mathbf{u}_2^T\, \mathbb{K}^{(M')}\, \mathbf{u}_2,$$

which implies that

$$\min_{u_2 \in \mathcal{U}_{M'}} \frac{\sum_{m=1}^{M'} \left(\ell_m^o(u_2)\right)^2}{\|u_2\|^2} \;=\; \min_{\mathbf{u}_2 \in \mathbb{R}^{M'}} \frac{\|\mathbb{K}^{(M')} \mathbf{u}_2\|_2^2}{\mathbf{u}_2^T\, \mathbb{K}^{(M')}\, \mathbf{u}_2} = \lambda_{\min}(\mathbb{K}^{(M')}). \tag{2.2.13}$$

Combining (2.2.12) and (2.2.13), we obtain

$$\sum_{m=1}^{M'} \left(\ell_m^o(u)\right)^2 = \sum_{m=1}^{M'} \left(\ell_m^o(u_2)\right)^2 \geq\; \lambda_{\min}(\mathbb{K}^{(M')})\, \|u_2\|^2.$$

Now, recalling the identity $2ab \geq -\frac{1}{\epsilon} a^2 - \epsilon b^2$ valid for any $\epsilon > 0$, and Lemma 2.2.1, we obtain:

$$\begin{aligned} \widetilde{J}_{M'}(u) = \widetilde{J}_{M'}(u_1 + u_2) \geq \;& \|\Pi_{\mathcal{Z}_N^\perp} u_1\|^2 + \|\Pi_{\mathcal{Z}_N^\perp} u_2\|^2 + 2\left(\Pi_{\mathcal{Z}_N^\perp} u_1, \Pi_{\mathcal{Z}_N^\perp} u_2\right) + \lambda_{\min}(\mathbb{K}^{(M')})\, \|u_2\|^2 \\ \geq \;& (1-\epsilon)\, \beta_{N,M'}^2 \|u_1\|^2 + \left(1 - \tfrac{1}{\epsilon}\right) \|\Pi_{\mathcal{Z}_N^\perp} u_2\|^2 + \lambda_{\min}(\mathbb{K}^{(M')}) \|u_2\|^2 \end{aligned}$$

Let us consider $\epsilon \in \left(\frac{1}{1+\lambda_{\min}(\mathbb{K}^{(M')})}, 1\right)$. Recalling that $\|\Pi_{\mathcal{Z}_N^\perp} u_2\| \leq \|u_2\|$, we obtain

$$\begin{aligned}\widetilde{J}_{M'}(u) \geq & \ (1-\epsilon)\beta_{N,M'}^2 \|u_1\|^2 + \left(\lambda_{\min}(\mathbb{K}^{(M')}) + 1 - \tfrac{1}{\epsilon}\right) \|u_2\|^2 \\ \geq & \ \min\left(\lambda_{\min}(\mathbb{K}^{(M')}) + 1 - \tfrac{1}{\epsilon},\ (1-\epsilon)\beta_{N,M'}^2\right) \underbrace{\left(\|u_1\|^2 + \|u_2\|^2\right)}_{=\|u\|^2}.\end{aligned}$$

Estimate (2.2.11) follows by considering $\epsilon = \frac{2}{2+\lambda_{\min}(\mathbb{K}^{(M')})}$. □

We observe that $c_{N,M}$ is monotonic increasing with $M$; therefore, it is asymptotically bounded from below in the limit $M \to \infty$. We further observe that $\lambda_{\min}(\mathbb{K}^{(M')}) > 0$ if and only if $\mathcal{U}_{M'}$ is a $M'$-dimensional space.

*Proof.* (Proposition 2.2.2). We first prove that $\eta_\xi^\star \in \mathcal{U}_M \cap \mathcal{Z}_N^\perp$ (Statement (i)). Thesis follows by observing that $J_\xi(z,\eta) = J_\xi(z, \Pi_{\mathcal{U}_M}\eta) + \xi\|\Pi_{\mathcal{U}_M^\perp}\eta\|^2$, and $J_\xi(z,\eta) = J_\xi(z+\Pi_{\mathcal{Z}_N}\eta, \Pi_{\mathcal{Z}_N^\perp}\eta) + \xi\|\Pi_{\mathcal{Z}_N}\eta\|^2$. We omit the details.

We now show that $(z_\xi^\star, \eta_\xi^\star)$ solves (2.1.5) if and only if $u_\xi^\star = z_\xi^\star + \eta_\xi^\star$ solves (2.2.7) (Statement (ii)). Exploiting Statement (i), we have

$$\min_{(z,\eta)\in\mathcal{Z}_N\times\mathcal{U}} J_\xi(z,\eta) = \min_{(z,\eta)\in\mathcal{Z}_N\times\mathcal{Z}_N^\perp} J_\xi(z,\eta).$$

Thesis follows by observing that $J_\xi^{(1)}(u) = J_\xi(\Pi_{\mathcal{Z}_N} u, \Pi_{\mathcal{Z}_N^\perp} u)$, and recalling that $\mathcal{U} = \mathcal{Z}_N \oplus \mathcal{Z}_N^\perp$.

We now prove (iii). Applying Lemma 2.2.2, we find that the objective function $J_\xi^{(1)} : \mathcal{U} \to \mathbb{R}$ is strictly convex if $\beta_{N,M} > 0$. Existence and uniqueness of the solution to (2.2.7) then follow from [74, Theorem 3, Chapter 8.2]. Exploiting Statement (ii), we find that the solution $(z_\xi^\star, \eta_\xi^\star)$ to (2.1.5) exists and is unique. Furthermore, recalling that the solution $u_\xi^\star$ must be a zero of the first variation of $J_\xi^{(1)}$, we obtain

$$\delta J(u_\xi^\star, v) = 2\xi(\Pi_{\mathcal{Z}_N^\perp} u_\xi^\star, v) + \frac{2}{M}\sum_{m=1}^{M}\left(\ell_m^o(u_\xi^\star) - \ell_m^{\text{obs}}\right)\ell_m^o(v) = 0. \qquad \forall v \in \mathcal{U},$$

which implies (2.2.8). Thesis follows. □

Before concluding, we present a number of observations. First, in Propositions 2.2.1 and 2.2.2, we rely on the assumption that $\mathcal{Z}_N \subset \mathcal{U}$. This is required to define $\beta_{N,M}$ in (2.2.2),

and also the single-field formulations (2.2.4) and (2.2.7). In section 2.3, we derive sufficient conditions for the well-posedness of (2.1.5) and (2.1.6) that do not rely on the hypothesis $\mathcal{Z}_N \subset \mathcal{U}$. Second, statements (i) of Propositions 2.2.1 and 2.2.2 are extremely important from a practical standpoint since they provide an *a priori* finite-dimensional representation formula for the solutions to (2.1.5) and (2.1.6). We rely on these finite-dimensional representations to derive efficient algebraic counterparts of the variational statements.

### 2.2.2 Connection with the problem of optimal recovery

We illustrate the connection between the PBDW formulation presented in this chapter and the problem of optimal recovery ([152]). This connection has first been observed by Binev et al. in [33] for perfect observations; in this section, we briefly review part of the analysis presented in [33], and we present the analogous result for noisy measurements.

Given the background space $\mathcal{Z}_N \subset \mathcal{U}$ and the linear functionals $\ell_1^o, \ldots, \ell_M^o \in \mathcal{U}'$, we introduce the compact sets

$$\mathcal{K}_N(\epsilon, \boldsymbol{\ell}^{\text{obs}}) = \left\{ u \in \mathcal{U} : \ \|\Pi_{\mathcal{Z}_N^\perp} u\| \leq \epsilon, \ \ell_m^o(u) = \ell_m^{\text{obs}}, \ m = 1, \ldots, M \right\}, \tag{2.2.14}$$

and

$$\mathcal{K}_{N,\xi}(\epsilon, \boldsymbol{\ell}^{\text{obs}}) = \left\{ u \in \mathcal{U} : \ J_\xi^{(1)}(u) = \xi \|\Pi_{\mathcal{Z}_N^\perp} u\|^2 + \frac{1}{M} \sum_{m=1}^{M} \left( \ell_m^o(u) - \ell_m^{\text{obs}} \right)^2 \leq \epsilon, \right\}, \tag{2.2.15}$$

where $\epsilon > 0$, and $\boldsymbol{\ell}^{\text{obs}} = (\ell_1^{\text{obs}}, \ldots, \ell_M^{\text{obs}})$ is the vector of experimental observations. We observe that the spaces $\mathcal{K}_N$ and $\mathcal{K}_{N,\xi}$ incorporate the two available pieces of information: the proximity of $u^{\text{true}}$ to the linear space $\mathcal{Z}_N$, and the experimental observations. In the former case, we impose that all elements of $\mathcal{K}_N$ interpolate data; in the latter case, we rely on the parameter $\xi$ to properly balance between proximity to $\mathcal{Z}_N$ and agreement with the experimental observations.

Given the closed set $\mathcal{K}_\cdot \subset \mathcal{U}$, the problem of optimal recovery corresponds to identify the field $u^\star \in \mathcal{U}$ that minimizes the error $\|u^\star - u^{\text{true}}\|$ in the worst-case scenario, provided that $u^{\text{true}} \in \mathcal{K}_\cdot$. More formally, we can introduce the optimal recovery algorithms associated with (2.2.14) and (2.2.15).

**Definition 2.2.1.** *A recovery algorithm is any measurable mapping $A : \mathbb{R}^M \to \mathcal{U}$. The*

optimal recovery algorithm $A_N^{\text{opt}}$ *associated with* $\mathcal{K}_N(\epsilon, \cdot)$ *satisfies*

$$A^{\text{opt}}(\boldsymbol{\ell}^{\text{obs}}) = \arg \inf_{\xi \in \mathcal{U}} \sup_{u \in \mathcal{K}_N(\epsilon, \boldsymbol{\ell}^{\text{obs}})} \|u - \xi\|, \tag{2.2.16}$$

*for any* $\boldsymbol{\ell}^{\text{obs}} \in \mathbb{R}^M$ *for which* $\mathcal{K}_{N,\delta}$ *is not empty. Similarly, we can define the optimal recovery* $A_{N,\xi}^{\text{opt}}$ *associated with* $\mathcal{K}_{N,\xi}$.

Next Proposition shows that the PBDW formulation is the optimal recovery algorithm.

**Proposition 2.2.3.** *Suppose that* $\beta_{N,M} > 0$. *Then, the PBDW algorithm* $A^{\text{PBDW}} : \mathbb{R}^M \to \mathcal{U}$ (2.2.4) *is the optimal recovery algorithm associated to* $\mathcal{K}_N(\epsilon, \cdot)$ *for any* $\epsilon > 0$. *Similarly, the regularized PBDW algorithm* $A_\xi^{\text{PBDW}} : \mathbb{R}^M \to \mathcal{U}$ (2.2.7) *is optimal for* $\mathcal{K}_{N,\xi}(\epsilon, \cdot)$ *for any* $\epsilon > 0$.

*Proof.* The optimality of (2.2.4) is proved in [33, Theorem 2.8]. On the other hand, we observe that[4]:

$$2\xi(\Pi_{\mathcal{Z}_N^\perp} u_\xi^\star,\, v) + \frac{2}{M} \sum_{m=1}^{M} \left(\ell_m^o(u_\xi^\star) - \ell_m^{\text{obs}}\right) \ell_m^o(v) = 0 \quad \forall\, v \in \mathcal{U}.$$

Thus, we find

$$J_\xi^{(1)}(u_\xi^\star + v) = J_\xi^{(1)}(u_\xi^\star) + \xi \|\Pi_{\mathcal{Z}_N^\perp} v\|^2 + \frac{1}{M} \sum_{m=1}^{M} (\ell_m^o(v))^2.$$

This implies that $u_\xi^\star + v \in \mathcal{K}_{N,\xi}(\epsilon, \boldsymbol{\ell}^{\text{obs}})$ if and only if $u_\xi^\star - v \in \mathcal{K}_{N,\xi}(\epsilon, \boldsymbol{\ell}^{\text{obs}})$. Then, optimality of (2.2.7) is a direct consequence of Remarks 2.2 and 2.3 in [33]. We omit the details. □

## 2.3 Algebraic formulation

In this section, we present the PBDW algebraic formulation, and we study the stability properties of the linear system. Then, as anticipated in section 2.2.1, we present a well-posedness result that does not rely on the assumption that $\mathcal{Z}_N \subset \mathcal{U}$.

[4] If $v \in \mathcal{U}_M$, this follows from (2.2.8); if $v \in \mathcal{U}_M^\perp$, this follows by observing that $\ell_m^o(v) = (q_m, v) = 0$ for $m = 1, \ldots, M$, and $(\Pi_{\mathcal{Z}_N^\perp} u_\xi^\star, v) = (\eta_\xi^\star, v) = 0$.

### 2.3.1 PBDW algebraic statement

In view of the algebraic formulation, we first introduce the matrices $\mathbb{K} \in \mathbb{R}^{M,M}$, $\mathbb{Z} \in \mathbb{R}^{N,N}$, $\mathbb{L} \in \mathbb{R}^{M,N}$ such that

$$\mathbb{K}_{m,m'} = (q_m, q_{m'}), \quad \mathbb{Z}_{n,n'} = (\zeta_n, \zeta_{n'}), \quad \mathbb{L}_{m,n} = \ell_m^o(\zeta_n), \tag{2.3.1}$$

for $m, m' = 1, \ldots, M$, and $n, n' = 1, \ldots, N$. Next Propositions show the algebraic counterparts of the PBDW statements (2.1.5) and (2.1.6). We note that the state estimation procedure does not require the calculation of the matrix $\mathbb{Z}$.

**Proposition 2.3.1.** *Let $\beta_{N,M} > 0$, and let $\xi > 0$. Then, the solution to* (2.1.5) $u_\xi^\star = z_\xi^\star + \eta_\xi^\star$ *is given by*

$$u_\xi^\star(\cdot) = \sum_{n=1}^{N} z_{\xi,n}^\star \zeta_n(\cdot) + \sum_{m=1}^{M} \eta_{\xi,m}^\star q_m(\cdot), \tag{2.3.2a}$$

*where the pair $(\boldsymbol{z}_\xi^\star, \boldsymbol{\eta}_\xi^\star) \in \mathbb{R}^N \times \mathbb{R}^M$ solves*

$$\begin{bmatrix} \xi M \mathbb{I} + \mathbb{K} & \mathbb{L} \\ \mathbb{L}^T & 0 \end{bmatrix} \begin{bmatrix} \boldsymbol{\eta}_\xi^\star \\ \boldsymbol{z}_\xi^\star \end{bmatrix} = \begin{bmatrix} \boldsymbol{\ell}_M^{\text{obs}} \\ \mathbf{0} \end{bmatrix}, \quad \boldsymbol{\ell}_M^{\text{obs}} = \begin{bmatrix} \ell_1^{\text{obs}} \\ \vdots \\ \ell_M^{\text{obs}} \end{bmatrix} \tag{2.3.2b}$$

*Equation* (2.3.2) *can be extended to $\xi = 0$ with the convention $u^\star = u_{\xi=0}^\star$.*

*Proof.* We first consider the case $\xi > 0$. Recalling Proposition 2.2.2 (Statement (i)), we have that $u_\xi^\star$ is of the form (2.3.2a). Then, substituting (2.3.2a) in (2.2.8) and choosing $q = q_m$, $p = \zeta_n$, we find

$$\begin{bmatrix} 2\xi\mathbb{K} + \frac{2}{M}\mathbb{K}^2 & \frac{2}{M}\mathbb{K}\mathbb{L} \\ \mathbb{L}^T & 0 \end{bmatrix} \begin{bmatrix} \boldsymbol{\eta}_\xi^\star \\ \boldsymbol{z}_\xi^\star \end{bmatrix} = \begin{bmatrix} \frac{2}{M}\mathbb{K}\boldsymbol{\ell}_M^{\text{obs}} \\ \mathbf{0} \end{bmatrix}.$$

Since $\mathbb{K}$ is invertible, thesis follows by multiplying the first equation by $\frac{M}{2}\mathbb{K}^{-1}$.

We now consider the case $\xi = 0$. Thesis follows by combining Proposition 2.2.1 (Statement (i)), and (2.2.5). We omit the details. □

We now wish to investigate the spectral properties of the linear system (2.3.2b). With this in mind, we first present a standard result (see, e.g., [141, Lemma 3.3]).

**Lemma 2.3.1.** *The inf-sup constant $\beta_{N,M}$ is the square root of the minimum eigenvalue of the following eigenproblem:*

$$\mathbb{L}^T \mathbb{K}^{-1} \mathbb{L} \, \mathbf{z}_n = \nu_n \, \mathbb{Z} \, \mathbf{z}_n, \qquad n = 1, \ldots, N. \tag{2.3.3}$$

*Proof.* Since $\sup_{\eta \in \mathcal{U}_M} \frac{(\eta, z)}{\|\eta\|} = \|\Pi_{\mathcal{U}_M} z\|$, we obtain:

$$\beta_{N,M}^2 = \inf_{z \in \mathcal{Z}_N} \sup_{\eta \in \mathcal{U}_M} \left( \frac{(\eta, z)}{\|\eta\| \|z\|} \right)^2 = \inf_{z \in \mathcal{Z}_N} \frac{\|\Pi_{\mathcal{U}_M} z\|^2}{\|z\|^2}.$$

We observe that for any $z \in \mathcal{Z}_N$ the projection onto $\mathcal{U}_M$ can be written as $\Pi_{\mathcal{U}_M} z = \sum_{m=1}^{M} \eta_m^z \, q_m$, where the vector $\boldsymbol{\eta}^z$ satisfies $\boldsymbol{\eta}^z = \mathbb{K}^{-1} \mathbb{L} \, \mathbf{z}$. Therefore, we find

$$\beta_{N,M}^2 = \inf_{\mathbf{z} \in \mathbb{R}^N} \frac{\mathbf{z}^T \mathbb{L}^T \mathbb{K}^{-1} \mathbb{L} \, \mathbf{z}}{\mathbf{z}^T \mathbb{Z} \mathbf{z}}.$$

Introducing the Lagrangian multiplier $\nu \in \mathbb{R}$, we can write the optimality conditions as

$$\begin{cases} \mathbb{L}^T \mathbb{K}^{-1} \mathbb{L} \, \mathbf{z} - \nu \mathbb{Z} \mathbf{z} & = \mathbf{0}; \\ \mathbf{z}^T \mathbb{Z} \mathbf{z} & = 1. \end{cases}$$

Thesis follows. □

Next Proposition provides a bound for the minimum eigenvalue of the saddle point system (2.3.2b).

**Proposition 2.3.2.** *Suppose that $\beta_{N,M} > 0$, and let $\zeta_1, \ldots, \zeta_N$ be an orthonormal basis of $\mathcal{Z}_N$. Let $\lambda_\xi^{\min}$ be the minimum (in absolute value) eigenvalue of the saddle point system* (2.3.2b). *Then, the following bound holds:*

$$|\lambda_\xi^{\min}| \geq \min \left( \lambda_{\min}(\mathbb{K}) + \xi M, \;\; \beta_{N,M}^2 - \xi M \frac{\lambda_{\max}(\mathbb{L}^T \mathbb{L})}{\lambda_{\min}(\mathbb{K})(\xi M + \lambda_{\min}(\mathbb{K}))} \right), \tag{2.3.4}$$

*and the bound holds with equality for $\xi = 0$.*

*Proof.* Following the argument in [27, Section 3.4], we observe that the saddle-point system (2.3.2b) is congruent to the block-diagonal matrix $\begin{bmatrix} \mathbb{K} + \xi M \mathbb{I} & 0 \\ 0 & -\mathbb{L}^T (\mathbb{K} + \xi M \mathbb{I})^{-1} \mathbb{L} \end{bmatrix}$.

Therefore, we find:

$$|\lambda_\xi^{\min}| = \min\left(\lambda_{\min}(\mathbb{K}) + \xi M,\ \lambda_{\min}\left(\mathbb{L}^T(\mathbb{K}+\xi M\mathbb{I})^{-1}\mathbb{L}\right)\right).$$

We now estimate $\lambda_{\min}\left(\mathbb{L}^T(\mathbb{K}+\xi M\mathbb{I})^{-1}\mathbb{L}\right)$. Towards this end, we first observe that

$$(\mathbb{K}+\xi M\mathbb{I})^{-1} = \mathbb{K}^{-1} - \xi M\mathbb{X}_\xi, \quad \mathbb{X}_\xi = (\mathbb{K}+\xi M\mathbb{I})^{-1}\,\mathbb{K}^{-1}.$$

Therefore, recalling standard linear algebra results and Lemma 2.3.1, we find

$$\begin{aligned}
\lambda_{\min}\left(\mathbb{L}^T(\mathbb{K}+\xi M\mathbb{I})^{-1}\mathbb{L}\right) &= \min_{\mathbf{v}} \frac{\mathbf{v}^T\mathbb{L}^T(\mathbb{K}+\xi M\mathbb{I})^{-1}\mathbb{L}\mathbf{v}}{\|\mathbf{v}\|_2^2} \\
&\geq \min_{\mathbf{v}} \frac{\mathbf{v}^T\mathbb{L}^T\mathbb{K}^{-1}\mathbb{L}\mathbf{v}}{\|\mathbf{v}\|_2^2} - \xi M \max_{\mathbf{v}} \frac{\mathbf{v}^T\mathbb{L}^T\mathbb{X}_\xi\mathbb{L}\mathbf{v}}{\|\mathbf{v}\|_2^2} \\
&\geq \beta_{N,M}^2 - \xi M\lambda_{\max}(\mathbb{X}_\xi)\lambda_{\max}(\mathbb{L}^T\mathbb{L}).
\end{aligned}$$

Thesis follows by observing that

$$\lambda_{\max}(\mathbb{X}_\xi) = \max_{\mathbf{v}} \frac{\mathbf{v}^T(\mathbb{K}+\xi M\mathbb{I})^{-1}\,\mathbb{K}^{-1}\mathbf{v}}{\|\mathbf{v}\|_2^2} \leq (\lambda_{\min}(\mathbb{K})+\xi M)^{-1}\ \frac{1}{\lambda_{\min}(\mathbb{K})}.$$

□

### 2.3.2 An improved well-posedness result

Proposition 2.3.3 shows a well-posedness result that does not rely on the assumption $\mathcal{Z}_N \subset \mathcal{U}$.

**Proposition 2.3.3.** *Let $\mathcal{X} = \mathcal{X}(\Omega)$ be a Hilbert space $\Omega$ such that $\mathcal{Z}_N \subset \mathcal{X}$, and $\ell_1^o, \ldots, \ell_M^o \in \mathcal{X}'$. Then, the solution $(z_\xi^\star, \eta_\xi^\star) \in \mathcal{Z}_N \times \mathcal{U}$ to (2.1.5) exists and is unique if and only if the matrix $\mathbb{L}$ has rank $N$. Furthermore, the state estimate $u_\xi^\star = z_\xi^\star + \eta_\xi^\star$ satisfies the representation formula (2.3.2). The same result holds for $\xi = 0$.*

*Proof.* We only prove the case $\xi > 0$ since the case $\xi = 0$ can be studied using the same argument. We observe that $J_\xi(z,\eta) = J_\xi(z, \Pi_{\mathcal{U}_M}\eta) + \xi\|\Pi_{\mathcal{U}_M^\perp}\eta\|^2$. Therefore, any solution $\eta_\xi^\star$ to (2.1.5) belongs to $\mathcal{U}_M$. This implies that any solution to (2.1.5) is of the form (2.3.2a).

Substituting (2.3.2a) in the minimization statement, we find

$$\min_{(\mathbf{z}^\star,\boldsymbol{\eta}^\star)\in\mathbb{R}^N\times\mathbb{R}^M} \xi\,\boldsymbol{\eta}^T\,\mathbb{K}\,\boldsymbol{\eta} + \frac{1}{M}\,\|\mathbb{K}\boldsymbol{\eta} + \mathbb{L}\boldsymbol{z} - \boldsymbol{\ell}_M^{\text{obs}}\|_2^2.$$

By deriving the stationary conditions, we find

$$\begin{cases} \left(\xi\mathbb{K} + \frac{1}{M}\mathbb{K}^2\right)\,\boldsymbol{\eta}^\star \,+\, \frac{1}{M}\mathbb{K}\mathbb{L}\mathbf{z}^\star & = \frac{1}{M}\mathbb{K}\mathbf{y} \\ \mathbb{L}^T\,\mathbb{K}\,\boldsymbol{\eta}^\star + \mathbb{L}^T\mathbb{L}\mathbf{z}^\star & = \mathbb{L}^T\mathbf{y} \end{cases} \tag{2.3.5}$$

By premultiplying $(2.3.5)_1$ by $M\mathbb{K}^{-1}$, we find

$$(\xi M\mathbb{I} + \mathbb{K})\,\boldsymbol{\eta}^\star + \mathbb{L}\mathbf{z}^\star = \mathbf{y}. \tag{2.3.6a}$$

If we now premultiply the latter equation by $\mathbb{L}^T$ and we subtract $(2.3.5)_2$, we obtain

$$\mathbb{L}^T\boldsymbol{\eta} = \mathbf{0}. \tag{2.3.6b}$$

Saddle system (2.3.6a) - (2.3.6b) is well-posed since $\mathbb{K}$ is invertible and $\mathbb{L}$ is full-rank by hypothesis. Thesis follows. □

We observe that if $\mathcal{Z}_N \subset \mathcal{U}$, the condition $\text{rank}(\mathbb{L}) = N$ is equivalent to $\beta_{N,M} > 0$ (cf. Lemma 2.3.1). Therefore, Proposition 2.3.3 is equivalent to Propositions 2.2.2 and 2.2.1 if $\mathcal{Z}_N \subset \mathcal{U}$. We further observe that the proof of Proposition 2.3.3 is closely related to the proof of [127, Theorem 5.1].

## 2.4 Computational procedure: offline-online computational decomposition

The algebraic formulation derived in section 2.3 allows us to decouple the computational procedure into two distinct stages. During the offline stage, which is performed before acquiring the experimental observations, we generate the approximation spaces $\mathcal{Z}_N$ and $\mathcal{U}_M$, and we assemble the linear saddle point system (2.3.2b). During the online stage, which is performed during the operations and possibly *in situ*, we acquire the experimental data $\ell_1^{\text{obs}}, \ldots, \ell_M^{\text{obs}}$, we select the regularizer weight $\xi$, and we compute the state estimate

by solving (2.3.2b). We observe that the offline stage is computationally extensive since we need to solve the bk model possibly several times. On the other hand, the online stage requires $\mathcal{O}(N+M)^3$ operations.

Algorithm 2.4.1 presents the computational procedure. In Chapter 3, for noise-free measurements, we present a Greedy procedure to select sensor locations (Step 3-Offline stage). We further remark that in our setting the update space $\mathcal{U}_M$ is induced by the norm $\|\cdot\|$ and the observation functionals: in Chapter 6, for the special case of pointwise measurements, we partially reverse this scheme. Finally, we have not yet discussed how to practically choose the hyper-parameter $\xi$: we address this question in Chapter 6.

**Algorithm 2.4.1** PBDW approach. Offline-online computational procedure

**Offline stage**

1: Choose the space $(\mathcal{U}, \|\cdot\|)$

2: Generate the background $\mathcal{Z}_N \subset \mathcal{U}$

3: (If possible) Select the observation functionals $\ell_1^o, \ldots, \ell_M^o \in \mathcal{U}'$

4: Compute $\mathcal{U}_M = \text{span}\{R_{\mathcal{U}}\ell_m^o\}_{m=1}^M$

5: Assemble the matrix in (2.3.2b)

**Onine stage**

1: Acquire the measurements $\ell_1^{\text{obs}}, \ldots, \ell_M^{\text{obs}}$

2: Choose the regularizer weight $\xi$

3: Solve the linear system (2.3.2b)

4: (If needed) Evaluate the state using (2.3.2a).

## 2.5 Connection with other formulations

### 2.5.1 Connection with other data assimilation procedures

In the statistical learning literature, PBDW is closely related to the approach presented in [127] by Kimeldorf and Wahba. In more detail, the two approaches are equivalent if we choose $\mathcal{Z}_N$ as the set of all polynomials of degree less or equal to $\kappa$, $\kappa > d/2 - 1$, and $\mathcal{U} = H^{\kappa+1}(\Omega)$ endowed with a proper inner product. We further observe that, by exploiting the connection with [127], we can re-interpret our formulation in a Bayesian setting as a

Gaussian linear system with improper prior (see [225]). In this work, we do not pursue this feature of the approach.

Furthermore, for $N = M$ PBDW formulation is equivalent to the solution to the Generalized Empirical Interpolation Method (GEIM, [140]), while for $\xi \to \infty$ and $\mathcal{Z}_N$ built using a Proper Orthogonal Decomposition (POD, [130]), PBDW is asymptotically equivalent to Gappy-POD ([75, 234]). We shall also observe that the use of the background space — as opposed to a background singleton element in the original 3D-VAR — is also found in nearfield acoustical holography (NAH, [47, 235]). We finally mention that the general PBDW formulation (2.1.5) is asymptotically equivalent to the "noise-free" formulation in the limit $\xi \to 0^+$: as stated in section 2.1.1, the latter corresponds to the original formulation presented in [142]. Next Proposition shows the two asymptotic results.

**Proposition 2.5.1.** *Let $\beta_{N,M} > 0$. Let $u_\xi^\star = \eta_\xi^\star + z_\xi^\star$ be the solution to* (2.1.5)*. Then, we have*

$$\lim_{\xi \to 0^+} \|u^\star - u_\xi^\star\| = 0, \quad \lim_{\xi \to \infty} \|u_\xi^\star - z_{\text{LS}}\| = 0, \tag{2.5.1}$$

*where $u^\star = z^\star + \eta^\star$ is the solution to* (2.1.6)*, and $z_{\text{LS}} = \arg\min_{z \in \mathcal{Z}_N} \sum_{m=1}^M (\ell_m^o(z) - \ell_m^{\text{obs}})^2$.*

*Proof.* Let us first consider the limit $\xi \to 0^+$. We just have to show that

$$\lim_{\xi \to 0^+} \left( \boldsymbol{u}_\xi^\star = \begin{bmatrix} \boldsymbol{\eta}_\xi^\star \\ \boldsymbol{z}_\xi^\star \end{bmatrix} \right) = \boldsymbol{u}_{\xi=0}^\star = \begin{bmatrix} \boldsymbol{\eta}_{\xi=0}^\star \\ \boldsymbol{z}_{\xi=0}^\star \end{bmatrix}$$

Exploiting Proposition 2.3.2, we can show that each eigenvalue of the saddle-point system (2.3.2b) satisfies $|\lambda_{\xi,j}| \geq \frac{1}{2} \min(\lambda_{\min}(\mathbb{K}), \beta_{N,M}^2) > 0$ for all $\xi \leq \bar{\xi}$, for some $\bar{\xi} > 0$. Therefore, we find $\|\boldsymbol{u}_\xi^\star\|_2 \leq C$ for all $\xi \leq \bar{\xi}$.

Let $\{\xi_j\}_j$ be a positive sequence such that $\xi_j \to 0^+$, and let $\boldsymbol{u}_{\xi_j}^\star$ be the solution to (2.3.2b) for $\xi = \xi_j$. Since $\{\boldsymbol{u}_{\xi_j}^\star\}_j$ is uniformly bounded, applying Bolzano-Weierstrass theorem, we obtain that, up to a subsequence, $\boldsymbol{u}_{\xi_\ell}^\star \to \widehat{\boldsymbol{u}}$. We further observe that

$$\begin{bmatrix} \boldsymbol{\ell}_M^{\text{obs}} \\ \mathbf{0} \end{bmatrix} = \begin{bmatrix} \mathbb{K} & \mathbb{L} \\ \mathbb{L}^T & 0 \end{bmatrix} \boldsymbol{u}_{\xi_\ell}^\star + \xi_\ell M \begin{bmatrix} \mathbb{I} & 0 \\ 0 & 0 \end{bmatrix} \underbrace{\boldsymbol{u}_{\xi_\ell}^\star}_{\ell \to \infty} \begin{bmatrix} \mathbb{K} & \mathbb{L} \\ \mathbb{L}^T & 0 \end{bmatrix} \widehat{\boldsymbol{u}}.$$

Since the linear system (2.3.2b) for $\xi = 0$ admits a unique solution, we must have $\widehat{\boldsymbol{u}} = \boldsymbol{u}_{\xi=0}^\star$.

Using the same reasoning, we find that $\boldsymbol{u}^\star_{\xi=0}$ is the only limit point of the uniformly bounded sequence $\{\boldsymbol{u}^\star_{\xi_j}\}_j$. Therefore, the entire sequence is convergent (see, e.g., [148, page 67]).

We now consider the case $\xi \to \infty$. As for the previous case, we must prove that for $\xi \to \infty$

$$\mathbf{z}^\star_\xi \to \mathbf{z}_{\rm LS} = (\mathbb{L}^T\mathbb{L})^{-1}\,\mathbb{L}^T\,\boldsymbol{\ell}^{\rm obs}_M, \quad \boldsymbol{\eta}^\star_\xi \to \mathbf{0}.$$

The proof exploits the same argument of the previous case, $\xi \to 0^+$. We omit the details. □

### 2.5.2 A two-stage regression procedure: connection with Kalman filter

We can rewrite the linear system (2.3.2b) as follows:

$$\begin{cases} \mathbb{L}^T(\xi M\mathbb{I} + \mathbb{K})^{-1}\mathbb{L}\,\mathbf{z}^\star_\xi = \mathbb{L}^T(\xi M\mathbb{I} + \mathbb{K})^{-1}\boldsymbol{\ell}^{\rm obs}_M \\ (\xi M\mathbb{I} + \mathbb{K})\boldsymbol{\eta}^\star_\xi = \boldsymbol{\ell}^{\rm obs}_M - \mathbb{L}\mathbf{z}^\star_\xi. \end{cases} \tag{2.5.2}$$

Formulation (2.5.2) is the algebraic counterpart of the following two-stage procedure:

$$\begin{cases} z^\star_\xi := \arg\min_{z\in\mathcal{Z}_N} \|\mathcal{L}_M(z) - \boldsymbol{\ell}^{\rm obs}_M\|_{\mathbb{W}_\xi}; \\ \eta^\star_\xi := \arg\min_{\eta\in\mathcal{U}} \xi\|\eta\|^2 + \dfrac{1}{M}\displaystyle\sum_{m=1}^{M}(\ell^o_m(\eta) - \ell^{\rm err}_m)^2, \quad \ell^{\rm err}_m := \ell^{\rm obs}_m - \ell^o_m(z^\star_\xi), \end{cases} \tag{2.5.3}$$

where $\mathbb{W}_\xi = (\mathbb{K} + \xi M\mathbb{I})^{-1}$, $\mathcal{L}_M(z) = [\ell^o_1(z), \ldots, \ell^o_M(z)]$, and $\|\mathbf{d}\|_{\mathbb{W}} = \sqrt{\mathbf{d}^T\mathbb{W}\mathbf{d}}$. Problem $(2.5.3)_1$ corresponds to a weighted least-square (generalized) regression problem, while $(2.5.3)_2$ corresponds to a generalized smoothing problem applied to the error field $u^{\rm true} - z^\star_\xi$.

Equation (2.5.3) clarifies the connection of our approach with Kalman filtering techniques ([123, 134]). The deduced-background estimate $z^\star_\xi \in \mathcal{Z}_N$ represents our *predicted state estimate* based on prior knowledge (here encoded in the background space); on the other hand, the update $\eta^\star_\xi \in \mathcal{U}_M$ represents the *innovation* induced by the measurements and only depends on the residuals $\ell^{\rm err}_m = \ell^{\rm obs}_m - \ell^o_m(z^\star_\xi)$.

We further observe that — from the perspective of approximation theory — PBDW formulation introduces a hierarchy between the approximation provided by the background space $\mathcal{Z}_N$, and the approximation provided by $\mathcal{U}_M$. In more detail, the background space $\mathcal{Z}_N$ should provide primary approximation, while the update space $\mathcal{U}_M$ is designed to complete any deficiency in $\mathcal{Z}_N$. This asymmetry between $\mathcal{Z}_N$ and $\mathcal{U}_M$ is motivated by the underlying

assumption that elements of $\mathcal{Z}_N$ have better *generalization properties* (see, e.g., [221]) than elements in $\mathcal{U}_M$ since they are directly informed by the mathematical model. In this respect, by adapting the parameter $\xi$, we can properly tune the relative importance of primary and secondary approximation.

## 2.6 Conclusions and objective of the next chapters

In this chapter, we presented the PBDW formulation of the variational data assimilation (state estimation) problem for systems modeled by PDEs. Below, we list the main features of the methodology.

**Projection-by-data:** PBDW is an approximation method that seeks solutions based on projection-by-data. In more detail, the bk model does not enter explicitly in the PBDW variational formulation since it is only employed to generate the background space $\mathcal{Z}_N$. This feature of the approach greatly simplifies the implementation of the computational procedure, and ultimately speeds up computations. Projection-by-data — a problem in approximation theory — rather than projection-by-model — a problem in PDE discretization — has also many advantages with respect to the mathematical theory. First, projection-by-data eliminates many of the standard requirements of projection-by-model related to initial and boundary conditions; for example, the domain $\Omega$ over which we reconstruct the state can be a subset of the bk domain $\Omega^{\text{bk}}$ over which the mathematical model is well-posed. Second, in projection-by-data, we can accomodate norms which may be considerably stronger than the norms required for well-posedness in projection-by-model. We extensively exploit these features of the formulation in Chapters 5 and 6.

**Variational formulation:** we remark that PBDW relies on a variational formulation. The variational formulation facilitates the construction of *a priori* error estimates informed by the analysis developed for PDEs and scattered data approximation. In Chapter 3, we present theoretical *a priori* bounds for the state estimation error in absence of noise. Then, in Chapter 6, we provide an error analysis for pointwise noisy measurements.

**Background space:** PBDW formulation incorporates background spaces that accommodate anticipated parametric uncertainty. The background space is constructed in two steps: (i) the identification of a parametrized PDE that models the phenomenon under con-

sideration and a suitable confidence region $\mathcal{P}^{\text{bk}}$ for the parameters of the model, and (ii) the application of a pMOR technique — such as the Weak-Greedy algorithm briefy summarised in Algorithm 2.1.1 — to generate a linear space appropriate for real-time evaluations.

**Correction of unmodeled physics:** as explained in section 2.5, PBDW provides a mechanism — the update $\eta_\xi^\star$ — to address the inevitable deficiencies of the bk model.

The PBDW formulation (2.1.6) was first presented and analysed in [142, 143] for perfect measurements ($\ell_m^{\text{obs}} = \ell_m^o(u^{\text{true}})$). In [142], for localised measurements, the authors proposed a Greedy strategy for the selection of sensor locations. In [143], the authors extended the analysis to imperfect measurements.

The original PBDW approach shows a number of deficiencies. First, in [142, 143], the authors did not propose an actionable strategy to quantify the uncertainty in the state estimate — apart from the heuristic error indicator in [143, section 5.7]. Second, the authors employed a traditional pMOR technique — the weak-Greedy algorithm reviewed in section 2.1.2 — to the manifold $\widehat{\mathcal{M}}^{\text{bk}}$ defined over $\Omega^{\text{bk}}$: as explained in section 2.1.2, if $\Omega$ is strictly contained in $\Omega^{\text{bk}}$, this strategy might either be unfeasible or might lead to inaccurate approximation spaces for the restricted manifold $\mathcal{M}^{\text{bk}}$. Third, due to the absence of tunable parameters, the original formulation did not provide tools to rationally balance inadequacies in the bk model and noise in the measurements. In particular, there was no attempt to incorporate the presence of noise in the actual state estimate. In addition, due to the choice $\mathcal{U} = H^1(\Omega)$, for localised measurements, the approximation properties of the update are poor, and it is not possible to efficiently adapt the shape of the Riesz representers during the online stage: this might lead to poor convergence in $M$.

Motivated by the previous discussion, in this thesis, we first review the PBDW formulation for perfect measurements presented in [142], and then we propose three contributions to the original formulation.

In **Chapter 3**, we present the PBDW formulation for perfect measurements. We review and slightly improve the error analysis presented in [142], and we present the Greedy strategy for the selection of sensor locations. We also contribute an analysis of a thermal experiment not previously considered.

In **Chapter 4**, we propose an experimental *a posteriori* estimation procedure for the

$L^2(\Omega)$ state-estimation error $\|u^{\text{true}} - u^\star\|_{L^2(\Omega)}$, and for the error in output $\mathcal{L}(u^{\text{true}}) - \mathcal{L}(u^\star)$, where $\mathcal{L} : L^2(\Omega) \to \mathbb{R}$. The procedure allows us to quantify the uncertainty in the state estimate. In addition, it can also be employed (i) to guide the data-driven enrichment of the PBDW background space $\mathcal{Z}_N$ (based on the algorithm first proposed in [143, section 5.8]), (ii) to improve the estimate of the $L^2$ output of interest, and (iii) to adaptively select the PBDW tunable parameters. The error estimation procedure has been presented in [213].

In **Chapter 5**, we present a computational procedure for the construction of the background space $\mathcal{Z}_N$ when $\Omega \subset \Omega^{\text{bk}}$. Our approach represents an extension of a computational strategy first studied theoretically in the context of approximation theory ([172]), and then applied in the context of generalized finite element method ([8]) and more recently in Port-Reduced static condensation Reduced Basis Element method ([204]).

In **Chapter 6**, we study the case of pointwise noisy measurements ($\ell_m^{\text{obs}} = u^{\text{true}}(x_m^{\text{obs}}) + \epsilon_m$). We rely on the theory of RKHS, which allows us to consider spaces $\mathcal{U}$ for which the Riesz representers $\{K_{x_m}\}_m$ associated with the observation functionals $\{\delta_{x_m}\}_m$ are explicitly known. We demonstrate that explicit expressions for the representers greatly improve the flexibility of the approach; in addition, we find much faster convergence with respect to the number of measurements $M$ than in the approach presented in [142, 143]. We present a rigorous *a priori* error analysis for the $L^2(\Omega)$ state-estimation error, $\|u^{\text{true}} - u^\star\|_{L^2(\Omega)}$, for (i) homoscedastic random noise (i.e., $\epsilon_m \overset{iid}{\sim} (0, \sigma^2)$), and (ii) systematic noise (i.e., $|\epsilon_m| \leq \delta$). We further discuss an adaptive procedure for the selection of the hyper-parameters of the PBDW formulation. The adaptive procedure and the error analysis have been presented in [212].

# Chapter 3

# The PBDW approach for perfect observations

We discuss the PBDW formulation for perfect measurements (2.1.6): given the $N$-dimensional background space $\mathcal{Z}_N \subset \mathcal{U}$, find $(z^\star, \eta^\star) \in \mathcal{Z}_N \times \mathcal{U}$ such that

$$(z^\star, \eta^\star) = \arg \min_{(z,\eta)\in\mathcal{Z}_N\times\mathcal{U}} \|\eta\| \quad \text{subject to} \quad \ell_m^o(z+\eta) = \ell_m^{\text{obs}}, \quad m = 1, \dots, M;$$

where $(\mathcal{U}, \|\cdot\|)$ is a Hilbert space over the domain of interest $\Omega$ and $\ell_1^o, \dots, \ell_M^o \in \mathcal{U}'$. We state upfront that in this chapter we rely on localized observations; in more detail, we consider $\ell_m^o(v) = \int_\Omega \omega_{d,\nu}(|x_m^{\text{obs}} - y|)v(y)\,dy$, where $\{x_m^{\text{obs}}\}_{m=1}^M \subset \Omega$ denote the transducers' locations, and $\omega_{d,\nu} : \mathbb{R} \to \mathbb{R}_+$ denotes a properly-chosen convolutational kernel associated with the transducer. In Chapter 2, we discussed the well-posedness of problem (2.1.6), and we presented a finite-dimensional formulation for the PBDW state estimate $u^\star = z^\star + \eta^\star$, which permits rapid computations. In this chapter, we provide an *a priori* bound for the state estimation error $\|u^{\text{true}} - u^\star\|$ (section 3.1), and we discuss a Greedy procedure for the selection of sensor locations $\{x_m^{\text{obs}}\}_{m=1}^M$ (section 3.2). In section 3.3, we present results for a synthetic acoustic problem. Finally, in section 3.4, we present the results for a physical thermal patch configuration.

## 3.1 Error analysis

Next Proposition contains the key result.

**Proposition 3.1.1.** *([241]) Suppose that $\beta_{N,M} > 0$. Then, the PBDW state estimate $u^\star$ satisfies*

$$\|u^{\text{true}} - u^\star\| \leq \frac{1}{\beta_{N,M}} \inf_{\eta \in \mathcal{U}_M \cap \mathcal{Z}_N^\perp} \inf_{z \in \mathcal{Z}_N} \|u^{\text{true}} - z - \eta\|, \tag{3.1.1}$$

*or, equivalently,*

$$\|u^{\text{true}} - u^\star\| \leq \frac{1}{\beta_{N,M}} \|u^{\text{true}} - \Pi_{\mathcal{Z}_N \oplus (\mathcal{U}_M \cap \mathcal{Z}_N^\perp)} u^{\text{true}}\|. \tag{3.1.2}$$

*Furthermore, the following estimates hold for background and update:*

$$\|\Pi_{\mathcal{Z}_N} u^{\text{true}} - z^\star\| \leq \frac{1}{\beta_{N,M}} \inf_{\eta \in \mathcal{U}_M \cap \mathcal{Z}_N^\perp} \inf_{z \in \mathcal{Z}_N} \|u^{\text{true}} - z - \eta\|, \tag{3.1.3a}$$

*and*

$$\|\Pi_{\mathcal{Z}_N^\perp} u^{\text{true}} - \eta^\star\| = \inf_{\eta \in \mathcal{U}_M \cap \mathcal{Z}_N^\perp} \inf_{z \in \mathcal{Z}_N} \|u^{\text{true}} - z - \eta\|. \tag{3.1.3b}$$

*Proof.* We observe that the error $u^{\text{true}} - u^\star \in \mathcal{U}_M^\perp$. Therefore, recalling Lemma 2.2.1, we find

$$\beta_{N,M} \|u^{\text{true}} - u^\star\| \leq \left( \inf_{\xi \in \mathcal{U}_M^\perp} \frac{\|\Pi_{\mathcal{Z}_N^\perp} \xi\|}{\|\xi\|} \right) \|u^{\text{true}} - u^\star\| \underbrace{\leq}_{\xi = u^{\text{true}} - u^\star} \|\Pi_{\mathcal{Z}_N^\perp}(u^{\text{true}} - u^\star)\|. \tag{3.1.4a}$$

By restricting $(2.2.5)_1$ to $q \in \mathcal{U}_M \cap \mathcal{Z}_N^\perp$, we find

$$(\eta^\star - u^{\text{true}}, q) = 0 \ \ \forall q \in \mathcal{U}_M \cap \mathcal{Z}_N^\perp \Rightarrow \eta^\star = \Pi_{\mathcal{U}_M \cap \mathcal{Z}_N^\perp} u^{\text{true}}.$$

As a result, we obtain

$$\|\Pi_{\mathcal{Z}_N^\perp}(u^{\text{true}} - u^\star)\| = \|\Pi_{\mathcal{Z}_N^\perp}(u^{\text{true}} - \eta^\star - z^\star)\| = \|\Pi_{\mathcal{Z}_N^\perp}(u^{\text{true}} - \eta^\star)\| = \|\Pi_{\mathcal{Z}_N^\perp}(\Pi_{(\mathcal{U}_M \cap \mathcal{Z}_N^\perp)^\perp} u^{\text{true}})\|. \tag{3.1.4b}$$

Here, the first equality follows from $u^\star = \eta^\star + z^\star$, the second equality follows from $z^\star \in \mathcal{Z}_N$, the third equality follows from $\eta^\star = \Pi_{\mathcal{U}_M \cap \mathcal{Z}_N^\perp} u^{\text{true}}$ and from the projection theorem. We can

then rewrite the latter expression as

$$\begin{aligned}\|\Pi_{\mathcal{Z}_N^\perp}(\Pi_{(\mathcal{U}_M\cap\mathcal{Z}_N^\perp)^\perp}u^{\text{true}})\| &= \inf_{z\in\mathcal{Z}_N}\|\Pi_{(\mathcal{U}_M\cap\mathcal{Z}_N^\perp)^\perp}u^{\text{true}}-z\| = \inf_{z\in\mathcal{Z}_N}\|\Pi_{(\mathcal{U}_M\cap\mathcal{Z}_N^\perp)^\perp}(u^{\text{true}}-z)\| \\ &= \inf_{z\in\mathcal{Z}_N}\inf_{\eta\in\mathcal{Z}_N^\perp\cap\mathcal{U}_M}\|u^{\text{true}}-z-\eta\|. \end{aligned} \tag{3.1.4c}$$

Here, the second equality follows from the fact that, since $\mathcal{U}_M\cap\mathcal{Z}_N^\perp\subset\mathcal{Z}_N^\perp$, we have $\mathcal{Z}_N\subset(\mathcal{U}_M\cap\mathcal{Z}_N^\perp)^\perp$. As a result, $\Pi_{(\mathcal{U}_M\cap\mathcal{Z}_N^\perp)^\perp}z=z$.

Combining (3.1.4a), (3.1.4b) and (3.1.4c), we obtain (3.1.1). Finally, (3.1.2) follows by observing that, since $\mathcal{Z}_N$ and $\mathcal{Z}_N^\perp\cap\mathcal{U}_M$ are orthogonal subspaces, we have that

$$\inf_{z\in\mathcal{Z}_N}\inf_{\eta\in\mathcal{Z}_N^\perp\cap\mathcal{U}_M}\|u^{\text{true}}-z-\eta\| = \|u^{\text{true}}-\Pi_{\mathcal{Z}_N\oplus(\mathcal{U}_M\cap\mathcal{Z}_N^\perp)}u^{\text{true}}\|.$$

We now show (3.1.3a) and (3.1.3b). The former follows directly from (3.1.2), recalling that $\eta^\star\in\mathcal{Z}_N^\perp$ and that the projection operator is linear with continuity constant equal to one:

$$\|\Pi_{\mathcal{Z}_N}u^{\text{true}}-z^\star\| = \|\Pi_{\mathcal{Z}_N}(u^{\text{true}}-u^\star)\| \le \|u^{\text{true}}-u^\star\| \le \frac{1}{\beta_{N,M}}\inf_{\eta\in\mathcal{U}_M\cap\mathcal{Z}_N^\perp}\inf_{z\in\mathcal{Z}_N}\|u^{\text{true}}-z-\eta\|.$$

To show (3.1.3b), we observe that $\|\Pi_{\mathcal{Z}_N^\perp}u^{\text{true}}-\eta^\star\| = \|\Pi_{\mathcal{Z}_N^\perp}(u^{\text{true}}-u^\star)\|$, and then we combine (3.1.4b) and (3.1.4c). □

Estimate (3.1.1) identifies three distinct contributions to the error in the field estimate. The first contribution, $\frac{1}{\beta_{N,M}}$, takes into account the stability of the formulation. The second contribution is the background best-fit error $\inf_{z\in\mathcal{Z}_N}\|u^{\text{true}}-z\|$: as discussed in section 2.1.2, this depends on (i) the modeling error $\epsilon_N^{\text{bk}}=\min_{\mu\in\mathcal{P}^{\text{bk}}}\|u^{\text{true}}-u^{\text{bk}}(\mu)\|$, and (ii) on the discretization error $\epsilon_{\text{disc},N}^{\text{bk}}=\max_{\mu\in\mathcal{P}^{\text{bk}}}\|\Pi_{\mathcal{Z}_N}u^{\text{bk}}(\mu)-u^{\text{bk}}(\mu)\|$; while the former is associated to the accuracy of the best-knowledge model, the latter is associated to the compression process. The third contribution is the update best-fit error $\inf_{\eta\in\mathcal{U}_M\cap\mathcal{Z}_N^\perp}\|\Pi_{\mathcal{Z}_N^\perp}u^{\text{true}}-\eta\|$, which depends on the approximation properties of the update space.

Estimates (3.1.3) strengthen the interpretation of the background and update given in section 2.5.2. In particular, we observe that if $u^{\text{true}}\in\mathcal{Z}_N$, we obtain that $u^{\text{true}}=u^\star=z^\star$ and $\eta^\star\equiv 0$. This observation shows that the update contribution is noticeable only if the

true field is not well-represented by its projection onto the background space.

## 3.2 Construction of the update space

### 3.2.1 Theoretical considerations

Error estimate (3.1.1) shows that the update space $\mathcal{U}_M$ should be designed based on two criteria: (i) the maximization of the stability constant $\beta_{N,M}$ to improve stability, and (ii) the minimization of the approximation error $\inf_{\eta \in \mathcal{U}_M \cap \mathcal{Z}_N^\perp} \|\Pi_{\mathcal{Z}_N^\perp} u^{\text{true}} - \eta\|$ to improve approximation. We thus seek a strategy that addresses both these issues.

With this in mind, we observe that the update space $\mathcal{U}_M := \text{span}\{R_{\mathcal{U}} \ell_m^o\}_{m=1}^M$ depends (i) on the choice of the ambient space $\mathcal{U}$ and on its inner product $(\cdot, \cdot)$, and (ii) on sensor locations $\{x_m^{\text{obs}}\}_m$. Since the use of high-order Sobolev spaces requires the use of proper Finite Element discretizations, in this chapter we consider $H_0^1(\Omega) \subset \mathcal{U} \subset H^1(\Omega)$ endowed with the inner product

$$(w, v) = \int_\Omega \nabla w \cdot \nabla v + \gamma^2 w\, v \, dx, \tag{3.2.1}$$

for some $\gamma > 0$. Hence the choice of $(\mathcal{U}, \|\cdot\|)$ reduces to the choice of the parameter $\gamma$. We observe that $\gamma$ influences the spatial length-scale of the Riesz elements $\{R_{\mathcal{U}} \ell_m^o\}_{m=1}^M$ and should be properly tuned based on the number of measurements available and on the expected length-scale of the true field. Example 3.2.1 illustrates the influence of the choice of $\gamma$ on $R_{\mathcal{U}} \ell^o$ for pointwise measurements in one dimension.

**Example 3.2.1.** ***(Riesz element associated with different norms)*** *Let us consider* $\Omega = (-1, 1)$ *and the functional* $\ell^o = \delta_{x^{\text{obs}}}$ *where* $x^{\text{obs}} = 0$ *and* $\delta$ *is the Dirac delta. We consider* $\mathcal{U} = H_0^1(-1, 1)$ *endowed with the inner product*

$$(w, v) = \int_{-1}^{1} w'v' + \gamma^2 wv \, dx.$$

*By tedious but straightforward calculations, we find that the Riesz element associated with* $\ell^o$ *is as follows*

$$R_{\mathcal{U}} \delta_0(x) = \tfrac{1}{2}(1 - |x|), \qquad \gamma = 0;$$

$$R_{\mathcal{U}} \delta_0(x) = \tfrac{1}{2\gamma(e^{2\gamma}+1)} \left(e^{2\gamma - \gamma|x|} - e^{\gamma|x|}\right), \quad \gamma > 0$$

*Figure 3-1 shows the plot of the Riesz elements for three different values of $\gamma$. To simplify the comparison, we normalize the $L^\infty(\Omega)$ norm of each Riesz representer to one.*

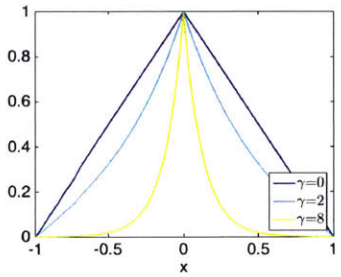


**Figure 3-1:** Example 3.2.1: plot of the Riesz elements $R_{\mathcal{U}}\delta_0$ for three different choices of $\gamma$. For visualization purposes, we normalize the $L^\infty(\Omega)$-norm of the Riesz elements to one.

### 3.2.2 Computational procedure

We set the value of the constant $\gamma$ in (3.2.1) *a priori*, and we choose the observation points $\{x_m^{\text{obs}}\}_{m=1}^M$ according to a Greedy strategy based on two stages. During the first (stability) stage, we maximize the constant $\beta_{N,M}$ in a Greedy manner. During the second (approximation) stage, we minimize the fill distance $h_{\mathcal{X}_M} := \sup_{x\in\Omega} \min_{m=1,\ldots,M} \|x - x_m^{\text{obs}}\|_2$ in a Greedy manner. Since the stability constant is a non-decreasing function of $M$ for a fixed $N$, the stability constant remains above the threshold in the second stage. We envision that the constant $\gamma$ should be selected based on the characteristic length-scale of the error field $u^{\text{true}} - z^\star$: however, it might be extremely difficult to estimate *a priori* this quantity. In the numerical section, we study the effect of the choice of $\gamma$ for a two-dimensional model problem.

Algorithm 3.2.1 summarises the computational procedure. Computational cost is dominated by the computation of the Riesz representations of the functionals $\ell_1^o, \ldots, \ell_M^o$. In the limit $M \gg N$ and assuming that $\Omega$ is discretized using a Finite Element mesh of size $\mathcal{N}$, the selection of the observation points during the approximation step has complexity $\mathcal{O}(\mathcal{N}M^2)$, while the cost of the actual construction of the update space — which involves the solution to $M$ linear systems — is roughly $\mathcal{O}(\mathcal{N}^s M)$, where $1 < s < 3$ is a suitable exponent, which depends on the sparsity pattern of the matrix associated with the inner product.

If $tol = 0$, all the observation centers are selected through the approximation loop. On the other hand, if $tol = 1$, all the centers are selected through the stability loop. A

representative value for *tol* used in our simulations is $tol = 0.2$. Computation of the least-stable mode $z_{\min,m}$ involves the solution to the dense eigenproblem (2.3.3).

**Algorithm 3.2.1** Greedy stability-approximation balancing (`SGreedy-plus`) algorithm

| | | |
|---|---|---|
| **Input** | $\mathcal{Z}_N$ | background space |
| | $M$ | number of sensors |
| | $tol > 0$ | threshold for the stability constant |
| **Output** | $\mathcal{U}_M$ | update space |

**Stability**

1: Compute $x_1^{\text{obs}} := \arg\max_{x\in\bar{\Omega}} |\zeta_1(x)|$, $m = 1$

2: **while** $m \leq M$ **do**

3: Compute $\beta_{N,m} = \min_{w\in\mathcal{Z}_N} \max_{v\in\mathcal{U}_m} \frac{(w,v)}{\|w\|\|v\|}$.

4: **if** $\beta_{N,m} \leq tol$ **then**

5: Compute $z_{\min,m} := \arg\min_{z\in\mathcal{Z}_N} \max_{v\in\mathcal{U}_m} \frac{(w,v)}{\|w\|\|v\|}$.

6: Compute $x_{m+1}^{\text{obs}} := \arg\max_{x\in\bar{\Omega}} |z_{\min,m}(x) - \Pi_{\mathcal{U}_m} z_{\min,m}(x)|$.

7: Set $\mathcal{U}_{m+1} = \mathcal{U}_m \cup \text{span}\{R_{\mathcal{U}}\ell(\cdot, x_{m+1}^{\text{obs}})\}$, $m = m + 1$.

8: **else**

9: `Break`

10: **end if**

11: **end while**

**Approximation**

1: **while** $m \leq M$ **do**

2: Compute $x_{m+1}^{\text{obs}} := \arg\max_{x\in\bar{\Omega}} \min_{m'=1,\ldots,m} \|x - x_{m'}^{\text{obs}}\|_2$.

3: Set $\mathcal{U}_{m+1} = \mathcal{U}_m \cup \text{span}\{R_{\mathcal{U}}\ell(\cdot, x_{m+1}^{\text{obs}})\}$.

4: $m = m + 1$.

5: **end while**

Since $\beta_{N,m} = 0$ for $m < M$, if $tol > 0$, at least the first $M$ points are selected within the first loop. As $\beta_{N,m} > tol$, the algorithm selects well-separated points in the attempt to reduce the approximation error. We further remark that in our implementation we control whether or not each point selected by the stability loop (Line 6) is well-separated from the

other observation centers: for $m \lesssim N$ the stability loop might select points that are too close to each other, especially for sufficiently large transducers' widths; this would ultimately lead to an ill-conditioned linear saddle-point system.

We observe that, for $N = M$, the point selection routine coincides with the routine proposed in [140] for the Generalized Empirical Interpolation Method (GEIM). We also observe that the stability stage is related to the E-optimality criteria considered in the design of experiments ([83]). On the other hand, the strategy for the approximation step is strongly related to the so-called *farthest-first traversal* approach to the minimax facility location problem (see, e.g, [167]), first proposed by Rosenkrantz et al. in [186].

We can interpret our procedure as a stabilization for the saddle-point system (2.3.2b). Assuming that $\zeta_1, \ldots, \zeta_N$ is an orthonormal basis of $\mathcal{Z}_N$, and recalling (cf. Proposition 2.3.2) that $|\lambda^{\min}| = \min\left(\lambda_{\min}(\mathbb{K}), \beta^2_{N,M}\right)$, we observe that the stability loop aims to maximize the minimum eigenvalue by maximizing the inf-sup constant, while the approximation loop aims to maximize $|\lambda^{\min}|$ by maximizing $\lambda_{\min}(\mathbb{K})$. We have indeed that for localised observations $\lambda_{\min}(\mathbb{K})$ depends on the minimum separation distance $\hat{h}_M = \min_{m,m'=1,\ldots,M,\, m\neq m'} \|x^{\text{obs}}_m - x^{\text{obs}}_{m'}\|_2$ between observation points. We refer to [197, 160] and [230, Chapter 12] for a rigorous analysis for pointwise measurements; for localized measurements, we are not aware of any theoretical result that relate $\lambda_{\min}(\mathbb{K})$ to $\hat{h}_M$. However, we empirically observe a strong correlation between these two quantities.

## 3.3 A synthetic problem: Helmholtz in $\mathbb{R}^2$

### 3.3.1 Problem definition

We illustrate the behavior of the PBDW formulation through a two-dimensional Helmholtz problem[1]. Towards this end, we first introduce the domains $\Omega^{\text{bk}}$ and $\Omega$, $\Omega = \Omega^{\text{bk}} = (0,1)^2$ and the mathematical problem:

$$\begin{cases} -(1 + i\epsilon\mu)\,\Delta u_g(\mu) \,-\, \mu^2 u_g(\mu) = \mu\left(2x_1^2 + e^{x_2}\right) + \mu g & \text{in } \Omega, \\ \partial_n\, u_g(\mu) = 0 & \text{on } \partial\Omega, \end{cases} \tag{3.3.1}$$

[1]The model problem is the same considered in [142, Section 3].

where $\mu > 0$ is the wave number, $\epsilon = 10^{-2}$ is a fixed dissipation, and $g \in L^2(\Omega)$ is a bias term that will be specified later. Here, the parameter $\mu > 0$ constitutes the anticipated, parametric uncertainty in the system, which might model our uncertainty in the speed of sound, while the function $g$ constitutes the unanticipated and non-parametric uncertainty in the system. Since $\Omega = \Omega^{\text{bk}}$, in what follows, we simply use the former to indicate both the domain of interest and the domain in which the mathematical model is properly defined.

We can restate problem (3.3.1) in weak form as

$$\mathcal{G}_g^\mu(u_g(\mu),\, v) = a^\mu(u_g^{\text{bk}}(\mu), v) \,-\, F_g^\mu(v) = 0 \qquad \forall\, v \in \mathcal{U}; \tag{3.3.2a}$$

where $\mathcal{U} = \mathcal{V}^{\text{bk}} = H^1(\Omega)$,

$$a^\mu(w, v) = (1 + i\epsilon\mu) \int_\Omega \nabla w \cdot \nabla \bar{v}\, d\,x \,-\, \mu^2 \int_\Omega w\, \bar{v}\, d\,x; \tag{3.3.2b}$$

and

$$F_g^\mu(v) \,=\, \mu \int_\Omega \left(2x_1^2 + e^{x_2} + g\right)\, \bar{v}\, d\,x. \tag{3.3.2c}$$

To assess the performance of the PBDW formulation for various configurations, we define the true field $u^{\text{true}}$ as the solution to (3.3.1) for some $\mu^{\text{true}} \in \mathcal{P}^{\text{bk}}$ and for the following two choices of the "bias" $g$

$$g := \begin{cases} 0 & \text{perfect model;} \\ \\ \tilde{g} \equiv 0.5(e^{-x_1} \,+\, 1.3\cos(1.3\pi x_2)) & \text{imperfect model.} \end{cases} \tag{3.3.3a}$$

On the other hand, we define the bk manifold as

$$\mathcal{M}^{\text{bk}} := \{u_{g=0}(\mu) :\, \mu \in \mathcal{P}^{\text{bk}}\}. \tag{3.3.3b}$$

Figure 3-2 shows the true field for three choices of the wave number $\mu$ and for the two choices of the bias $g$. We approximate the solution using a triangular $\mathbb{P}^5$ finite element discretization ($\mathcal{N} = 3312$). The use of a high-order method is here motivated by the smoothness of the true field.

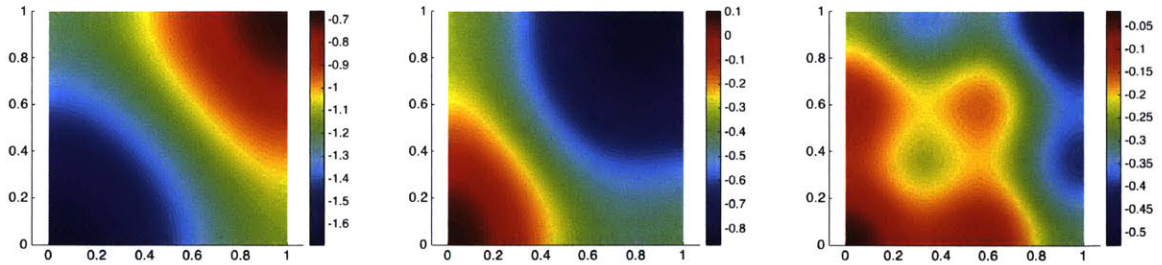

(a) $\Re(u^{\text{true}})$, $\mu = 2$, $g = 0$ (b) $\Re(u^{\text{true}})$, $\mu = 5$, $g = 0$ (c) $\Re(u^{\text{true}})$, $\mu = 10$, $g = 0$

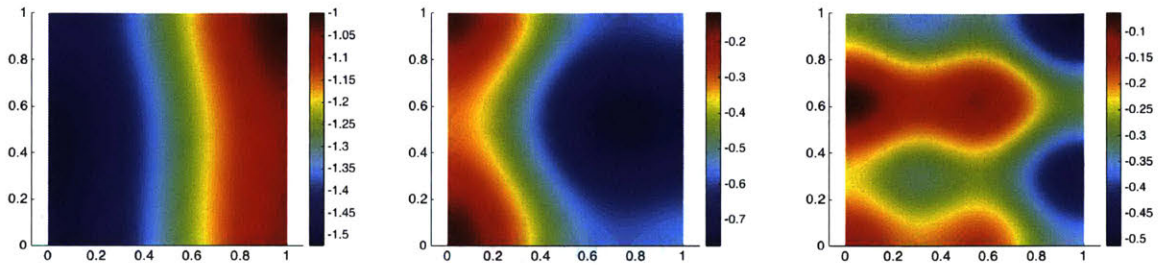

(d) $\Re(u^{\text{true}})$, $\mu = 2$, $g = \tilde{g}$ (e) $\Re(u^{\text{true}})$, $\mu = 5$ , $g = \tilde{g}$ (f) $\Re(u^{\text{true}})$, $\mu = 10$, $g = \tilde{g}$

**Figure 3-2:** Application to a synthetic acoustic problem: visualization of the truth solutions associated with the synthetic Helmholtz problem for perfect ($g = 0$ ) and imperfect ($g = \tilde{g}$) models.

### 3.3.2 Construction of the PBDW spaces

Recalling the definition of the inner product for $\mathcal{U}$ in (3.2.1), we build the background spaces $\{\mathcal{Z}_N\}_N$ using the weak-Greedy algorithm based on the residual estimator

$$\Delta_N^{\text{bk}}(\mu) = \inf_{z \in \mathcal{Z}_N} \|G^{\text{bk},\mu}(u^{bk}(\mu))\|_{\mathcal{U}'};$$

where $\|\cdot\|_{\mathcal{U}'}$ denotes the dual norm. Figure 3-3 shows the behavior of the best-fit error over $\mathcal{P}^{\text{bk}}_{\text{train}} \subset \mathcal{P}^{\text{bk}}$

$$E_N^{\text{rel}} := \max_{\mu \in \mathcal{P}^{\text{bk}}_{\text{train}}} \frac{\|\Pi_{\mathcal{Z}_N^\perp} u^{\text{true}}(\mu)\|}{\|u^{\text{true}}(\mu)\|}, \tag{3.3.4}$$

where $\mathcal{P}^{\text{bk}}_{\text{train}}$ is a uniform discretization of $\mathcal{P}^{bk}$, $|\mathcal{P}^{\text{bk}}_{\text{train}}| = 20$. We observe that for the perfect model $E_N^{\text{rel}}$ rapidly converges to zero as $N$ increases. On the other hand, in the case of imperfect model, $E_N^{\text{rel}}$ exhibits a plateau for $N \geq 4$. This can be explained recalling the discussion in section 2.1.2: as $N$ increases, the modeling error dominates over the discretization error.

In this synthetic example, we model the observation by a Gaussian convolution with

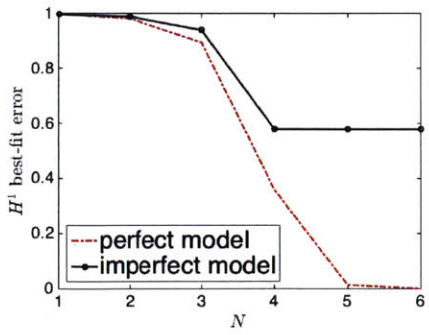


**Figure 3-3:** Application to a synthetic acoustic problem: best-fit error $E_N^{\text{rel}}$ (3.3.4) for perfect and imperfect model ($\gamma = 1$).

standard deviation $r = 0.02$:

$$\ell(v,\ x) \ = \ C(x) \int_{\Omega} \exp\left(-\frac{1}{2r^2}\|x-y\|_2^2\right)\ v(y)\, dy;$$

where $C(x) > 0$ is such that $\ell(1,\ x) \equiv 1$ for all $x \in \Omega$. Figure 3-4 shows the behavior of the stability constant $\beta_{N,M}$ with $M$ for three different choices of the threshold in Algorithm 3.2.1 and for three different values of $N$ for $\gamma = 1$. On the other hand, Figure 3-5 shows the behavior of the condition number of the matrix (2.3.2b) with $M$. We remark that the stabilization stage of Algorithm 3.2.1 is performed only for $tol > 0$, while the approximation stage is performed only for $tol < 1$.

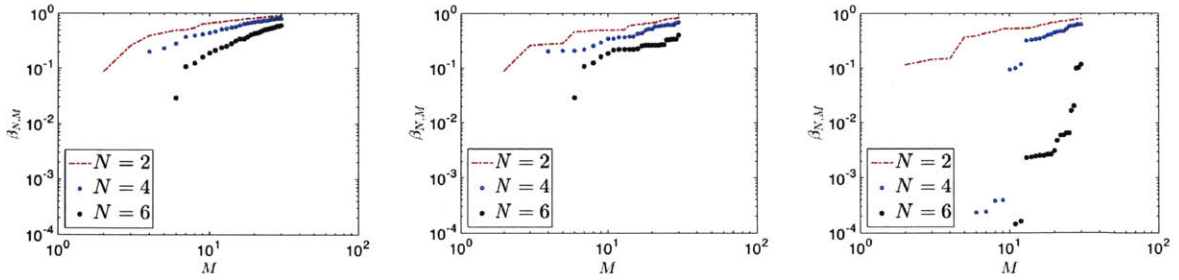


**(a)** $tol = 1$ **(b)** $tol = 0.2$ **(c)** $tol = 0$

**Figure 3-4:** Application to a synthetic acoustic problem: behavior of $\beta_{N,M}$ with $M$ for three different choices of the threshold $tol$ in Algorithm 3.2.1 and for three different values of $N$ ($\gamma = 1$).

We observe that the stabilization stage of Algorithm 3.2.1 significantly improves the stability of the variational formulation and consequently of the saddle point linear system. We further observe that for large values of $M$ the condition number of the saddle system is slightly smaller if we consider $tol < 1$.

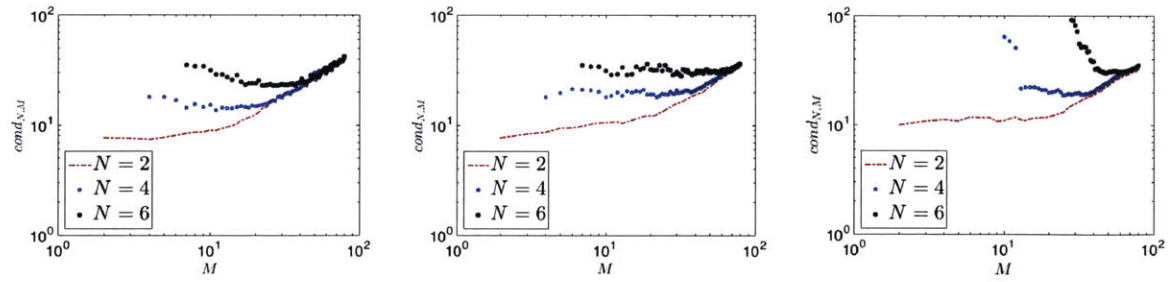


**(a)** $tol = 1$ **(b)** $tol = 0.2$ **(c)** $tol = 0$

**Figure 3-5:** Application to a synthetic acoustic problem: behavior of the condition number of the matrix (2.3.2b) with $M$ for three different choices of $tol$ in Algorithm 3.2.1 and for three different values of $N$ ($\gamma = 1$).

### 3.3.3 Results of the data assimilation procedure

We first visualize the PBDW state estimates for two distinct choices of $u^{\text{true}}$. We consider $\mu = 7.5$, and we consider $u^{\text{true}} = u_{g=0}(\mu)$ and $u^{\text{true}} = u_{g=\tilde{g}}(\mu)$; PBDW state estimates are based on the background $\mathcal{Z}_{N=5}$ and on $M = 32$ measurements chosen using Algorithm 3.2.1 with $tol = 0.2$. Figure 3-6 shows (the real part of) the true state, the PBDW state estimate $u^\star$, the deduced background $z^\star$ and the update $\eta^\star$. We observe that for $u^{\text{true}} = u_{g=0}(\mu)$ the update $\eta^\star$ is negligible; the reason is that the true state is well-approximated by its projection over $\mathcal{Z}_N$. On the other hand, for $u^{\text{true}} = u_{g=\tilde{g}}(\mu)$ we observe that the update is appreciable, and plays a significant role in improving the accuracy of the state estimate $u^\star$. These results strenghten the interpretation of the components of the PBDW state estimate provided in Chapter 2.

We now assess the performance of the data assimilation procedure. Towards this end, we compute the maximum $L^2$ error over $\mathcal{P}^{\text{bk}}_{\text{train}} \subset \mathcal{P}^{\text{bk}}$

$$E^{\text{rel}}_{\text{max}} := \max_{\mu \in \mathcal{P}^{\text{bk}}_{\text{train}}} \frac{\|u^{\text{true}}(\mu) - u^\star(\mu)\|_{L^2(\Omega)}}{\|u^{\text{true}}(\mu)\|_{L^2(\Omega)}}, \tag{3.3.5}$$

where $u^\star(\mu)$ denotes the PBDW state estimate associated with $u^{\text{true}}(\mu)$, and $|\mathcal{P}^{\text{bk}}_{\text{train}}| = 20$. Figure 3-7 shows the behavior of $E^{\text{rel}}_{\text{max}}$ with $M$ for three different choices of the threshold in Algorithm 3.2.1 and for three different values of $N$. We observe that the stabilization procedure for the selection of the sensors' locations leads to a significant improvement of the performances for small values of $M$. On the other hand, as $M$ increases, our results show that selecting well-separated observation points improves performances. We further observe

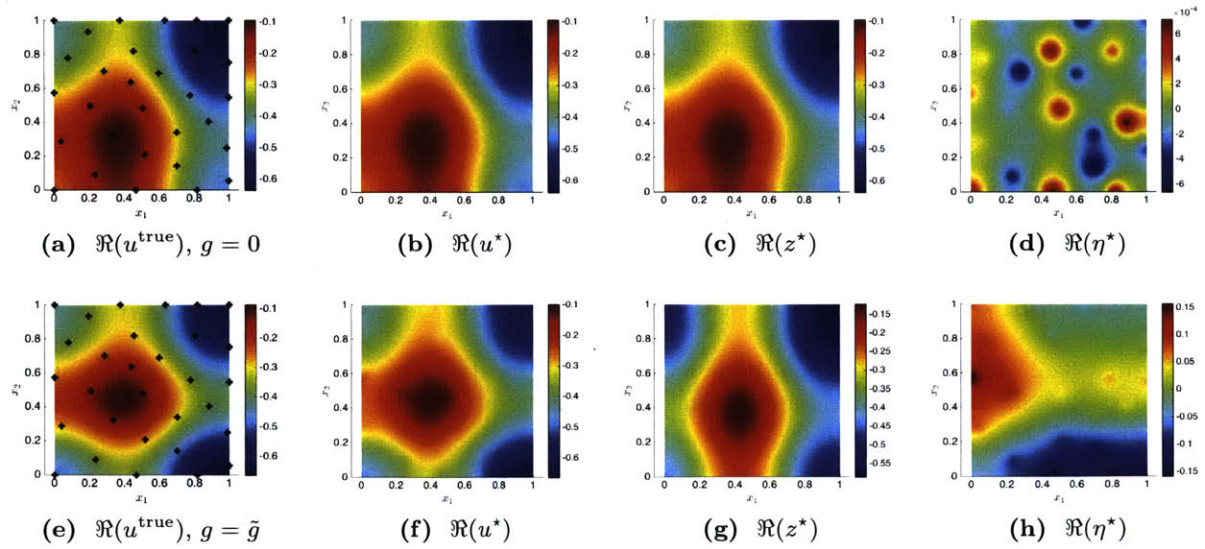

**(a)** $\Re(u^{\text{true}})$, $g = 0$ **(b)** $\Re(u^\star)$ **(c)** $\Re(z^\star)$ **(d)** $\Re(\eta^\star)$

**(e)** $\Re(u^{\text{true}})$, $g = \tilde{g}$ **(f)** $\Re(u^\star)$ **(g)** $\Re(z^\star)$ **(h)** $\Re(\eta^\star)$

**Figure 3-6:** Application to a synthetic acoustic problem: visualization of the PBDW state estimates for $N = 5$, $M = 32$. The states in Figures (a) and (e) correspond to $\mu = 7.5$. The black points in Figures (a) and (e) indicate the transducers' locations.

that increasing $N$ improves performances in the case of perfect model; on the other hand, in the case of imperfect model, increasing $N$ from 4 to 6 does not have any effect. This is in good agreement with the plot in Figure 3-3.

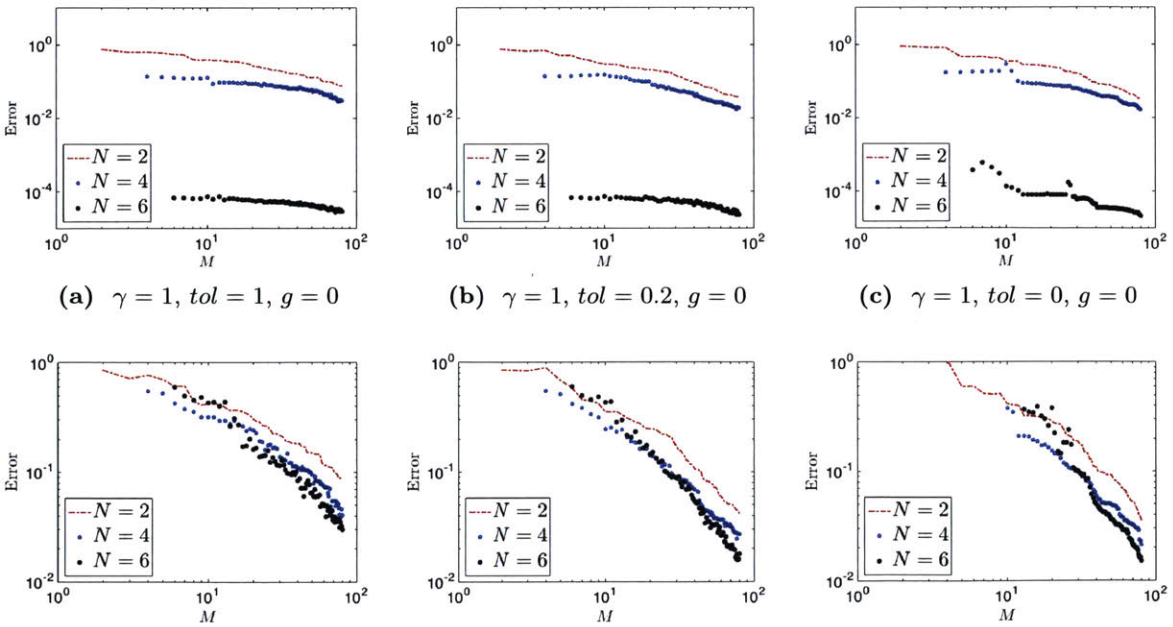


**(a)** $\gamma = 1$, $tol = 1$, $g = 0$ **(b)** $\gamma = 1$, $tol = 0.2$, $g = 0$ **(c)** $\gamma = 1$, $tol = 0$, $g = 0$

**(d)** $\gamma = 1$, $tol = 1$ , $g = \tilde{g}$ **(e)** $\gamma = 1$, $tol = 0.2$ , $g = \tilde{g}$ **(f)** $\gamma = 1$, $tol = 0$ , $g = \tilde{g}$

**Figure 3-7:** Application to a synthetic acoustic problem: behavior of $E^{\text{rel}}_{\text{max}}$ (3.3.5) with $M$ for three different choices of *tol* in Algorithm 3.2.1 and for three different values of $N$.

Figure 3-8 shows the anticipated and unanticipated mean fractions of the state

$$\text{mean}_{\mu \in \mathcal{P}^{\text{bk}}_{\text{train}}} \frac{\|z^\star(\mu)\|}{\|u^\star(\mu)\|}, \qquad \text{anticipated},$$

and

$$\text{mean}_{\mu \in \mathcal{P}^{\text{bk}}_{\text{train}}} \frac{\|\eta^\star(\mu)\|}{\|u^\star(\mu)\|}, \qquad \text{unanticipated}.$$

We observe that in the case of perfect model the update component of the state is essentially negligible, while it is significant in the case of imperfect model to address the deficiencies of the primary approximation. This confirms the results in Figure 3-6.

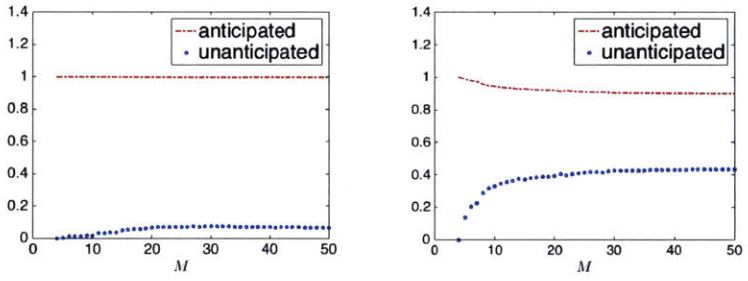


**(a)** $g = 0$ **(b)** $g = \tilde{g}$

**Figure 3-8:** Application to a synthetic acoustic problem: behavior of the anticipated and unanticipated fractions of the state for perfect and imperfect models ($N = 4$, $tol = 0.2$, $\gamma = 1$).

Figure 3-9 investigates the behavior of $E^{\text{rel}}_{\text{max}}$ (3.3.5) with $M$ for three different choices of $\gamma$ in (3.2.1). We observe that while in the case of perfect model, performances are essentially independent of the choice of $\gamma$, in the case of imperfect model — in which the secondary approximation provided by the update is crucial to guarantee an accurate reconstruction — the choice of the parameter $\gamma$ is extremely important for large values of $M$. As $\gamma$ increases, the smoothing effect of the $H^1$ term in the inner product (3.2.1) decreases, and $R_{\mathcal{U}}\ell^o_m$ approaches $C(x)\exp\left(-\frac{1}{2r^2}\|\cdot - x^{\text{obs}}_m\|^2_2\right)$, which clearly is not suited to capture the low-order components of the error $u^{\text{true}} - z^\star$. On the other hand, for sufficiently large $M$, we envision that too small values of $\gamma$ might not be able to capture high-order components of the error $u^{\text{true}} - z^\star$. We further address this point in Chapter 6.

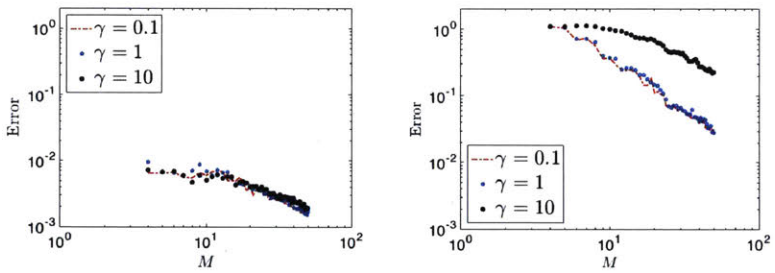


**(a)** $g = 0$ **(b)** $g = \tilde{g}$

**Figure 3-9:** Application to a synthetic acoustic problem: behavior of $E^{\text{rel}}_{\max}$ (3.3.5) with $M$ for three different choices of $\gamma$ ($N = 4$, $tol = 0.2$).

## 3.4 A physical system: the thermal patch experiment

### 3.4.1 Experimental apparatus

The thermal patch system consists of a 1.5[mm] thick acrylic sheet heated from behind by a resistive patch. Heat is generated through an electrical resistance with input power equal to $0.667W$. The goal of the data assimilation procedure is to estimate the temperature field over a portion $\Omega^{\text{obs,dim}}$ of the external surface of the plate at the steady-state limit.

We use an IR camera (`Fluke Ti 9`) to take measurements in the rectangular region $\Omega^{\text{obs,dim}} = [-23.85, 23.85] \times [-17.85, 17.85]$[mm] centered on the patch. Figure 3-10 shows the IR camera. After the patch power is turned on, we take measurements using a sampling time of 4 seconds until steady state is reached; the total duration of the experiment is roughly 5 minutes. The external temperature is about $20^oC$, roughly constant throughout the experiment. Each surface measurement taken from the IR camera corresponds to $160 \times 120$ pixel-wise measurements; the pixel size is roughly $\Delta h^{\text{device}} = 0.3$[mm], which is much smaller than the spatial length scale of the phenomenon of interest.

In view of the mathematical description of the problem, we present formal definitions for the geometric quantities involved. First, we introduce the domain $\Omega^{\text{bk,dim}} \subset \mathbb{R}^3$ corresponding to the three-dimensional acrylic sheet. We denote by $\Gamma^{\text{patch,dim}} \subset \mathbb{R}^2$ the surface of the sheet attached to the patch, and we denote by $\Gamma^{\text{in,dim}}$ the face of the sheet that contains $\Gamma^{\text{patch,dim}}$. We recall that $\Omega^{\text{obs,dim}} \subset \partial\Omega^{\text{bk,dim}}$ is the region in which the IR camera takes measurements. Then, we introduce the Cartesian coordinate system $x_1^{\text{dim}} x_2^{\text{dim}} x_3^{\text{dim}}$; according to our definitions, the IR camera takes measurements in the $x_1^{\text{dim}} x_3^{\text{dim}}$ plane. Figure 3-11 clarifies the definitions of $\Omega^{\text{obs,dim}}$, $\Omega^{\text{bk,dim}}$, $\Gamma^{\text{patch,dim}}$ and $\Gamma^{\text{in,dim}}$ and shows the

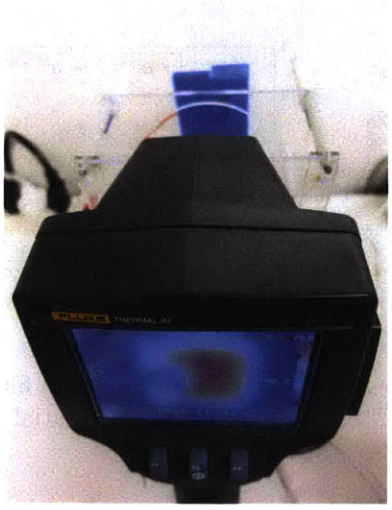

**Figure 3-10:** Thermal patch experiment: IR camera.

characteristic dimensions of the patch.

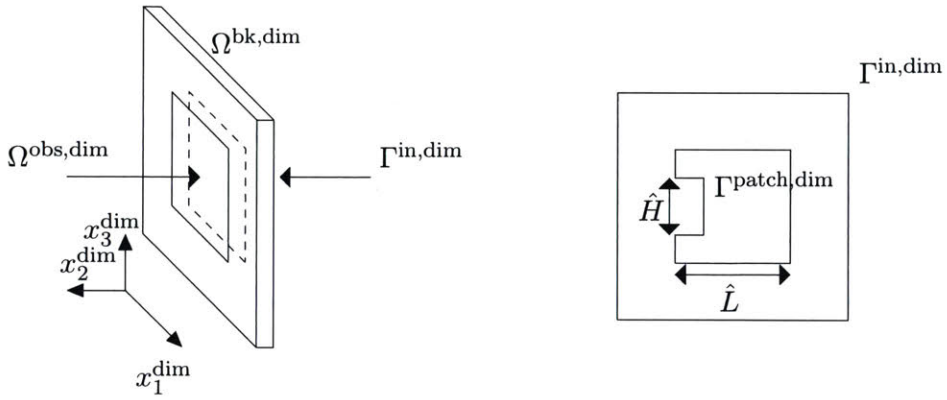


**Figure 3-11:** Thermal patch experiment: mathematical description of the acrylic sheet. $\hat{L} = 22.606\text{mm}$, $\hat{H} = 9.271\text{mm}$.

In order to estimate the noise level in the dataset, we compute the difference $u^{\text{obs,dim}} - u^{\text{filt,dim}}$ where the field $u^{\text{obs,dim}}$ is obtained directly from the IR camera, and $u^{\text{filt,dim}}$ is obtained applying a Wiener filter (see, e.g., [136]) based on a 3 by 3 pixel averaging to the field $u^{\text{obs,dim}}$. Figure 3-12 shows two spatial slices of the difference $u^{\text{obs,dim}} - u^{\text{filt,dim}}$. By comparing $u^{\text{filt,dim}}$ and $u^{\text{obs,dim}}$, we deduce that the magnitude of noise in the measurements is approximately $\pm 0.5^o C$, roughly independent of the spatial position.

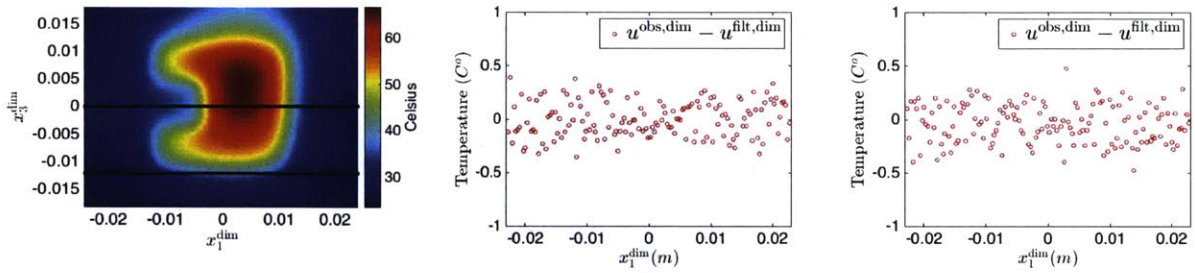


**(a)** $u^{\text{obs,dim}}$ **(b)** $x_3^{\dim} = 0.2\text{mm}$ **(c)** $x_3^{\dim} = -12.0\text{mm}$

**Figure 3-12:** Thermal patch experiment: comparison between filtered and unfiltered fields. Figure (a): observed thermal field $u^{\text{obs,dim}}$. Figures (b) and (c): spatial slices of the difference $u^{\text{obs,dim}} - u^{\text{filt,dim}}$.

### 3.4.2 Engineering motivation

We shall now motivate this model problem from the engineering standpoint. Full-field information is typically not available; in practical applications, we envision a system with a local sensor or a small sensor array. For this reason, we want to design a data assimilation state estimation procedure that is able to reconstruct the full field based on a small amount of local measurements.

Since the IR camera provides full-field information, in this work, we synthetize local measurements – the experimental input to our methods – from the IR camera to obtain $\ell_m^{\text{obs}} = \ell(u^{\text{obs}}, x_m^{\text{obs}})$ where the observation functional $\ell(\cdot, x_m^{\text{obs}})$ is designed to represent a local measurement in the sensor location $x_m^{\text{obs}} \in \Omega^{\text{obs}}$. We observe that the IR camera permits us to conduct convergence studies that would typically not be feasible in actual field deployment.

### 3.4.3 Mathematical model and background space

We resort to a steady-state heat-transfer model in which we rely on a Robin boundary condition to describe the heat-exchange between the patch and the sheet. In more detail, we consider the bk model for the thermal field $u^{\text{bk,dim}} : \Omega^{\text{bk,dim}} \to \mathbb{R}$:

$$\begin{cases} -\Delta u^{\text{bk,dim}} = 0, & \text{in } \Omega^{\text{bk,dim}}, \\ \kappa \partial_n u^{\text{bk,dim}} + \gamma(u^{\text{bk,dim}} - \Theta^{\text{room,dim}}) = g^{\dim} \chi_{\Gamma^{\text{patch,dim}}} & \text{on } \Gamma^{\text{in,dim}}, \\ \kappa \partial_n u^{\text{bk,dim}} = 0 & \text{on } \partial\Omega^{\text{bk,dim}} \setminus \Gamma^{\text{in,dim}}, \end{cases} \tag{3.4.1}$$

where $\gamma$ is the convective heat transfer coefficient, $\kappa$ is the thermal conductivity of acrylic, $\Theta^{\text{room,dim}} = 20^oC(= 293K)$ is the room temperature, and $g^{\text{dim}}$ is the incoming flux, which models the heat exchange between the patch and the plate. Textbook values for the model parameters are $\kappa = 0.2[\text{W}/(\text{m} \cdot \text{K})]$, $\gamma = 10[\text{W}/(\text{m}^2 \cdot \text{K})]$. We remark that the value of $\gamma$ is computed as $\gamma = \frac{Nu\kappa_{\text{air}}}{\hat{L}}$. Here, $\kappa_{\text{air}} = 0.0257[\text{W}/(\text{m} \cdot \text{K})]$ is the thermal conductivity of air, $\hat{L} = 22.606\text{mm}$ is the length of the edge of the patch (see Figure 3-11), $Nu = 0.59(\text{Ra})^{1/4}$ is the Nusselt number, and $\text{Ra} = 5.9 \cdot 10^4$ is the Rayleigh number defined as $\text{Ra} = \frac{\beta g \Delta\Theta \hat{L}^3}{\nu\alpha}$, where $g = 9.81[\text{m}/\text{s}^2]$, $\nu = 1.81 \cdot 10^{-5}[\text{m}^2/\text{s}]$ is the kinematic viscosity of air, $\beta = 1/300[1/\text{K}]$ is the thermal expansion coefficient, $\alpha = 1.9 \cdot 10^{-5}[\text{m}^2/\text{s}]$ is the thermal diffusivity of air, and $\Delta\Theta = 50^oC(= 50K)$ is a rough approximation of the temperature difference between the far-field and the center of the patch.

Given the thermal field $u^{\text{bk,dim}}$, we introduce the non-dimensional counterpart

$$u^{\text{bk}}(x) = \frac{u^{\text{bk,dim}}(\hat{L}x) - \Theta^{\text{room,dim}}}{\Delta\Theta}. \tag{3.4.2}$$

We observe that $u^{\text{bk}} = u^{\text{bk}}(\mu)$ satisfies

$$\begin{cases} -\Delta u^{\text{bk}}(\mu) = 0, & \text{in}\,\Omega^{\text{bk}}, \\ \partial_n u^{\text{bk}}(\mu) + \mu u^{\text{bk}}(\mu) = g & \text{on}\,\Gamma^{\text{in}}, \\ \partial_n u^{\text{bk}}(\mu) = 0 & \text{on}\,\partial\Omega^{\text{bk}} \setminus \Gamma^{\text{in}}, \end{cases} \tag{3.4.3a}$$

where $\mu = \hat{L}\gamma/\kappa \approx 1.13$ and $g$ is defined as follows:

$$g(x) = C\,\chi_{\Gamma^{\text{patch}}}(x). \tag{3.4.3b}$$

We observe that $u^{\text{bk}}$ depends on the parameters $\mu$ and $C$. Since the model is linear with respect to $C$ and our ultimate goal is to define a linear space associated with the bk manifold, we can simply set $C = 1$. On the other hand, assuming that the estimate of $\kappa$ is accurate and that $\gamma \approx 10 \pm 5\text{W}/\text{m}^2$, we obtain that $\mu \in \mathcal{P}^{\text{bk}} = [0.5650, 1.650]$. We can thus define the bk manifold as follows:

$$\mathcal{M}^{\text{bk}} = \left\{ u^{\text{bk}}(\mu)|_{\Omega^{\text{obs}}} : \mu \in \mathcal{P}^{\text{bk}} \right\}. \tag{3.4.4}$$

We further introduce the weak form of the bk model (3.4.3): given $\mu \in \mathcal{P}^{\text{bk}}$, find $u^{\text{bk}}(\mu) \in \mathcal{V}^{\text{bk}}$ such that

$$\mathcal{G}^{\text{bk},\mu}(u^{\text{bk}}(\mu),\ v) = a^{\mu}(u^{\text{bk}}(\mu), v)\ - F^{\mu}(v) = 0 \qquad \forall v \in \mathcal{V}^{\text{bk}}; \tag{3.4.5a}$$

where $\mathcal{V}^{\text{bk}} = H^1(\Omega^{\text{bk}})$,

$$a^{\mu}(w, v) = \int_{\Omega^{\text{bk}}} \nabla w \cdot \nabla v \, dx \ + \ \mu \int_{\Gamma^{\text{in}}} w \, v \, ds; \tag{3.4.5b}$$

and

$$F(v) \ = \ \int_{\Gamma^{\text{patch}}} v \, dx. \tag{3.4.5c}$$

We observe that our parametrized model encodes the uncertainty in the material properties $\gamma$ and $\kappa$. On the other hand, it does not take into account the nonlinear effects associated to natural convection, and to the heat-exchange between the patch and the sheet. The latter represent the non-parametric uncertainty in the model.

The background space $\mathcal{Z}_N$ associated with (3.4.3)-(3.4.4) is built using the weak-Greedy algorithm. More in detail, we apply the weak-Greedy algorithm based on the residual estimator

$$\Delta_N^{\text{bk}}(\mu) = \inf_{z \in \mathcal{Z}_N^{\text{bk}}} \|G^{\text{bk},\mu}(u^{\text{bk}}(\mu))\|_{(\mathcal{V}^{\text{bk}})'}$$

to build $\mathcal{Z}_N^{\text{bk}} \subset \mathcal{V}^{\text{bk}}$, where $\|\cdot\|_{(\mathcal{V}^{\text{bk}})'}$ denotes the dual norm. Then, we restrict the space $\mathcal{Z}_N^{\text{bk}}$ to the domain of interest $\Omega = \Omega^{\text{obs}}$ to form $\mathcal{Z}_N$. To compute the solution to the bk model, we appeal to a $\mathbb{P}^3$ continuous Finite Element discretization based on $\mathcal{N} = 40000$ degrees of freedom.

### 3.4.4 Best-knowledge and observed thermal fields

We now show plots of the observed and bk fields. For convenience, we consider non-dimensional fields – which are based on the non-dimensionalization (3.4.2). Furthermore, to simplify the comparison, we scale the bk fields such that $\max_{x \in \overline{\Omega}^{\text{obs}}} u^{\text{bk}}(x) = \max_{x \in \overline{\Omega}^{\text{obs}}} u^{\text{obs}}(x)$. This corresponds to adjust the value of $C$ in the bk model (3.4.3). Figures 3-13(a), (b) and (c) show the non-dimensional observed field $u^{\text{obs}}$ as measured by the IR camera, the bk field

$u^{\text{bk}}$ for $\mu = 1.13$ and the error field $u^{\text{obs}} - u^{\text{bk}}$. Figures 3-13(d), (e) and (f) show the bk field $u^{\text{bk}}$ for three different values of $\mu$. We observe that $u^{\text{bk}}$ is symmetric with respect to $x_3 = 0$ for each value of $\mu$ , while $u^{\text{obs}}$ is markedly asymmetric. This is clearly related to the nonlinear effects of natural convection.

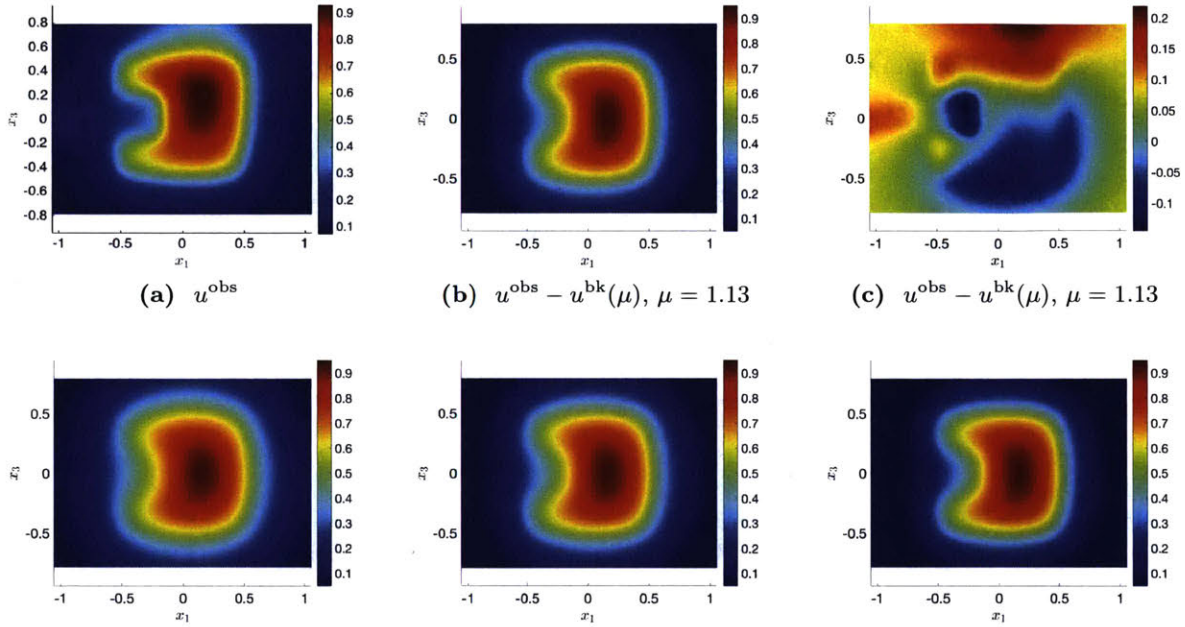

**(a)** $u^{\text{obs}}$ **(b)** $u^{\text{obs}} - u^{\text{bk}}(\mu)$, $\mu = 1.13$ **(c)** $u^{\text{obs}} - u^{\text{bk}}(\mu)$, $\mu = 1.13$

**(d)** $u^{\text{bk}}(\mu)$, $\mu = 0.565$ **(e)** $u^{\text{bk}}(\mu)$, $\mu = 1$ **(f)** $u^{\text{bk}}(\mu)$, $\mu = 1.565$

**Figure 3-13:** Thermal patch experiment: comparison between observed field and bk solutions.

Figure 3-14 shows the basis $\zeta_1, \zeta_2, \zeta_3$ of the three-dimensional space $\mathcal{Z}_N$, while Figure 3-15 shows the behavior of the $L^2$ relative *discretization error* computed as

$$E_N^{\text{rel,bk}} := \max_{\mu \in \mathcal{P}^{\text{bk}}_{\text{train}}} \frac{\|u^{\text{bk}}(\mu) - \Pi_{\mathcal{Z}_N, L^2} u^{\text{bk}}(\mu)\|_{L^2(\Omega^{\text{obs}})}}{\|u^{\text{bk}}(\mu)\|_{L^2(\Omega^{\text{obs}})}}, \tag{3.4.6}$$

where $\Pi_{\mathcal{Z}_N, L^2}$ denotes the projection over $\mathcal{Z}_N$ with respect to the $L^2$ norm, $\mathcal{P}^{\text{bk}}_{\text{train}}$ is a uniform discretization of $\mathcal{P}^{\text{bk}}$, $N_{\text{train}} = 20$, and of the $L^2$ relative *best-fit error* computed as

$$E_N^{\text{rel,best-fit}} := \frac{\|u^{\text{obs}} - \Pi_{\mathcal{Z}_N, L^2} u^{\text{obs}}\|_{L^2(\Omega^{\text{obs}})}}{\|u^{\text{obs}}\|_{L^2(\Omega^{\text{obs}})}}. \tag{3.4.7}$$

We observe that for $N > 3$ the best-fit error remains essentially constant, while the discretization error decreases exponentially with $N$.

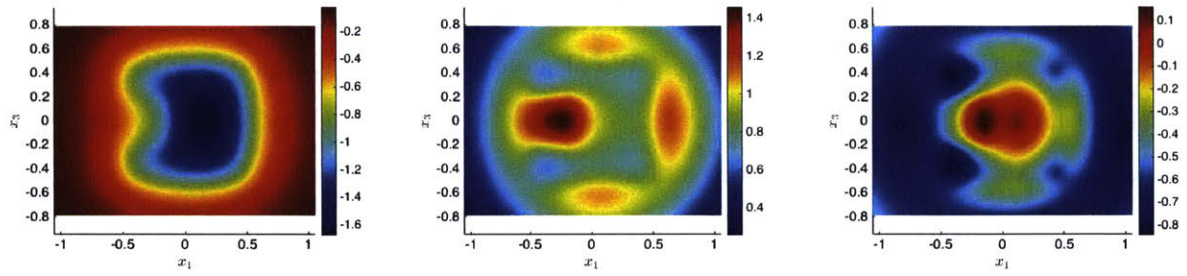

(a) $\zeta_1$ (b) $\zeta_2$ (c) $\zeta_3$

**Figure 3-14:** Thermal patch experiment: basis of the background space obtained using the weak-Greedy algorithm.

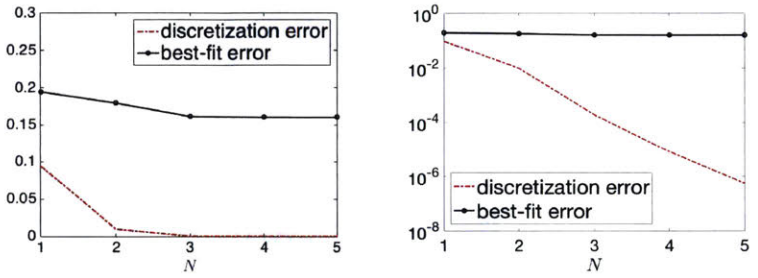


(a) (b)

**Figure 3-15:** Thermal patch experiment: behavior of the $L^2$ relative *discretization error* (3.4.6) and of the $L^2$ relative best-fit error (3.4.7) in linear (Figure (a)) and logarithmic (Figure (b)) scale.

### 3.4.5 Numerical results

We now present the results of the application of the PBDW data assimilation procedure to the thermal patch problem. We here apply our procedure to the non-dimensional field, and we synthesize local measurements to obtain $\ell_m^{\text{obs}} = \ell(u^{\text{obs}}, x_m^{\text{obs}})$ where

$$\ell(v,\ x) \ = \ C(x) \int_{\Omega^{\text{obs}}} \exp\left(-\frac{1}{2r^2}\|x-y\|_2^2\right)\ v(y)\, dy,$$

$r > 0$ and $C(x) > 0$ is such that $\ell(1,\ x) \equiv 1$ for all $x \in \Omega$. Recalling the definitions of Chapter 3.4, our goal is to estimate the thermal field in $\Omega = \Omega^{\text{obs}}$.

Figure 3-16 shows the behavior of $E_{N,M}^{\text{rel}}$,

$$E_{N,M}^{\text{rel}} := \frac{\|u^{\text{obs}}(\mu) - u_{N,M}^{\star}(\mu)\|_{L^2(\Omega)}}{\|u^{\text{obs}}(\mu)\|_{L^2(\Omega)}}, \tag{3.4.8}$$

with respect to $M$ for four values of $N$ and for two values of $r$, $r = 0.02$ ($r^{\text{dim}} = 0.452$[mm]), and $r = 0.1$ ($r^{\text{dim}} = 2.26$[mm]). To build the update space, we set $\gamma = 1$ in the inner product

(3.2.1), and we run the SGreedy-plus algorithm using the threshold $tol = 0.2$. We observe that reducing the value of $r$ deteriorates the performance of our approach. This issue does not seem to be solvable by simply tuning the value of $\gamma$. We argue that this is related to the fact that as $r \to 0^+$, the PBDW becomes inconsistent: we have indeed that as $r$ goes to zero the dual norm of the functional $\ell(\cdot, x_m^{\text{obs}})$ diverges.

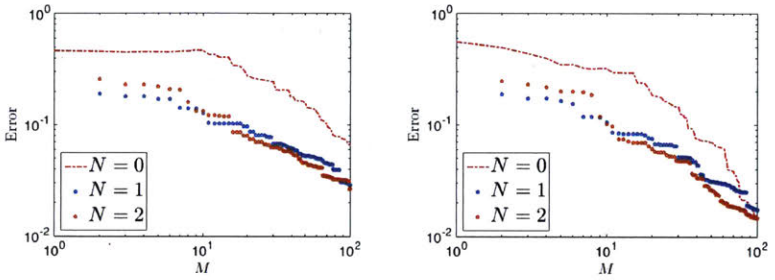


**(a)** $r_{\text{Gauss}} = 0.02$ **(b)** $r_{\text{Gauss}} = 0.1$

**Figure 3-16:** Application to the thermal patch experiment: behavior of $E^{\text{rel}}_{N,M}$ (3.4.8) with $M$ for three values of $N$ and for two values of $r_{\text{Gauss}}$ ($\gamma = 1$, $tol = 0.2$).

Figure 3-17 shows the behavior of the anticipated and unanticipated fractions of the state. We observe that due to the model error the unanticipated fraction is significant.

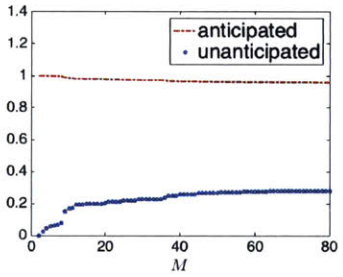


**Figure 3-17:** Application to the thermal patch experiment: behavior of the anticipated and unanticipated fractions of the state ($\gamma = 1$, tol $= 0.2$, $r_{\text{Gauss}} = 0.1$, $N = 2$).

## 3.5 Conclusions

In this chapter, we discussed the PBDW approach for perfect measurements. We presented an *a priori* error analysis, which shows the quasi-optimality of the PBDW state estimate, and an adaptive procedure for the selection of the observation centers. Numerical results illustrated the role of the different elements of the formulation — namely, the background space, the inner product, and the choice of the observation centers.

The use of rapid-convergent background spaces $\{\mathcal{Z}_N\}_N$ allows us to properly take into account parametric uncertainty in the system, and thus leads to accurate state reconstructions in the case of moderate model error. In addition, the stabilization strategy for the selection of the observation centers allows us to consider $N \simeq M$. On the other hand, numerical results showed that the main issue of the formulation is the slow convergence with $M$. This is explained by the poor approximation properties provided by the update space, especially for nearly pointwise measurements. We address this issue in the case of pointwise measurements in Chapter 6.

# Chapter 4

# *A posteriori* error estimation and output prediction

We present and analyze an experimental $L^2$-*a posteriori* error estimation procedure based on Monte Carlo sampling of observation functionals. Given $J$ possibly noisy local measurements over the domain $\Omega$, $\{\ell_j^{\text{obs}}\}_{j=1}^J$, and a state estimate $u^\star$ for the true field $u^{\text{true}}$, we provide confidence intervals for the $L^2$ error in state $E = \|u^{\text{true}} - u^\star\|_{L^2(\Omega)}$, and the error in $L^2$ outputs $E_{\mathcal{L}} = |\mathcal{L}(u^{\text{true}}) - \mathcal{L}(u^\star)|$. We further present an adaptive strategy, which relies on the proposed error estimation procedure, to automatically enrich the PBDW background space $\mathcal{Z}_N$ based on unmodeled physics identified through data assimilation of a select few configurations.

We provide an outline of the chapter. In section 4.1, we introduce the problem of validation and we introduce our method; we further illustrate the application of our techniques to three data assimilation tasks. In section 4.2, we derive a confidence interval $\widehat{C}_{\mathcal{L}}$ for the error in $L^2$ functional outputs; we also unfold the confidence interval to develop estimates for the output $\mathcal{L}(u^{\text{true}})$. In section 4.3, we discuss how to extend our technique to the estimation of the $L^2$ error in state. Then, in section 4.4, we illustrate the application to subsequent state estimation. Finally, in sections 4.5 and 4.6 we present a number of numerical results.

## 4.1 Validation: definition and application to output prediction and state estimation

### 4.1.1 A posteriori error estimation

According to the definition of AIAA ([57]), validation ([163]) is *the process of determining the degree to which a model is an accurate representation of the real world from the perspective of the intended uses of the model.* From a mathematical standpoint, validation is the process of estimating the error in our model in a suitable metric of interest, e.g. a suitable norm or seminorm.

Given the estimate $u^\star$ of the system's state $u^{\text{true}}$ over a specified spatial domain $\Omega \subset \mathbb{R}^d$, our goal is to estimate the $L^2(\Omega)$ state-estimation error, and the error in $L^2(\Omega)$ output functionals based on $J$ experimental measurements $\{\ell_j^{\text{obs}}\}_{j=1}^J$. We shall denote by $E = \|u^{\text{true}} - u^\star\|_{L^2(\Omega)}$ the $L^2(\Omega)$ state-estimation error, and by $E_{\mathcal{L}} = |\mathcal{L}(u^{\text{true}}) - \mathcal{L}(u^\star)|$ the error in the $L^2$ output $\mathcal{L} : L^2(\Omega) \to \mathbb{R}$. We shall further describe the measurements as $\ell_j^{\text{obs}} = \ell(u^{\text{true}}, x_j^{\text{obs}}, \nu) + \epsilon_j$, where $x_j^{\text{obs}} \in \Omega$ is the transducer location, the constant $\nu > 0$ denotes the spatial width of the transducer, and $\epsilon_j$ is a random disturbance. The functional $\ell(\cdot, x_j^{\text{obs}}, \nu)$ takes into account the averaging process performed by the experimental device.

In this work we follow a frequentist approach to derive confidence intervals for the error in state and output. For either $E_{\mathcal{L}}$ or $E$, we first build a Monte Carlo estimate for the error (denoted by either $\widehat{E}_{\mathcal{L}}$ or $\widehat{E}$). Then, we build lower and upper error bounds for the difference between the estimated error and the true error (either $E_{\mathcal{L}} - \widehat{E}_{\mathcal{L}}$ or $E - \widehat{E}$) based on standard large-sample methods (see, e.g., [183, Chapter 8]). In more detail, we identify three different error sources, here called finite-$\nu$ error, finite-$J$ error, and finite-noise error. Finite-$\nu$ error is related to the finite spatial width $\nu$ of the transducer (which prevents us from computing pointwise values of the error field). Finite-$J$ error is related to the finite number of measurements available. Finally, finite-noise error is related to the random error in the measurements. We propose actionable lower and upper error bounds that take into account finite-$J$ and finite-noise error in the estimate. Furthermore, we develop a mathematical theory to assess the conditions under which finite-$\nu$ error is small. We observe that, while we prescribe a probabilistic model for the observational disturbances, we do not make any assumption on the error field $u^{\text{true}} - u^\star$ apart from a very weak regularity hypothesis.

Large-sample methods — on which we rely to address finite-$J$ and finite-noise errors —

have already been extensively used to assess the accuracy of computational models in the field of Validation and Verification (see, e.g., [196]). However, the idea of applying a Monte Carlo approach to estimate the $L^2$ error in state and the error in output evaluations is new: rather than comparing experimental measurements of the output with simulation prediction for the output, we exploit (quasi-)pointwise experimental measurements to deduce the error in output functionals of interest.

From the perspective of uncertainty quantification, our method complements Bayesian techniques [49, 50, 55, 164, 165] in that we make few assumptions on the error field $u^{\text{true}} - u^\star$. If substantial prior information about the error field is available, we envision that our approach might be outperformed by suitable Bayesian techniques. In absence of such information our frequentist approach can still be applied and will yield good results in particular if the model error is not too large.

From the perspective of uncertainty reduction, our approach may be viewed as the experimental extension of recent efforts in variance reduction techniques for Monte Carlo simulations. In more detail, the idea of using a surrogate model – in this case the state estimate $u^\star$ – to reduce the variance of a Monte Carlo process is related to the classical control variates method (see, e.g., [189, Chapter 4]) and to a number of more recent works for the estimation of statistical outputs of stochastic ODEs ([94, 95]), and stochastic PDEs ([13, 224, 161]).

Our method relies on the assumption that sensor locations are drawn randomly from a given distribution and that the disturbance is homoscedastic. Measurements in arbitrary spatial points can be acquired by appealing to robotic observation platforms. We refer to [142] for an application of the former data acquisition system to acoustics. On the other hand, we observe that in distributed sensor networks ([68, 187]) locations should be selected among a set of candidate grid points; in section 4.2, we discuss how to extend our procedure to this scenario. Finally, the assumption of homoscedastic random noise is convenient for the analysis and is reasonably accurate in many engineering applications. In Appendix B, we discuss the extension of our theory to heteroscedastic noise.

### 4.1.2 Applications

Although the validation procedure is primarily designed to assess the accuracy of the (PBDW) state estimate $u^\star$, we further apply our error estimator to three different tasks:

output prediction, data-driven empirical enrichment of the PBDW background space $\mathcal{Z}_N$, and adaptive selection of the PBDW tunable parameters. The first two tasks are illustrated in this chapter, while the third task is discussed in Chapter 6.

**Output prediction:** exploiting the linearity of $\mathcal{L}$, we employ our technique to provide lower and upper bounds for the quantity of interest $\mathcal{L}(u^{\text{true}})$. We demonstrate that, by applying the Monte Carlo procedure to the output error instead of to the true field, and exploiting the proximity of $u^\star$ to $u^{\text{true}}$, we can significantly reduce the variance of the process and thus improve the output estimate $\mathcal{L}(u^\star)$ for the output $\mathcal{L}(u^{\text{true}})$.

**Data-driven empirical enrichment of the PBDW background space $\mathcal{Z}_N$:** we provide a strategy to systematically incorporate the unmodelled physics identified by the update $\eta^\star \in \mathcal{U}_M$ to augment the background space $\mathcal{Z}_N$ for subsequent data assimilation. The goal is to reduce the number of observations for future configurations. The strategy, which is designed for a many-query scenario and was first presented in [143], relies on the *a posteriori* error estimator to guide the data-driven enrichment.

**Adaptive selection of the PBDW tunable parameters:** as explained in Chapter 2, PBDW depends on the tunable parameter $\xi > 0$, and potentially also on other parameters related to the norm $\|\cdot\|$ of the space $\mathcal{U}$. In Chapter 6, we discuss a strategy to systematically select the value(s) of the hyper-parameter(s) based on estimates of the error in state.

## 4.2 *A posteriori* error estimation in $L^2$ functionals

### 4.2.1 General framework

We first introduce the problem we wish to address together with a number of definitions and assumptions. Given the true deterministic field $u^{\text{true}} : \Omega^{\text{obs}} \to \mathbb{R}$, an estimate for $u^{\text{true}}$, $u^\star : \Omega^{\text{obs}} \to \mathbb{R}$, and the associated state estimation error $e := u^{\text{true}} - u^\star$, we wish to exploit $J$ local assessment observations to compute a confidence interval $\widehat{C}_{\mathcal{L}}$ for the error

$$E_{\mathcal{L}} = \mathcal{L}(e), \tag{4.2.1}$$

where $\mathcal{L} : L^2(\Omega) \to \mathbb{R}$ is of the form

$$\mathcal{L}(w) := \int_\Omega \zeta(x) w(x)\, dx, \tag{4.2.2}$$

and the kernel $\zeta : \Omega \mapsto \mathbb{R}$ is a $L^2(\Omega)$ function such that $\mathcal{L}$ is bounded in $L^2(\Omega)$.

In order to develop the mathematical analysis, we assume that the $\nu$-neighborhood $\Omega_\nu$ of $\Omega$, $\Omega_\nu := \{x \in \Omega^{\text{obs}} : \text{dist}(x, \Omega) < \nu\}$, is compactly embedded in $\Omega^{\text{obs}}$, $\Omega_\nu \subset\subset \Omega^{\text{obs}}$, for some $\nu > 0$.

We model the experimental observations at "point" $x_j^{\text{obs}}$ as

$$\ell_j^{\text{obs}} = \ell(u^{\text{true}}, \nu, x_j^{\text{obs}}) + \varepsilon_j, \qquad j = 1, \ldots, J. \tag{4.2.3}$$

The random variables $\varepsilon_1, \ldots, \varepsilon_J$ are $J$ independent identically distributed (i.i.d.) random variables such that $\varepsilon_j \sim (0, \sigma^2)$ for $j = 1, \ldots, J$. The functional $\ell(\cdot, \nu, x_j^{\text{obs}}) : L^2(\Omega^{\text{obs}}) \to \mathbb{R}$ is defined as the convolution

$$\ell(w, \nu, x_j^{\text{obs}}) = \int_{\Omega^{\text{obs}}} \omega_{d,\nu}(|x - x_j^{\text{obs}}|) w(x)\, dx. \tag{4.2.4a}$$

The convolutional kernel $\omega_{d,\nu}$ is given by

$$\omega_{d,\nu}(r) = \frac{C(d)}{\nu^d} \omega\left(\frac{r}{\nu}\right), \tag{4.2.4b}$$

where $\nu, C(d) > 0$ are given constants, and $\omega(\cdot)$ is a positive function such that $\omega(\rho) = 0$ for $\rho \geq 1$. We emphasize that the constant $\nu > 0$ reflects the filter width of the transducer, assumed small compared to the characteristic length-scale of the true field, while $x_j^{\text{obs}} \in \Omega$ reflects the transducer position. Finally, the function $\omega$ describes the local averaging process and is analogous to the spread function employed in blurring/deblurring of images. In anticipation of the analysis, we also introduce the low-pass filter operator $\mathcal{F}_\nu : L^2(\Omega^{\text{obs}}) \to L^2(\Omega)$ such that

$$\mathcal{F}_\nu(w)(x) = \ell(w, \nu, x), \qquad \forall\, x \in \Omega. \tag{4.2.5}$$

We can now introduce the limited observations error estimator $\widehat{E}_{\mathcal{L}}$ as

$$\widehat{E}_{\mathcal{L}}(J, \nu) := \frac{|\Omega|}{J} \sum_{j=1}^{J} \zeta(x_j^{\text{obs}})\, \ell_j^{\text{err}}. \tag{4.2.6}$$

Here, $\ell_1^{\text{err}}, \ldots, \ell_J^{\text{err}}$ are defined as

$$\ell_j^{\text{err}} = \ell_j^{\text{obs}} - \ell(u^\star, \nu, x_j^{\text{obs}}). \tag{4.2.7a}$$

We observe that $\{\ell_j^{\text{obs}}\}_j$ are taken experimentally, while $\{\ell(u^\star, \nu, x_j^{\text{obs}})\}_j$ are computed numerically. Recalling (4.2.5) and (4.2.3), we also observe that

$$\ell_j^{\text{err}} = \ell(u^{\text{true}}, \nu, x_j^{\text{obs}}) + \varepsilon_j - \ell(u^\star, \nu, x_j^{\text{obs}}) = \mathcal{F}_\nu(e)(x_j^{\text{obs}}) + \varepsilon_j. \tag{4.2.7b}$$

In order to address the problem of estimating $E_{\mathcal{L}}$ using the pointwise estimator $\widehat{E}_{\mathcal{L}}$, we identify three different sources of error.

**Finite-$\nu$ error**: since the transducers have finite spatial width, we can only measure an approximation of the pointwise values of $u^{\text{true}}$.

**Finite-$J$ error**: since the number of measurements is limited, only a finite number of error evaluations are available.

**Finite-noise error**: since measurements are affected by homoscedastic error, we can only observe a noisy value of $\ell(u^{\text{true}}, \nu, x_j^{\text{obs}})$.

To formalize these definitions, we introduce the perfect unlimited observations error estimator

$$\widehat{E}_{\mathcal{L}}^{\infty}(\nu) = \mathcal{L}(\mathcal{F}_\nu(e)), \tag{4.2.8}$$

and then the finite-$\nu$ error

$$\Delta_{\mathcal{L}}^{\nu}(\nu) := |E_{\mathcal{L}} - \widehat{E}_{\mathcal{L}}^{\infty}(\nu)|, \tag{4.2.9}$$

and the combined finite-$J$ and finite-noise error

$$\Delta_{\mathcal{L}}^{J,\sigma}(J, \nu) := |\widehat{E}_{\mathcal{L}}^{\infty}(\nu) - \widehat{E}_{\mathcal{L}}(J, \nu)|. \tag{4.2.10}$$

We emphasize that $\Delta_{\mathcal{L}}^{\nu}$ is deterministic, while $\Delta_{\mathcal{L}}^{J,\sigma}$ is random.

We now present the outline of the remainder of this section. In section 4.2.2, we propose an actionable procedure to estimate a confidence interval for $\widehat{E}_{\mathcal{L}}^{\infty}(\nu)$. Then, in section 4.2.3,

we illustrate how to exploit the confidence interval for $\widehat{E}_{\mathcal{L}}^{\infty}(\nu)$ to update the estimate of the output $\mathcal{L}(u^{\text{true}})$. In these two sections, we assume that the finite-$\nu$ error is negligible. Finally, in section 4.2.4, we provide conditions under which the finite-$\nu$ error is small.

### 4.2.2 Construction of the confidence interval

#### Finite-noise and finite-$J$ error

In order to derive an asymptotic bound for the finite-noise and finite-$J$ error, it is first convenient to introduce a probabilistic interpretation of the quantities introduced in section 4.2.1. Towards this end, we assume that the observation points $\{x_j^{\text{obs}}\}_{j=1}^J$ are realizations of the $J$ i.i.d. random variables $X_1, \dots, X_J \sim \text{Uniform}(\Omega)$ such that $X_i$ and $\varepsilon_j$ are independent for each $i, j = 1, \dots, J$. As a consequence, recalling (4.2.7), we have that $\{\ell_j^{\text{err}}\}_{j=1}^J$ are realizations of the i.i.d. random variables $L_j^{\text{err}} = \mathcal{F}_\nu(e)(X_j) + \varepsilon_j$ and

$$\hat{E}_{\mathcal{L}}^{\infty}(\nu) = \mathbb{E}\left[|\Omega|\,\zeta(X_j)\,L_j^{\text{err}}\right] = \mathbb{E}\left[Z_j^{\text{obs}}\right], \tag{4.2.11}$$

where $Z_j^{\text{obs}} = |\Omega|\zeta(X_j)L_j^{\text{err}}$ is introduced to simplify the notation.

We observe that $\widehat{E}_{\mathcal{L}}$ is the sample mean associated with the realizations $\{z_j^{\text{obs}} = |\Omega|\,\zeta(x_j^{\text{obs}})\ell_j^{\text{err}}\}_{j=1}^J$; therefore, $\widehat{E}_{\mathcal{L}}$ is an unbiased estimator for $\widehat{E}_{\mathcal{L}}^{\infty}(\nu)$, and we can apply the Central Limit Theorem (see, e.g., [119, Theorem 21.1]) to derive an approximate confidence interval for $\hat{E}_{\mathcal{L}}^{\infty}$. We thus obtain:

$$\begin{aligned}\widehat{C}_{\mathcal{L}}^{J,\sigma}(J,\nu,\alpha) &= \left[\widehat{E}_{\mathcal{L},\text{LB}}^{J,\sigma}(J,\nu,\alpha), \widehat{E}_{\mathcal{L},\text{UB}}^{J,\sigma}(J,\nu,\alpha)\right] \\ &= \left[\widehat{E}_{\mathcal{L}}(J,\nu) - \frac{1}{\sqrt{J}}\,\widehat{se}_{\mathcal{L},J}^{\text{obs}} t_{1-\alpha/2}(J-1), \widehat{E}_{\mathcal{L}}(J,\nu) + \frac{1}{\sqrt{J}}\,\widehat{se}_{\mathcal{L},J}^{\text{obs}} t_{1-\alpha/2}(J-1)\right]\end{aligned} \tag{4.2.12}$$

where $t_{1-\alpha/2}(J-1)$ is the $(1-\alpha/2)$ quantile of the t-distribution with $J-1$ degrees of freedom, and $\widehat{se}_{\mathcal{L},J}^{\text{obs}} = \sqrt{\frac{1}{J-1}\sum_{j=1}^J (z_j^{\text{obs}} - \bar{z}^{\text{obs}})^2}$, $\bar{z}^{\text{obs}} = \frac{1}{J}\sum_{j=1}^J z_j^{\text{obs}}$.

The confidence interval $\widehat{C}_{\mathcal{L}}^{J,\sigma}$ is asymptotically correct for $\widehat{E}_{\mathcal{L}}^{\infty}$, its size vanishes as $J$ goes to infinity, and it can be computed in real time ($\mathcal{O}(J)$-computational complexity). In addition, the quantity $\frac{1}{\sqrt{J}}\widehat{se}_{\mathcal{L},J}^{\text{obs}} t_{1-\alpha/2}(J-1)$ asymptotically bounds the finite-$J$ and finite-noise error $\Delta_{\mathcal{L}}^{J,\sigma}$ in (4.2.10) with confidence $1-\alpha$. We remark that this procedure can be extended to the case of multiple outputs. We refer to [51] for a thorough analysis of multivariate normal confidence regions. We further observe that other non-parametric

strategies for the construction of confidence regions can be applied in lieu of the normal confidence intervals employed in this work. In this respect , we mention bootstrap confidence intervals (see [71, 69] and [228, Chapter 8] ).

Our construction relies on the assumption that we can take measurements in arbitrary spatial points. Next remark shows how to extend our approach to the case in which sensor locations should be selected among a set of candidate grid points.

**Remark 4.2.1.** *We shall now discuss the case in which sensor locations should be selected among a set of candidate grid points* $\{x_i^{\text{grid}}\}_{i=1}^{\mathcal{N}}$. *With this in mind, we shall define the functional* $\mathcal{L}^{\text{grid}} : C(\Omega) \to \mathbb{R}$ *as*

$$\mathcal{L}^{\text{grid}}(u) = |\Omega| \sum_{i=1}^{\mathcal{N}} u(x_i^{\text{grid}})\, \zeta(x_i^{\text{grid}})\, w_i, \tag{4.2.13}$$

*where* $\{w_i\}_{i=1}^{\mathcal{N}}$ *is a set of suitable weights such that* $\sum_{i=1}^{\mathcal{N}} w_i = 1$. *We shall further define the probability distribution* $P^{\text{grid}}$ *such that* $P^{\text{grid}}(x_i^{\text{grid}}) = w_i$, $i = 1, \ldots, \mathcal{N}$.

*Exploiting the definitions above, it is straightforward to verify that if* $X_1, \ldots, X_J$ *are i.i.d. random variables such that* $X_j \sim P^{\text{grid}}$ *then*

$$\mathbb{E}\left[|\Omega|\zeta(X_j)L_j^{\text{err}}\right] = \mathcal{L}^{\text{grid}}(\mathcal{F}_\nu(e)), \quad j = 1, \ldots, J.$$

*Therefore, provided that* $|\mathcal{L}^{\text{grid}}(\mathcal{F}_\nu(e)) - \mathcal{L}(\mathcal{F}_\nu(e))|$ *is small, we can rely on* $\widehat{C}_{\mathcal{L}}^{J,\sigma}$ *to estimate* $\widehat{E}_{\mathcal{L}}^{\infty}(\nu)$. *This observation suggests (for smooth problems) a grid informed by high-order quadrature schemes.*

### Computational procedure

Algorithm 4.2.1 outlines the computational procedure to generate the confidence interval $\widehat{C}_{\mathcal{L}}^{J,\sigma}$ for $\widehat{E}_{\mathcal{L}}^{\infty}(\nu)$. Provided that $\Delta_{\mathcal{L}}^{\nu}(\nu)$ is negligible, we can rely on the same procedure to estimate $E_{\mathcal{L}}$.

The computational cost associated with the procedure is very limited. If the approximated field $u^\star$ is discretized through the Finite Element method ([18]), calculation of $\ell(u^\star, \nu, x_j^{\text{obs}})$ requires a search to find the element of the FE triangulation to which $x_j^{\text{obs}}$ belongs. For structured grids, this operation is independent of the mesh size, while for unstructured grids it scales in general with the size of the mesh. In both cases, the cost is

negligible if compared to the cost of acquiring experimental data.

If sensor locations should be selected among a set of grid points $\{x_i^{\text{grid}}\}_{i=1}^{\mathcal{N}}$ (cf. Remark 4.2.1), we first introduce the functional $\mathcal{L}^{\text{grid}}$ (4.2.13) by selecting the weights $\{w_i\}_{i=1}^{\mathcal{N}}$; then we draw $\{x_j^{\text{obs}}\}_j$ from $X_1, \dots, X_J \sim P^{\text{grid}}$, and we collect the corresponding experimental results $\{\ell_j^{\text{obs}}\}_j$. The remainder of the Algorithm (steps 2-4) remains unchanged.

**Algorithm 4.2.1** Confidence region for $\widehat{E}_{\mathcal{L}}^{\infty}(\nu)$

| | | |
|---|---|---|
| **Input** | $J$ | number of measurements |
| | $u^\star : \Omega^{\text{obs}} \mapsto \mathbb{R}$ | approximated field |
| **Output** | $\widehat{C}_{\mathcal{L}}^{J,\sigma}$ | confidence interval for $\widehat{E}_{\mathcal{L}}^{\infty}(\nu)$ |

1: Draw $\{x_j^{\text{obs}}\}_{j=1}^{J}$ from $X_1, \dots, X_J \sim \text{Uniform}(\Omega)$, and collect the experimental results $\{\ell_j^{\text{obs}}\}_{j=1}^{J}$.

2: Compute $\ell_j^{\text{err}} = \ell_j^{\text{obs}} - \ell(u^\star, \nu, x_j^{\text{obs}})$ for $j = 1, \dots, J$.

3: $\widehat{E}_{\mathcal{L}}(J, \nu) := \frac{|\Omega|}{J} \sum_{j=1}^{J} \ell_j^{\text{err}} \zeta(x_j^{\text{obs}})$.

4: Compute the confidence region $\widehat{C}_{\mathcal{L}}^{J,\sigma}$ of (4.2.12).

### 4.2.3 Variance analysis and output updates

Proposition 4.2.1 provides a formula for the asymptotic behavior of the square of $\widehat{se}_{\mathcal{L},J}^{\text{obs}}$ defined in (4.2.12).

**Proposition 4.2.1.** *Let $\{X_j\}_j$ and $\{\varepsilon_j\}_j$ be two i.i.d. random sequences such that $X_j \sim$ Uniform$(\Omega)$ and $\varepsilon_j \sim (0, \sigma^2)$. Then, if $X_j$ and $\varepsilon_j$ are independent for all $j$, we have*

$$\lim_{J \to \infty} \left( \widehat{se}_{\mathcal{L},J}^{\text{obs}} \right)^2 = |\Omega|^2 \left( \mathbb{V}\left[ \zeta(X)\, \mathcal{F}_\nu(e)(X) \right] + \mathbb{E}[\zeta(X)^2]\, \sigma^2 \right), \tag{4.2.14}$$

*where the limit is in the almost sure sense.*

*Proof.* Recalling the law of large numbers, it is sufficient to show that

$$\mathbb{V}[Z^{\text{obs}}] = |\Omega|^2 \left( \mathbb{V}\left[ \zeta(X)\, \mathcal{F}_\nu(e)(X) \right] + \mathbb{E}[\zeta(X)^2]\, \sigma^2 \right),$$

where $Z^{\text{obs}} = |\Omega| \zeta(X)(\mathcal{F}_\nu(e)(X) + \varepsilon)$, and $X \sim \text{Uniform}(\Omega)$ and $\varepsilon \sim (0, \sigma^2)$ are two inde-

pendent random variables. Since $X, \varepsilon$ are independent, $\mathbb{E}[f(X)\, g(\varepsilon)] = \mathbb{E}[f(X)]\, \mathbb{E}[g(\varepsilon)]$ for any pair $(f, g)$ of measurable functions (see, e.g., [119, Theorem 10.1]). Therefore, we obtain

$$\begin{aligned}\mathbb{E}[Z^{\text{obs}}] = &\ \mathbb{E}[|\Omega|\zeta(X)(\mathcal{F}_\nu(e)(X) + \varepsilon)] \\ = &\ |\Omega|\Big(\mathbb{E}[\zeta(X)\mathcal{F}_\nu(e)(X))] + \mathbb{E}[\zeta(X)]\ \underbrace{\mathbb{E}[\varepsilon]}_{=0}\Big) = |\Omega|\mathbb{E}[\zeta(X)\mathcal{F}_\nu(e)(X)],\end{aligned}$$

and

$$\begin{aligned}\mathbb{E}[\big(Z^{\text{obs}}\big)^2] = &\ |\Omega|^2\Big(\mathbb{E}[(\zeta(X)\mathcal{F}_\nu(e)(X))^2] + \mathbb{E}[\zeta(X)^2]\ \underbrace{\mathbb{E}[\varepsilon^2]}_{=\sigma^2} + 2\mathbb{E}[\zeta(X)^2\mathcal{F}_\nu(e)(X)]\ \underbrace{\mathbb{E}[\varepsilon]}_{=0}\Big). \\ = &\ |\Omega|^2\Big(\mathbb{E}[(\zeta(X)\mathcal{F}_\nu(e)(X))^2] + \mathbb{E}[\zeta(X)^2]\sigma^2\Big).\end{aligned}$$

Thesis follows recalling that $\mathbb{V}[W] = \mathbb{E}[W^2] - (\mathbb{E}[W])^2$ for any random variable $W$. □

The limit (4.2.14) and the confidence interval (4.2.12) show that the variance of the Monte Carlo process is the sum of two contributions: the first one is related to the accuracy of the state estimate $u^\star$, the second one is related to the magnitude of the noise. The first term vanishes when $u^{\text{true}} = u^\star$ (perfect approximation), while the second term vanishes when the measurements are noise-free. Provided that the noise is small, if the error $e = u^{\text{true}} - u^\star$ is also small, we can accurately estimate the error for modest values of $J$.

Due to the linearity of $\mathcal{L}$, and provided that the finite-$\nu$ error is negligible, we can also use our error estimator $\widehat{E}_{\mathcal{L}}$ to improve the estimate for the output. We have indeed that

$$\lim_{J\to\infty} \mathcal{L}(u^\star) + \widehat{E}_{\mathcal{L}}(J, \nu) = \mathcal{L}(u^\star - \mathcal{F}_\nu(u^\star)) + \mathcal{L}(\mathcal{F}_\nu(u^{\text{true}})) \simeq \mathcal{L}(u^{\text{true}}). \tag{4.2.15}$$

Clearly, the variance associated with the process $\mathcal{L}(u^\star) + \widehat{E}_{\mathcal{L}}(J, \nu)$ satisfies (4.2.14). On the other hand, if we apply the Monte Carlo procedure to the true field, we obtain

$$\lim_{J\to\infty} \left(\widehat{se}^{\text{obs}}_{\mathcal{L},J}\right)^2 = |\Omega|^2 \left(\mathbb{V}\left[\zeta(X)\, \mathcal{F}_\nu(u^{\text{true}})(X)\right] + \mathbb{E}[\zeta(X)^2]\, \sigma^2\right).$$

Thus, by applying the Monte Carlo procedure to the output error instead of to the true field, we can significantly reduce the variance associated to the process and thus improve the output estimate even for modest values of $J$. This idea is related to control variates method for variance reduction ([189]), and also to multi-level Monte Carlo approaches ([94,

95, 13, 224, 161]). In section 4.5, we assess numerically the practical relevance of (4.2.15).

### 4.2.4 Analysis of the finite-$\nu$ error

In section 4.2.2, we have proposed an actionable procedure to compute a confidence region $\widehat{\mathcal{C}}_{\mathcal{L}}^{J,\sigma}$ for $\widehat{E}_{\mathcal{L}}^{\infty}(\nu)$. In this section, we investigate under what assumptions we can neglect the finite-$\nu$ error $\Delta_{\mathcal{L}}^{\nu}(\nu) = |E_{\mathcal{L}} - \widehat{E}_{\mathcal{L}}^{\infty}(\nu)|$ and then interpret $\widehat{\mathcal{C}}_{\mathcal{L}}^{N,\sigma}$ as an appropriate confidence interval for $E_{\mathcal{L}}$. We refer to Appendix A for a rigorous discussion of the finite-$\nu$ error.

We present the error bound for $\Delta_{\mathcal{L}}^{\nu}(\nu)$. We assume that the filter width $\nu$ is such that $\Omega_\nu \subset\subset \Omega$; we further assume that $\omega(r) \leq M$ for all $r \geq 0$ and for some $M > 0$. Then, if $\nabla e \in L^q(\Omega_\nu)$ for some $q > d$, we have

$$|E_{\mathcal{L}} - \hat{E}_{\mathcal{L}}^{\infty}| \leq C_\omega \nu^{1-d/q} |\Omega|^{1/2} \|\zeta\|_{L^2(\Omega)} \|\nabla e\|_{L^q(\Omega_\nu)}, \tag{4.2.16}$$

where $C_\omega$ depends on the exponent $q$, on the dimension $d$, and on the filter shape $\omega$. We observe that bound (4.2.16) is not actionable since $\|\nabla e\|_{L^q(\Omega_\nu)}$ is unknown; in section 4.5, we investigate numerically the actual magnitude of $\Delta_{\mathcal{L}}^{\nu}(\nu)$ for the problems considered.

Unlike finite-$J$ and finite-noise error, finite-$\nu$ error admits a physical interpretation: it is a balance between the filter width $\nu$ and the characteristic spatial length scale of the error field. Furthermore, finite-$\nu$ error is related to the so-called *minimum detectable signal* in radar systems [185] since it represents a way of assessing the maximum accuracy of our estimate. However, in radar systems this concept has a different physical interpretation: it is the ratio between signal and noise.

## 4.3 *A posteriori* $L^2$ error estimation

### 4.3.1 General framework

We now tailor the analysis of section 4.2 to the *a posteriori* error estimation of the $L^2(\Omega)$-error $E = \|u^{\text{true}} - u^\star\|_{L^2(\Omega)}$. Due to the nonlinearity of $E$, the procedure is more involved; however, the same ideas apply also to this case.

Given $\{\ell_j^{\text{err}}\}_{j=1}^J$ introduced in (4.2.7), we define the limited observations error estimator

$$\widehat{E}(J,\nu) := \sqrt{\frac{|\Omega|}{J}\sum_{j=1}^{J}(\ell_j^{\text{err}})^2}. \tag{4.3.1}$$

Then, we define the perfect unlimited observations error estimator

$$\widehat{E}^{\infty}(\nu) := \|\mathcal{F}_\nu(e)\|_{L^2(\Omega)}. \tag{4.3.2}$$

Finally, we define the finite-$\nu$ error

$$\Delta^{\nu}(\nu) := |E - \widehat{E}^{\infty}(\nu)|, \tag{4.3.3}$$

and the combined finite-$N$ and finite-noise error

$$\Delta^{J,\sigma}(J,\nu) := |\widehat{E}^{\infty}(\nu) - \widehat{E}(J,\nu)|. \tag{4.3.4}$$

In the remainder of this section, we first propose a confidence interval for $\widehat{E}^{\infty}(\nu)$, and we present an error bound for $\Delta^{\nu}(\nu)$.

### 4.3.2 Construction of the confidence interval

#### Finite-noise and finite-$J$ error

We first consider the case in which the variance $\sigma^2$ associated with the random noise is known *a priori*. Given $J$ i.i.d. random variables $X_1,\ldots,X_J \sim \text{Uniform}(\Omega)$, we define the random variables $Y_j^{\text{obs}} = |\Omega|(\,(L_j^{\text{err}})^2 - \sigma^2\,)$, where $L_j^{\text{err}} = \mathcal{F}_\nu(e)(X_j) + \varepsilon_j$. We observe that $\mathbb{E}\left[Y_j^{\text{obs}}\right] = \left(\widehat{E}^{\infty}(\nu)\right)^2$. Therefore, assuming that $\sigma^2$ is known and exploiting the positivity of $\widehat{E}^{\infty}(\nu)$, we can apply the Central Limit Theorem to derive an approximate confidence interval for $\widehat{E}^{\infty}(\nu)$:

$$\widehat{C}^{J,\sigma}(J,\nu,\alpha,\sigma) = \left[\sqrt{\left(\left(\widehat{E}_{\text{mod}}(J,\nu,\sigma)\right)^2 - \frac{1}{\sqrt{J}}t_{1-\alpha/2}(J-1)\widehat{se}_{Y^{\text{obs}},J}\right)_+}, \sqrt{\left(\left(\widehat{E}_{\text{mod}}(J,\nu,\sigma)\right)^2 + \frac{1}{\sqrt{J}}t_{1-\alpha/2}(J-1)\widehat{se}_{Y^{\text{obs}},J}\right)_+}\right] \tag{4.3.5a}$$

Here, $(a)_+ = \max\{a, 0\}$, the modified estimator $\widehat{E}_{\text{mod}}$ is defined as

$$\widehat{E}_{\text{mod}}(J, \nu, \sigma) = \sqrt{\left(\left(\widehat{E}(J, \nu)\right)^2 - |\Omega|\sigma^2\right)_+}, \tag{4.3.5b}$$

while $t_{1-\alpha/2}(J-1)$ is the $(1-\alpha/2)$ quantile of the t-distribution with $J-1$ degrees of freedom, and $\widehat{se}_{Y^{\text{obs}},J}$ is the sample standard deviation associated with $Y^{\text{obs}}$:

$$\widehat{se}_{Y^{\text{obs}},J} := \sqrt{\frac{1}{J-1}\sum_{j=1}^{J}\left(|\Omega|\,(\ell_j^{\text{err}})^2 - \left(\widehat{E}(J, \nu)\right)^2\right)^2}. \tag{4.3.5c}$$

We now consider the case in which $\sigma \in [\sigma_{\text{LB}}, \sigma_{\text{UB}}]$ for some known constants $\sigma_{\text{LB}}, \sigma_{\text{UB}} > 0$. Since $\widehat{se}_{Y^{\text{obs}},J}$ is independent of $\sigma^2$, the noise variance $\sigma^2$ only shifts the confidence region $\widehat{C}^{J,\sigma}$ along the real axis. Therefore, finite-$J$ and finite-noise errors can be asymptotically decoupled in the limit of $J \to \infty$. The latter observation helps us manage uncertainty through the value of $\sigma^2$: if we are confident that $\sigma \in [\sigma_{\text{LB}}, \sigma_{\text{UB}}]$, we can modify (4.3.5) as follows:

$$\widehat{C}^{J,\sigma}(J, \nu, \alpha, \sigma) = \left[\sqrt{\left(\left(\widehat{E}_{\text{mod,LB}}(J, \nu, \sigma)\right)^2 - \frac{1}{\sqrt{J}}t_{1-\alpha/2}(J-1)\widehat{se}_{Y^{\text{obs}},J}\right)_+}, \sqrt{\left(\left(\widehat{E}_{\text{mod,UB}}(J, \nu, \sigma)\right)^2 + \frac{1}{\sqrt{J}}t_{1-\alpha/2}(J-1)\widehat{se}_{Y^{\text{obs}},J}\right)_+}\right] \tag{4.3.6a}$$

where $\widehat{E}_{\text{mod,LB}}(J, \nu, \sigma)$, and $\widehat{E}_{\text{mod,UB}}(J, \nu, \sigma)$ are defined as

$$\widehat{E}_{\text{mod,LB}}(J, \nu, \sigma) = \sqrt{\left(\left(\widehat{E}(J, \nu)\right)^2 - |\Omega|\sigma_{\text{UB}}^2\right)_+}, \quad \widehat{E}_{\text{mod,UB}}(J, \nu, \sigma) = \sqrt{\left(\left(\widehat{E}(J, \nu)\right)^2 - |\Omega|\sigma_{\text{LB}}^2\right)_+} \tag{4.3.6b}$$

### Computational procedure

Algorithm 4.3.1 summarizes the computational procedure. Unlike the case of $L^2$ outputs, we must provide an estimate for $\sigma^2$. As for $L^2$ functionals, if the finite-$\nu$ error is modest, we can employ the same procedure to estimate $E$.

**Algorithm 4.3.1** Confidence region for $\widehat{E}^{\infty}(\nu)$

| | | |
|---|---|---|
| **Input** | $J$ | number of measurements |
| | $\sigma_{\text{LB}}, \sigma_{\text{UB}}$ | lower and upper bound for the noise standard deviation $\sigma$ |
| | $u^\star : \Omega^{\text{obs}} \mapsto \mathbb{R}$ | approximated field |
| **Output** | $\widehat{C}^{J,\sigma}$ | confidence interval for $\widehat{E}^{\infty}(\nu)$ |

1: Draw $\{x_j^{\text{obs}}\}_j$ from $X_1, \ldots, X_J \sim \text{Uniform}(\Omega)$, and collect the experimental results $\{\ell_j^{\text{obs}}\}_j$.

2: Compute $\ell_j^{\text{err}} = \ell_j^{\text{obs}} - \ell(u^\star, \nu, x_j^{\text{obs}})$ for $j = 1, \ldots, J$.

3: $\widehat{E}(J, \nu) := \sqrt{\frac{|\Omega|}{J} \sum_{j=1}^{J} (\ell_j^{\text{err}})^2}$.

4: Compute the confidence region $\widehat{C}^{J,\sigma}$ of (4.3.6).

### 4.3.3 Analysis of the finite-$\nu$ error

Following the discussion in section 4.2.4, we assume that (i) $\Omega_\nu \subset\subset \Omega$, (ii) $\omega(r) \leq M$ for all $r \geq 0$ and for some $M > 0$, and (iii) $\nabla e \in L^q(\Omega_\nu)$ for some $q > d$. Then, it is possible to prove the following estimate

$$\Delta^\nu(\nu) \leq C_\omega \sqrt{|\Omega|}\, \nu^{1-d/q}\, \|\nabla e\|_{L^q(\Omega_\nu)}, \tag{4.3.7}$$

where $C_\omega > 0$. As for $L^2$ functionals, finite-$\nu$ error $\Delta^\nu(\nu)$ depends on the balance between filter width $\nu$ and characteristic spatial length scale of the error field. We refer to Appendix A for the proof of (4.3.7), and to the numerical results for a rigorous assessment of the practical effect of this contribution for a controlled synthetic example.

## 4.4 Application to subsequent state estimation

We consider the scenario in which during the offline stage (cf. Algorithm 2.4.1, Chapter 2.4) we have the opportunity to acquire data from a number of system configurations (associated with different values of the parameter). Our goal is to exploit these offline experimental data to reduce the number of observations for future configurations. Towards this end, we wish to augment the background space $\mathcal{Z}_{N_{\text{bk}}}$ based on the results of the PBDW data assimilation procedure. To differentiate between offline and online measurements, we denote by $M_{\text{off}}$ the amount of experimental measurements available offline, and by $M_{\text{on}}$ the amount

of experimental measurements available during the online stage. We here assume that $M_{\text{on}} < M_{\text{off}}$.

Algorithm 4.4.1 summarises the computational procedure used to augment the background space during the offline stage. This procedure was first proposed in [143, section 5.8]. The function $[u^\star] = \texttt{PBDW}\,(\mathcal{Z}_N, \{x_m^{\text{obs}}\}_{m=1}^M, \{\ell_m^{\text{obs}}\}_{m=1}^M)$ indicates the application of the PBDW state estimation procedure based on the background $\mathcal{Z}_N$, and on the measurements $\{\ell_m^{\text{obs}} = \ell(u^{\text{true}}, \nu, x_m^{\text{obs}})\}_{m=1}^M$; the function $\widehat{E}(J, \nu) = \texttt{a-posteriori}(u^\star, \{x_j^{\text{obs}}\}_{j=1}^J, \{\ell_j^{\text{obs}}\}_{j=1}^J)$ refers to the application of Algorithm 4.3.1 for $\sigma_{\text{LB}} = \sigma_{\text{UB}} = 0$, and $\{\ell_j^{\text{obs}} = \ell(u^{\text{true}}, \nu, x_j^{\text{obs}})\}_{j=1}^J$. Finally, we denote by $\{\mathcal{C}_k\}_{k=1}^K$ the system configurations associated with the available offline experiments, and we denote by $u^{\text{true}}(\mathcal{C}_k)$ and $u^\star(\mathcal{C}_k)$ the true state and the state estimate associated with the configuration $\mathcal{C}_k$. The procedure can be easily extended to noisy measurements. In section 4.6, we present numerical results for a synthetic acoustic problem; we refer to [143, section 5.8] for an application to a physical system.

**Algorithm 4.4.1** Data-Driven Empirical Enrichment of the background space

| | | |
|---|---|---|
| **Input** | $\mathcal{Z}_{N_{\text{bk}}}$ | background space |
| | $M_{\text{off}}$ ($J_{\text{off}}$) | number of offline measurements used for training (validation) |
| | $M_{\text{on}}$ | number of online measurements used for training |
| | $N_{\max}$ | maximum dimension of the background space |
| | $\{\mathcal{C}_k\}_{k=1}^K$ | system configurations available for comprehensive testing |
| **Output** | $\mathcal{Z}_{N_{\max}}$ | enriched background space |

1: **for** $N = N_{\text{bk}}, \ldots, N_{\max} - 1$ **do**
2: Choose transducers' locations $\{x_m^{\text{obs}}\}_{m=1}^{M_{\text{off}}}$, $\{x_j^{\text{obs}}\}_{j=1}^{J_{\text{off}}}$
3: **for** $k = 1, \ldots, K$ **do**
4: Compute the state estimate $[u^\star(\mathcal{C}_k)] = \texttt{PBDW}\,(\mathcal{Z}_N, \{x_m^{\text{obs}}\}_{m=1}^{M_{\text{on}}}, \{\ell_m^{\text{obs}}(\mathcal{C}_k)\}_{m=1}^{M_{\text{on}}})$
5: Estimate the $L^2$ error $\widehat{E}_k(J_{\text{off}}, \nu) = \texttt{a-posteriori}(u^\star, \{x_j^{\text{obs}}\}_{j=1}^{J_{\text{off}}}, \{\ell_j^{\text{obs}}(\mathcal{C}_k)\}_{j=1}^{J_{\text{off}}})$.
6: **end for**
7: Compute $k^\star := \arg\max_{k=1,\ldots,K} \dfrac{\widehat{E}_k(J_{\text{off}}, \nu)}{\|u^\star(\mathcal{C}_k)\|_{L^2(\Omega)}}$
8: Compute the state estimate $[u^\star(\mathcal{C}_{k^\star})] = \texttt{PBDW}\,(\mathcal{Z}_N, \{x_m^{\text{obs}}\}_{m=1}^{M_{\text{off}}}, \{\ell_m^{\text{obs}}(\mathcal{C}_{k^\star})\}_{m=1}^{M_{\text{off}}})$
9: Compute $\mathcal{Z}_{N+1} \equiv \mathcal{Z}_N \oplus \text{span}\{u^\star(\mathcal{C}_{k^\star}) - \Pi_{\mathcal{Z}_N} u^\star(\mathcal{C}_{k^\star})\}$.
10: **end for**

At each iteration of the external `for` loop, we first estimate the state for each configuration $\mathcal{C}_k$ based on $M_{\text{on}}$ measurements, and we estimate the $L^2$ error $\|u^{\text{true}}(\mathcal{C}_k) - u^\star(\mathcal{C}_k)\|_{L^2(\Omega)}$. Then, we compute the index $k^\star$ that maximizes the error estimate over all configurations. Finally, we estimate the state for the $k^\star$-th configuration based on $M_{\text{off}}$ measurements and we augment the space $\mathcal{Z}_N$ with the update $\eta^\star(\mathcal{C}_{k^\star}) = u^\star(\mathcal{C}_{k^\star}) - \Pi_{\mathcal{Z}_N} u^\star(\mathcal{C}_{k^\star})$. We note that the error estimator $\widehat{E}$ plays the same role as the error bound $\Delta_N^{\text{bk}}(\mu)$ in the weak-Greedy algorithm (cf. Algorithm 2.1.1, Chapter 2.1.2). This is possible because Greedy techniques do not exploit the structure of the parameter (or configuration) space, which is not in general observable in the current framework. We further observe that we perform state estimation based on $M_{\text{off}}$ measurements only once per iterations.

The value $N_{\max}$ should be chosen based on (i) the offline computational and experimental budget (i.e., the amount of offline experiments that can be performed), and (ii) the amount of online experimental measurements $M_{\text{on}}$. To explain the latter, we shall remember that we should at least guarantee that the PBDW state estimation procedure is stable: this implies that the inf-sup constant $\beta_{N,M_{\text{on}}}$ should exceed a given threshold for $N = N_{\text{bk}}, \ldots, N_{\max}$. The condition $\beta_{N,M_{\text{on}}} \geq tol$ for $N = N_{\text{bk}}, \ldots, N_{\max}$ can then be easily imposed as additional termination condition in the external `for` loop in Algorithm 4.4.1.

## 4.5 Numerical results (I): error estimation

### 4.5.1 Application to a synthetic thermal problem

We first assess our computational procedures through a synthetic problem. Towards this end, we consider the parametric problem:

$$\begin{cases} -\nabla \cdot (\kappa(\mu)\nabla u(\mu)) = 0 & \text{in } \Omega^{\text{obs}} \\ \kappa(\mu)\frac{\partial u(\mu)}{\partial n} = g & \text{on } \Gamma_1 \cup \Gamma_2 \cup \Gamma_3 \\ u(\mu) = 0 & \text{on } \Gamma_4 \end{cases} \tag{4.5.1a}$$

where $\Omega^{\text{obs}} = \bigcup_{i=1}^{9} \Omega_i$, and

$$\kappa(x,\mu) = \begin{cases} 1 & \text{in } \Omega_1, \\ \mu_i & \text{in } \Omega_{i+1},\ i = 1,\ldots,8; \end{cases} \qquad g(x) = \begin{cases} 1 & \text{on } \Gamma_1, \\ 0 & \text{on } \Gamma_2, \\ 1 - 2x_1 & \text{on } \Gamma_3. \end{cases} \tag{4.5.1b}$$

Figure 4-1 shows the computational domain. We consider the domain of interest $\Omega = \Omega_5$. In order to assess our method, we generate the true field $u^{\text{true}}$ and the approximate field $u^\star$ by considering the solution to (4.5.1) obtained using a Finite Element (FE) solver for different choices of the parameter $\mu$:

$$u^{\text{true}} = u(\mu^{\text{true}} = [1,1,1,1,1,1,1,1,1]), \quad u^\star = u(\mu^\star = [1, 1.2, 1.5, 0.6, 1.6, 1.3, 1.1, 1]).$$

We resort to a $\mathbb{P}^3$ Finite Element discretization with $\mathcal{N} = 37249$ degrees of freedom. Figure 4-2 shows the true field and the error field over $\Omega^{\text{obs}}$ and highlights the domain of interest $\Omega$.

Local experimental observations are assumed to be truncated Gaussians with $\nu = 2r_{\text{Gauss}}$, and standard deviation equal to $r_{\text{Gauss}}$:

$$\omega_{d,\nu}(r) = C(r_{\text{Gauss}}, d) \exp\left(-\frac{r^2}{2r_{\text{Gauss}}^2}\right) \chi_{\{r<2r_{\text{Gauss}}\}}(r). \tag{4.5.2}$$

In all the simulations, we consider observations of the form

$$\ell_j^{\text{obs}} = \ell\left(u^{\text{true}}, \nu, x_j^{\text{obs}}\right) + \epsilon_j,$$

where $\epsilon_1, \ldots, \epsilon_J$ are realizations of the i.i.d. Gaussian random variables $\varepsilon_1, \ldots, \varepsilon_J \sim \mathcal{N}(0, \sigma^2)$.

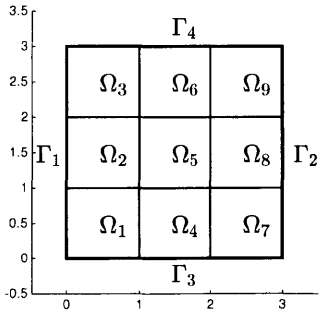


**Figure 4-1:** Thermal block synthetic problem: computational domain.

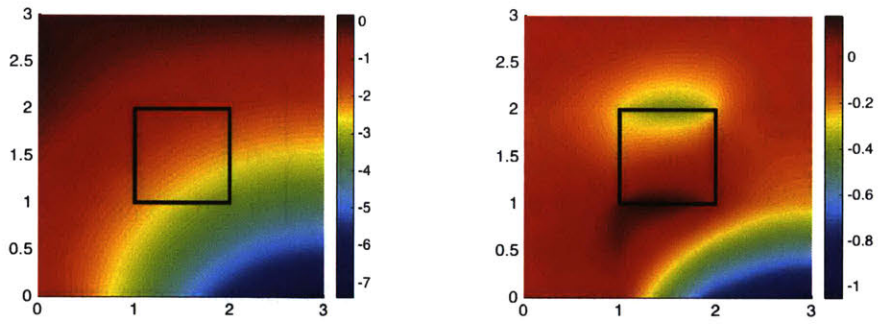

(a) $u^{\text{true}}$ (b) $u^{\text{true}} - u^\star$

**Figure 4-2:** Thermal block synthetic problem: visualization of the true field and of the error field. The domain $\Omega$ is the rectangular region inside the black boundary.

### Error in $L^2$ outputs

We first consider the case of $L^2$ outputs. We wish to estimate the error associated with the output

$$\mathcal{L}(u^{\text{true}}) = \frac{1}{|\Omega|} \int_\Omega u^{\text{true}} \, dx,$$

corresponding to $\zeta = 1/|\Omega|$. For this choice of $\mathcal{L}$, we have

$$\mathcal{L}(u^{true}) = -1.9588, \quad \mathcal{L}(u^\star) = -1.8464.$$

Figure 4-3 shows the behavior of the error estimator $\widehat{E}_{\mathcal{L}}$ and of the lower and upper bounds $\widehat{E}^{J,\sigma}_{\mathcal{L},\text{LB}}$ and $\widehat{E}^{J,\sigma}_{\mathcal{L},\text{UB}}$ with respect to $J$ for two values of $\sigma$. In this test, we consider $\alpha = 0.1$, $r_{\text{Gauss}} = 0.1$. We observe that in the noise-free case ($\sigma = 0$), $\widehat{E}_{\mathcal{L}}$ is an accurate approximation of $E_{\mathcal{L}}$ for $J \gtrsim 5$, and that $\widehat{C}^{J,\sigma}_{\mathcal{L}}$ is a meaningful confidence interval for $E_{\mathcal{L}}$ for $J \gtrsim 10$. By comparing Figure 4-3(a), and Figure 4-3(b), we observe that the convergence with $J$ depends on the magnitude of noise as expected from the theory (see equation (4.2.14)).

Figure 4-4 shows that we can use our procedure to build a confidence interval for $\mathcal{L}(u^{\text{true}})$. This observation confirms the result in (4.2.15). We observe that we can use our strategy to update the estimate for $\mathcal{L}(u^{\text{true}})$ for $J \gtrsim 10$ in the noise-free case, and for $J \gtrsim 20$ in the noisy case.

Figure 4-5 shows the behavior of the size of the confidence interval, $|\widehat{C}^{J,\sigma}_{\mathcal{L}}|$, for two different choices of $\sigma$, and for $u^\star = 0$ and $u^\star = u(\mu^\star)$. We denote by $\widehat{C}^{J,\sigma}_{\mathcal{L},1}$ the region

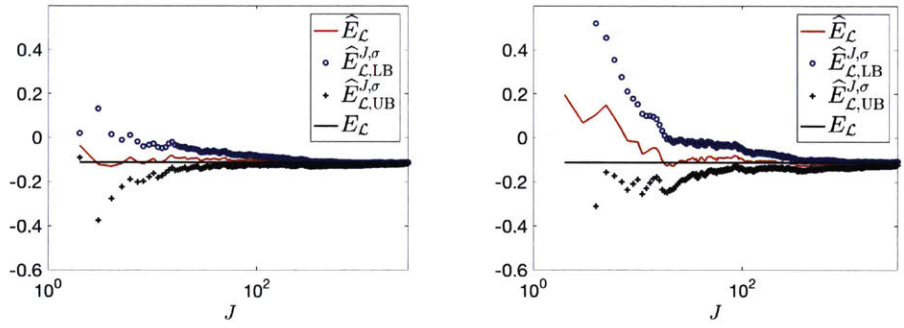


**(a)** $\sigma = 0$ **(b)** $\sigma = 0.25$

**Figure 4-3:** Thermal block synthetic problem: $(1-\alpha)$- confidence interval for the output error ($\alpha = 0.1$, $r_{\text{Gauss}} = 0.1$, $\mathcal{L}(u^{\text{true}} - u^\star) = -0.1124$ ).

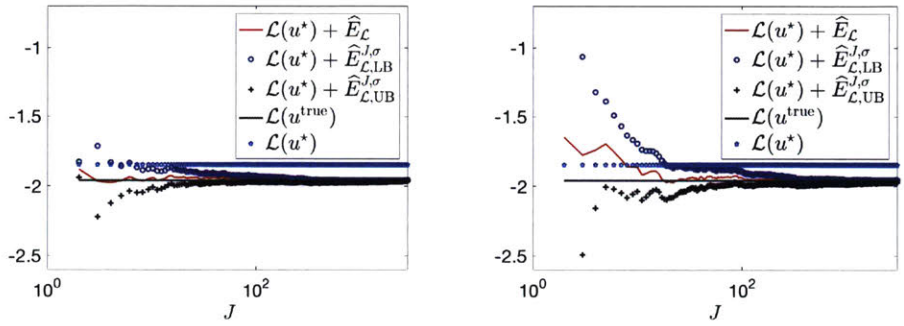


**(a)** $\sigma = 0$ **(b)** $\sigma = 0.25$

**Figure 4-4:** Thermal block synthetic problem: $(1-\alpha)$-confidence interval for the output ($\alpha = 0.1$, $r_{\text{Gauss}} = 0.1$, $\mathcal{L}(u^{\text{true}}) = -1.9288$ ).

associated with $u^\star = u(\mu^\star)$, and by $\widehat{C}^{J,\sigma}_{\mathcal{L},2}$ the region associated with $u^\star = 0$. As in the previous test, we set $\alpha = 0.1$, $r_{\text{Gauss}} = 0.1$. We observe that $|\widehat{C}^{J,\sigma}_{\mathcal{L},1}(J = 10)| \approx |\widehat{C}^{J,\sigma}_{\mathcal{L},2}(J = 150)|$ in the noise-free case, and $|\widehat{C}^{J,\sigma}_{\mathcal{L},1}(J = 10)| \approx |\widehat{C}^{J,\sigma}_{\mathcal{L},2}(J = 40)|$ in the noisy case. The results show that our procedure takes advantage of the proximity of $u^\star$ to $u^{\text{true}}$ to reduce the variance of the process. We observe that the variance reduction strategy is less effective in the presence of experimental noise: this is in good agreement with estimate (4.2.14).

### $L^2$ error

We now consider the problem of estimating the $L^2$ error. Figure 4-6 shows the behavior of $\widehat{E}$, $\widehat{E}_{\text{mod}}$, and the lower and upper bounds $\widehat{E}^{J,\sigma}_{\text{LB}}$ and $\widehat{E}^{J,\sigma}_{,\text{UB}}$ with respect to $J$ and for two values of $\sigma$. In this test, we consider $\alpha = 0.1$, $r_{\text{Gauss}} = 0.05$, and we assume that we know the value of $\sigma$. We observe that our procedure provides a meaningful upper bound for the error for $J \gtrsim 5$ in the noise-free case, and for $J \gtrsim 20$ in the noisy case.

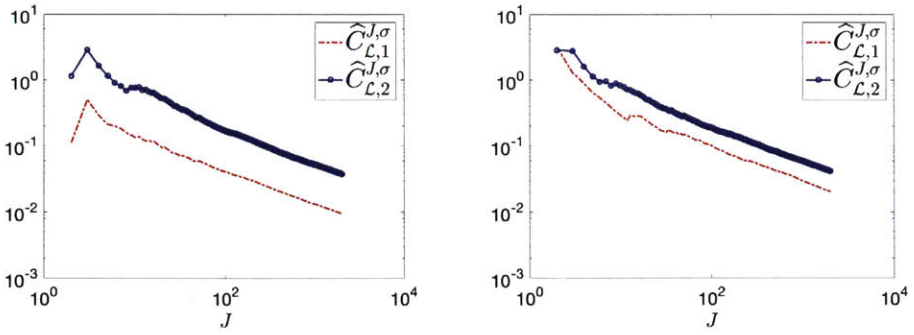


**(a)** $\sigma = 0$ **(b)** $\sigma = 0.25$

**Figure 4-5:** Thermal block synthetic problem: size of the confidence interval $|\widehat{C}^{J,\sigma}_{\mathcal{L}}|$ for two different choices of $\sigma$, and for $u^\star = 0$ and $u^\star = u(\mu^\star)$ ( $\alpha = 0.1$, $r_{\text{Gauss}} = 0.1$).

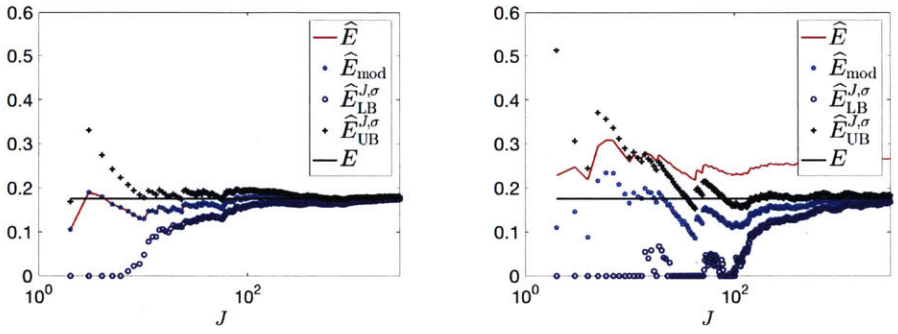


**(a)** $\sigma = 0$ **(b)** $\sigma = 0.2$

**Figure 4-6:** Thermal block synthetic problem: confidence intervals for the $L^2(\Omega)$ error for two different choices of $\sigma$ ($\alpha = 0.1$, $r_{\text{Gauss}} = 0.05$, $\|u^{\text{true}} - u^\star\|_{L^2(\Omega)} = 0.1756$).

### Finite-$\nu$ error

In Figure 4-7, we investigate the effect of the finite width $\nu$ in output error and $L^2$ error estimation[1]. Figure 4-7(a) a shows the behavior of $\widehat{E}_{\mathcal{L}}$, $\widehat{E}^{J,\sigma}_{\mathcal{L},\text{LB}}$ and $\widehat{E}^{J,\sigma}_{\mathcal{L},\text{UB}}$ with respect to $r_{\text{Gauss}}$ for $J = 2000$. Similarly, Figure 4-7(b) shows the behavior of $\widehat{E}$, $\widehat{E}^{J,\sigma}_{\text{LB}}$ and $\widehat{E}^{J,\sigma}_{\text{UB}}$ with $r_{\text{Gauss}}$ for the same value of $J$. We observe that as $r_{\text{Gauss}}$ increases, $\widehat{E}$ and the size of the confidence regions $\mathcal{C}^{J,\sigma}_{\mathcal{L}}$ and $\mathcal{C}^{J,\sigma}$ decrease. We further observe that, for our particular choice of the linear functional and of the error field, the effect of the filter spread is extremely limited.

[1]For $r_{\text{Gauss}} \geq 0.5$, condition $\Omega_\nu \subset\subset \Omega^{\text{obs}}$ does not hold; in this case, we simply adjust the constant $C = C(r_{\text{Gauss}}, d, x)$ in (4.5.2) by imposing that $\ell(1, \nu, x) = 1$ for any $x \in \Omega$.

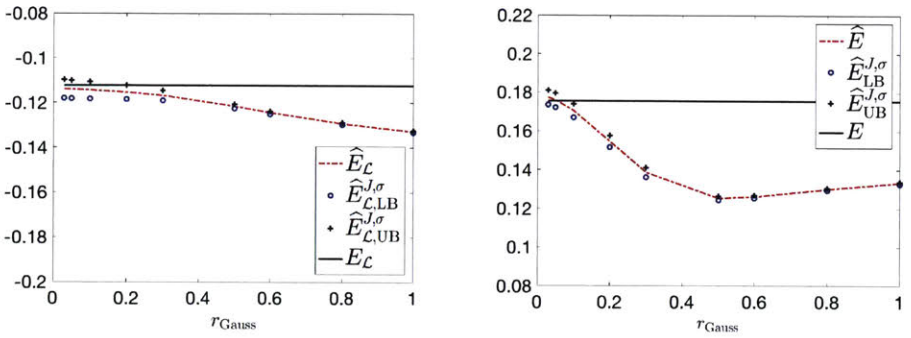


**(a)** output error **(b)** $L^2(\Omega)$ error

**Figure 4-7:** Thermal block synthetic problem: confidence intervals for output error and $L^2(\Omega)$ error for different values of $r_{\text{Gauss}}$ ($\sigma = 0$, $\alpha = 0.1$, $J = 2000$).

### Analysis of the finite-grid case

We now consider the case in which sensor locations should be selected among a set of grid points $\{x_j^{\text{grid}}\}_{j=1}^{\mathcal{J}}$. Towards this end, we consider two different cases: (i) a 10 by 10 grid of equispaced sensors in $\Omega$, and (ii) a 10 by 10 grid associated with the Gaussian quadrature points in $\Omega$. Figure 4-8 shows the grids. For the first grid we define $\mathcal{L}^{\text{grid}}$ (4.2.13) using uniform weights $w_j = \frac{1}{100}$, while for the second grid we consider the weights associated with Gaussian quadrature.

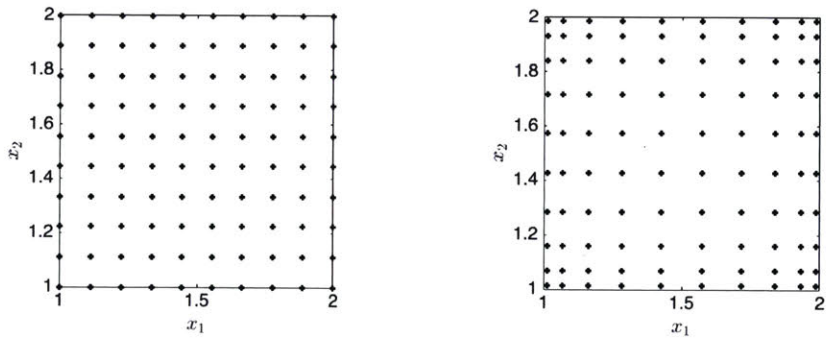


**(a)** Uniform **(b)** Gaussian

**Figure 4-8:** Thermal block synthetic problem: sensor grids.

Figure 4-9 shows the behavior of the confidence intervals for $E_{\mathcal{L}}$ and for $\mathcal{L}(u^{\text{true}})$. We here set $r_{\text{Gauss}} = 0.1$. We observe that for the Gaussian case results are comparable with the results shown in Figures 4-3 and 4-4; on the other hand, for the uniform case we observe that $\mathcal{L}^{\text{grid}}(\mathcal{F}_\nu(e)) - \mathcal{L}(\mathcal{F}_\nu(e))$ is not negligible.

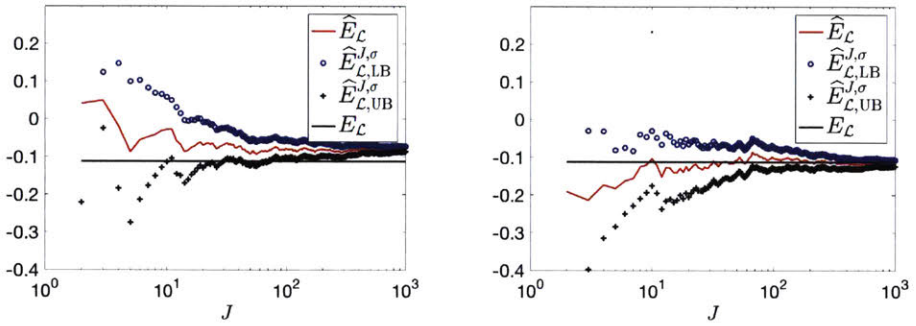


**(a)** Uniform **(b)** Gaussian

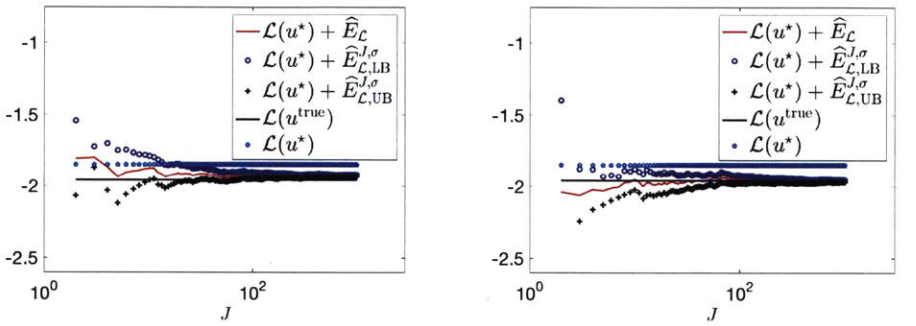


**(c)** Uniform **(d)** Gaussian

**Figure 4-9:** Thermal block synthetic problem: confidence intervals for the output error and for the $L^2(\Omega)$ error for different values of $r_{\mathrm{Gauss}}$ for two finite grids ($\sigma = 0$, $r_{\mathrm{Gauss}} = 0.1$, $\alpha = 0.1$).

### Validity of the large-sample approximation

We now assess the validity of the normal approximation, which has been exploited to derive the asymptotic confidence intervals $\widehat{C}^{J,\sigma}_{\mathcal{L}}$ (4.2.12), and $\widehat{C}^{J,\sigma}$ (4.3.6). With this in mind, for given values of $J$ and $\alpha$, we select $n_{\mathrm{train}} = 10^3$ different samples $\{\{x_n^{\mathrm{obs}}(i)\}_{n=1}^{J}\}_{i=1}^{n_{\mathrm{train}}}$ and, for each sample, we compute the error estimator $\widehat{E}_{\mathcal{L}}(J,\nu,i)$ and the confidence interval $\widehat{C}^{J,\sigma}_{\mathcal{L}}(J,\nu,\alpha,i)$, $i = 1,\ldots,n_{\mathrm{train}}$. Then, we estimate the confidence level of the confidence interval as

$$\widehat{CL}(J) := \frac{\mathrm{card}\left\{i \in \{1,\ldots,n_{\mathrm{train}}\} : \; E_{\mathcal{L}} \in \widehat{C}^{J,\sigma}_{\mathcal{L}}(J,\nu,\alpha,i)\right\}}{n_{\mathrm{train}}}, \tag{4.5.3}$$

where $\mathrm{card}\{\cdot\}$ denotes the cardinality of the set. If the normal assumption holds, we expect that $\widehat{CL}(J) \approx 1-\alpha$. Therefore, the difference $|\widehat{CL}(J) - 1 + \alpha|$ can be exploited to assess the validity of the normal approximation. We can then repeat the same analysis for the $L^2$ error.

Figure 4-10 shows the results for the output error. In this simulation, we consider $\sigma = 0$ (perfect measurements), $\alpha = 0.1$ and $r_{\text{Gauss}} = 0.03$. Figures 4-10(a) and 4-10(b) show the histograms of the distribution of $\widehat{E}_{\mathcal{L}}(J, \nu, i)$ for two different values of $J$. The red continuous line indicates the true value of the error, while the black dashed line denotes the mean of $\widehat{E}_{\mathcal{L}}(J, \nu, i)$ over the $n_{\text{train}}$ samples. We observe that for both $J = 3$ and $J = 8$ the distribution of $\widehat{E}_{\mathcal{L}}(J, \nu, i)$ is approximately normal. Figure 4-10(c) shows the behavior of $\widehat{CL}(J)$ with $J$. As expected, $\widehat{CL}(J)$ converges to $1 - \alpha$ as $J$ increases.

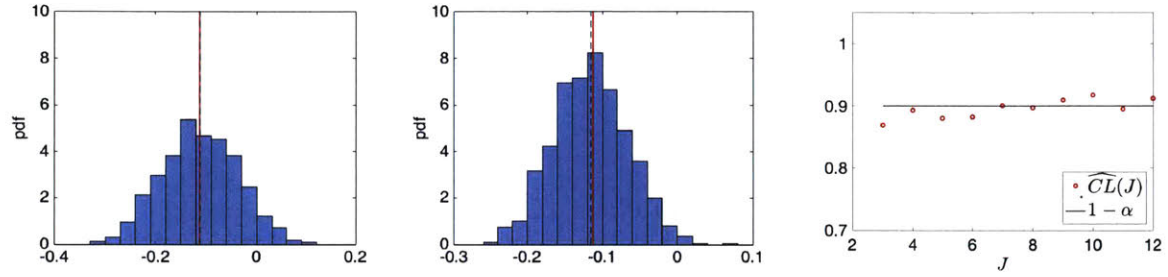


**(a)** $J = 3$ **(b)** $J = 8$ **(c)**

**Figure 4-10:** Thermal block synthetic problem: assessment of the Gaussianity assumption for output error confidence intervals ($r_{\text{Gauss}} = 0.03$, $\alpha = 0.1$, $\sigma = 0$).

Figure 4-11 shows results for the $L^2$ error. While for $J = 3$ the distribution of $\widehat{E}(J, \nu, i)$ is slightly asymmetric (Figure 4-11(a)), for $J = 8$ the distribution is approximately normal (Figure 4-11(b)). This is a consequence of the Central Limit Theorem. We further observe that the confidence level $\widehat{CL}(J)$ associated with $\{\widehat{C}^{J,\sigma}(J, \nu, \alpha, i)\}_{i=1}^{n_{\text{train}}}$ does not converge to $1 - \alpha$. This is a consequence of the shift determined by the presence of finite-$\nu$ error.

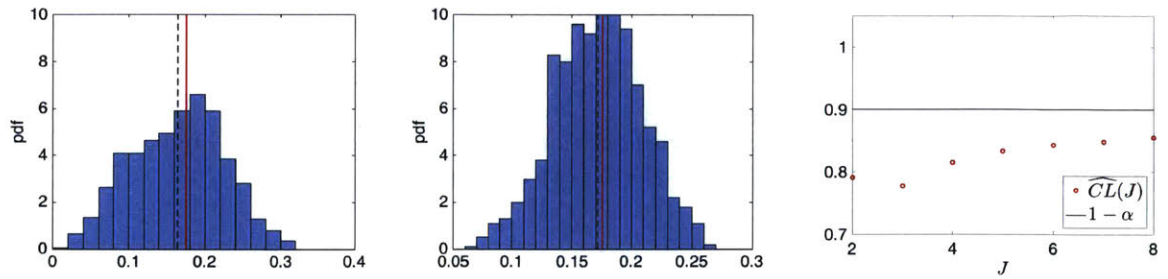


**(a)** $J = 3$ **(b)** $J = 8$ **(c)**

**Figure 4-11:** Thermal block synthetic problem: assessment of the Gaussianity assumption for $L^2(\Omega)$ error confidence intervals ($r_{\text{Gauss}} = 0.03$, $\alpha = 0.1$, $\sigma = 0$).

### 4.5.2 Application to the thermal patch experiment

We present results for the thermal patch problem introduced in Chapter 3.4. Given the domain $\Omega = (-0.5\widehat{L}, 0.5\widehat{L}) \times (-0.5\widehat{L}, 0)$ ($\widehat{L} = 22.606$mm), we wish to estimate the error associated with the output

$$\mathcal{L}(u^{\text{obs}}) = \frac{1}{|\Omega|} \int_{\Omega} u^{\text{true}} \, dx,$$

and the $L^2$ error over $\Omega$, $\|u^{\text{obs}} - u^\star\|_{L^2(\Omega)}$. We recall that $u^{\text{obs}}$ corresponds to the dimensional thermal field estimated by the IR camera, and that $[x] = \text{m}$. With some abuse of notation, in this section we omit the superscript $^{\text{dim}}$ to indicate dimensional quantities.

We now introduce the state estimate $u^\star$ generated by solving the bk model (3.4.3) for $\mu = 1$. We observe that

$$\mathcal{L}(u^{\text{obs}}) = 50.0640^o C, \qquad \mathcal{L}(u^\star) = 52.5965^o C,$$

and[2]

$$\|u^{\text{obs}} - u^\star\|_{L^2(\Omega)} = 0.0529[C^o \times \text{m}].$$

Figure 4-12 shows the observed field $u^{\text{obs}}$, the error field $e^{\text{obs}} = u^{\text{obs}} - u^\star$, and the domain $\Omega$.

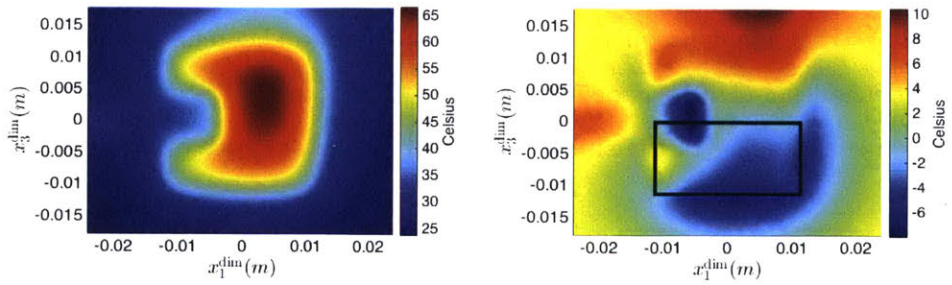


**(a)** $u^{\text{obs}}$ **(b)** $u^{\text{obs}} - u^\star$

**Figure 4-12:** Thermal patch problem: visualization of the observed field and of the error field. The domain $\Omega$ is the rectangular region inside the black curve.

Figure 4-13 shows the results. We observe that for $J \simeq 10$ the 90% confidence interval for the output error contains the true value, and has a half-amplitude equal to $1^o C$ (Figure 4-13(a)); therefore, we can use $\widehat{E}_{\mathcal{L}}$ to update the estimate of the output (Figure 4-13(b)).

[2]To provide a benchmark value, we observe that $\|u^{\text{obs}} - \mathcal{L}(u^{\text{obs}})\|_{L^2(\Omega)} = 0.1275[C^o \times \text{m}]$.

Similarly, we are able to construct meaningful confidence intervals for the $L^2$ error for $J \gtrsim 10$ (Figure 4-13(c)). This shows that, also in this case, our procedure is able to provide accurate confidence intervals for modest values of $J$.

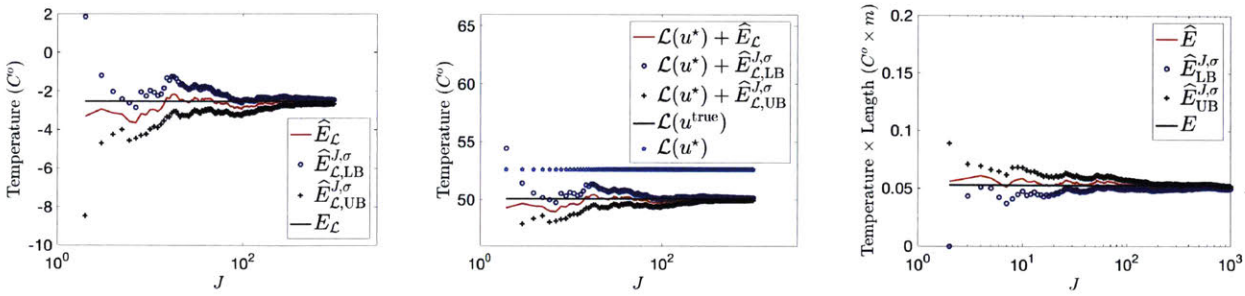


**(a)** output error **(b)** output **(c)** $L^2(\Omega)$ error

**Figure 4-13:** Thermal patch: confidence intervals for the output error, the output, and the $L^2(\Omega)$ error ($\alpha = 0.1$, $r_{\mathrm{Gauss}} = 0.09\mathrm{mm}$, $\mathcal{L}(u^{\mathrm{obs}} - u^\star) = -2.5325^o C$, $\|u^{\mathrm{obs}} - u^\star\|_{L^2(\Omega)} = 0.0529[C^o \times \mathrm{m}]$).

## 4.6 Numerical results (II): data assimilation

We discuss the application of the data-driven enrichment procedure presented in section 4.4 to the acoustic model problem introduced in Chapter 3.3. For this test, we set $\Omega = \Omega^{\mathrm{obs}} = (0,1)^2$, and we consider truncated Gaussians with $\nu/2 = r_{\mathrm{Gauss}} = 0.05$; since $\Omega_\nu$ is not embedded in $\Omega^{\mathrm{obs}}$, we adjust the constant $C = C(r_{\mathrm{Gauss}}, \nu, x)$ by imposing that $\ell(1, \nu, x) = 1$ for all $x \in \Omega$. We generate $\mathcal{Z}_{N_{\mathrm{bk}} \equiv 2}$ based on the bk model corresponding to $g = 0$. Then, we consider $n_{\mathrm{train}} = 15$ offline experiments associated with the true model corresponding to $g = \tilde{g}$, and $n_{\mathrm{train}}$ different frequencies in $\mathcal{P}^{\mathrm{bk}} = [2, 10]$. During the offline stage, we consider either $M_{\mathrm{off}} = 32$ or $M_{\mathrm{off}} = 64$ for training, and $J_{\mathrm{off}} = 10$ for validation. We further assume that the number of measurements available during the online stage is equal to $M_{\mathrm{on}} = 10$. During the online stage, we compute the PBDW solution for different backgrounds and $M_{\mathrm{on}} = 10$ experimental measurements, and we assess online performance by computing the relative $L^2$ error

$$E^{\mathrm{rel,on}}(\mu) := \|u^{\mathrm{true}}(\mu) - u^\star(\mu)\|_{L^2(\Omega)} / \|u^{\mathrm{true}}(\mu) - u^\star(\mu)\|_{L^2(\Omega)}, \tag{4.6.1}$$

for $n_{\mathrm{test}} = 100$ different values of the parameter $\mu \in \mathcal{P}^{\mathrm{bk}}$.

Figure 4-14 shows the the behavior of the relative $L^2$ error $E^{\mathrm{rel,on}}$ for different background spaces — we remark that the background $N = 2$ corresponds to the case in which no offline

enrichment is performed — and for $M_{\text{on}} = 10$ online measurements. The black dots denote the values of the parameters associated with the configurations $\mathcal{C}_{k^\star}$ selected during the offline Greedy procedure. We observe that the offline enrichment dramatically reduces the state estimation error over all frequencies. This shows that acoustic applications are particularly suited to the enrichment due to the modal structure of the solution to the PDE. Interestingly, the Greedy procedure selects updates associated with resonance frequencies.

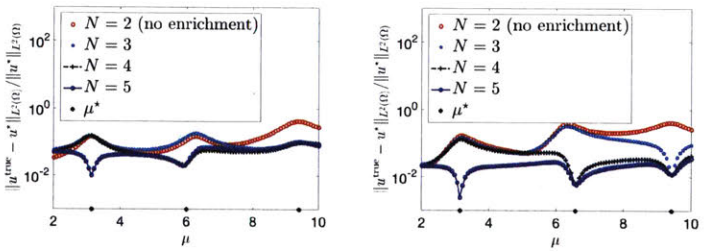


**(a)** $M_{\text{off}} = 32$ **(b)** $M_{\text{off}} = 64$

**Figure 4-14:** Data-driven enrichment for a synthetic acoustic problem. Behavior of $E^{\text{rel,on}}(\mu)$ (4.6.1) with respect to $\mu$ for several $N$ ($N_{\text{bk}} = 2$, $M_{\text{off}} = 32, 64$, $J^{\text{off}} = 10$, $n_{\text{train}} = 15$, $n_{\text{test}} = 100$, $M_{\text{on}} = 10$). The black dots denote the values of the parameters indirectly selected during the offline Greedy procedure.

## 4.7 Conclusions

We proposed a Monte Carlo experimental procedure that provides confidence intervals for the $L^2$ error in state and the error in $L^2$ outputs. The procedure relies on a state estimate $u^\star$ for the true field $u^{\text{true}}$ and on $J$ possibly noisy local experimental functionals, and is based on the identification of three different sources of error: the finite-$\nu$, the finite-$J$ error, and the finite-noise error. Our approach implicitly takes advantage of variance reduction, through the proximity of $u^\star$ to $u^{\text{true}}$, to provide tight confidence intervals even for modest values of $J$.

Numerical results for a synthetic model problem and for the experimental thermal patch configuration illustrate the elements of the methodology, and clarify the role played by the finite-$\nu$, the finite-$J$ error, and the finite-noise error. While finite-$J$ and finite-noise errors can be bound through an asymptotically rigorous statistical procedure, the effect of $\nu$ depends on the spatial scale of the field and on the transducer resolution, and can only be assessed on a case-by-case basis.

We also illustrated the application of our error estimation procedure to two data assim-

ilation tasks: output prediction and data-driven enrichment of the background space $\mathcal{Z}_N$ in the PBDW framework. For output prediction, we exploit the linearity of the functional to provide lower and upper bounds for the quantity of interest $\mathcal{L}(u^{\text{true}})$. Due to the modest variance of the process $e = u^{\text{true}} - u^\star$, we can obtain meaningful confidence intervals for $\mathcal{L}(u^{\text{true}})$ for moderate values of $J$. For the enrichment of the background space $\mathcal{Z}_N$, we rely on the *a posteriori* error estimator $\widehat{E}$ to properly enrich the background in a Greedy fashion. Numerical results for a synthetic problem demonstrated the effectivity of the approach.

# Chapter 5

# The PBDW approach for localised state estimation

We study the application of PBDW to the problem of localised state estimation. In more detail, we study the case in which the bk model is (i) defined over a domain $\Omega^{\text{bk}}$ that strictly contains the domain of interest $\Omega$, and (ii) depends on a high- (possibly infinite-) dimensional set of parameters. Since in PBDW the bk model is only employed to generate the background space, the focus of this chapter is on the development of efficient strategies for the construction of local approximation spaces $\{\mathcal{Z}_N\}_N$, which can then be employed in the PBDW formulation.

We first motivate the problem from an engineering standpoint, we introduce the general idea of the localisation procedure, and we discuss a simple model problem that explains under which condition localisation is feasible (section 5.1). Then, we propose the computational strategy (section 5.2), and we present a number of theoretical results concerning the optimality of our construction (section 5.3). Finally, in section 5.4, we present numerical results for two synthetic acoustic problems.

## 5.1 Preliminary discussion

### 5.1.1 Localisation strategy

For practical applications, bk mathematical models might be characterized by extremely high-dimensional parametric uncertainty. In the process of defining the model, we have

indeed to specify potential topology variations in the structure, material properties, initial and boundary conditions, just to mention a few; since all these quantities are typically subject to uncertainty, the effective number of parameters associated with the mathematical model of a full engineering system might number in the hundreds.

In many cases, we are interested in performing state estimation in a subregion of the whole system: for acoustic applications, active systems for noise cancellation rely on the estimation of the sound pressure level in a particular region of interest; in damage identification, engineers are often able to anticipate the region of the structure of interest that is more likely prone to failure, and consequently monitor only specific components of the structure. Once we restrict the model to the domain of interest, we have to face two different sources of uncertainty: (i) uncertainty in the physical parameters, and (ii) uncertainty in the boundary conditions at the interface. While we might reasonably assume that the former source of uncertainty leads to a low-dimensional parametrization, the latter clearly leads to a high-dimensional and possibly infinite-dimensional parameter space.

To address the uncertainty related to boundary conditions, in this work we propose a two-stage localisation procedure. If we denote by $\Omega^{\text{pb}}$ the domain associated with the full system, and by $\Omega \subset \Omega^{\text{pb}}$ the domain of interest in which we want to estimate the state, we introduce the bk domain $\Omega^{\text{bk}}$ such that $\Omega \subset \Omega^{\text{bk}} \subset \Omega^{\text{pb}}$. The domain $\Omega^{\text{bk}}$ is chosen to exclude many parameters associated with $\Omega^{\text{pb}} \setminus \Omega^{\text{bk}}$. We further denote by $\Gamma^{\text{in}}$ the portion of $\partial\Omega^{\text{bk}}$ in which boundary conditions are uncertain. Then, we define our bk mathematical model as follows:

$$\mathcal{G}^{\text{bk},\mu}(u_g^{\text{bk}}(\mu), v) = f(v), \ \ \forall\, v \in \mathcal{V}_0^{\text{bk}}, \quad u_g^{\text{bk}}|_{\Gamma^{\text{in}}} = g, \qquad \mu \in \mathcal{P}^{\text{bk}}, \ \ g \in \widetilde{\mathcal{T}}. \tag{5.1.1}$$

Here, $\mathcal{V}^{\text{bk}} = \mathcal{V}^{\text{bk}}(\Omega^{\text{bk}})$ is a Hilbert space defined over $\Omega^{\text{bk}}$, $\mathcal{V}_0^{\text{bk}} := \{v \in \mathcal{V}^{\text{bk}} : v|_{\Gamma^{\text{in}}} \equiv 0\}$, $\widetilde{\mathcal{T}} \subset \mathcal{T}$ is a, possibly infinite-dimensional, subset of the Sobolev space $\mathcal{T} = \mathcal{T}(\Gamma^{\text{in}})$, $\mu$ denotes the parametric uncertainty in the model, $\mathcal{G}^{\text{bk},\mu} : \mathcal{V}^{\text{bk}} \times \mathcal{V}_0^{\text{bk}} \to \mathbb{R}$ is a parametrized variational form defined over $\Omega^{\text{bk}}$, and $f \in (\mathcal{V}_0^{\text{bk}})'$ is associated with the external forces acting on the system. Based on the previous definitions, we can define the bk manifolds:

$$\widehat{\mathcal{M}}^{\text{bk}} := \left\{ u_g^{\text{bk}}(\mu) : \ \ \mu \in \mathcal{P}^{\text{bk}}, \ g \in \widetilde{\mathcal{T}} \right\} \subset \mathcal{V}^{\text{bk}}, \quad \widetilde{\mathcal{T}} \subset \mathcal{T}, \tag{5.1.2a}$$

and

$$\mathcal{M}^{\mathrm{bk}} := \left\{ u_g^{\mathrm{bk}}(\mu)|_\Omega : \ \mu \in \mathcal{P}^{\mathrm{bk}},\ g \in \widetilde{\mathcal{T}} \right\} \subset \mathcal{Y}, \quad \widetilde{\mathcal{T}} \subset \mathcal{T}, \tag{5.1.2b}$$

where $\mathcal{Y} = \mathcal{Y}(\Omega)$ is a suitable Hilbert space defined over $\Omega$.

The objective of this chapter is to propose a model-order-reduction strategy that generates local hierarchical approximation spaces $\mathcal{Z}_1 \subset \ldots \subset \mathcal{Z}_{N_{\max}}$ for the bk manifold $\mathcal{M}^{\mathrm{bk}}$ in (5.1.2b). We observe that if $\widetilde{\mathcal{T}}$ is infinite-dimensional, we cannot expect that the manifold $\widehat{\mathcal{M}}^{\mathrm{bk}}$ can be well-approximated by a low-dimensional linear space. In the next subsection, we explain — through the vehicle of a particular model problem — why $\mathcal{M}^{\mathrm{bk}}$ might nevertheless be well-approximated by a linear space.

### 5.1.2 A model problem

In order to get insights about the reduction task described in the previous section, we shall consider the following differential problem associated with a semi-infinite wave-guide ([96]):

$$\begin{cases} -\Delta u_g^{\mathrm{bk}}(\mu) - \mu^2\, u_g^{\mathrm{bk}}(\mu) = 0, & \text{in } \Omega^{\mathrm{bk}} = (0,\infty)\times(0,1), \\ \partial_{x_2}\, u_g^{\mathrm{bk}}(x;\mu) = 0 & x \in (0,\infty)\times\{0,1\}, \\ u_g^{\mathrm{bk}}(x;\mu) = g(x) & x \in \Gamma^{\mathrm{in}} := \{0\}\times(0,1), \end{cases} \tag{5.1.3}$$

where $g \in \widetilde{\mathcal{T}} \subset \mathcal{T} := H^{1/2}(\Gamma^{\mathrm{in}})$. We then define the domain of interest $\Omega = (L,\infty)\times(0,1)$. For simplicity, we set $\mathcal{P}^{\mathrm{bk}} = \{\bar{\mu}\}$ and we omit the dependence on $\mu$. By exploiting separation of variables, we obtain that

$$u_g^{\mathrm{bk}}(x_1,x_2) \;=\; \sum_{n=1}^{N_{\mathrm{prop}}} c_n(g)\, e^{-i\alpha_n x_1}\, \cos(n\pi x_2) \;+\; \sum_{n=N_{\mathrm{prop}}+1}^{\infty} c_n(g) e^{-\alpha_n x_1}\, \cos(n\pi x_2),$$

where $N_{\mathrm{prop}} = \lfloor \frac{\bar{\mu}}{\pi} \rfloor$, $\alpha_n^2 = |n^2\pi^2 - \bar{\mu}^2|$ and the coefficients $\{c_n\}_n$ depend on the boundary condition $g$. We observe that the first $N_{\mathrm{prop}}$ modes do not decay as $x_1 \to \infty$, while the remaining modes decay exponentially as $x_1 \to \infty$. For this reason, we refer to the former as *propagating modes* and to the latter as *evanescent modes*.

Let us now suppose that our goal is to approximate the bk manifold $\mathcal{M}^{\mathrm{bk}}$ through a $N$-

dimensional linear space $\mathcal{Z}_N$ under the assumption that $\widetilde{\mathcal{T}} = \{g \in \mathcal{T} : |c_n(g)| \leq C,\ \forall n \geq 1\}$. For the sake of argument, we aim to guarantee that the $L^2$ best-fit error associated with the bk manifold, $\epsilon_N^{\text{bk}} = \sup_{w \in \mathcal{M}^{\text{bk}}} \inf_{z \in \mathcal{Z}_N} \|w - z\|_{L^2(\Omega)}$, is below a fixed tolerance *tol*. We can distinguish between two scenarios:

$N_{\text{prop}} > N$: since the dimension of the approximation space is less than the number of propagating modes, we cannot accurately approximate the manifold $\mathcal{M}^{\text{bk}}$ through a $N$-dimensional linear space for any $L > 0$;

$N_{\text{prop}} < N$: in this case we can approximate all propagating modes; therefore, if the effect of the evanescent modes is negligible, we can approximate the manifold $\mathcal{M}^{\text{bk}}$ through a $N$-dimensional linear space.

In the latter case, we can indeed choose $\mathcal{Z}_N = \text{span}\{\zeta_n\}_{n=1}^N$ with $\zeta_n(x_1, x_2) = e^{-i\alpha_n x_1} \cos(n\pi x_2)$ if $n \leq N_{\text{prop}}$, and $\zeta_n(x_1, x_2) = e^{-\alpha_n x_1} \cos(n\pi x_2)$ if $N > N_{\text{prop}}$. Then, assuming that we are interested in bounding the $L^2$-error, it is easy to verify that

$$\inf_{z \in \mathcal{Z}_N} \|u_g^{\text{bk}} - z\|_{L^2(\Omega)}^2 = \sum_{n=N+1}^{\infty} (c_n(g))^2 \frac{e^{-\alpha_n L}}{4\alpha_n} \leq C^2 \sum_{n=N+1}^{\infty} \frac{e^{-\alpha_n L}}{4\alpha_n} =: \epsilon_N^{\text{bk,UB}}.$$

If $L$ is sufficiently large, $\epsilon_N^{\text{bk,UB}}$ is below the specified tolerance *tol*. We have thus shown that there exists a space $\mathcal{Z}_N$ that meets our requirements; we then say that $\mathcal{M}^{\text{bk}}$ is $N$-reducible. We highlight that our definition of reducibility depends on the dimension $N$ of the approximation space — which is ultimately related in our setting to the number $M$ of available experimental observations — on the tolerance ($tol > 0$), and also on the norm of interest (the $L^2$ norm).

The discussion of this section exemplifies two separate issues related to the problem at hand. The first is related to the possibility of "reducing" a given bk manifold to a $N$-dimensional linear space. This is strongly related to the PDE considered and is independent of the particular reduction algorithm used to build $\mathcal{Z}_N$. The second issue is related to the development of actionable computational procedures to identify the reduced space $\mathcal{Z}_N$: in this respect, we observe that standard pMOR strategies — such as the Weak-Greedy algorithm employed in the previous chapters — are not well-suited for this problem due to the high-dimensionality of the parameter space. The remainder of this chapter is devoted to the development of an actionable computational procedure to build rapid convergent localised approximation spaces $\{\mathcal{Z}_N\}_N$.

## 5.2 Methodology

We shall first introduce some notation and preliminary assumptions. We define the solution maps $\widehat{A} : \mathcal{T} \times \mathcal{P}^{\text{bk}} \to \mathcal{V}^{\text{bk}}$ and $A : \mathcal{T} \times \mathcal{P}^{\text{bk}} \to \mathcal{Y}$ such that

$$\widehat{A}(g;\mu) = u_g^{\text{bk}}(\mu), \quad A(g;\mu) = u_g^{\text{bk}}(\mu)|_\Omega, \qquad \forall\, g \in \mathcal{T}, \;\; \mu \in \mathcal{P}^{\text{bk}}. \tag{5.2.1}$$

We assume that $A$ and $\widehat{A}$ are linear operators such that $A(0;\mu) \equiv 0$, and $\widehat{A}(0;\mu) \equiv 0$. Recalling (5.1.1), this corresponds to assume that $\mathcal{G}^{\text{bk},\mu}$ is a bilinear continuous inf-sup stable form and $f \equiv 0$. We note that the extension to $f \neq 0$ is straightforward, while the extension to nonlinear operators appears difficult and is beyond the scope of this work. We further endow the Hilbert space $\mathcal{T}$ with the inner product $(\cdot,\cdot)_\mathcal{T}$ and the norm $\|\cdot\|_\mathcal{T}$. We denote by $(\cdot,\cdot)_\mathcal{Y}$ the inner product of $\mathcal{Y}$, and by $\|\cdot\|_\mathcal{Y}$ the induced norm. We also denote by $\Pi_\mathcal{Q}^\mathcal{Y}(\cdot)$ the projection operator onto $\mathcal{Q} \subset \mathcal{Y}$ in $\mathcal{Y}$, and by $\Pi_{\mathcal{Q}'}^\mathcal{T}(\cdot)$ the projection operator onto $\mathcal{Q}' \subset \mathcal{T}$ in $\mathcal{T}$. We remark that in our setting the space $\mathcal{Y}$ does not have to coincide with the space $\mathcal{U}$ employed in the PBDW formulation.

We first consider the case $\mathcal{P}^{\text{bk}} = \{\bar{\mu}\}$ (section 5.2.1), and then we consider the extension to the more general case $\mathcal{P}^{\text{bk}} \neq \{\bar{\mu}\}$ (section 5.2.2). To simplify notation, if $\mathcal{P}^{\text{bk}} = \{\bar{\mu}\}$, we omit the dependence on the parameter. We state upfront that our procedure intends — but does not assume — that the bk manifold can be well-approximated by a $N$-dimensional linear space. We come back to this point in the analysis.

### 5.2.1 The case $\mathcal{P}^{\text{bk}} = \{\bar{\mu}\}$

We introduce the *transfer eigenproblem* as follows: find $(\phi_n, \lambda_n) \in (\mathcal{T}, \mathbb{R}_+)$ such that

$$(A(\phi_n),\, A(g))_\mathcal{Y} \;=\; \lambda_n(\phi_n,\, g)_\mathcal{T} \qquad \forall\, g \in \mathcal{T}, \tag{5.2.2}$$

where $\lambda_1 \geq \lambda_2 \ldots \geq 0$. Then, for any $N > 0$, we define the *transfer eigenspace*

$$\mathcal{Z}_N^{\text{te}} := \text{span}\{A(\phi_n)\}_{n=1}^N. \tag{5.2.3}$$

If we introduce the finite-dimensional discretization of $\mathcal{T}$, $\mathcal{T}_{\mathcal{N}_{\text{in}}} = \text{span}\{g_1, \ldots, g_{\mathcal{N}_{\text{in}}}\} \subset \mathcal{T}$, we can define the semi-discrete transfer eigenproblem: find $(\phi_n^{\mathcal{N}_{\text{in}}}, \lambda_n^{\mathcal{N}_{\text{in}}}) \in (\mathcal{T}_{\mathcal{N}_{\text{in}}}, \mathbb{R}_+)$ such

that

$$(A(\phi_n^{\mathcal{N}_{\text{in}}}),\, A(g))_{\mathcal{Y}} \;=\; \lambda_n^{\mathcal{N}_{\text{in}}}(\phi_n^{\mathcal{N}_{\text{in}}},\, g)_{\mathcal{T}} \qquad \forall\, g \in \mathcal{T}_{\mathcal{N}_{\text{in}}}, \tag{5.2.4}$$

where $\lambda_1^{\mathcal{N}_{\text{in}}} \geq \lambda_2^{\mathcal{N}_{\text{in}}} \ldots \geq \lambda_{\mathcal{N}_{\text{in}}}^{\mathcal{N}_{\text{in}}} \geq 0$. Then, for any $N > 0$, we define the semi-discrete transfer eigenspace:

$$\mathcal{Z}_N^{\text{te},\mathcal{N}_{\text{in}}} := \text{span}\{A(\phi_n^{\mathcal{N}_{\text{in}}})\}_{n=1}^{N}. \tag{5.2.5}$$

Eigenproblem (5.2.4) can also be restated in a fully algebraic form as

$$\mathbb{U}\,\boldsymbol{\phi}_j^{\mathcal{N}_{\text{in}}} = \lambda_n^{\mathcal{N}_{\text{in}}} \mathbb{T} \boldsymbol{\phi}_n^{\mathcal{N}_{\text{in}}}, \qquad \text{for } n = 1, \ldots, \mathcal{N}_{\text{in}}, \tag{5.2.6a}$$

where $\mathbb{U}, \mathbb{T} \in \mathbb{R}^{\mathcal{N}_{\text{in}},\mathcal{N}_{\text{in}}}$ are given by

$$\mathbb{U}_{i,i'} = (A(g_i), A(g_{i'}))_{\mathcal{Y}}, \quad \mathbb{T}_{i,i'} = (g_i, g_{i'})_{\mathcal{T}}, \quad i, i' = 1, \ldots, \mathcal{N}_{\text{in}}, \tag{5.2.6b}$$

and the vectors $\{\boldsymbol{\phi}_n^{\mathcal{N}_{\text{in}}}\}_n$ are related to the transfer-eigenmodes $\{\boldsymbol{\phi}_j^{\mathcal{N}_{\text{in}}}\}_n$ by the relation

$$\phi_n^{\mathcal{N}_{\text{in}}} = \sum_{i=1}^{\mathcal{N}_{\text{in}}} (\boldsymbol{\phi}_n^{\mathcal{N}_{\text{in}}})_i \, g_i. \tag{5.2.6c}$$

We observe that eigenproblem (5.2.6) is not fully actionable since evaluations of the map $A(\cdot)$ involve the solution to a PDE: we should thus replace $A$ with the corresponding FE counterpart $A^{\text{FE}}$. To simplify notation, we here omit the superscript $^{\text{FE}}$.

We recall that the transfer eigenproblem (5.2.2) has been first introduced and studied in the approximation theory literature (see, e.g., [172]). More recently, Babuška and Lipton in [8] employed the transfer eigenmodes to define local approximation spaces in the framework of Generalized Finite Element method ([151, 7]). Similarly, Smetana and Patera in [204] exploited the eigenmodes associated with the transfer eigenproblem in the context of Port-Reduced static condensation Reduced Basis Element (PR-scRBE, [171, 72]) method.

The transfer eigenproblem is tightly connected to the eigenproblem obtained using POD. In more detail, if we choose an orthonormal basis $\{g_n\}_{n=1}^{\mathcal{N}_{\text{in}}}$ for $\mathcal{T}_{\mathcal{N}_{\text{in}}}$, (5.2.6) reduces to the

eigenproblem

$$\mathbb{U}\,\phi_n^{\mathcal{N}_{\text{in}}} = \lambda_n^{\mathcal{N}_{\text{in}}}\phi_n^{\mathcal{N}_{\text{in}}}, \qquad \text{for } n = 1, \ldots, \mathcal{N}_{\text{in}};$$

this corresponds to the eigenproblem obtained by applying POD based on the method of snapshots ([202]) to the set $\{A(g_n)\}_{n=1}^{\mathcal{N}_{\text{in}}}$. We observe that, unlike the reduced space generated by POD, the reduced space $\mathcal{Z}_N^{\text{te},\mathcal{N}_{\text{in}}}$ is independent of the particular basis of $\mathcal{T}_{\mathcal{N}_{\text{in}}}$ employed.

### 5.2.2 The case $\mathcal{P}^{\text{bk}} \neq \{\bar{\mu}\}$

If $\mathcal{P}^{\text{bk}} \neq \{\bar{\mu}\}$, we adopt a two-stage procedure based on the combination of the method presented above and POD. We first consider a finite-dimensional discretization of $\mathcal{P}^{\text{bk}}$, $\mathcal{P}^{\text{bk}}_{\text{train}} = \{\mu^i\}_{i=1}^{n_{\text{train}}}$. Then, we solve $n_{\text{train}}$ transfer eigenproblems, one for each value of the parameter, to obtain $n_{\text{train}}$ $N$-dimensional transfer eigenspaces $\{\mathcal{Z}_N^{\text{te},\mathcal{N}_{\text{in}}}(\mu^i)\}_{i=1}^{n_{\text{train}}}$. Finally, we generate the background space $\mathcal{Z}_N$ by applying POD to the set of snapshots $\{A(\phi_n^{\mathcal{N}_{\text{in}},i};\mu^i)\}_{i,n}$, where $\|\phi_n^{\mathcal{N}_{\text{in}},i}\|_{\mathcal{T}} = 1$ for all $i = 1, \ldots, n_{\text{train}}$ and $n = 1, \ldots, N$. Algorithm 5.2.1 summarises the computational procedure. We refer to [204] for a different strategy to construct $\mathcal{Z}_N$ when $\mathcal{P}^{\text{bk}} \neq \{\bar{\mu}\}$.

**Algorithm 5.2.1** Construction of the localized reduced space

| | | |
|---|---|---|
| **Input** | $\mathcal{P}^{\text{bk}}_{\text{train}} = \{\mu^i\}_{i=1}^{n_{\text{train}}} \subset \mathcal{P}^{\text{bk}}$ | discretized parameter space |
| | $N$ | dimension of the background space |
| **Output** | $\mathcal{Z}_N$ | background space |

1: Define the basis $\{g_1, \ldots, g_{\mathcal{N}_{\text{in}}}\}$ for $\mathcal{T}_{\mathcal{N}_{\text{in}}}$.

2: **for** $i = 1 \ldots n_{\text{train}}$ **do**

3: Compute the first $N$ normalised eigenmodes $\{\phi_n^{\mathcal{N}_{\text{in}},i}\}_{n=1}^{N}$ associated with $A^i := A(\cdot;\mu^i)$ using (5.2.4), ($\|\phi_n^{\mathcal{N}_{\text{in}},i}\|_{\mathcal{T}} = 1$, $i = 1, \ldots, n_{\text{train}}$, $n = 1, \ldots, N$).

4: **end for**

5: Apply POD to the set of snapshots $\{A(\phi_n^{\mathcal{N}_{\text{in}},i};\mu^i)\}_{n=1,\ldots,N,\, i=1,\ldots,n_{\text{train}}}$ to generate $\mathcal{Z}_N \subset \mathcal{Y}$.

We observe that

$$\|A(\phi_n^{\mathcal{N}_{\text{in}},i};\mu^i)\|_{\mathcal{Y}}^2 = (A(\phi_n^{\mathcal{N}_{\text{in}},i};\mu^i),\, A(\phi_n^{\mathcal{N}_{\text{in}},i};\mu^i)) = \lambda_n^{\mathcal{N}_{\text{in}},i}\,(\phi_n^{\mathcal{N}_{\text{in}},i},\, \phi_n^{\mathcal{N}_{\text{in}},i})_{\mathcal{T}} = \lambda_n^{\mathcal{N}_{\text{in}},i}.$$

Therefore, the POD reduction implicitly takes into account the relative importance — quantified by the value of the corresponding transfer eigenvalue — of the different snapshots. Recalling the connection between transfer eigenspace and POD, we can reinterpret the procedure described in Algorithm (5.2.1) as a Hierarchical Approximate Proper Orthogonal Decomposition (HAPOD, [108, 169]). Using terminology introduced in [108], our approach corresponds to a *distributed approximated POD*. We exploit this connection in the analysis. We finally observe that the construction of $\mathcal{Z}_N$ requires the solution to $n_{\text{train}} \cdot \mathcal{N}_{\text{in}}$ PDEs in the bk domain $\Omega^{\text{bk}}$, the solution to $n_{\text{train}}$ eigenproblems of size $\mathcal{N}_{\text{in}}$, and the solution to an eigenproblem of size $n_{\text{train}} \cdot N$. Although computations can be trivially parallelized, we envision that Algorithm 5.2.1 is affordable only for moderate values of $n_{\text{train}}$. Therefore, our technique can be applied only to low-dimensional parameter spaces $\mathcal{P}^{\text{bk}}$.

## 5.3 Analysis

### 5.3.1 Optimal approximation spaces

In view of the analysis, we present a first definition of optimality in the sense of Kolmogorov ([172]).

**Definition 5.3.1.** *Given $N > 0$, we say that $Z_N^{\text{kolm}} \subset \mathcal{Y}$ is the optimal $N$-dimensional approximation space for $A(\mathcal{T}) := \{A(g) : g \in \mathcal{T}\}$ if and only if*

$$Z_N^{\text{kolm}} = \arg \inf_{Z_N \subset \mathcal{Y},\, \dim Z_N = N} d\left(A(\mathcal{T}), Z_N\right), \tag{5.3.1a}$$

*where $d\left(A(\mathcal{T}), Z_N\right)$ is defined as*

$$d\left(A(\mathcal{T}), Z_N\right) = \sup_{g \in \mathcal{T}} \frac{\|A(g) - \Pi_{Z_N}^{\mathcal{Y}} A(g)\|_{\mathcal{Y}}}{\|g\|_{\mathcal{T}}}. \tag{5.3.1b}$$

*We say that $d_N(A(\mathcal{T})) = d\left(A(\mathcal{T}), Z_N^{\text{kolm}}\right)$ is the Kolmogorov $N$-width associated with the manifold $A(\mathcal{T})$.*

Several variants of Kolmogorov $N$-width have been proposed in the literature. In the MOR literature, provided that the manifold $\mathcal{M}^{\text{bk}}$ is compact, Kolmogorov $N$-width is defined as (see, e.g., [56])

$$\hat{d}_N(\mathcal{M}^{\text{bk}}) = \inf_{Z_N \subset \mathcal{Y},\, \dim Z_N = N} \sup_{u \in \mathcal{M}^{\text{bk}}} \|u - \Pi^{\mathcal{Y}}_{Z_N} u\|_{\mathcal{Y}}. \tag{5.3.2}$$

Kolmogorov $N$-widths measure the performance of the best linear approximation space of size $N$: they thus provide a lower bound for the best-fit error associated with any $N$-dimensional linear space obtained using a model-reduction technique. For this reason, we can interpret them as measures of the reducibility of the manifold $\mathcal{M}^{\text{bk}}$. *A priori* results for the convergence of the $N$-width with $N$ are limited to a few model problems: see [100, Example 3.4], [188, Section 8.1.1], [215, Example 2.5], and [8, Theorem 3.3]. Several empirical studies suggest that $N$-widths converge rapidly for diffusion-dominated problems, and significantly less rapidly for advection-dominated problems. Recalling the example in section 5.1.2, this is strongly related to the concept of evanescence.

Next Proposition shows an interesting relation between (5.3.1b) and (5.3.2).

**Proposition 5.3.1.** *Let us assume that $\widetilde{\mathcal{T}}$ is the ball of radius $C$ in $\mathcal{T}$, and let us consider the bk manifold $\mathcal{M}^{\text{bk}} = A(\widetilde{\mathcal{T}})$. Let us further define the optimal space*

$$Z_N^{\text{kolm},2} := \arg \inf_{Z_N \subset \mathcal{Y},\, \dim Z_N = N} \sup_{u \in \mathcal{M}^{\text{bk}}} \|u - \Pi^{\mathcal{Y}}_{Z_N} u\|_{\mathcal{Y}}.$$

*Then, $Z_N^{\text{kolm},2} = Z_N^{\text{kolm}}$, and $\hat{d}_N(\mathcal{M}^{\text{bk}}) = C\, d(A(\mathcal{T}))$.*

*Proof.* Using the definition of $\mathcal{M}^{\text{bk}}$, we first obtain:

$$\begin{aligned} Z_N^{\text{kolm},2} &= \arg\inf_{Z_N \subset \mathcal{Y},\, \dim Z_N = N} \sup_{u \in \mathcal{M}^{\text{bk}}} \|u - \Pi^{\mathcal{Y}}_{Z_N} u\|_{\mathcal{Y}} \\ &= \arg\inf_{Z_N \subset \mathcal{Y},\, \dim Z_N = N} \sup_{g \in \mathcal{T}, \|g\|_{\mathcal{T}} \le C} \|A(g) - \Pi^{\mathcal{Y}}_{Z_N} A(g)\|_{\mathcal{Y}} \end{aligned}$$

Since $A - \Pi^{\mathcal{Y}}_{Z_N} A : \mathcal{T} \to \mathcal{Y}$ is a linear operator, we find

$$Z_N^{\text{kolm},2} = \arg\inf_{Z_N \subset \mathcal{Y},\, \dim Z_N = N} \sup_{g \in \mathcal{T}, \|g\|_{\mathcal{T}} = C} \|A(g) - \Pi^{\mathcal{Y}}_{Z_N} A(g)\|_{\mathcal{Y}}$$

Finally, multiplying by $\frac{C}{C}$ and recalling (5.3.1), we find

$$Z_N^{\text{kolm},2} = \arg C \left( \inf_{Z_N \subset \mathcal{Y}, \dim Z_N = N} \sup_{g \in \mathcal{T}} \frac{\|A(g) - \Pi_{Z_N}^{\mathcal{Y}} A(g)\|_{\mathcal{Y}}}{\|g\|_{\mathcal{T}}} \right) = Z_N^{\text{kolm}}.$$

This proves the first statement of the proof. The second statement can be shown using the same argument. □

We now provide another definition of optimality. For simplicity, we state the definition for a finite set of snapshots rather than a continuous manifold. We refer to [28, section 2.3] for the generalization of this definition to manifolds.

**Definition 5.3.2.** *Given $N > 0$, and the set of snapshots $\mathcal{S} = \{u_i\}_{i=1}^{|\mathcal{S}|}$, we say that $Z_N^{\ell^2} \subset \mathcal{Y}$ is the optimal $N$-dimensional approximation space for $\mathcal{S}$ in the $\ell^2$-sense if and only if*

$$Z_N^{\ell^2} = \arg \inf_{Z_N \subset \mathcal{Y}, \dim Z_N = N} d^{\ell^2}(\mathcal{S}, Z_N) := \frac{1}{|\mathcal{S}|} \sum_{i=1}^{|\mathcal{S}|} \|u_i - \Pi_{Z_N}^{\mathcal{Y}} u_i\|_{\mathcal{Y}}^2. \tag{5.3.3}$$

*We further define $d_N^{\ell^2}(\mathcal{S}) := d^{\ell^2}(\mathcal{S}, Z_N^{\ell^2})$*

### 5.3.2 The case $\mathcal{P}^{\text{bk}} = \{\bar{\mu}\}$

We first state the key result of this section. We refer to [172, Chapter 4, Theorem 2.2] for the proof.

**Proposition 5.3.2.** *Let $A : \mathcal{T} \to \mathcal{Y}$ defined in (5.2.1) be a linear compact operator. Then, for any $N > 0$ the space $\mathcal{Z}_N^{\text{te}}$ defined in (5.2.3) is the optimal $N$-dimensional approximation space for $A(\mathcal{T})$, i.e., $\mathcal{Z}_N^{\text{te}} = Z_N^{\text{kolm}}$. Furthermore,*

$$d(A(\mathcal{T})) = \sqrt{\lambda_{N+1}}. \tag{5.3.4}$$

Exploiting Proposition 5.3.1, provided that $\widetilde{\mathcal{T}}$ is the ball of radius $C$ in $\mathcal{T}$, it follows that $\mathcal{Z}_N^{\text{te}} = Z_N^{\text{kolm},2}$ and $\hat{d}_N(\mathcal{M}^{\text{bk}}) = C\sqrt{\lambda_{N+1}}$. Next Proposition provides a bound on the performance of the semi-discrete transfer eigenspace $Z_N^{\text{te},\mathcal{N}_{\text{in}}}$ (5.2.5).

**Proposition 5.3.3.** *Let $\mathcal{T}_{\mathcal{N}_{\text{in}}} = \text{span}\{g_1, \ldots, g_{\mathcal{N}_{\text{in}}}\} \subset \mathcal{T}$, and let $\mathcal{Z}_N^{\text{te},\mathcal{N}_{\text{in}}}$ be the corresponding*

*semi-discrete transfer eigenspace* (5.2.5) *computed based on* (5.2.6). *For any* $g \in \mathcal{T}$, *we have*

$$\|A(g) - \Pi^{\mathcal{Y}}_{\mathcal{Z}_N^{\mathrm{te},\mathcal{N}_{\mathrm{in}}}} A(g)\|_{\mathcal{Y}} \leq \|A\|_{\mathcal{L}(\mathcal{T}^{\perp}_{\mathcal{N}_{\mathrm{in}}},\mathcal{Y})} \|\Pi^{\mathcal{T}}_{\mathcal{T}^{\perp}_{\mathcal{N}_{\mathrm{in}}}} g\|_{\mathcal{T}} + \sqrt{\lambda^{\mathcal{N}_{\mathrm{in}}}_{N+1}} \|g\|_{\mathcal{T}}, \tag{5.3.5}$$

*where* $\lambda^{\mathcal{N}_{\mathrm{in}}}_{N+1}$ *is the* $N+1$ *eigenvalue of the semi-discrete eigenproblem* (5.2.4).

*Proof.* Exploiting the linearity of the operator $A$ and applying (5.3.4) in the finite dimensional case, we find

$$\begin{aligned}
\inf_{\phi \in \mathcal{Z}_N^{\mathrm{te},\mathcal{N}_{\mathrm{in}}}} \|A(g) - \phi\|_{\mathcal{Y}} \leq & \inf_{\phi \in \mathcal{Z}_N^{\mathrm{te},\mathcal{N}_{\mathrm{in}}}} \|A(g) - A\left(\Pi^{\mathcal{T}}_{\mathcal{T}_{\mathcal{N}_{\mathrm{in}}}} g\right)\|_{\mathcal{Y}} + \|A\left(\Pi^{\mathcal{T}}_{\mathcal{T}_{\mathcal{N}_{\mathrm{in}}}} g\right) - \phi\|_{\mathcal{Y}} \\
\leq & \|A\|_{\mathcal{L}(\mathcal{T}^{\perp}_{\mathcal{N}_{\mathrm{in}}},\mathcal{Y})} \|\Pi^{\mathcal{T}}_{\mathcal{T}^{\perp}_{\mathcal{N}_{\mathrm{in}}}} g\|_{\mathcal{T}} + \inf_{\phi \in \mathcal{Z}_N^{\mathrm{te},\mathcal{N}_{\mathrm{in}}}} \|A\left(\Pi^{\mathcal{T}}_{\mathcal{T}_{\mathcal{N}_{\mathrm{in}}}} g\right) - \phi\|_{\mathcal{Y}} \\
\leq & \|A\|_{\mathcal{L}(\mathcal{T}^{\perp}_{\mathcal{N}_{\mathrm{in}}},\mathcal{Y})} \|\Pi^{\mathcal{T}}_{\mathcal{T}^{\perp}_{\mathcal{N}_{\mathrm{in}}}} g\|_{\mathcal{T}} + \underbrace{d(A(\mathcal{T}_{\mathcal{N}_{\mathrm{in}}}), \mathcal{Z}_N^{\mathrm{te},\mathcal{N}_{\mathrm{in}}})}_{=\sqrt{\lambda^{\mathcal{N}_{\mathrm{in}}}_{N+1}}} \|g\|_{\mathcal{T}},
\end{aligned}$$

Thesis follows. □

Proposition 5.3.3 is extremely important in the context of data assimilation. In many engineering applications, the set of possible inputs might be very high dimensional, but it might be well-approximated by a lower dimensional space. Proposition 5.3.3 shows that we can reduce the dimension of the discrete input space without significantly deteriorating the approximation properties of $\mathcal{Z}_N^{\mathrm{te},\mathcal{N}_{\mathrm{in}}}$. This leads to a two-step reduction, the former on the input port (based for instance on a polynomial expansion) and the second one in the interior of the domain (based on the transfer eigenproblem). We observe that by reducing $\mathcal{N}_{\mathrm{in}}$, we can substantially reduce the offline computational cost, which is dominated by the solution to $\mathcal{N}_{\mathrm{in}}$ PDEs in the large domain $\Omega^{\mathrm{bk}}$.

### Sufficient conditions for compactness

Proposition 5.3.2 shows that the reduced space built by solving the transfer eigenproblem is optimal in the sense of Kolmogorov if the solution map $A$ (5.2.1) is compact. We now provide sufficient conditions under which the solution map associated with a given mathematical model is compact.

**Hypothesis 1.** ***(geometry and functional spaces)*** *Let* $\Omega^{\mathrm{bk}} \subset \mathbb{R}^d$ *be a* $d$*-dimensional Lipschitz domain, let* $\Gamma^{\mathrm{in}} \subset \partial\Omega^{\mathrm{bk}}$ *be an open set and let* $\Omega \subset \overline{\Omega}^{\mathrm{bk}}$ *be either a* $d$*-dimensional*

*open set or a $(d-1)$-dimensional open set. Then, let us introduce the space $\mathcal{V}^{\text{bk}} = H^s(\Omega^{\text{bk}})$, the space $\mathcal{T} = H^{s-1/2}(\Gamma^{\text{in}})$, and the space $\mathcal{Y}$ to be either $H^s(\Omega)$ if $\Omega$ is $d$-dimensional or $H^{s-1/2}(\Omega)$ if $\Omega$ is $(d-1)$-dimensional.*

*We assume that $\Omega$ and $\Gamma^{\text{in}}$ satisfy the condition*

$$\operatorname{dist}(\overline{\Omega}, \overline{\Gamma}^{\text{in}}) = \min_{x \in \overline{\Omega}} \min_{y \in \overline{\Gamma}^{\text{in}}} \|x - y\|_2 > 0. \tag{5.3.6}$$

*Furthermore, we assume that $s$ is a strictly positive integer, $s \geq 1$.*

**Hypothesis 2.** ***(solution operators)*** *We assume that $\widehat{A} : \mathcal{T} \to \mathcal{V}^{\text{bk}}$ is a linear continuous operator, $\widehat{A} \in \mathcal{L}(\mathcal{T}, \mathcal{V}^{\text{bk}})$, and that $\mathcal{G}^{\text{bk}} : \mathcal{V}^{\text{bk}} \times \mathcal{V}_0^{\text{bk}} \to \mathbb{R}$ is a continuous bilinear form. We further assume that for any $d$-dimensional domain $\Omega^\star \subset \Omega^{\text{bk}}$, $\operatorname{dist}(\overline{\Omega}^\star, \overline{\Gamma}^{\text{in}}) > 0$, there exists $C = C(\Omega^{\text{bk}}, \Omega^\star) > 0$ such that for any $g \in \mathcal{T}$*

$$\|\widehat{A}(g)\|_{H^s(\Omega^\star)} \leq C(\Omega^{\text{bk}}, \Omega^\star) \|\widehat{A}(g)\|_{H^{s-1}(\Omega^{\text{bk}})}. \tag{5.3.7}$$

We briefly comment on the two hypotheses. Recalling the continuity of the trace operator, Hypothesis 1 implies that there exist $C(\mathcal{V}^{\text{bk}}, \mathcal{T})$, $C(\mathcal{V}^{\text{bk}}, \mathcal{Y}) > 0$ such that

$$\|u|_{\Gamma^{\text{in}}}\|_{\mathcal{T}} \leq C(\mathcal{V}^{\text{bk}}, \mathcal{T}) \|u\|_{\mathcal{V}^{\text{bk}}}, \qquad \|u|_{\Omega}\|_{\mathcal{Y}} \leq C(\mathcal{V}^{\text{bk}}, \mathcal{Y}) \|u\|_{\mathcal{V}^{\text{bk}}}, \qquad \forall\, u \in \mathcal{V}^{\text{bk}}.$$

Combining the latter with Hypothesis 2, since $g = \widehat{A}(g)|_{\Gamma^{\text{in}}}$, we find that

$$\frac{1}{C(\mathcal{V}^{\text{bk}}, \mathcal{T})^2} \|g\|_{\mathcal{T}}^2 \leq \|\widehat{A}(g)\|_{\mathcal{V}^{\text{bk}}}^2 \leq \|\widehat{A}\|_{\mathcal{L}(\mathcal{T}, \mathcal{V}^{\text{bk}})}^2 \|g\|_{\mathcal{T}}^2.$$

This implies that we can endow $\mathcal{T}$ with the inner product $(g, g')_{\mathcal{T}} = (\widehat{A}(g),\, \widehat{A}(g'))_{\mathcal{V}^{\text{bk}}}$.

Next result motivates the previous hypotheses.

**Proposition 5.3.4.** *Let Hypotheses 1 and 2 hold. Then, the operator $A$ is compact from $\mathcal{T}$ to $\mathcal{Y}$.*

*Proof.* We must show that given the sequence $\{g_n\}_n \subset \mathcal{T}$, $\|g_n\|_{\mathcal{T}} \leq C$, then the sequence $\{A(g_n)\}_n$ admits a strongly convergent subsequence in $\mathcal{Y}$. Recalling that $\widehat{A} \in \mathcal{L}(\mathcal{T}, \mathcal{V}^{\text{bk}})$, the sequence $\{\widehat{A}(g_n)\}_n$ is bounded in $\mathcal{V}^{\text{bk}}$. Then, due to Banach Alaoglu theorem (see, e.g., [192, Theorem 6.12]), there exists a subsequence $\{\widehat{A}(g_{n_m})\}_m$ that converges weakly to

$\bar{u} \in \mathcal{V}^{\text{bk}}$. Recalling the definition of weak convergence, and recalling that for any $\phi \in \mathcal{V}_0^{\text{bk}}$, $\mathcal{G}^{\text{bk}}(\cdot, \phi) \in (\mathcal{V}^{\text{bk}})'$, we have that

$$0 = \mathcal{G}^{\text{bk}}\left(\widehat{A}(g_{n_m}), \phi\right) \to \mathcal{G}^{\text{bk}}(\bar{u}, \phi) = 0 \qquad \forall\, \phi \in \mathcal{V}_0^{\text{bk}}.$$

This implies that $\bar{u} = \widehat{A}(\bar{u}|_{\Gamma^{\text{in}}})$. Then, exploiting (5.3.7), we find that for any $\Omega^\star \subset \Omega^{\text{bk}}$, dist $(\overline{\Omega}^\star, \overline{\Gamma}^{\text{in}}) > 0$,

$$\|\bar{u} - \widehat{A}(g_{n_m})\|_{H^s(\Omega^\star)} \leq C(\Omega^{\text{bk}}, \Omega^\star)\|\bar{u} - \widehat{A}(g_{n_m})\|_{H^{s-1}(\Omega^{\text{bk}})}.$$

Since $\mathcal{V}^{\text{bk}} = H^s(\Omega^{\text{bk}})$ is compactly embedded in $H^{s-1}(\Omega^{\text{bk}})$ (see, e.g., [181, Theorem 1.3.5]), we have that $\|\bar{u} - \widehat{A}(g_{n_m})\|_{H^{s-1}(\Omega^{\text{bk}})} \to 0$ as $m \to \infty$.

In order to complete the proof, we must distinguish two cases. If $\Omega \subset \mathbb{R}^d$, then thesis follows by substituting $\Omega^\star = \Omega$ and observing that $\|\bar{u} - \widehat{A}(g_{n_m})\|_{H^s(\Omega)} = \|\bar{u} - A(g_{n_m})\|_{\mathcal{Y}}$. On the other hand, if $\Omega \subset \mathbb{R}^{d-1}$, thesis follows by considering $\Omega^\star$ such that $\Omega \subset \partial\Omega^\star$ and then invoking the continuity of the trace operator from $H^s(\Omega^\star)$ to $H^{s-1/2}(\Omega)$. □

Exploiting Proposition 5.3.4, given a particular bk model, we can assess whether or not the reduced space based on the transfer eigenmodes is optimal by verifying Hypotheses 1 and 2. We observe that Hypothesis 1 depends only on the geometry and can be trivially checked. On the other hand, Hypothesis 2 depends on the particular differential operator and should be checked separately. Typically, the hardest condition to verify is inequality (5.3.7), known as *Caccioppoli's inequality*. In Appendix C, we show that the differential operators associated with (i) linear damped elastodynamics, (ii) Stokes flow, (iii) advection-diffusion-reaction equation, and (iv) Helmholtz equation satisfy this inequality.

### 5.3.3 The case $\mathcal{P}^{\text{bk}} \neq \{\bar{\mu}\}$

Exploiting the connection with Hierarchical Approximate Proper Orthogonal Decomposition, we can show the following Proposition. We refer to [108, Corollary 3.5] for the proof. We observe that the result does not address whether or not our construction is optimal and in which sense; this is the subject of ongoing research.

**Proposition 5.3.5.** *Let $\{g_1, \ldots, g_{\mathcal{N}_{\text{in}}}\} \subset \mathcal{T}$ be an orthonormal basis of $\mathcal{T}_{\mathcal{N}_{\text{in}}}$. Let us define $\epsilon_N^{\text{te,i}} = \sum_{n=N+1}^{\mathcal{N}_{\text{in}}} \lambda_n^{\mathcal{N}_{\text{in}},i}$ for $i = 1, \ldots, n_{\text{train}}$, where $\{\lambda_n^{\mathcal{N}_{\text{in}},i}\}_{n=1}^{\mathcal{N}_{\text{in}}}$ are the transfer eigenvalues*

*associated with* (5.2.4). *Let us further define* $\epsilon_N^{\text{POD}} = \sum_{n=N+1}^{Nn_{\text{train}}} \lambda_n^{\text{POD}}$, *where* $\{\lambda_n^{\text{POD}}\}_{n=1}^{Nn_{\text{train}}}$ *are the POD eigenvalues. Then, if* $\epsilon^\star > 0$ *and* $\omega \in (0,1)$ *satisfy*

$$\epsilon_N^{\text{te,i}} \leq \frac{\sqrt{1-\omega^2}}{\sqrt{n_{\text{train}}-1}}\epsilon^\star \;\; i = 1,\dots,n_{\text{train}}; \qquad \epsilon_N^{\text{POD}} \leq \frac{\sqrt{\mathcal{N}_{\text{in}}}}{\sqrt{n_{\text{train}}}}\omega\epsilon^\star, \tag{5.3.8a}$$

*the following holds*

$$\frac{1}{\mathcal{N}_{\text{in}} n_{\text{train}}} \sum_{n=1}^{\mathcal{N}_{\text{in}}} \sum_{i=1}^{n_{\text{train}}} \|A(g_n;\mu^i) - \Pi_{\mathcal{Z}_N}^{\mathcal{Y}} A(g_n;\mu^i)\|_{\mathcal{Y}}^2 \leq (\epsilon^\star)^2. \tag{5.3.8b}$$

*Furthermore, the number of POD modes associated with* $\{A(g,\mu^i)\}_{i,n}$ *required to obtain the accuracy* $\tilde{\epsilon} = \sqrt{\frac{1-\omega^2}{n_{\text{train}}-1}}\epsilon^\star$ *is greater or equal than* $N$*:*

$$N \leq \min\left\{N' \in \{1,\dots,n_{\text{train}}\cdot\mathcal{N}_{\text{in}}\} : \; d_{N'}^{\ell^2}(\{A(g_n;\mu^i)\}_{n,i}) \leq \tilde{\epsilon}^2\right\}, \tag{5.3.8c}$$

*where* $d_N^{\ell^2}$ *is introduced in Definition 5.3.2.*

## 5.4 Numerical results

### 5.4.1 Application to a two-dimensional acoustic problem

#### Problem definition

We consider the following model problem:

$$\begin{cases} -(1+\epsilon i)\Delta u^{\text{true}}(\mu) - \mu^2 u^{\text{true}}(\mu) = f & \text{in } \Omega^{\text{pb}}; \\ \partial_n u^{\text{true}}(\mu) = 0 & \text{on } \partial\Omega^{\text{pb}} \setminus \Gamma; \\ u^{\text{true}}(\mu) = g^{\text{true}} & \text{on } \Gamma; \end{cases} \tag{5.4.1}$$

where $\epsilon = 10^{-4}$, $f(x) = \frac{10}{2\pi\sigma^2}\exp\big(-\frac{1}{2\sigma^2}\big((x_1+0.75)^2 + (x_2-1.5)^2\big)\big)$, $\sigma = 0.2$, $\Omega^{\text{pb}} = (-1,3)\times(0,3)\setminus\Omega^{\text{cut}}$, $\Omega^{\text{cut}} = (-0.75,-0.5)\times(0,1)$, $\Gamma = \{-1\}\times(0,3)$. In all numerical simulations, we consider $g^{\text{true}} = g_k(x_2) = \sin(\pi k x_2)$ for $k = 1,2,3$ and we consider different choices of $\mu$. We then consider the domain of interest $\Omega = (2,3)^2$.

We consider the bk domain $\Omega^{\text{bk}} = (0,3)^2$ and the bk model

$$\begin{cases} -(1+\epsilon i)\Delta u_g^{\text{bk}}(\mu) - \mu^2 u_g^{\text{bk}}(\mu) = 0 & \text{in } \Omega^{\text{bk}}; \\ \partial_n u_g^{\text{bk}}(\mu) = 0 & \text{on } \partial\Omega^{\text{bk}} \setminus \Gamma^{\text{in}}; \\ u_g^{\text{bk}}(\mu) = g & \text{on } \Gamma^{\text{in}}; \end{cases} \tag{5.4.2}$$

where $\Gamma^{\text{in}} = \{0\} \times (0,3)$. We observe that for $f|_{\Omega^{\text{bk}}} \equiv 0$ and for any $g^{\text{true}} \in H^{1/2}(\Gamma)$ in (5.4.1) we have that the true field belongs to the bk manifold associated with (5.4.2), that is $u^{\text{true}} \in \mathcal{M}^{\text{bk}} := \{u_g^{\text{bk}}(\mu) = u_g(\mu)|_\Omega : \mu \in \mathcal{P}^{\text{bk}}, g \in \mathcal{T} = H^{1/2}(\Gamma^{\text{in}})\}$. Provided that the effect of the source term in $\Omega^{\text{bk}}$ is limited, we expect that the true field is close to the bk manifold $\mathcal{M}^{\text{bk}}$. Figure 5-1(a) shows the geometry.

Computations are based on a P4 FE discretization with $\mathcal{N}^{\text{pb}} = 12289$ degrees of freedom in $\Omega^{\text{pb}}$, $\mathcal{N}^{\text{bk}} = 9409$ degrees of freedom in $\Omega^{\text{bk}}$, and $\mathcal{N} = 1089$ degrees of freedom in $\Omega$. Figure 5-2 shows the field $u^{\text{true}}(\mu)$ for different $g^{\text{true}}$ and $\mu$. Figure 5-3 shows the variations in $\|u^{\text{true}}(\mu)\|_{H^1(\Omega^{\text{pb}})}$ as a function of $\mu$ for $g^{\text{true}} = g_1$; note that there are ten resonances in the parameter range $\mathcal{P}^{\text{bk}} = [2,4]$.

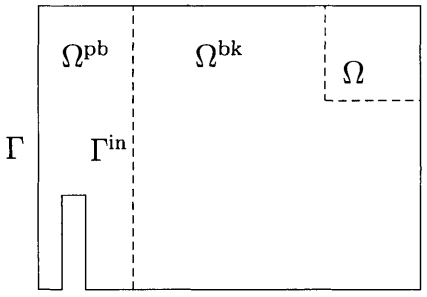


**Figure 5-1:** Application to a two-dimensional acoustic problem: computational domain.

**The case $\mathcal{P}^{\text{bk}} = \{\bar{\mu}\}$**

We first introduce the transfer eigenproblem and the transfer eigenspace. We consider $\mathcal{Y} = H^1(\Omega)$ endowed with the inner product $(u,v)_{\mathcal{Y}} = \int_\Omega \nabla u \cdot \nabla \bar{v} + u\bar{v}\, dx$; we consider $\mathcal{V}^{\text{bk}} = H^1(\Omega^{\text{bk}})$ endowed with the inner product $(u,v)_{\mathcal{V}^{\text{bk}}} = \int_{\Omega^{\text{bk}}} \nabla u \cdot \nabla \bar{v} + u\bar{v}\, dx$; and we consider $\mathcal{T} = H^{1/2}(\Gamma^{\text{in}})$ endowed with the inner product $(u,v)_{\mathcal{T}} = (E(u), E(v))_{\mathcal{V}^{\text{bk}}}$, where

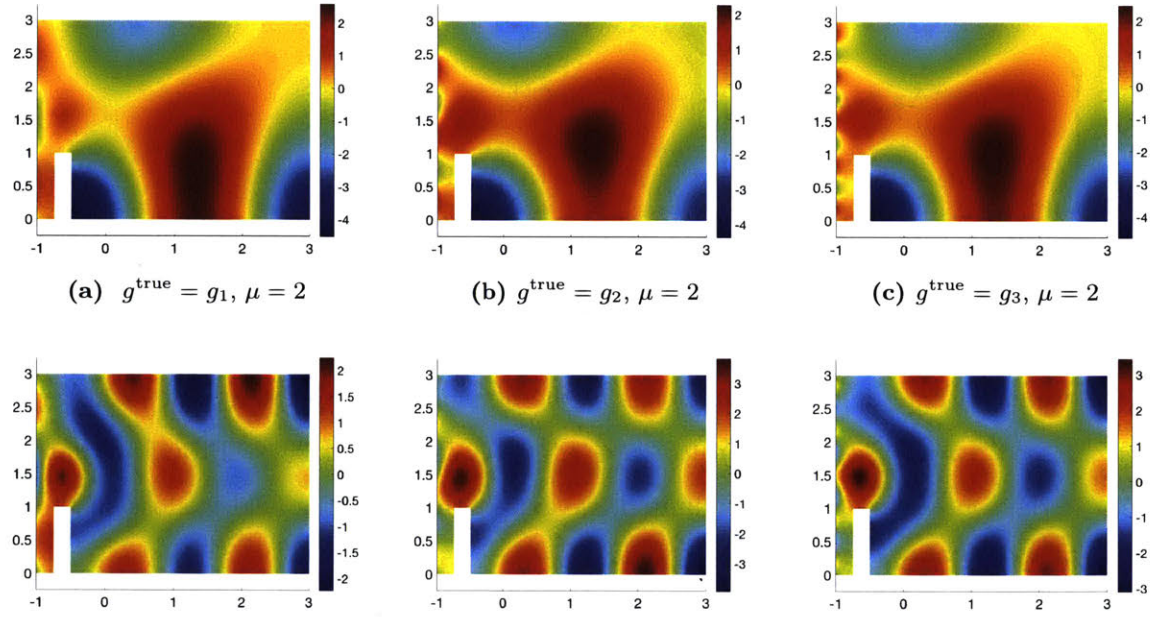

(a) $g^{\text{true}} = g_1$, $\mu = 2$ (b) $g^{\text{true}} = g_2$, $\mu = 2$ (c) $g^{\text{true}} = g_3$, $\mu = 2$

(d) $g^{\text{true}} = g_1$, $\mu = 4$ (e) $g^{\text{true}} = g_2$, $\mu = 4$ (f) $g^{\text{true}} = g_3$, $\mu = 4$

**Figure 5-2:** Application to a two-dimensional acoustic problem: visualization of the true field $u^{\text{true}}(\mu)$.

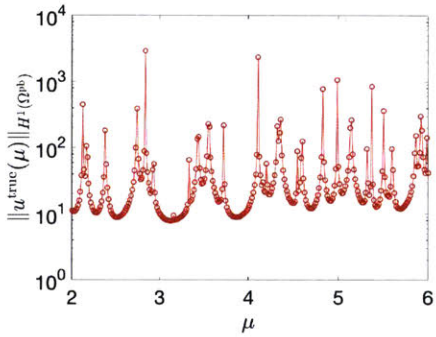


**Figure 5-3:** Application to a two-dimensional acoustic problem: behavior of $\|u_g^{\text{bk}}(\mu)\|_{H^1(\Omega^{\text{bk}})}$ with $\mu$ ( $g = g_1$).

$E : \mathcal{T} \to \mathcal{V}^{\text{bk}}$ is defined as the solution to the following PDE:

$$-\Delta E(g) + E(g) = 0 \ \text{ in}\,\Omega^{\text{bk}}, \quad \partial_n E(g) = 0 \ \text{ on}\,\partial\Omega^{\text{bk}} \setminus \Gamma^{\text{in}}; \quad E(g) = g \ \text{ on}\,\Gamma^{\text{in}}.$$

Finally, we consider a $\mathcal{N}_{\text{in}} = 20$-dimensional discretization of the input space $\mathcal{T}$ based on Legendre polynomials.

Figure 5-4(a) shows the behavior of $\sqrt{\lambda_{N+1}^{\mathcal{N}_{\text{in}}}}$ with $N$ for three different values of $\mu$, while

Figure 5-4(b) shows the behavior of the relative $H^1$ best-fit error

$$E_N^{\text{rel}} = \max_{k=1,2,3} \frac{\|u_k^{\text{true}}(\mu) - \Pi_{Z_N^{\text{te},\mathcal{N}_{\text{in}}}} u_k^{\text{true}}(\mu)\|_{\mathcal{Y}}}{\|u_k^{\text{true}}(\mu)\|_{\mathcal{Y}}} \tag{5.4.3}$$

where $u_k^{\text{true}}(\mu)$ is the solution to (5.4.1) for $g^{\text{true}} = g_k$. We observe that $\sqrt{\lambda_{N+1}^{\mathcal{N}_{\text{in}}}} \gtrsim E_N^{\text{rel}}$: this can be explained by recalling Proposition 5.3.2, and observing that the source term $f$ in (5.4.1) is negligible far from $x^\star = (-0.75, 1.5)$. We also observe that the transfer eigenvalues increase as $\mu$ increases: this is in good agreement with the discussion in section 5.1.2 for the semi-infinite wave-guide.

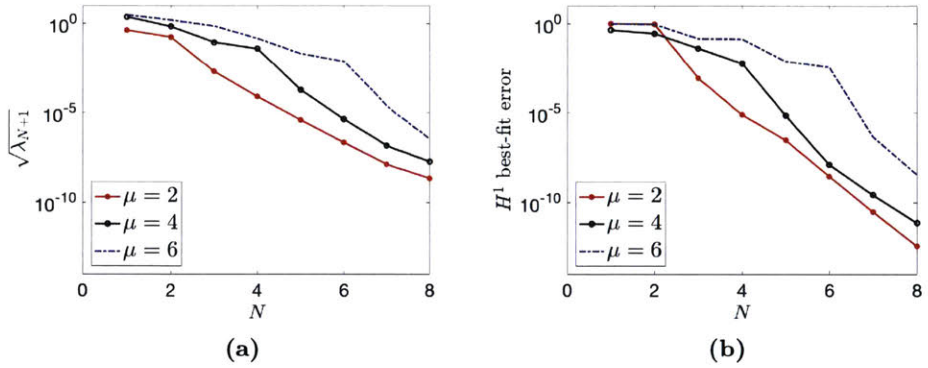


**Figure 5-4:** Application to a two-dimensional acoustic problem: transfer eigenproblem. Behavior of $\sqrt{\lambda_{N+1}^{\mathcal{N}_{\text{in}}}}$ (Figure (a)), and of the $H^1$ best-fit error (5.4.3) (Figure (b)), for three values of $\mu$ ($\mathcal{N}_{\text{in}} = 20$).

Figure 5-5 shows the performance of the data assimilation procedure. We here apply PBDW based on Gaussian functionals ($r_{\text{Gauss}} = 0.1$), with observation centers selected based on SGreedy-plus algorithm ($tol = 0.2$) and $\mathcal{U} = \mathcal{Y}$. To assess performance, we both consider $L^2$ and $H^1$ maximum relative error over the three choices of the Dirichlet datum $g_k(x_2) = \sin(\pi k x_2)$, $k = 1, 2, 3$. By comparing Figures 5-5(a) and (b) with Figure 5-4(b), we observe that, for sufficiently large $M$, the state estimation error is of the same order as $\|u^{\text{true}} - \Pi_{Z_N}^{\mathcal{Y}} u^{\text{true}}\|_{\mathcal{Y}}$: this is in agreement with the *a priori* result shown in Chapter 3. We further observe that convergence with $M$ due to the secondary approximation provided by the update space is slow: the estimated convergence rate in $L^2$ norm is roughly $M^{-1}$ for all values of $N$ considered[1] we address this issue in Chapter 6.

[1] In more detail, $E_{\max}^{\text{rel,L}^2} \approx M^{-1.0}$ for $N = 1, 3$, $E_{\max}^{\text{rel,L}^2} \approx M^{-1.1}$ for $N = 5, 6, 7$.

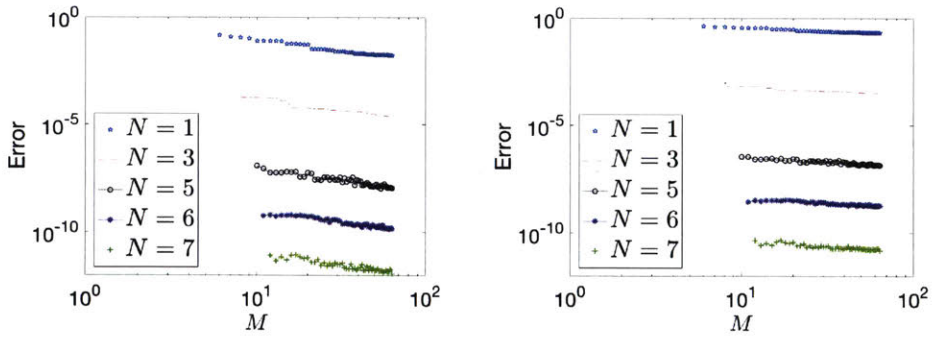


(a) $L^2$ (b) $H^1$

**Figure 5-5:** Application to a two-dimensional acoustic problem: behavior of the relative $L^2$ and $H^1$ errors ($\mu = 2$).

### The case $\mathcal{P}^{\text{bk}} \neq \{\bar{\mu}\}$

We first study the behavior of the eigenvalues associated with the application of Algorithm 5.2.1. We here set $n_{\text{train}} = 11$ and $\mathcal{N}_{\text{in}} = 20$, and we consider different values of $N$. Figure 5-6(a) shows the behavior of the transfer eigenvalues $\lambda_n^{\mathcal{N}_{\text{in}}}$ for different values of $\mu \in [2, 4]$, while Figure 5-6(b) shows the behavior of the POD eigenvalues $\lambda_n^{\text{POD}}$ for different choices of $N$. We observe exponential convergence of the POD eigenvalues. We further observe that POD eigenvalues are weakly affected by the value $N$: this means that only the first few transfer eigenmodes contribute to the final background $\mathcal{Z}_N$.

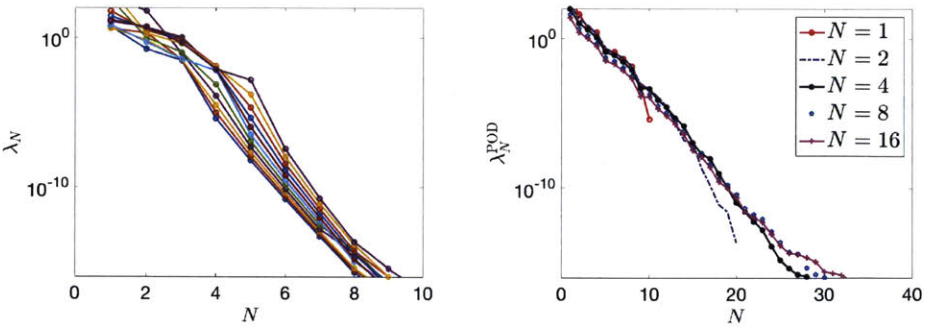


(a) (b)

**Figure 5-6:** Application to a two-dimensional acoustic problem: application of Algorithm 5.2.1. Figure (a): behavior of the transfer eigenvalues $\lambda_n^{\mathcal{N}_{\text{in}}}$ for different values of $\mu \in [2, 4]$. Figure (b): behavior of the POD eigenvalues $\lambda_n^{\text{POD}}$ for different choices of $N$ ($n_{\text{train}} = 11$, $\mathcal{N}_{\text{in}} = 20$).

Figure 5-7 shows the performance of the data assimilation procedure. As in the previous example, we here apply PBDW based on Gaussian functionals ($r_{\text{Gauss}} = 0.1$), with observation centers selected based on SGreedy-plus algorithm ($tol = 0.2$) and $\mathcal{U} = \mathcal{Y}$. To

assess performance, we consider $H^1$ maximum relative error over the three choices of the Dirichlet datum $g_k(x_2) = \sin(\pi k x_2)$, $k = 1, 2, 3$, and $n_{\text{test}} = 5$ different values of $\mu$ in $\mathcal{P}^{\text{bk}}$. To interpret results, we also report the behavior of the relative $H^1$ best-fit error. We observe that our procedure is able to generate an extremely accurate background space for the bk manifold $\mathcal{M}^{\text{bk}}$.

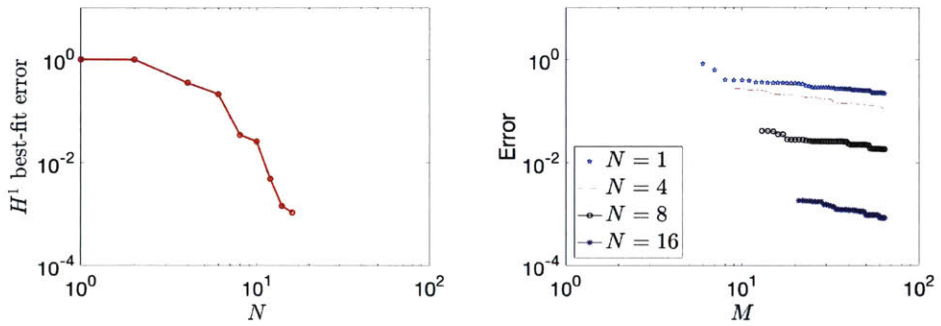


**(a)** **(b)** $H^1$

**Figure 5-7:** Application to a two-dimensional acoustic problem: data assimilation results. Figure (a): behavior of the $H^1$ best-fit error with $N$. Figure (b): behavior of the PBDW relative $H^1$ error with $M$. ($n_{\text{train}} = 11$, $\mathcal{N}_{\text{in}} = 20$, $n_{\text{test}} = 5$).

### 5.4.2 Application to a three-dimensional acoustic problem

We now consider the three-dimensional model problem:

$$\begin{cases} -(1+\epsilon i)\Delta u_g(\mu) - \mu^2 u_g(\mu) = 0 & \text{in } \Omega^{\text{pb}} = \Omega^{\text{bk}}; \\ \partial_n u_g(\mu) = 0 & \text{on } \partial\Omega^{\text{pb}} \setminus \Gamma^{\text{in}}; \\ u_g(\mu) = g & \text{on } \Gamma^{\text{in}}; \end{cases} \tag{5.4.4}$$

where $\epsilon = 10^{-4}$, $\Omega^{\text{pb}} = (-1.5, 1.5)\times(0,3)\times(0,3)\setminus\Omega^{\text{cut}}$, $\Omega^{\text{cut}} = (-0.5, 0.5)\times(0.25, 0.5)\times(0,1)$, $\Gamma^{\text{in}} = (-1.5, 1.5) \times \{0\} \times (0,3)$, and we choose $\Omega = (-1.5, 1.5) \times (2,3) \times (2,3)$. Figure 5-8 shows the geometry. In this example, we consider the bk manifold $\mathcal{M}^{\text{bk}} = \{u_g^{\text{bk}}(\mu)|_\Omega = u_g(\mu)|_\Omega : \mu \in \mathcal{P}^{\text{bk}} = [2,4], g \in \mathcal{T} = H^{1/2}(\Gamma^{\text{in}})\}$; for simplicity, we consider $\Omega^{\text{pb}} = \Omega^{\text{bk}}$, and

we consider $u^{\text{true}} = u_g(\mu)$ with

$$g = g_k(x_1, x_3) = \begin{cases} x_1 \cos(x_3^2) & k = 1; \\ (x_1 - x_3)\log(1 + (x_1 + x_3)^2) & k = 2; \\ \sin(3\pi x_1 x_3) & k = 3. \end{cases}$$

Computations are based on a P3 FE discretization with $\mathcal{N}^{\text{bk}} = 50389$ degrees of freedom in $\Omega^{\text{bk}}$, and $\mathcal{N} = 6253$ degrees of freedom in $\Omega$. Figure 5-9 shows the solution to (5.4.4) for $g = g_k$, $k = 1, 2, 3$, and $\mu = 4$. Figure 5-10 shows the variations in $\|u_g^{\text{true}}(\mu)\|_{H^1(\Omega^{\text{bk}})}$ as a function of $\mu$ for $g = g_1$; note that there are several resonances in the parameter range considered.

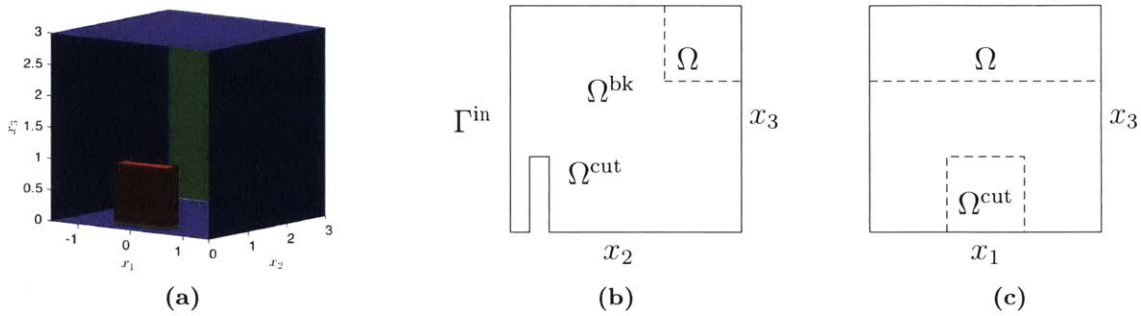


**(a)** **(b)** **(c)**

**Figure 5-8:** Application to a three-dimensional acoustic problem: bk and extracted domains.

### The case $\mathcal{P}^{\text{bk}} = \{\bar{\mu}\}$

We first introduce the transfer eigenproblem and the transfer eigenspace. We consider $\mathcal{Y} = H^1(\Omega)$, $\mathcal{V}^{\text{bk}} = H^1(\Omega^{\text{bk}})$, and $\mathcal{T} = H^{1/2}(\Gamma^{\text{in}})$, each of them endowed with the same inner products considered in section 5.4.1. We further discretize $\mathcal{T}$ through a 6 by 6 tensorized Legendre polynomial expansion ($\mathcal{N}_{\text{in}} = 36$).

Figure 5-11(a) shows the behavior of $\sqrt{\lambda_{N+1}^{\mathcal{N}_{\text{in}}}}$ with $N$ for three different values of $\mu$, while Figure 5-11(b) shows the behavior of the relative $H^1$ best-fit error $E_N^{\text{rel}}$ defined in (5.4.3). We observe that eigenvalues decay exponentially with a rate that strongly depends on the wave number $\mu$. We further observe that, for the choices of $g$ considered, only a subset of modes actively contribute to reduce the best-fit error. Interestingly, the same pattern is also empirically observed in [204, Figure 6.4]. We recall that (cf. Figure 5-10) there are several resonances close to $\mu = 4$ and $\mu = 6$, and, due to (approximate) symmetry,

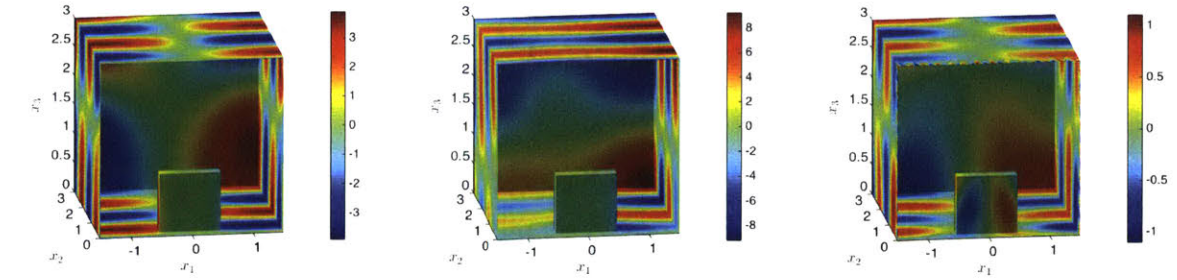

(a) $g = g_1$, $\mu = 4$ (b) $g = g_2$, $\mu = 4$ (c) $g = g_3$, $\mu = 4$

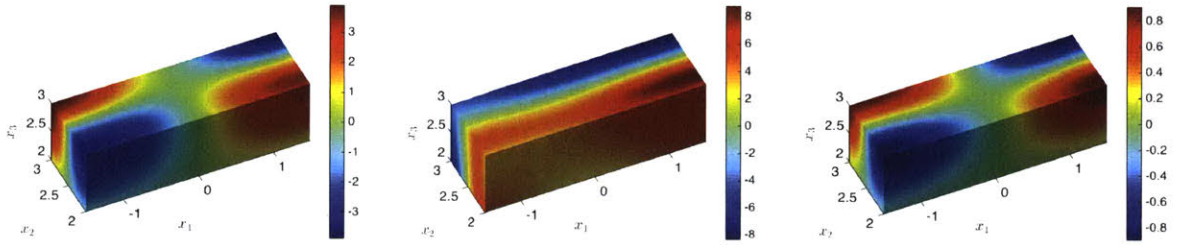

(d) $g = g_1$, $\mu = 4$ (e) $g = g_2$, $\mu = 4$ (f) $g = g_3$, $\mu = 4$

**Figure 5-9:** Application to a three-dimensional acoustic problem: visualization of the true field $u_g^{\text{true}}(\mu)$.

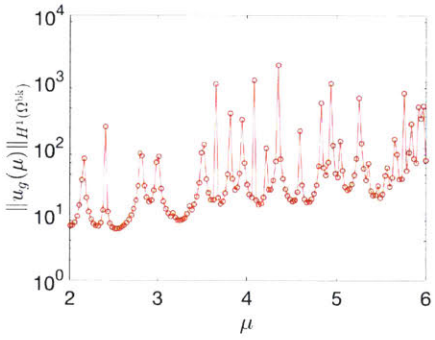


**Figure 5-10:** Application to a three-dimensional acoustic problem: behavior of $\|u_g^{\text{true}}(\mu)\|_{H^1(\Omega^{\text{bk}})}$ with $\mu$ ( $g = g_1$).

many quasi-multiple eigenvalues: the former explains the slow convergence of the transfer eigenvalues; the latter explains the staircase convergence of the best-fit error (essentially, we must go through various symmetries which provide roughly the same eigenvalue before finally arriving at the modal structure relevant to our particular solution).

### The case $\mathcal{P}^{\text{bk}} \neq \{\bar{\mu}\}$

We first study the behavior of the eigenvalues associated with the application of Algorithm 5.2.1. We here set $n_{\text{train}} = 8$ and $\mathcal{N}_{\text{in}} = 36$, and we consider several values of $N$. Figure

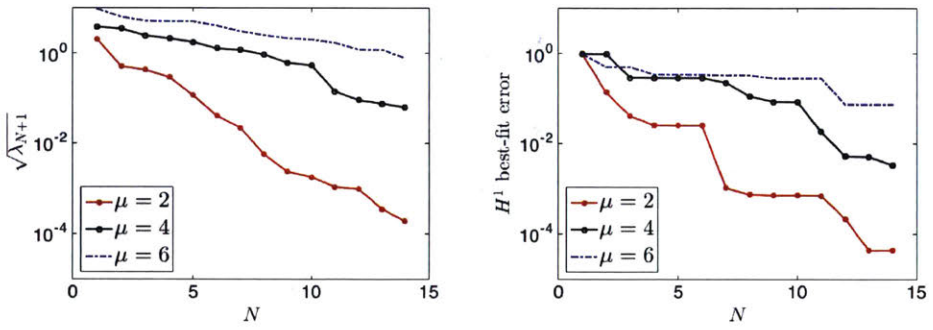


**Figure 5-11:** Application to a three-dimensional acoustic problem: transfer eigenproblem. Behavior of $\sqrt{\lambda_{N+1}^{\mathcal{N}_{\text{in}}}}$ (Figure (a)), and of the $H^1$ relative best-fit error for three values of $\mu$ ($\mathcal{N}_{\text{in}} = 36$).

5-12(a) shows the behavior of the transfer eigenvalues $\lambda_n^{\mathcal{N}_{\text{in}}}$ for different values of $\mu \in [2, 4]$, while Figure 5-12(b) shows the behavior of the POD eigenvalues $\lambda_n^{\text{POD}}$ for different choices of $N$. As in the previous case, we observe exponential convergence of the POD eigenvalues.

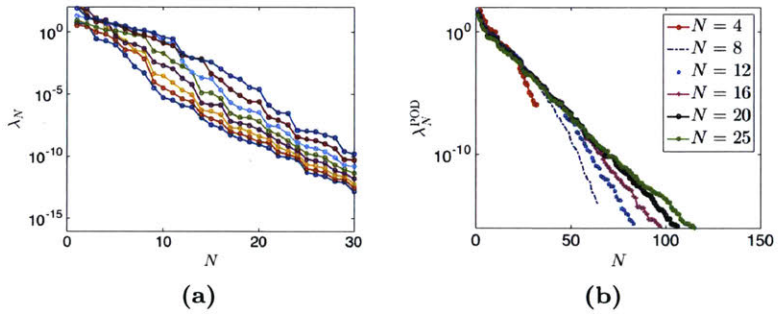


**Figure 5-12:** Application to a three-dimensional acoustic problem: application of Algorithm 5.2.1. Figure (a): behavior of the transfer eigenvalues $\lambda_n^{\mathcal{N}_{\text{in}}}$ for different values of $\mu \in [2, 4]$. Figure (b): behavior of the POD eigenvalues $\lambda_n^{\text{POD}}$ for different choices of $N$ ($n_{\text{train}} = 8$, $\mathcal{N}_{\text{in}} = 36$).

Figure 5-13 shows the performance of the data assimilation procedure. As in the previous example, we here apply PBDW based on Gaussian functionals ($r_{\text{Gauss}} = 0.1$), with observation centers selected based on SGreedy-plus algorithm ($tol = 0.2$) and $\mathcal{U} = \mathcal{Y}$. To assess performance, we consider $H^1$ maximum relative error over the three choices of the Dirichlet datum $g_k(x_2) = \sin(\pi k x_2)$, $k = 1, 2, 3$, and $n_{\text{test}} = 5$ different values of $\mu$ in $\mathcal{P}^{\text{bk}}$. To interpret results, we also report the behavior of the $H^1$ best-fit error. We observe that, as $N$ increases, the background accurately represents the elements of the bk manifolds.

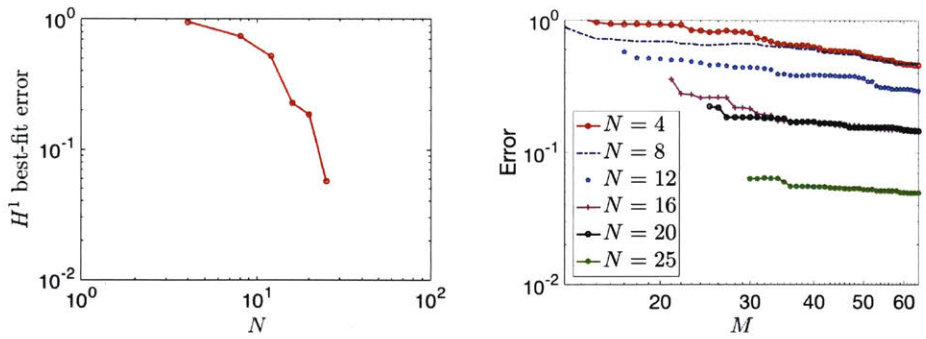


**Figure 5-13:** Application to a three-dimensional acoustic problem: data assimilation results. Figure (a): behavior of the $H^1$ best-fit error with $N$. Figure (b): behavior of the PBDW relative $H^1$ error with $M$. ($n_{\text{train}} = 8$, $\mathcal{N}_{\text{in}} = 36$, $n_{\text{test}} = 5$).

## 5.5 Conclusions

In this chapter, we presented a model reduction procedure for the construction of local approximation spaces associated with parametric manifolds. This procedure is then employed to generate background spaces $\{\mathcal{Z}_N\}_N$ for localised state estimation in the PBDW framework. The key elements of the technique are the transfer eigenproblem to manage uncertainty in the boundary conditions, and a POD to manage uncertainty in the model parameters. As explained in section 5.1, in developing our technique, we intended, but we did not assume, that the localised solution manifold $\mathcal{M}^{\text{bk}}$ is reducible.

Theoretical and numerical results were presented to demonstrate the effectivity of our approach. If the uncertainty is confined to the boundary conditions of the PDE model, we proved that our approach is optimal in the sense of Kolmogorov for a wide class of linear inf-sup stable elliptic operators. In addition, numerical results for two acoustic problems demonstrated that, for moderate wave numbers, it is possible to generate accurate local approximation spaces even in presence of high-dimensional uncertainty at the boundaries of the domain.

We finally highlight that our procedure relies on the assumption that the underlined PDE model is linear and elliptic. Extensions of the procedure to nonlinear problems do not appear to be straightforward.

# Chapter 6

# The PBDW approach for noisy measurements

We here discuss the PBDW formulation for pointwise noisy measurements. We introduce the $M$ experimental observations $\mathcal{Y}_M = \{y_1, \ldots, y_M\}$ such that

$$y_m = u^{\text{true}}(x_m^{\text{obs}}) + \epsilon_m, \qquad m = 1, \ldots, M. \tag{6.0.1}$$

Here, $\epsilon_1, \ldots, \epsilon_M$ are unknown disturbances caused by either systematic error in the data acquisition system or experimental random noise, while $\mathcal{X}_M = \{x_1^{\text{obs}}, \ldots, x_M^{\text{obs}}\}$ denote the $M$ distinct observation centers contained in the domain of interest $\Omega \subset \mathbb{R}^d$ associated with the measurements $\mathcal{Y}_M$. Then, given the background space $\mathcal{Z}_N \subset C(\Omega)$ and the Hilbert space $(\mathcal{U}, \|\cdot\|)$, the PBDW state estimate $u_\xi^\star$ associated with the dataset $\mathcal{D}_M = \{(x_m^{\text{obs}}, y_m)\}_{m=1}^M$ is the solution to the minimization statement:

$$(z_\xi^\star, \eta_\xi^\star) = \arg \min_{(z,\eta)\in\mathcal{Z}_N\times\mathcal{U}} \ \xi\|\eta\|^2 + \frac{1}{M}\sum_{m=1}^{M} (z(x_m^{\text{obs}}) + \eta(x_m^{\text{obs}}) - y_m)^2;$$

which corresponds to (2.1.5) for $\ell_m^o = \delta_{x_m^{\text{obs}}}$, and $\ell_m^{\text{obs}} = y_m$, $m = 1, \ldots, M$.

We provide an outline of the chapter. In section 6.1, we introduce the key elements of the theory of Reproducing Kernel Hilbert Spaces (RKHS), and we comment on their application to our framework. We then present *a priori* (section 6.2) and *a posteriori* (section 6.3) error analyses for the $L^2$ state estimation error, and we discuss an adaptive strategy to improve performance (section 6.4). Finally, we present numerical results for a

synthetic model problem, and for the experimental thermal patch configuration.

## 6.1 Reproducing Kernel Hilbert Spaces for PBDW

### 6.1.1 Theoretical background

Reproducing Kernel Hilbert Spaces (RKHS) are ubiquitous in several fields of applied mathematics and engineering. The notion of Reproducing Kernel was first introduced by Stanislaw Zaremba in 1907, and then systematically studied by Aronszajn in 1950 ([5]). Since then, RKHS have become central in the modern theory of learning for regression and pattern recognition ([201, 199]), scattered data approximation ([41, 230]), and meshless methods for solving PDEs ([19]). General introductions of the theory of RKHS are provided in Berlinet, Thomas-Agnan ([29]), and Wendland ([230]). We shall here present a brief overview of the main definitions and central results from the perspective of scattered data approximation.

An Hilbert space $(\mathcal{U}, \|\cdot\|)$ is a RKHS if the point evaluation functionals are continuous, i.e. $\delta_x \in \mathcal{U}'$ for all $x \in \Omega$. This is equivalent (cf. [230, Theorem 10.2]) to assume that there exists a function $K : \Omega \times \Omega \to \mathbb{R}$ such that (i) $K(\cdot, x) \in \mathcal{U}$ for all $x \in \Omega$, and (ii) $(K(\cdot, x), f) = f(x)$ for all $x \in \Omega$ and $f \in \mathcal{U}$. The function $K$ is called Reproducing Kernel. With some abuse, in what follows, we use notation $K_x = K(\cdot, x)$. We observe that $K_x$ is simply the Riesz element associated with the point evaluation functional $\delta_x$, $K_x = R_{\mathcal{U}}\delta_x$.

A function $K : \Omega \times \Omega \to \mathbb{R}$ is a symmetric positive definite (SPD) kernel if (i) $K(x, y) = K(y, x)$ for all $x, y \in \Omega$, and (ii) for any set of $N$ distinct points in $\Omega$, $\{x_n^{\text{obs}}\}_{n=1}^N \subset \Omega$, the matrix $\mathbb{K} \in \mathbb{R}^{N,N}$ defined as $\mathbb{K}_{n,n'} = K(x_n^{\text{obs}}, x_{n'}^{\text{obs}})$ is positive definite. It is easy to verify that if $\mathcal{U}$ is a RKHS such that point evaluation functionals are linearly independent then the corresponding reproducing kernel is SPD (cf. [230, Theorem 10.4]). The converse is also true: given the SPD kernel $K$ there exists a RKHS for which $K$ is the reproducing kernel, which is referred to as *native space* of $K$. The latter result is known as Moore-Aronszajn theorem and was first proved in [5].

Given the SPD kernel $K$, it is important to characterize the regularity of the corresponding native space $\mathcal{U} = \mathcal{U}(K)$. Next Theorem and the subsequent corollary address this point. Given the function $f \in L^2(\mathbb{R}^d)$, we denote by $\hat{f}$ the corresponding Fourier transform.

**Theorem 6.1.1.** *([230, Theorem 10.12]) Suppose that $\Phi \in C(\mathbb{R}^d) \cap L^1(\mathbb{R}^d)$ is a real-valued function such that $K : \Omega \times \Omega \to \mathbb{R}$ defined as $K(x, y) = \Phi(x - y)$ is a SPD kernel. Then,*

*the real space*

$$\mathcal{G} = \left\{ f \in L^2(\mathbb{R}^d) \cap C(\mathbb{R}^d) : \ \frac{\hat{f}}{\sqrt{\hat{\Phi}}} \in L^2(\mathbb{R}^d) \right\} \tag{6.1.1a}$$

*endowed with the inner product*

$$(f, g) = \frac{1}{(2\pi)^{d/2}} \int_{\mathbb{R}^d} \frac{\hat{f}(\omega)\overline{\hat{g}(\omega)}}{\widehat{\Phi}(\omega)} \, d\omega \tag{6.1.1b}$$

*is the native space of $K$.*

**Corollary 6.1.2.** *([230, Corollary 10.13]) Suppose that $\Phi \in C(\mathbb{R}^d) \cap L^1(\mathbb{R}^d)$ satisfies*

$$c_1(1 + \|\omega\|_2^2)^{-s} \leq \widehat{\Phi}(\omega) \leq c_2(1 + \|\omega\|_2^2)^{-s}, \quad \omega \in \mathbb{R}^d, \tag{6.1.2}$$

*for some $c_1, c_2 > 0$ and $s > d/2$. Let us further suppose that $K(x, y) = \Phi(x - y)$ is a SPD kernel. Then, the native space associated with $K$ coincides with the Sobolev space $H^s(\mathbb{R}^d)$.*

An important class of kernels, which is employed in the numerical simulations, is given by the compactly supported radial basis functions of minimal degree (csRBFs), also known as Wendland functions. This class of kernels was first proposed by Wendland in [229], and is defined as $K_\chi(x, y) = \phi_{d,k}(\gamma\|x - y\|_2)$ where $\chi = [k, \gamma]$ and

$$\phi_{d,k}(r) = \begin{cases} p_{d,k}(r) & 0 \leq r \leq 1; \\ 0 & r > 1. \end{cases} \tag{6.1.3a}$$

The polynomial $p_{d,k}$ has the following form for $k = 0, 1$ and for all $d$:

$$p_{d,k}(r) = \begin{cases} (1 - r)^{\ell_{d,k}} & k = 0 \\ (1 - r)^{\ell_{d,k}+1} \left((\ell_{d,k} + 1)r + 1\right) & k = 1 \end{cases} \tag{6.1.3b}$$

and $\ell_{d,k} = \left\lfloor \frac{d}{2} \right\rfloor + k + 1$. We observe that it is possible to generalize (6.1.3b) to the more general case $k \in \mathbb{N}$; we refer to [230, Table 9.1] for the explicit formulas.

Next result clarifies the connection between csRBF and Sobolev spaces. We refer to [230, Theorem 10.35] for the proof.

**Theorem 6.1.3.** *Let us consider the compactly supported RBF $K_\chi$, $K_\chi(x, y) = \phi_{d,k}(\gamma\|x - y\|_2)$, introduced in (6.1.3). Let $\Omega = \mathbb{R}^d$, and let either one of these conditions hold: (i)*

$d \geq 3$, $k \geq 0$, *or (ii)* $d \geq 1$, $k > 0$. *Then, the native space for* $K_\chi$ *is the Sobolev space* $H^{(d+1)/2+k}(\mathbb{R}^d)$.

We observe that by restricting ourselves to csRBF kernels, the choice of the inner product reduces to the choice of the parameters $\chi = [k, \gamma]$: the parameter $k$ determines the Sobolev regularity of the native space, while the constant $\gamma$ influences the characteristic length-scale of the elements of the update space. Recalling the scaling property of Fourier transform and (6.1.1), for fixed $k$ we find that the Kernel $K_\gamma(x, y) = \phi_{d,k}(\gamma\|x - y\|_2)$ induces the inner product

$$(f, g)_\gamma = \frac{\gamma}{(2\pi)^{d/2}} \int_{\mathbb{R}^d} \frac{\hat{f}(\omega)\overline{\hat{g}}(\omega)}{\widehat{\Phi}(\omega/\gamma)}\, d\omega,$$

where $\widehat{\Phi}$ is the Fourier transform of $\Phi(x) = \phi_{d,k}(\|x\|_2)$. We observe that as $\gamma$ decreases, we penalize more and more high-frequency modes.

### 6.1.2 PBDW for pointwise measurements with explicit kernels

**Algorithm 6.1.1** PBDW approach for pointwise measurements. Offline-online computational procedure

**Offline stage**

1: Choose a family of kernels (e.g. (6.1.3))

2: Generate the background $\mathcal{Z}_N \subset \mathcal{U}$

3: (If possible) Select the observation centers $x_1^{\text{obs}}, \ldots, x_M^{\text{obs}} \in \Omega$

4: Compute the matrix $\mathbb{L}$ (2.3.1)

**Onine stage**

1: Acquire the measurements $y_1, \ldots, y_M$

2: Choose the parameters of the kernel and the regularizer weight $\xi$ (cf. section 6.4)

3: Assemble the matrix (2.3.2b) and solve the linear system (2.3.2b)

4: (If needed) Evaluate the state using (2.3.2a).

The duality between RKHS and SPD kernels has important implications for our discussion. In Chapters 3, 4 and 5 we first proposed an inner product $(\cdot, \cdot)$ and then we appealed to a FE discretization to compute the Riesz representations of the observation functionals

(cf. Algorithm 2.4.1, Chapter 2). For pointwise measurements, we might first propose an explicit SPD kernel, and then appeal to Moore-Aronszajn theorem to recover the variational formulation. This prevents us from having to solve $M$ FE problems to build the update space $\mathcal{U}_M$. In addition, since $K$ is known explicitly, we can efficiently adapt the characteristic length-scale of the elements of the update space during the online stage. As discussed in Chapter 3, this might be extremely important for sufficiently large values of $M$.

Algorithm 6.1.1 summarises the computational procedure. We observe that during the online stage we should first select the parameters of the kernel. We discuss how to practically select these parameters in section 6.4. We further observe that, although we can compute the solution to (2.3.2b), the matrix $\mathbb{Z}$ (2.3.1) is not in general computable. As a consequence, we cannot estimate the inf-sup constant $\beta_{N,M}$ (2.2.2). Therefore, we cannot directly apply the SGreedy-plus algorithm described in Chapter 3 to select the observation centers.

## 6.2 *A priori* error analysis for pointwise noisy measurements

We present *a priori* estimates for the $L^2(\Omega)$ state-estimation error $\|u^{\text{true}} - u^\star_\xi\|_{L^2(\Omega)}$. We state upfront that in this section we assume that $\mathcal{Z}_N \subset \mathcal{U}$. The importance of the error analysis is twofold. First, it motivates our formulation from a theoretical viewpoint. Second, it provides insights about the role of the different pieces of our formulation: the regularization parameter $\xi$, the background space $\mathcal{Z}_N$, the kernel $K$ and the centers $\mathcal{X}_M$.

In order to derive error bounds for the $L^2(\Omega)$ state-estimation error $\|u^{\text{true}} - u^\star_\xi\|_{L^2(\Omega)}$, we must first introduce assumptions on our dataset $\mathcal{D}_M$. To our knowledge, three different scenarios have been considered so far.

1. *Random-design regression*: the pairs $\{(x_m^{\text{obs}}, y_m)\}_{m=1}^M$ are drawn independently from a joint unknown distribution $\rho_{(X,Y)}$. In this case, the objective of learning is to estimate the conditional expectation $\mathbb{E}[Y|X = x]$.

2. *Fixed-design regression*: the centers $\mathcal{X}_M = \{x_1^{\text{obs}}, \ldots, x_M^{\text{obs}}\}$ are fixed (non-random) points in $\Omega$, while the responses $\mathcal{Y}_M = \{y_m\}_{m=1}^M$ satisfy $y_m = u^{\text{true}}(x_m^{\text{obs}}) + \epsilon_m$, where $u^{\text{true}} : \Omega \to \mathbb{R}$ is the deterministic field of interest and $\epsilon_1, \ldots, \epsilon_M$ are independent identically distributed (i.i.d.) random variables with zero mean and variance $\sigma^2$, $\epsilon_m \sim (0, \sigma^2)$.

3. *Scattered data approximation*: both centers $\mathcal{X}_M$ and responses $\mathcal{Y}_M$ are non-random, and we assume that there exists some unknown $\delta > 0$ such that $|y_m - u^{\text{true}}(x_m^{\text{obs}})| \leq \delta$ for all $m = 1, \ldots, M$.

The first scenario has been extensively studied in the statistical learning literature (see, e.g., [174, 221]). We refer to [99] for a complete review of the error bounds available. The second scenario has also been studied in statistics; we refer to the survey [91] for further details about a specific class of kernels. Finally, the third scenario has been studied in approximation theory and radial basis functions (see, e.g., [230]). From the modeling perspective, the first scenario refers to the case in which we do not have control on the observation centers, the second scenario addresses the problem of random error in the measurements, and the third scenario addresses the problem of systematic deterministic error. In this thesis, we provide error bounds for the second and the third scenarios.

### 6.2.1 Preliminaries

In view of the proofs of the error bounds, we introduce a regularized formulation of the APBDW statement proposed in this work: given $\lambda \geq 0$, $\xi > 0$, find $u^\star_{\lambda,\xi} \in \mathcal{U}$ such that

$$u^\star_{\lambda,\xi} = \arg\min_{u \in \mathcal{U}} J^{(1)}_{\lambda,\xi}(u) := \xi \|u\|^2_{\lambda,N} + \frac{1}{M} \sum_{m=1}^{M} \Big( u(x_m^{\text{obs}}) - y_m \Big)^2, \tag{6.2.1}$$

where the seminorm $\|\cdot\|_{\lambda,N}$ is defined as

$$\|w\|^2_{\lambda,N} = \lambda \|\Pi_{\mathcal{Z}_N} w\|^2 + \|\Pi_{\mathcal{Z}_N^\perp} w\|^2. \tag{6.2.2}$$

We observe that for any $\lambda > 0$, the function $\|\cdot\|_{\lambda,N}$ is a norm equivalent to $\|\cdot\|$. We also observe that for $\lambda = 0$, problem (6.2.1) corresponds to (2.2.7).

Next Proposition summarizes a number of properties of problem (6.2.1).

**Proposition 6.2.1.** *Let $\beta_{N,M} > 0$. Then, the following hold.*

1. *For any $\lambda > 0$, the solution to* (6.2.1) *exists and is unique. Furthermore, if we introduce $\eta^\star_{\lambda,\xi} = \Pi_{\mathcal{Z}_N^\perp} u^\star_{\lambda,\xi}$, $z^\star_{\lambda,\xi} = \Pi_{\mathcal{Z}_N} u^\star_{\lambda,\xi}$, we have that $\eta^\star_{\lambda,\xi} \in \text{span}\{\Pi_{\mathcal{Z}_N^\perp} K_{x_m^{\text{obs}}}\}_{m=1}^M$ and $z^\star_{\lambda,\xi} \in \text{span}\{\Pi_{\mathcal{Z}_N} K_{x_m^{\text{obs}}}\}_{m=1}^M$.*

2. *For any $\xi > 0$, the solution $u^\star_{\lambda,\xi}$ converges to the solution $u^\star_\xi$ to* (2.2.7) *when $\lambda \to 0^+$.*

*3. For any $\lambda \geq 0$, the following bounds hold:*

$$\|u^{\text{true}} - u^{\star}_{\lambda,\xi}\|_{\lambda,N} \leq 2\|u^{\text{true}}\|_{\lambda,N} + \frac{\delta}{2\sqrt{\xi}}, \tag{6.2.3a}$$

*and*

$$\|u^{\text{true}} - u^{\star}_{\lambda,\xi}\|_{\ell^2(\mathcal{X}_M)} \leq \sqrt{M}\left(\delta + \frac{\sqrt{\xi}}{2}\|u^{\text{true}}\|_{\lambda,N}\right), \tag{6.2.3b}$$

*where* $\|u\|_{\ell^2(\mathcal{X}_M)} := \sqrt{\sum_{m=1}^{M}(u(x_m^{\text{obs}}))^2}$.

We prove each statement separately.

*Proof.* (*statement 1*) For any $\lambda > 0$, $u \mapsto \|u\|^2_{\lambda,N}$ is strictly convex, while $u \mapsto V_M(u)$ is convex. This implies that for any $\xi > 0$ the objective function $J_{\lambda,\xi}(u) = \xi\|u\|^2_{\lambda,N} + V_M(u)$ is strictly convex. Therefore, existence and uniqueness of the solution to (6.2.1) follow from [74, Theorem 3, Chapter 8.2]. We observe that $x \in \Omega \mapsto \Phi_x^{\lambda,N} = \frac{1}{\lambda}\Pi_{\mathcal{Z}_N}K_x + \Pi_{\mathcal{Z}_N^{\perp}}K_x$, is the Riesz representer associated with $\delta_x$ in $(\mathcal{U}, \|\cdot\|_{\lambda,N})$. We have indeed that for all $v \in \mathcal{U}$ and $x \in \Omega$

$$(\Phi_x^{\lambda,N}, v)_{\lambda,N} = \frac{\lambda}{\lambda}(\Pi_{\mathcal{Z}_N}K_x, v) + (\Pi_{\mathcal{Z}_N^{\perp}}K_x, v) = (K_x, \Pi_{\mathcal{Z}_N}v + \Pi_{\mathcal{Z}_N^{\perp}}v) = (K_x, v) = v(x).$$

Exploiting the representer theorem (see, e.g., [230, Theorem 16.1]), we have that $u^{\star}_{\lambda,\xi} \in \text{span}\{\Phi^{\lambda,N}_{x_m^{\text{obs}}}\}_{m=1}^{M}$. As a result, we have that $\eta^{\star}_{\lambda,\xi} \in \text{span}\{\Pi_{\mathcal{Z}_N^{\perp}}\Phi^{\lambda,N}_{x_m^{\text{obs}}}\}_{m=1}^{M}$, and $z^{\star}_{\lambda,\xi} \in \text{span}\{\Pi_{\mathcal{Z}_N}\Phi^{\lambda,N}_{x_m^{\text{obs}}}\}_{m=1}^{M}$ for any $\lambda > 0$. □

*Proof.* (*statement 2*) Let $\{\lambda_j\}_j$ be a real sequence such that $\lambda_j \to 0^+$. Exploiting the first statement of Proposition 6.2.1, we have that sequences $\{\eta^{\star}_{\lambda_j,\xi}\}_j$, $\{z^{\star}_{\lambda_j,\xi}\}_j$ belong to finite dimensional spaces that do not depend on $\lambda$. Furthermore, applying Lemma 2.2.2, it is possible to verify that they are uniformly bounded for all $j$. Therefore, applying Bolzano-Weierstrass theorem, the sequence $\{u^{\star}_{\lambda_j,\xi} = \eta^{\star}_{\lambda_j,\xi} + z^{\star}_{\lambda_j,\xi}\}_j$ admits a strongly convergent subsequence $\{u^{\star}_{\lambda_k,\xi}\}_k$ to $\widehat{u}^{\star}_{\xi} \in \mathcal{U}$.

We now show that $\widehat{u}^{\star}_{\xi} = u^{\star}_{\xi}$. We first observe that

$$J^{(1)}_{\lambda_k,\xi}(u^{\star}_{\lambda_k,\xi}) = \lambda_k \underbrace{\|z^{\star}_{\lambda_k,\xi}\|^2}_{\leq C} + \|\eta^{\star}_{\lambda_k,\xi}\|^2 + \frac{1}{M}\sum_{m=1}^{M}\left(u^{\star}_{\lambda_k,\xi}(x_m^{\text{obs}}) - y_m\right)^2 \to J^{(1)}_{\xi}(\widehat{u}^{\star}_{\xi}), \qquad k \to \infty.$$

We further observe that for any $\lambda_k > 0$

$$J^{(1)}_{\lambda_k,\xi}(u^\star_{\lambda_k,\xi}) \leq J^{(1)}_{\lambda_k,\xi}(u^\star_\xi), \qquad k = 1, 2, \ldots,$$

and by taking the limit on both sides, we obtain

$$J^{(1)}_\xi(\widehat{u}^\star_\xi) \leq J^{(1)}_\xi(u^\star_\xi)$$

Since $u^\star_\xi$ is the unique minimizer of (2.2.7), we must have $u^\star_\xi = \widehat{u}^\star_\xi$. Furthermore, by the same argument, $u^\star_\xi$ is the only limit point of the sequence; therefore, the entire sequence converges to $\widehat{u}^\star_\xi$. Thesis follows. □

*Proof.* (*statement 3*) For $\lambda > 0$, $\|\cdot\|_{\lambda,N}$ is a norm for $\mathcal{U}$; therefore, estimates (6.2.3a) and (6.2.3b) follow directly from [129, Corollary 4.3] and [129, Lemma 4.5]. The extension to $\lambda = 0$ follows by observing that $u^\star_{\lambda,\xi}$ converges to $u^\star_\xi$ when $\lambda \to 0^+$ (cf. statement 2). □

Given the observation centers $\mathcal{X}_M$, and the background space $\mathcal{Z}_N$, we define the constant $C_{N,\mathcal{X}_M}$ as

$$C_{N,\mathcal{X}_M} := \sup_{u \in \mathcal{U}} \frac{\|u\|^2_{L^2(\Omega)}}{h^{2\tau}_{\mathcal{X}_M} \|\Pi_{\mathcal{Z}_N^\perp} u\|^2 + h^d_{\mathcal{X}_M} \|u\|^2_{\ell^2(\mathcal{X}_M)}}, \tag{6.2.4}$$

where $h_{\mathcal{X}_M}$ is the fill distance defined as

$$h_{\mathcal{X}_M} = \sup_{x \in \Omega} \min_{m=1,\ldots,M} \|x - x^{\text{obs}}_m\|_2. \tag{6.2.5}$$

We anticipate that the constant $C_{N,\mathcal{X}_M}$ enters in the upper bounds for the state-estimation error. Next Lemma shows a bound for $C_{N,\mathcal{X}_M}$ that depends on the constant $c_{N,M}$ introduced in (2.2.10).

**Lemma 6.2.1.** *Let $\Omega$ be a Lipschitz domain and let $\mathcal{U}$ be the Sobolev space $H^\tau(\Omega)$ with $\tau > d/2$. Let us assume that the inf-sup constant $\beta_{N,M}$ defined in (2.2.2) is strictly positive and $h_{\mathcal{X}_M} < 1$. Then, the constant $C_{N,\mathcal{X}_M}$ defined in (6.2.4) is bounded by*

$$C_{N,\mathcal{X}_M} \leq \frac{1}{\min\{c_{N,M}, 1 - h^{2\tau-d}_{\mathcal{X}_M}\}} C, \tag{6.2.6}$$

*where $c_{N,M}$ is defined in* (2.2.10) *and $C$ depends on the domain $\Omega$ and on $(\cdot,\cdot)$.*

*Proof.* Let us define the constant

$$\widehat{C}_{\mathcal{X}_M} := \sup_{u\in\mathcal{U}} \frac{\|u\|^2_{L^2(\Omega)}}{h^{2\tau}_{\mathcal{X}_M}\|u\|^2 + h^d_{\mathcal{X}_M}\|u\|^2_{\ell^2(\mathcal{X}_M)}}.$$

Recalling [129, Theorem 4.8], $\widehat{C}_{\mathcal{X}_M}$ is bounded from above by a constant $C$ that does not depend on $M$.

Since $\beta_{N,M} > 0$, recalling Lemma 2.2.2, we have that

$$\|\Pi_{\mathcal{Z}_N^\perp} u\|^2 + \|u\|^2_{\ell^2(\mathcal{X}_M)} \geq c_{N,M}\|u\|^2,$$

where $c_{N,M} > 0$ is given by the expression in (2.2.10). Then, we observe that

$$\begin{aligned} h^{2\tau}_{\mathcal{X}_M}\|\Pi_{\mathcal{Z}_N^\perp} u\|^2 + h^d_{\mathcal{X}_M}\|u\|^2_{\ell^2(\mathcal{X}_M)} &= h^{2\tau}_{\mathcal{X}_M}\left(\|\Pi_{\mathcal{Z}_N^\perp} u\|^2 + \|u\|^2_{\ell^2(\mathcal{X}_M)}\right) + \left(h^d_{\mathcal{X}_M} - h^{2\tau}_{\mathcal{X}_M}\right)\|u\|^2_{\ell^2(\mathcal{X}_M)} \\ &\geq c_{N,M} h^{2\tau}_{\mathcal{X}_M}\|u\|^2 + \left(1 - h^{2\tau-d}_{\mathcal{X}_M}\right) h^d_{\mathcal{X}_M}\|u\|^2_{\ell^2(\mathcal{X}_M)} \\ &\geq \min\{c_{N,M}, 1 - h^{2\tau-d}_{\mathcal{X}_M}\}\left(h^{2\tau}_{\mathcal{X}_M}\|u\|^2 + h^d_{\mathcal{X}_M}\|u\|^2_{\ell^2(\mathcal{X}_M)}\right). \end{aligned}$$

As a result,

$$C_{N,\mathcal{X}_M} = \sup_{u\in\mathcal{U}} \frac{\|u\|^2_{L^2(\Omega)}}{h^{2\tau}_{\mathcal{X}_M}\|\Pi_{\mathcal{Z}_N^\perp} u\|^2 + h^d_{\mathcal{X}_M}\|u\|^2_{\ell^2(\mathcal{X}_M)}} \leq \underbrace{\left(\sup_{u\in\mathcal{U}} \frac{\|u\|^2_{L^2(\Omega)}}{h^{2\tau}_{\mathcal{X}_M}\|u\|^2 + h^d_{\mathcal{X}_M}\|u\|^2_{\ell^2(\mathcal{X}_M)}}\right)}_{\leq C} \frac{1}{\min\{c_{N,M}, 1 - h^{2\tau-d}_{\mathcal{X}_M}\}}$$

Thesis follows. □

Exploiting the definition of $c_{N,M}$ (2.2.10), we find that $C_{N,\mathcal{X}_M}$ is asymptotically bounded as $M \to \infty$ for fixed $N$; on the other hand, the dependence on $N$ heavily depends on the background $\mathcal{Z}_N$. Practical estimates of $C_{N,\mathcal{X}_M}$ require the solution to a a generalized eigenproblem[1], which involves the matrix $\mathbb{Z}$ in (2.3.1); this requires that the basis $\zeta_1, \ldots, \zeta_N$ satisfies $\zeta_n(\cdot) = \sum_{k=1}^{K_n} a_{n,k} K_{\tilde{x}_{n,k}}(\cdot)$ for some $\{a_{n,k}\}_k$ and $\{\tilde{x}_{n,k}\} \subset \Omega$, $n = 1, \ldots, N$.

[1]We refer to [103] for a discussion on the use of meshless methods based on csRBF for the solution to eigenproblems.

### 6.2.2 An *a priori* error bound for scattered data approximation

We state the main result of this section.

**Proposition 6.2.2.** *Let $\Omega$ be a Lipschitz domain and let $\mathcal{U}$ be the Sobolev space $H^\tau(\Omega)$ with $\tau > d/2$. Let $\beta_{N,M}$ in (2.2.2) be strictly positive. Let us further assume that measurements are of the form $y_m = u^{\text{true}}(x_m^{\text{obs}}) + \epsilon_m$ with $|\epsilon_m| \leq \delta$ for $m = 1, \dots, M$.*

*Then, if $u^{\text{true}} \in \mathcal{U}$, the following holds:*

$$\|u^{\text{true}} - u_\xi^\star\|_{L^2(\Omega)}^2 \leq C_{N,\mathcal{X}_M} \left( h_{\mathcal{X}_M}^{2\tau} \left( 2\|\Pi_{\mathcal{Z}_N^\perp} u^{\text{true}}\| + \frac{\delta}{2}\frac{1}{\sqrt{\xi}} \right)^2 + h_{\mathcal{X}_M}^d M \left( \delta + \frac{\sqrt{\xi}}{2}\|\Pi_{\mathcal{Z}_N^\perp} u^{\text{true}}\| \right)^2 \right), \tag{6.2.7}$$

*where $C_{N,\mathcal{X}_M}$ is defined in (6.2.4), and $h_{\mathcal{X}_M}$ is defined in (6.2.5).*

*Proof.* The proof replicates the argument of [129, Theorem 4.11]. Recalling the definition of $C_{N,\mathcal{X}_M}$, we have

$$\|u^{\text{true}} - u_\xi^\star\|_{L^2(\Omega)}^2 \leq C_{N,\mathcal{X}_M} \left( h_{\mathcal{X}_M}^{2\tau} \|\Pi_{\mathcal{Z}_N^\perp}(u^{\text{true}} - u_\xi^\star)\|^2 + h_{\mathcal{X}_M}^d \|u^{\text{true}} - u_\xi^\star\|_{\ell^2(\mathcal{X}_M)}^2 \right).$$

Then, using (6.2.3a) and (6.2.3b), we obtain

$$\|u^{\text{true}} - u_\xi^\star\|_{L^2(\Omega)}^2 \leq C_{N,\mathcal{X}_M} \left( h_{\mathcal{X}_M}^{2\tau} \left( 2\,\|\Pi_{\mathcal{Z}_N^\perp} u^{\text{true}}\|^2 + \frac{\delta}{2}\frac{1}{\sqrt{\xi}} \right)^2 + h_{\mathcal{X}_M}^d M \left( \delta + \frac{\sqrt{\xi}}{2}\|\Pi_{\mathcal{Z}_N^\perp} u^{\text{true}}\| \right)^2 \right),$$

which is the thesis. □

**Remark 6.2.1.** *For quasi-uniform grids, $h_{\mathcal{X}_M} \sim M^{-1/d}$, for $M \to \infty$, the right-hand side reduces to*

$$\|u^{\text{true}} - u_\xi^\star\|_{L^2(\Omega)}^2 \lesssim \mathcal{O}\left( \|\Pi_{\mathcal{Z}_N^\perp} u^{\text{true}}\|^2 \, h_{\mathcal{X}_M}^{2\tau} \left(1 + \frac{1}{\Lambda}\right)^2 + \delta^2 \, (1+\Lambda)^2 \right) \tag{6.2.8a}$$

*where*

$$\Lambda = \frac{\sqrt{\xi}\|\Pi_{\mathcal{Z}_N^\perp} u^{\text{true}}\|}{\delta}, \tag{6.2.8b}$$

*By minimizing with respect to $\Lambda$, we obtain that the asymptotically optimal choice of $\xi$*

*is*

$$\xi = \left( \frac{\delta}{\|\Pi_{\mathcal{Z}_N^\perp} u^{\text{true}}\|} \right)^{2/3} h_{\mathcal{X}_M}^{4/3\tau}. \tag{6.2.9a}$$

*For this choice of the hyper-parameter, we obtain:*

$$\|u^{\text{true}} - u_\xi^\star\|_{L^2(\Omega)}^2 \lesssim \mathcal{O}\left( \|\Pi_{\mathcal{Z}_N^\perp} u^{\text{true}}\|^{2/3} h_{\mathcal{X}_M}^{2/3\tau} \delta^{4/3} + \delta^2 \right) \qquad M \to \infty. \tag{6.2.9b}$$

*We observe that for any finite $\delta > 0$, we do not expect convergence in a $L^2$ sense. We also observe that the optimal value of $\xi$ is directly proportional to $\delta$, inversely proportional to the background best-fit error $\|\Pi_{\mathcal{Z}_N^\perp} u^{\text{true}}\|$ and decreases as $M$ increases.*

**Remark 6.2.2.** *In the case of perfect measurements, estimate* (6.2.7) *reduces to*

$$\|u^{\text{true}} - u_\xi^\star\|_{L^2(\Omega)}^2 \leq \frac{1}{4} C_{N,\mathcal{X}_M} \|\Pi_{\mathcal{Z}_N^\perp} u^{\text{true}}\|^2 \left( 16 h_{\mathcal{X}_M}^{2\tau} + h_{\mathcal{X}_M}^d M\xi \right). \tag{6.2.10}$$

*We can decouple the right-hand side of* (6.2.10)*, as the product of two terms: (i) $C_{N,\mathcal{X}_M} \|\Pi_{\mathcal{Z}_N^\perp} u^{\text{true}}\|^2$, and (ii) $16 h_{\mathcal{X}_M}^{2\tau} + h_{\mathcal{X}_M}^d M\xi$. Recalling that $C_{N,\mathcal{X}_M}$ is asymptotically independent of $M$ (cf. Lemma 6.2.1 and* (2.2.10)*), we find that the first contribution is independent of the number of measurements $M$; on the other hand, the second contribution is independent of the background $\mathcal{Z}_N$. We thus observe a multiplicative effect between $M$ convergence (associated with the update) and $N$ convergence (associated with the deduced background). We note, however, that while the $M$ term is guaranteed to decrease as $M$ increases, in general it is not possible to guarantee that $C_{N,\mathcal{X}_M} \|\Pi_{\mathcal{Z}_N^\perp} u^{\text{true}}\|^2$ is monotonic decreasing with $N$. We investigate such multiplicative effect of the approach in the numerical results.*

### 6.2.3 *A priori* error bounds for fixed-design regression

In view of the presentation of the main result, we define the matrix $\mathbb{A}_\xi \in \mathbb{R}^{N+M,N+M}$,

$$\mathbb{A}_\xi := \begin{bmatrix} \xi M \mathbb{I} + \mathbb{K} & \mathbb{L} \\ \mathbb{L}^T & 0 \end{bmatrix}, \tag{6.2.11a}$$

associated with the linear system (2.3.2b). Then, we introduce $\Sigma \in \mathbb{R}^{N+M,N+M}$,

$$\Sigma := \begin{bmatrix} \mathbb{I} & 0 \\ 0 & 0 \end{bmatrix}. \tag{6.2.11b}$$

Finally, we introduce $\mathbb{M} \in \mathbb{R}^{N+M,N+M}$ such that

$$\mathbb{M}_{i,i'} := \int_\Omega \psi_i(x)\,\psi_{i'}(x)\,dx, \qquad \psi_i(x) = \begin{cases} K_{x_j^{\text{obs}}} & i = 1,\dots,M \\ \zeta_{i-M} & i = M+1,\dots,M+N \end{cases} \tag{6.2.11c}$$

We further decompose the datum $\mathbf{y}_M$ as

$$\mathbf{y}_M = \mathbf{y}_M^{\text{true}} + \boldsymbol{\epsilon}, \qquad \mathbf{y}_M^{\text{true}} = [u^{\text{true}}(x_1^{\text{obs}}),\dots,u^{\text{true}}(x_M^{\text{obs}})], \quad \boldsymbol{\epsilon} = [\epsilon_1,\dots,\epsilon_M],$$

and we define $\boldsymbol{\epsilon}_{aug} = [\boldsymbol{\epsilon}, \mathbf{0}] \in \mathbb{R}^{M+N}$. We observe that $\mathbb{V}(\boldsymbol{\epsilon}_{aug}) = \sigma^2\Sigma$, where $\Sigma$ is defined in (6.2.11). Then, we introduce the solution $u_\xi^{\star,\sigma=0}$ to (2.2.7) for $\mathbf{y}_M = \mathbf{y}_M^{\text{true}}$ and the vectors of coefficients $\mathbf{u}^\star, \mathbf{u}^{\star,\sigma=0} \in \mathbb{R}^{M+N}$,

$$\mathbf{u}^\star = \begin{bmatrix} \boldsymbol{\eta}^\star \\ \boldsymbol{z}^\star \end{bmatrix}, \quad \mathbf{u}^{\star,\sigma=0} = \begin{bmatrix} \boldsymbol{\eta}^{\star,\sigma=0} \\ \boldsymbol{z}^{\star,\sigma=0} \end{bmatrix},$$

associated with $u_\xi^\star$ and $u_\xi^{\star,\sigma=0}$.

We can now state the error bound.

**Proposition 6.2.3.** *Let $\Omega$ be a Lipschitz domain and let $\mathcal{U}$ be the Sobolev space $H^\tau(\Omega)$ with $\tau > d/2$. Let $\beta_{N,M}$ in (2.2.2) be strictly positive. Then, if $u^{\text{true}} \in \mathcal{U}$, the following holds:*

$$\mathbb{E}\left[\|u^{\text{true}} - u_\xi^\star\|^2_{L^2(\Omega)}\right] \le \frac{1}{2} C_{N,\mathcal{X}_M} \left(16 h_{\mathcal{X}_M}^{2\tau} + h_{\mathcal{X}_M}^d M\xi\right) \|\Pi_{\mathcal{Z}_N^\perp} u^{\text{true}}\|^2 + 2\sigma^2 \mathcal{T}^\sigma, \tag{6.2.12}$$

*where $\mathcal{T}^\sigma = \text{trace}\left(\mathbb{A}_\xi^{-1}\,\mathbb{M}\,\mathbb{A}_\xi^{-1}\,\Sigma\right)$. Furthermore, if $u^{\text{true}} \in \mathcal{Z}_N$, we have*

$$\mathbb{E}\left[\|u^{\text{true}} - u_\xi^\star\|^2_{L^2(\Omega)}\right] = \sigma^2 \mathcal{T}^\sigma. \tag{6.2.13}$$

*Proof.* We observe that

$$\|u_\xi^\star - u_\xi^{\star,\sigma=0}\|^2_{L^2(\Omega)} = (\mathbf{u}^\star - \mathbf{u}^{\star,\sigma=0})^T\,\mathbb{M}\,(\mathbf{u}^\star - \mathbf{u}^{\star,\sigma=0}) = \boldsymbol{\epsilon}_{aug}^T \left(\mathbb{A}_\xi^{-1}\,\mathbb{M}\,\mathbb{A}_\xi^{-1}\right) \boldsymbol{\epsilon}_{aug}.$$

Then, applying [183, Theorem C, Chapter 14.4], we find

$$\mathbb{E}\left[\|u_\xi^\star - u_\xi^{\star,\sigma=0}\|^2_{L^2(\Omega)}\right] = \sigma^2 \operatorname{trace}\left(\mathbb{A}_\xi^{-1}\,\mathbb{M}\,\mathbb{A}_\xi^{-1}\,\Sigma\right). \tag{6.2.14}$$

We now distinguish two cases. If $u^{\text{true}} \in \mathcal{Z}_N$, then $u_\xi^{\star,\sigma=0} = u^{\text{true}}$ and (6.2.14) implies (6.2.13). On the other hand, if $u^{\text{true}} \notin \mathcal{Z}_N$ thesis follows by observing that

$$\mathbb{E}\left[\|u_\xi^\star - u^{\text{true}}\|^2_{L^2(\Omega)}\right] \leq 2\,\|u^{\text{true}} - u_\xi^{\star,\sigma=0}\|^2_{L^2(\Omega)} + 2\,\mathbb{E}\left[\|u_\xi^\star - u_\xi^{\star,\sigma=0}\|^2_{L^2(\Omega)}\right]$$

and then combining estimates (6.2.10) and (6.2.14). □

We observe that (6.2.12) can be easily extended to correlated noise by appropriately modifying the matrix $\Sigma$. We further observe that, unlike in the previous case, it is not evident how to provide explicit estimates for the optimal value of $\xi$. However, since $\mathcal{T}^\sigma$ is computable, in the case of perfect model, we can estimate numerically the optimal value of $\xi$ *a priori*. We investigate this aspect in the numerical section.

## 6.3 *A posteriori* error analysis for pointwise noisy measurements

Next result provides the identity of interest.

**Proposition 6.3.1.** *Let $\{x_j^{\text{obs}}\}_{j=1}^J$ be drawn independently from an uniform distribution over $\Omega$. Let $y_j = u^{\text{true}}(x_j^{\text{obs}}) + \delta_j + \epsilon_j$, where $\epsilon_1, \dots \epsilon_J$ are i.i.d. random variables such that $\epsilon_j \sim (0, \sigma^2)$ and $\delta_1, \dots, \delta_J$ are deterministic unknown disturbances. Let us further assume that $\{x_j^{\text{obs}}\}_{j=1}^J$ and $\{\epsilon_j\}_{j=1}^J$ are independent random sequences.*

*Then, we have that the mean squared error*

$$MSE_J := \frac{1}{J}\sum_{j=1}^{J}\left(y_i - u_\xi^\star(x_j^{\text{obs}})\right)^2 \tag{6.3.1}$$

*satisfies*

$$\mathbb{E}[MSE_J] = E^2_{\text{mean}} + \sigma^2 + \frac{1}{J}\sum_{j=1}^{J}\delta_j^2 - \frac{2}{|\Omega| J}\sum_{j=1}^{J}\delta_j\left(\int_\Omega u^{\text{true}}(x) - u_\xi^\star(x)\,dx\right) \tag{6.3.2}$$

*where* $E^2_{\text{mean}}$ *is defined as follows:*

$$E^2_{\text{mean}} := \frac{1}{|\Omega|} \int_\Omega \left(u^{\text{true}}(x) - u^\star_\xi(x)\right)^2 \, dx. \tag{6.3.3}$$

*Proof.* To simplify notation, we introduce the random sequence $\{e_j = u^{\text{true}}(x_j^{\text{obs}}) - u^\star_\xi(x_j^{\text{obs}})\}_{j=1}^J$. We observe that $e_1, \ldots, e_J$ are i.i.d. and $\mathbb{E}[e_j^2] = \frac{1}{|\Omega|}\|u^{\text{true}} - u^\star_{\lambda,\xi}\|^2_{L^2(\Omega)}$. Then, exploiting linearity of the expected value operator and the fact that $\{x_j^{\text{obs}}\}_{j=1}^J$ and $\{\epsilon_j\}_{j=1}^J$ are independent, we find

$$\mathbb{E}[MSE_J] = \mathbb{E}\left[e_1^2\right] + \mathbb{E}\left[\epsilon_1^2\right] + \frac{1}{J}\sum_{j=1}^J \delta_j^2 - \frac{2}{J}\sum_{j=1}^J \delta_j \, \mathbb{E}[e_j].$$

Thesis follows. □

We observe that $MSE_J = \frac{1}{|\Omega|}\widehat{E}(J, \nu = 0)$ where $\widehat{E}$ is the error estimator defined in Chapter 4.3.1 for $\ell(\cdot, x, \nu = 0) = \delta_x$. As discussed in Chapter 4, in absence of systematic noise ($\delta_j \equiv 0$), identity (6.3.2) reduces to

$$\mathbb{E}[MSE_J] = E^2_{\text{mean}} + \sigma^2. \tag{6.3.4}$$

Estimate (6.3.4) shows that for random noise ($\delta_j \equiv 0$) the mean squared error (6.3.1) can be used to asymptotically bound the squared $L^2(\Omega)$ error. Furthermore, since $\sigma^2$ is independent of the state estimate, minimizing the mean squared error is equivalent to minimize the $L^2(\Omega)$ error. The latter observation motivates the adaptive strategy presented in section 6.4.

## 6.4 Adaptivity

As observed in the previous sections, our procedure depends on a fair amount of design choices, which include the choice of a number of hyper-parameters and the choice of the observation centers and background space $\mathcal{Z}_N$. In section 6.4.1, we discuss how to exploit the error analysis to perform some design choices *a priori*. Then, in section 6.4.2, we discuss the adaptive strategy used to tune the parameters of the formulation after having acquired data.

### 6.4.1 *A priori* considerations

We recall that the PBDW state estimate $u_\xi^\star$ is given by

$$u_\xi^\star := \arg\min_{u\in\mathcal{U}} \xi\|\Pi_{\mathcal{Z}_N^\perp} u\|^2 + \frac{1}{M}\sum_{m=1}^{M}\Big(u(x_m^{\text{obs}}) - y_m\Big)^2 \tag{6.4.1}$$

where $\mathcal{Z}_N = \text{span}\{\zeta_n\}_{n=1}^N$. We observe that the formulation depends on the regularization parameter $\xi$, the sensor locations $\mathcal{X}_M = \{x_m^{\text{obs}}\}_{m=1}^M$ and the choice of the reproducing kernel $K$ associated with $(\mathcal{U}, \|\cdot\|)$.

The hyper-parameter $\xi > 0$ controls the amount of regularization introduced: for $\xi = 0$, the solution to (6.4.1) interpolates exactly the data while for $\xi \to \infty$, the solution to (6.4.1) converges to the least-squares solution. Our error analysis shows that the choice of $\xi$ strongly depends on the noise variance $\sigma^2$ and on the maximum systematic error $\delta$ and also on the accuracy of the model $\|\Pi_{\mathcal{Z}_N^\perp} u^{\text{true}}\|$; in some applications, noise level can be estimated from reanalysis, on the other hand, it is extremely difficult to estimate $\|\Pi_{\mathcal{Z}_N^\perp} u^{\text{true}}\|$ *a priori*.

Since in this work we employ csRBF kernels, the choice of the kernel $K$ reduces to the choice of the hyper-parameters $k$ and $\gamma$ in $K_\chi(x,y) = \phi_{d,k}(\gamma\|x-y\|_2)$, where $\phi_{d,k}$ is defined in (6.1.3). As stated in Proposition 6.1.3, the parameter $k$ determines the Sobolev regularity of the RKHS. Recalling estimate (6.2.9) and Proposition 6.1.3, the optimal value of $k$ should minimise $\|\Pi_{\mathcal{Z}_N^\perp} u^{\text{true}}\| h_{\mathcal{X}_M}^{(d+1)/2+k}$: it is thus extremely problem-dependent. The parameter $\gamma$ regulates the length scale of the kernel functions. In our experience, for small values of $M$, the choice of $\gamma$ weakly influences the results; we can thus pick $\gamma$ *a priori* such that the kernel functions $\{K_{x_m^{\text{obs}}}\}_m$ share the same length scale with the elements of $\mathcal{Z}_N$. On the other hand, for larger values of $M$, the choice of $\gamma$ significantly influences the performance of the method and it must be adapted using data. We remark that by changing $k$ and $\gamma$ we effectively modify the inner product $(\cdot,\cdot)$ and thus the penalization term $\|\cdot\|$ in (6.4.1).

If we neglect the effect of the sensor locations on the stability constant $C_{N,\mathcal{X}_M}$, the error analysis suggests to choose the observation centers to minimize the fill distance $h_{\mathcal{X}_M}$ in (6.2.5). For $N \simeq M$, sensor location might influence significantly the value of $C_{N,\mathcal{X}_M}$. As a result, it might be worth to choose the observation centers to maximize $C_{N,\mathcal{X}_M}$ for any given $M$. In Chapter 3, we presented a Greedy strategy (cf. Algorithm 3.2.1) for the selection of the observation centers that tries to maximize the inf-sup constant $\beta_{N,M}$ defined

in (2.2.2) in a Greedy manner. In this respect, we observe that calculations of $\beta_{N,M}$ (and also $C_{N,\mathcal{X}_M}$) involve computation of the matrix $\mathbb{Z}$ in (2.3.1). As observed in section 6.2.1, computation of accurate approximations of the matrix $\mathbb{Z}$ for general background spaces is unfeasible. Extension of Algorithm 3.2.1 to pointwise measurements is the topic of ongoing research.

In our numerical simulations, we choose adaptively the regularization parameter $\xi$ and the kernel parameter $\gamma$, while we pick $k$ *a priori*, and we simply consider equispaced observation centers. We remark that equispaced observation centers prevent us from considering $N \simeq M$. In the next section, we present the algorithm used to perform online adaptation. We note that our adaptation procedure could be also applied to automatically select the hyper-parameter $k$.

### 6.4.2 Adaptive procedure

In the Statistical Learning literature, several approaches have been presented to tune the design parameters of reguralized regression formulations; we refer to [104, Chapter 7] and to [128] for a thorough overview. The adaptive strategy depends on the size of the dataset, which in our context corresponds to the amount of available transducers. If we denote by $L$ the number of available transducers and by $\mathcal{D}_L = \{(x_\ell^{\text{obs}}, y_\ell)\}_{\ell=1}^L$ the corresponding dataset, for large values of $L$, the holdout method is the most widely used approach. On the other hand, for small values of $L$, $\kappa$-fold cross-validation is typically employed. In the remainder of this section, we briefly review these techniques and we discuss their application to our problem.

The holdout method partitions the dataset $\mathcal{D}_L$ into the two mutually exclusive subsets $\mathcal{D}_M = \{(x_m^{\text{obs}}, y_m)\}_{m=1}^M$ and $\mathcal{D}_J = \{(x_j^{\text{obs}}, y_j)\}_{j=1}^J$. Given the finite dimensional search space $\mathfrak{H}^{hyper}$ for $(\xi, \gamma)$, we generate the state estimate $u_{\xi,\gamma}^\star$ based on the training set and then we compute the mean squared error over the validation set

$$MSE_J(\xi, \gamma) = \frac{1}{J} \sum_{j=1}^{J} \left( y_j - u_{\xi,\gamma}^\star(x_j^{\text{obs}}) \right)^2, \tag{6.4.2}$$

for each $(\xi, \gamma)$ in $\mathfrak{H}^{hyper}$. Finally, we choose the state estimate associated with the choice of $(\xi, \gamma)$ that minimizes $MSE_J(\xi, \gamma)$ over $\mathfrak{H}^{hyper}$. Recalling Proposition 6.3.1, if $\{x_j^{\text{obs}}\}_j$ are drawn from an uniform distribution over $\Omega$ and the disturbances are homoscedastic,

this choice of the hyper-parameters asymptotically minimizes the $L^2$ state-estimation error. This result holds independently of the strategy employed to compute the state estimate and thus independently of the strategy employed to select the training observation centers. As discussed in Chapter 4, if $u^\star_{\xi,\gamma}$ is an accurate description of the true field $u^{\text{true}}$, $MSE_J$ rapidly converges to its expected value. Therefore, the number $J$ of measurements that should be reserved for validation is modest.

Cross-validation is based on the partition of the dataset $\mathcal{D}_L$ into $\kappa$ equal-sized subsamples (folds) $\{\mathcal{D}_L^{(k)}\}_{k=1}^{\kappa}$. Of the $\kappa$ folds, a single fold is retained for testing and the remaining $\kappa-1$ folds are used for training. The procedure is then repeated $\kappa$ times with each of the $\kappa$ folds used once as the validation dataset. In the limit $L = \kappa$, the procedure is known as Leave-One-Out Cross-Validation (LOOCV). We observe that, even for moderate $L$, $\kappa$-fold Cross-Validation can be quite expensive if $\kappa \approx L$. For this reason, generalized cross-validation strategies, which focus on computing computationally inexpensive approximations of the error indicator, have been developed. We refer to [104, Chapter 7.10] and to the references therein for further details.

In this paper, we exclusively employ holdout validation and we refer to a future work for the application of more advanced cross-validation strategies. Motivated by the previous discussion, in this work, we here choose the validation sensors by sampling uniformly over $\Omega$.

## 6.5 Numerical results

### 6.5.1 Application to a synthetic two-dimensional acoustic problem

We first consider the two-dimensional acoustic problem introduced in Chapter 3.3. To assess the performance, we introduce the relative $L^2$ error averaged over $|\mathcal{P}^{\text{bk}}_{\text{train}}| = n_{\text{train}}$ fields associated with different choices of the parameter $\mu$:

$$E^{\text{rel}}_{\text{avg}}(n_{\text{train}}) := \frac{1}{n_{\text{train}}} \sum_{\mu \in \mathcal{P}^{\text{bk}}_{\text{train}}} \frac{\|u^{\text{true}}(\mu) - u^\star_\xi(\mu)\|_{L^2(\Omega)}}{\|u^{\text{true}}(\mu)\|_{L^2(\Omega)}}. \tag{6.5.1}$$

In all our numerical tests, we consider noisy observations with additive Gaussian noise:

$$y_\ell = u^{\text{true}}(x_\ell) + \epsilon_\ell, \qquad \epsilon_\ell \overset{iid}{\sim} \mathcal{N}(0, \sigma^2). \tag{6.5.2}$$

As in Chapter 3.3, we build the background spaces $\{\mathcal{Z}_N\}_N$ using the weak-Greedy algorithm. We employ csRBF with $k = 1$; recalling Proposition 6.1.3, this corresponds to $\mathcal{U} = H^{2.5}(\mathbb{R}^2)$.

### 6.5.2 Results of the data assimilation procedure (noise-free case)

We first visualize the PBDW state estimates for two distinct choices of $u^{\text{true}}$. We consider $\mu = 6.6$, and we consider $u^{\text{true}} = u_{g=0}(\mu)$ and $u^{\text{true}} = u_{g=\tilde{g}}(\mu)$; PBDW state estimates are based on the background $\mathcal{Z}_{N=5}$ and on $M = 25$ equispaced measurements. We rely on holdout validation ($J = 12$) to choose the value of the hyper-parameters $\xi, \gamma$. Figure 6-1 shows (the real part of) the true state, the PBDW state estimate $u_\xi^\star$, the deduced background $z_\xi^\star$ and the update $\eta_\xi^\star$. As observed in Chapter 3 (cf. Figure 3-6), for $u^{\text{true}} = u_{g=0}(\mu)$ the update $\eta_\xi^\star$ is negligible; the reason is that the true state is well-approximated by its projection over $\mathcal{Z}_N$. On the other hand, for $u^{\text{true}} = u_{g=\tilde{g}}(\mu)$ we observe that the update is appreciable, and plays a significant role in improving the accuracy of the state estimate $u_\xi^\star$. These results strenghten the interpretation of the components of the PBDW state estimate provided in Chapter 2: $z_\xi^\star$ addresses the parametric uncertainty in the model, while $\eta^\star$ accomodates non-parametric uncertainty.

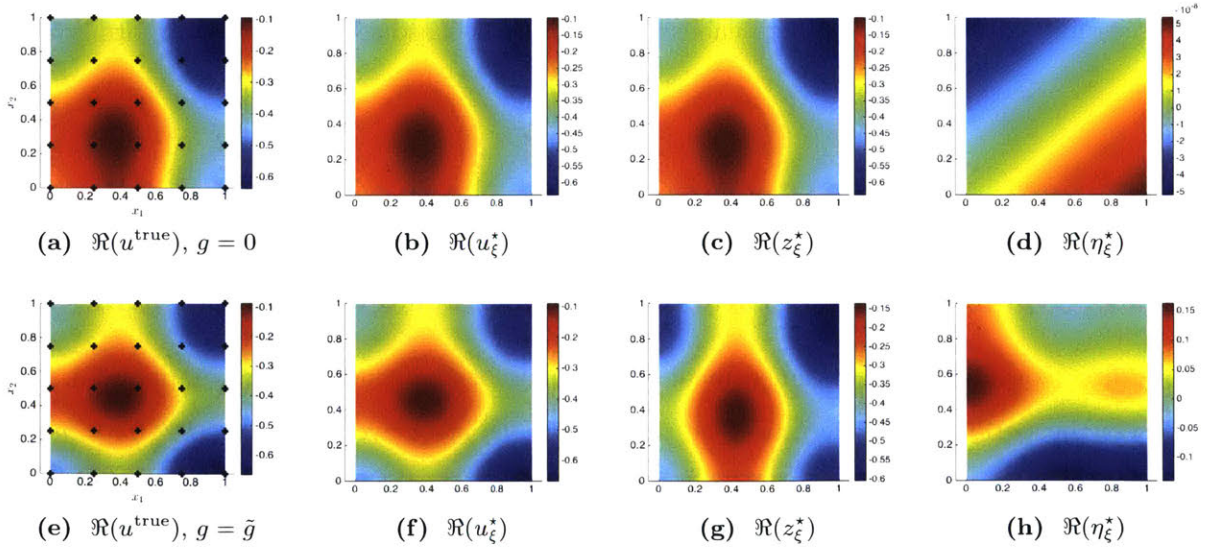

**(a)** $\Re(u^{\text{true}})$, $g = 0$ **(b)** $\Re(u_\xi^\star)$ **(c)** $\Re(z_\xi^\star)$ **(d)** $\Re(\eta_\xi^\star)$

**(e)** $\Re(u^{\text{true}})$, $g = \tilde{g}$ **(f)** $\Re(u_\xi^\star)$ **(g)** $\Re(z_\xi^\star)$ **(h)** $\Re(\eta_\xi^\star)$

**Figure 6-1:** Application to a two-dimensional acoustic problem: visualization of the PBDW state estimates for $N = 5$, $M = 25$, $J = 12$ (perfect measurements). The states in Figures (a) and (e) correspond to $\mu = 6.6$.

Figure 6-2 shows the convergence of $E_{\text{avg}}^{\text{rel}}$ with $N$ for fixed $M$ and noise-free measurements. We compute $E_{\text{avg}}^{\text{rel}}$ using (6.5.1) based on $n_{\text{train}} = 20$ fields. We observe that conver-

gence with $N$ is in good qualitative agreement with the behavior of the best-fit error

$$E_N^{\text{rel}} := \frac{1}{n_{\text{train}}} \sum_{\mu \in \mathcal{P}_{\text{train}}^{\text{bk}}} \frac{\|u^{\text{true}}(\mu) - \Pi_{\mathcal{Z}_N, L^2} u^{\text{true}}(\mu)\|_{L^2(\Omega)}}{\|u^{\text{true}}(\mu)\|_{L^2(\Omega)}},$$

where $\Pi_{\mathcal{Z}_N, L^2}$ is the projection operator with respect to the $L^2$ inner product. If $u^{\text{true}} \in \mathcal{M}^{\text{bk}}$, we observe fast convergence with $N$; on the other hand, if $u^{\text{true}} \notin \mathcal{M}^{\text{bk}}$, we reach a strictly positive plateau.

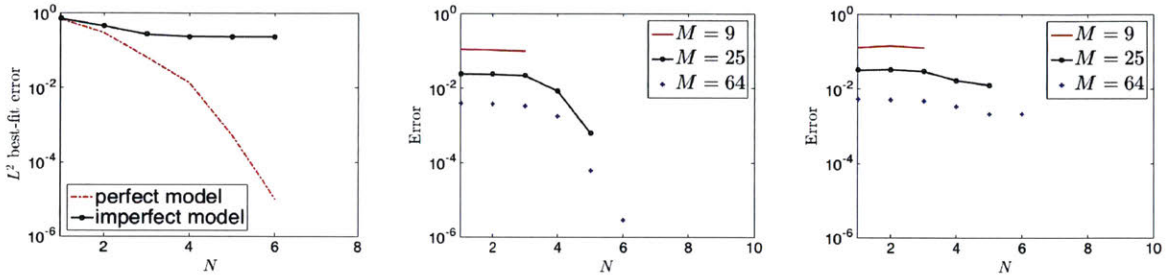


**(a)** $L^2$-best fit **(b)** $g = 0$ **(c)** $g = \tilde{g}$

**Figure 6-2:** Application to a two-dimensional acoustic problem: convergence of $E_{\text{avg}}^{\text{rel}}$ with $N$ for fixed $M$ for perfect ($g = 0$) and imperfect ($g = \tilde{g}$) model. Figure (a) shows the $L^2$-best-fit error.

Figure 6-3 shows the convergence with $M$ for fixed $N$ and noise-free measurements. We assess performance by computing $E_{\text{avg}}^{\text{rel}}$ in (6.5.1) averaged over $n_{\text{train}} = 20$ fields. We observe that, with the exception of $N = 5$ for perfect model, the rate of convergence with $M$ weakly depends on the value of $N$: in this test, we observe $E_{\text{avg}}^{\text{rel}} \simeq M^{-s}$ with $s \in [1.3, 1.5]$ for all cases considered. This empirically confirms the multiplicative effect between $N$ convergence and $M$ convergence observed in Remark 6.2.2. A possible explanation for the contrasting results for the case ($N = 5, g = 0$) is due to discretization effects: since in this case the error $u^{\text{true}} - z_\xi^\star$ is highly oscillatory, the adaptive procedure selects large value of the parameter $\gamma$ that are not well-resolved by the Finite Element mesh used to estimate the norms and to compute the true solution.

### 6.5.3 Comparison with $H^1$-PBDW

We now wish to compare the approach presented in this chapter with the original PBDW approach discussed in Chapter 3. We refer to the former as adaptive PBDW (A-PBDW) and to the latter as $H^1$-PBDW. For $N = 5$, we compare the behavior of the averaged $L^2$-relative error $E_{\text{avg}}^{\text{rel}}$ (6.5.1) for $n_{\text{train}} = 10$ different fields. We consider both the case of perfect model

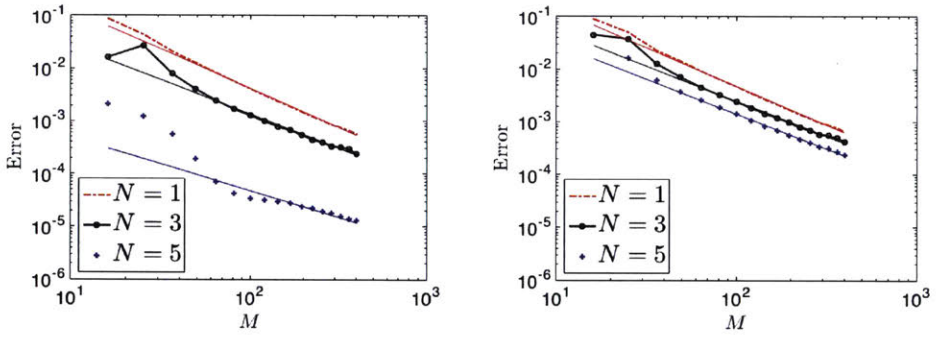


**(a)** $g = 0$ **(b)** $g = \tilde{g}$

**Figure 6-3:** Application to a two-dimensional acoustic problem: convergence of $E_{\text{avg}}^{\text{rel}}$ with $M$ for fixed $N$ for perfect ($g = 0$) and imperfect ($g = \tilde{g}$) model ($I = M/2$). Estimated convergence rates for perfect model: $-1.48$ ($N = 1$), $-1.30$ ($N = 3$), and $-1.00$ ($N = 5$). Estimated convergence rates for imperfect model: $-1.46$ ($N = 1$), $-1.32$ ($N = 3$), and $-1.32$ ($N = 5$).

and the case of imperfect model. For $H^1$-PBDW we consider Gaussian functionals with standard deviations $r_{\text{Gauss}} = 0.01$ and $r_{\text{Gauss}} = 0.02$. In all cases, we consider the same set of training points chosen based on the SGreedy-plus algorithm presented in Chapter 3. We remark that for A-PBDW we use pointwise measurements, while for $H^1$-PBDW measurements are evaluations of the Gaussian functionals.

Figure 6-4 shows the results[2]. We observe that A-PBDW significantly outperforms $H^1$-PBDW. The difference becomes even more evident if we consider a smaller value of $r_{\text{Gauss}}$.

### 6.5.4 Interpretation of the hyper-parameters $\gamma$ and $\xi$

We investigate the connection between the optimal value of $\xi$ and the signal-to-noise ratio. In Figure 6-5, we compute the mean squared error over the validation set for the estimation of the state associated with the parameter $\mu = 5.8$. We consider $M = 225$ and we compute the mean squared error based on $J = 110$ measurements. We both consider the case of perfect model ( $g = 0$), and the case of imperfect model ($g = \tilde{g}$). For this test, we employ the background $\mathcal{Z}_{N=5}$. We observe that the optimal $\xi$ depends on model error and on noise level. In more detail, we observe that for $g = 0$, the adaptive procedure selects large values of $\xi$ regardless of the noise level, while for $g = \tilde{g}$ it selects $\xi \approx 10^{-7}$ for $\sigma = 0.05$ and $\xi \approx 10^{-5}$ for $\sigma = 0.4$. Therefore, the optimal $\xi$ increases as noise increases, and decreases as

[2]We note that, as a result of validation, A-PBDW requires $3/2M$ measurements, while $H^1$-PBDW only requires $M$ measurements. We argue, however, that the use of $J = M/2$ measurements is unnecessary for noise-free observations. In addition, we might significantly reduce the gap by resorting to more advanced cross-validation strategies.

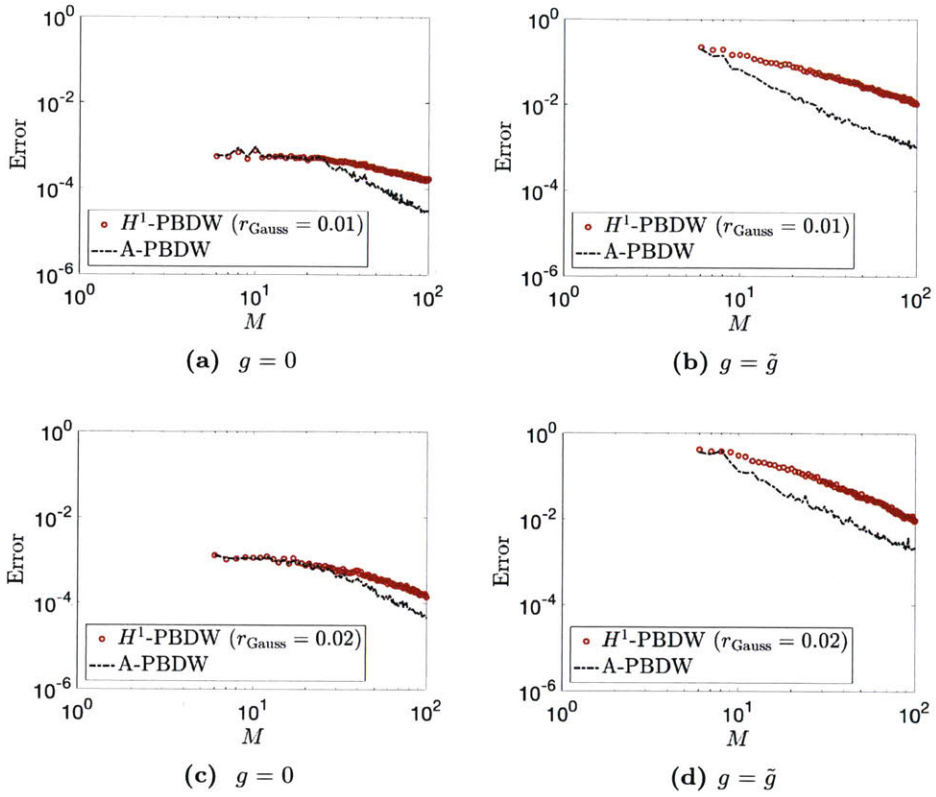


**(a)** $g = 0$ **(b)** $g = \tilde{g}$

**(c)** $g = 0$ **(d)** $g = \tilde{g}$

**Figure 6-4:** Application to a two-dimensional acoustic problem: convergence of $E_{\text{avg}}^{\text{rel}}$ with $M$ for fixed $N$ for adaptive PBDW (A-PBDW) and for $H^1$-PBDW ($N = 5$, $\gamma = 1$).

best-fit error increases. The latter empirical observation is in good agreement with (6.2.9a), although the latter has been rigorously shown only for systematic noise.

In Figure 6-6, we investigate the influence of the kernel parameter $\gamma$. We study the behavior of $E_{\text{avg}}^{\text{rel}}$ with $M$ associated with $n_{\text{train}} = 10$ different values of the parameter $\mu$, for the five-dimensional background $\mathcal{Z}_{N=5}$ and for two different search spaces $\mathfrak{H}^{hyper}$: in more detail, in the first case we seek $\gamma$ in $\{0.1, 0.5, 1\}$, and in the second case we choose $\gamma$ in $\{3, 3.5, 4\}$. Since we consider perfect measurements, results are not sensitive to the choice of $\xi$. We observe that in the perfect-model case (Figure 6-6(a)) large values of $\gamma$ significantly improve performance; on the other hand, in the imperfect model case (Figure 6-6(b)), the first choice of $\mathfrak{H}^{hyper}$ leads to more accurate results for all values of $M$ considered. This can be explained by observing that $\gamma$ has to match the length-scale of the field $u^{\text{true}} - z_\xi^\star$, and strongly depends on the distance between observations (and thus $M$). This test motivates the importance of adapting the value of $\gamma$. We remark that adaptation in $\gamma$ relies on the availability of explicit expressions for the Riesz elements $K_{x_m}$.

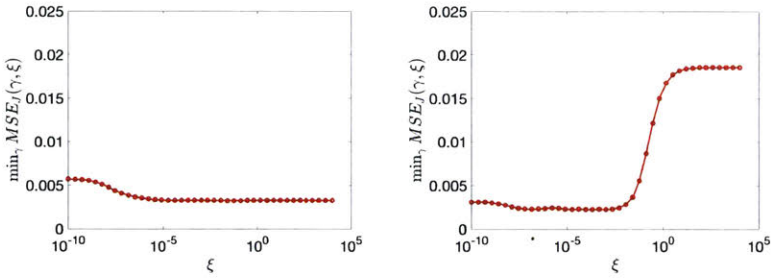


**(a)** $\sigma = 0.05$, $g = 0$ **(b)** $\sigma = 0.05$, $g = \tilde{g}$

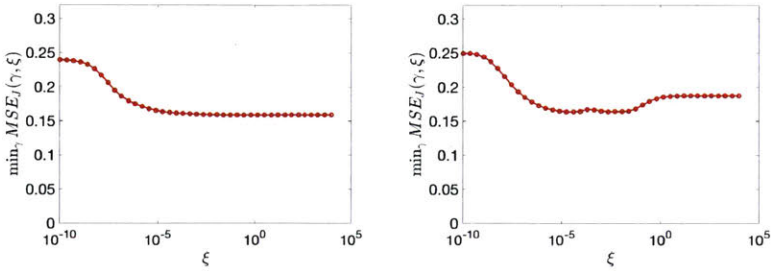


**(c)** $\sigma = 0.4$, $g = 0$ **(d)** $\sigma = 0.4$, $g = \tilde{g}$

**Figure 6-5:** Application to a two-dimensional acoustic problem: interpretation of $\xi$. Results correspond to $u^{\text{true}} = u_g(\mu = 5.8)$. ($M = 225$, $J = 112$, $N = 5$).

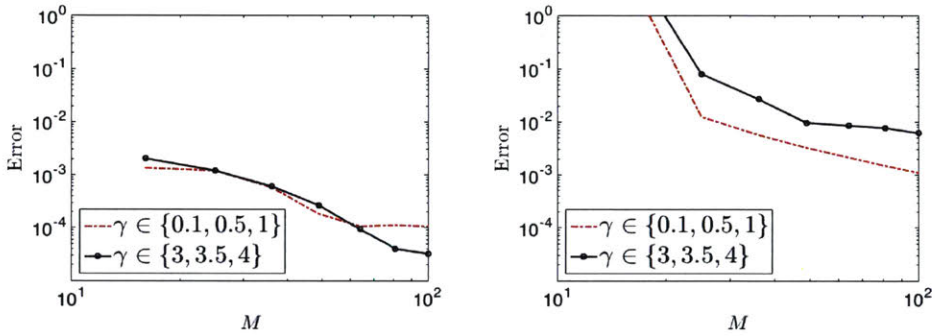


**(a)** $g = 0$, $N = 5$ **(b)** $g = \tilde{g}$, $N = 5$

**Figure 6-6:** Application to a two-dimensional acoustic problem: interpretation of $\gamma$ ($N = 5$, $\sigma = 0$).

### 6.5.5 Noisy measurements

We first study the behavior of the constant $\mathcal{T}^\sigma$ introduced in (6.2.12). Figures 6-7(a) and (b) show the behavior of $\mathcal{T}^\sigma$ for equispaced measurements with respect to the value of $\xi$ and for two values of $\gamma$. We observe that $\mathcal{T}^\sigma$ is monotonic decreasing in $\xi$ and reaches a lower bound for $\xi \to \infty$. Figure 6-7(c) shows the behavior of $\min_\xi \mathcal{T}^\sigma$ with respect to the number of measurements: $\min_\xi \mathcal{T}^\sigma$ is independent of $\gamma$ and converges to 0 with rate $M^{-1}$.

Figure 6-8 shows performance in presence of noise. As in the previous tests, we assess performance by computing $E^{\text{rel}}_{\text{avg}}$ in (6.5.1) for $n_{\text{train}} = 1$ ($\mu = 6.6$); to take into account

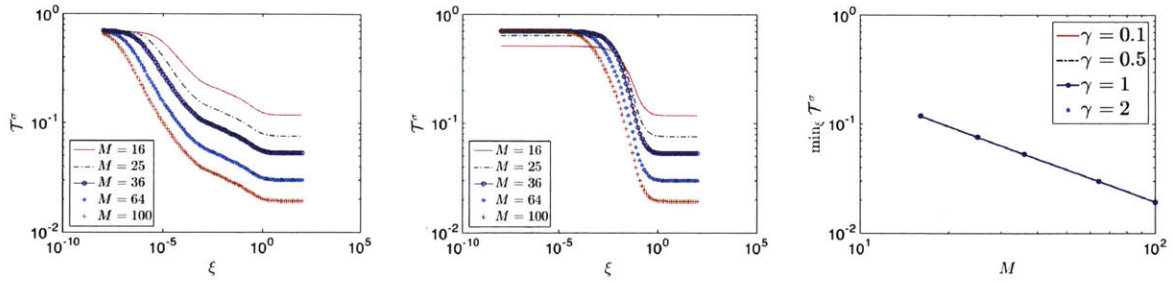


**(a)** $\gamma = 0.1$ **(b)** $\gamma = 2$ **(c)** $\gamma = 2$

**Figure 6-7:** Application to a two-dimensional acoustic problem: $\mathcal{T}^\sigma$. Figures (a) and (b): behavior of $\mathcal{T}^\sigma$ with $\xi$ for $\gamma = 0.1$ and $\gamma = 2$. Figure (c): behavior of $\min_\xi \mathcal{T}^\sigma$ with $M$ for several values of $\gamma$.

randomness in the results, we average over 24 realizations of the random noise. We consider the background $\mathcal{Z}_{N=5}$. In the case of perfect model, the estimated convergence rate in the noisy case is roughly $M^{-0.5}$ for all values of standard deviations $\sigma$ considered: this is in agreement with the results shown in Figure 6-7(c) and with the mathematical analysis. On the other hand, in the case of imperfect model, the estimated convergence rate in the noisy case is roughly $M^{-0.4}$. Interestingly, also in this case, the convergence rate weakly depends on $\sigma$.

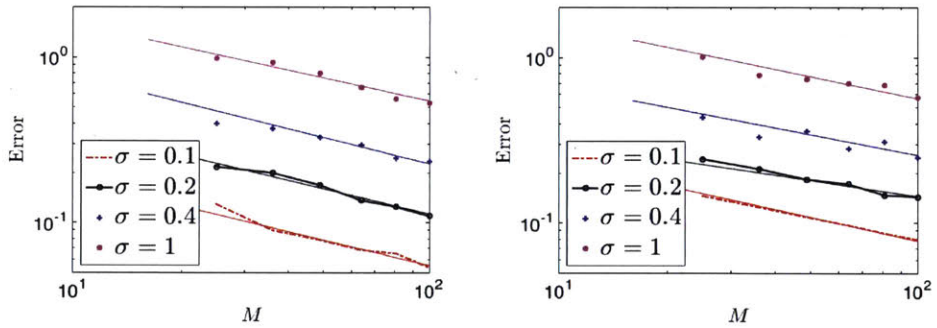


**(a)** $g = 0$, $N = 5$ **(b)** $g = \tilde{g}$, $N = 5$

**Figure 6-8:** Application to a two-dimensional acoustic problem: convergence with $M$ for fixed $N$ for perfect ($g = 0$) and imperfect ($g = \tilde{g}$) model in presence of homoscedastic Gaussian noise. Estimated convergence rates for perfect model: $-0.5114$ ($\sigma = 0.1$), $-0.5091$ ($\sigma = 0.2$), $-0.5297$ ($\sigma = 0.4$), and $-0.4641$ ($\sigma = 1$). Estimated convergence rates for imperfect model: $-0.4759$ ($\sigma = 0.1$), $-0.3235$ ($\sigma = 0.2$), $-0.4155$ ($\sigma = 0.4$), and $-0.4443$ ($\sigma = 1$).

### 6.5.6 Application to the thermal patch experiment

We apply our procedure to the thermal patch configuration. For this test, we interpret pixel-wise measurements as pointwise evaluations associated with the center of the pixel. As in the previous test, we perform holdout validation for $\xi$ and $\gamma$ with $J = M/2$. We assess perfor-

mance by computing the relative mean squared error $MSE^{\text{rel}} = \|u^{\text{obs}} - u^{\star}_{\xi}\|^2_{L^2(\Omega)} / \|u^{\text{obs}}\|^2_{L^2(\Omega)}$ based on the full-field information. Figure 6-9 shows the convergence of $MSE^{\text{rel}}$ with $M$ for three values of $N$.

We observe that, while including the first snapshot leads to a substantial improvement in the performances, considering $N > 1$ does not lead to any substantial improvement. We further observe that for $M \approx 100$ we reach the estimated noise level

$$\sigma_{\text{est}} := \frac{\|\frac{0.5^o C}{\Delta\Theta}\|_{L^2(\Omega)}}{\|u^{\text{obs}}\|_{L^2(\Omega)}}.$$

As $M$ increases, $MSE^{\text{rel}}$ becomes significantly lower than $\sigma^2_{\text{est}}$: this can be explained by observing that for large values of $M$ the amount of pixels used for learning (training plus validation) is not negligible compared to the entire dataset. For $M = 100$, the amount of pixels used for learning is 150, which is 8% of the total number of pixels. This introduces a bias in our calculation of the relative MSE, $MSE^{\text{rel}}$.

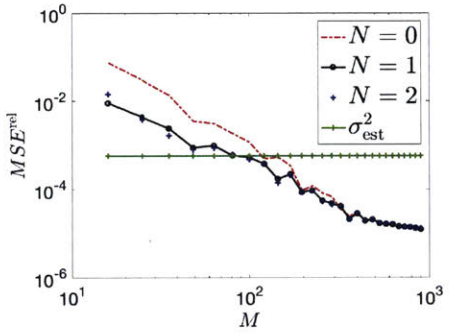


**Figure 6-9:** Application to the thermal patch experiment: convergence of the relative mean squared error $MSE^{\text{rel}}$ with $M$ for fixed $N$.

## 6.6 Conclusions

In this chapter, we extended the PBDW formulation to pointwise noisy measurements. The extension relies on an adaptive procedure that properly takes into account the noise level, and the characteristic length-scale of the difference $u^{\text{true}} - z^{\star}_{\xi}$. Adaptation in the value of $\xi$ allows us to properly weight the trust in the bk model with respect to the trust in the experimental measurements. The use of explicit kernels allows us to perform online adaptation to tune the characteristic length-scale of the update functions. We presented

*a priori* and *a posteriori* error estimates for the $L^2$ state-estimation error to motivate the approach from a theoretical standpoint.

We also presented several numerical results to illustrate the different elements of the formulation. In more detail, numerical experiments demonstrated (i) a multiplicative effect between $N$ convergence (associated with the primary approximation provided by the background $\mathcal{Z}_N$) and $M$ convergence (associated with the secondary approximation provided by the update $\mathcal{U}_M$), (ii) the practical importance of adapting the shape of the Riesz representers based on data, (iii) $L^2$ convergence of the PBDW estimate to the true state even for noisy measurements, and (iv) the improvement in the convergence rate with $M$ with respect to the $H^1$-PBDW formulation considered in the previous chapters.

# Part II

# Simulation-Based Classification

# Chapter 7

# The microtruss problem

In this chapter, the first one of the second part of the thesis, we introduce the damage identification problem considered in this work: the microtruss problem. This physical companion experiment will serve to illustrate and motivate the definitions given in Chapter 1.3.2, and the computational approach proposed in Chapter 8. We first introduce the experimental apparatus and procedure (section 7.1); then, following the general paradigm proposed in [78] and outlined in Chapter 1.4.2, we provide an actionable definition of damage (section 7.2), we describe the data acquisition system, and we introduce the experimental outputs (section 7.3). In section 7.4, we propose a parametrized mathematical model for the structure of interest which shall serve to estimate the experimental outputs, and we introduce a mathematical description of the space of system configurations. In section 7.5, we formalize the problem of feature extraction and we present the choice of the features for the microtruss problem, and in section 7.6, we state the classification problem and we summarize all the key definitions.

## 7.1 Experimental apparatus

We consider the acrylic microtruss system shown in Figure 7-1. The microtruss consists of a 4 by 4 lattice of blocks of size $\ell_{\text{block}} \times \ell_{\text{block}}$, $\ell_{\text{block}} = 0.25$[in], linked together by horizontal and vertical joints of size $L_{\text{joint}} \times h_{\text{joint}}$, $L_{\text{joint}} = 1$[in] and $h_{\text{joint}} = 0.015$[in]. The depth of the microtruss is equal to $d_{\text{mtruss}} = 1$[in]. We state upfront that the actual geometry of the microtruss is to be considered uncertain due to the (3d-printing) manufacturing process. For this reason, the values reported above should be interpreted as nominal, and we shall

refer to the configuration described above as the *nominal geometry*. We resort to cartesian coordinates; since the geometry is independent of the third dimension, we use notation

$$x^{\text{dim}} = L_{\text{joint}}\, x = L_{\text{joint}}\, x_1 \mathbf{e}_1 + L_{\text{joint}}\, x_2 \mathbf{e}_2 = L_{\text{joint}} \begin{bmatrix} x_1 \\ x_2 \end{bmatrix}$$

to indicate a physical point in the microtruss; here $\mathbf{e}_1$ and $\mathbf{e}_2$ are the canonical unit vectors, and $L_{\text{joint}} = 1[\text{in}]$ is the non-dimensionalization constant. In what follows we exclusively refer to non-dimensional quantities unless otherwise indicated. We refer to the blocks using the matrix notation $(i, j)$, $i, j = 1, \ldots, 4$: the $i$-index corresponds to the $x_1$ position and is ordered from left to right in Figure 7-1(b); the $j$-index corresponds to the $x_2$ position and is ordered from bottom to top in Figure 7-1(b).

Our goal is to detect the presence of added mass on top of block $(1, 4)$ and of block $(4, 4)$. More precisely, we wish to distinguish between $K = 4$ states of damage: no added mass ($y = 1$), added mass on top of block $(1, 4)$ ($y = 2$), added mass on top of block $(4, 4)$ ($y = 3$), added mass on top of both block $(1, 4)$ and block $(4, 4)$ ($y = 4$). Note that state 1 shall correspond to no damage, and states 2, 3, and 4 shall correspond to different damage configurations. We refer to the case of no added mass as the undamaged case. Figure 7-1(c) shows the detail of the added mass on top of block $(1, 4)$ for a particular experimental configuration. Added mass is of the same material as the microtruss system.

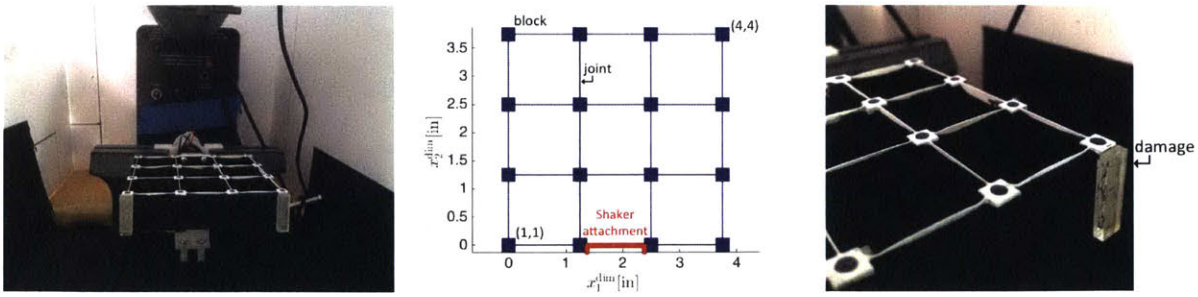


**(a)** **(b)** **(c)**

**Figure 7-1:** Microtruss experiment. Figure (a): experimental apparatus. Figure (b): schematic of undamaged configuration at rest. Figure (c): detail of the added mass on top of block $(1, 4)$.

## 7.2 Definition of damage

In view of the definition of damage, we first introduce the non-dimensional ratios

$$s_L := 1 + \frac{V_{\text{left}}}{V_{\text{nom}}}, \qquad s_R := 1 + \frac{V_{\text{right}}}{V_{\text{nom}}}, \tag{7.2.1}$$

where $V_{\text{nom}} = h\,\ell_{\text{block}}\,d_{\text{mtruss}}$, $h = \frac{1}{2}(d_{\text{block}} - h_{\text{joint}})$, is a nominal volume, $V_{\text{left}}$ is the volume of the added mass on top of block $(1,4)$, and $V_{\text{right}}$ is the volume of the added mass on top of block $(4,4)$. We observe that the ratios in (7.2.1) do not rely on any model of the structure.

We can now introduce the function $\bar{f}^{\text{dam}} : [1,2]^2 \to \{1,2,3,4\}$ such that

$$\bar{f}^{\text{dam}}(s_L, s_R) = \begin{cases} 1 & s_L, s_R \leq 1.5, \\ 2 & s_L > 1.5,\ s_R \leq 1.5, \\ 3 & s_L \leq 1.5,\ s_R > 1.5, \\ 4 & s_L, s_R > 1.5. \end{cases} \tag{7.2.2}$$

The function $\bar{f}^{\text{dam}}$ reflects our actionable definition of damage for the structure of interest; given the system configuration described by the pair $(s_L, s_R)$, $y = \bar{f}^{\text{dam}}(s_L, s_R)$ denotes the corresponding state of damage. For this reason, we refer to $\bar{f}^{\text{dam}}$ as the *damage function.* From an engineering perspective, equation (7.2.2) implies that system configurations should be classified as damaged only if the added mass is "substantial", in our case of volume larger than $0.5V_{\text{nom}} \approx 0.37 \cdot 10^{-3}[\text{in}^3]$. We remark that, from a practical perspective, the proper choice of the threshold is extremely important and should be related to appropriate safety factors ([242]). In section 7.6 we shall provide a general form for the damage function in terms of the system configuration.

## 7.3 Data acquisition and experimental outputs

We rely on a camera to acquire measurements of the $x_2$ displacement of the 16 respective centers of the blocks as a function of time $t$ associated with $Q_f$ different time-harmonic inputs. The camera is carefully calibrated to permit its use for precise measurement. A stroboscope flashing at the 10 Hz frame rate of the camera "freezes" the oscillation of the blocks to yield crisp images suitable for subsequent processing. Frequencies of excitation are offset by 0.1 Hz from integer values to ensure that each set of 100 consecutively captured im-

ages corresponds to 100 equally spaced instants in a single period of oscillation. Excitations are imposed by a linear voice coil actuator attached to the joint between blocks $(2,1)$ and $(3,1)$; Figure 7-1(b) highlights in red the region of the microtruss attached to the actuator. A linear flexure bearing is used to ensure that the excitation is imposed almost exclusively in the $x_2$ direction.

We introduce the system configuration $\mathcal{C}$ associated with the particular specimen considered; we defer the formal definition of $\mathcal{C}$ to section 7.4. Then, we denote by $\{f^q\}_{q=1}^{Q_f} \subset \mathcal{I}_f := [20, 80][\text{Hz}]$ the input frequencies and we denote by $\{q_{i,j}^{\text{exp}}(t^\ell, f^q; \mathcal{C})\}_{\ell=1}^{L}$ the raw time signal for the $x_2$-displacement obtained experimentally for the block $(i,j)$ and the frequency $f^q$. Finally, we introduce the fitted amplitude $\{\overline{A}_{i,j}^{\text{exp}}(f^q;\mathcal{C})\}_{i,j,q}$ and phase $\{\overline{\phi}_{i,j}^{\text{exp}}(f^q;\mathcal{C})\}_{i,j,q}$ such that[1]

$$q_{i,j}^{\text{exp}}(t^\ell, f^q; \mathcal{C}) \approx \overline{A}_{i,j}^{\text{exp}}(f^q;\mathcal{C}) \cos\left(2\pi f^q t^\ell + \overline{\phi}_{i,j}^{\text{exp}}(f^q;\mathcal{C})\right), \quad i,j = 1,\ldots,4, \ell = 1,\ldots,L. \tag{7.3.1}$$

It is convenient to rescale amplitudes and phases as follows:

$$A_{i,j}^{\text{exp}}(f^q;\mathcal{C}) := \frac{A_{\text{nom}}}{\overline{A}_{2,1}^{\text{exp}}(f^q;\mathcal{C})} \overline{A}_{i,j}^{\text{exp}}(f^q;\mathcal{C}), \qquad \phi_{i,j}^{\text{exp}}(f^q;\mathcal{C}) = \overline{\phi}_{i,j}^{\text{exp}}(f^q;\mathcal{C}) - \overline{\phi}_{2,1}^{\text{exp}}(f^q;\mathcal{C}), \tag{7.3.2}$$

for $A_{\text{nom}} = 0.25$. Figure 7-2 demonstrates the accuracy of the time-harmonic fit for the blocks $(1,4)$ and $(4,4)$ in absence of added masses. In section 7.4, we describe how we shall estimate $\{A_{i,j}^{\text{exp}}(f^q;\mathcal{C})\}$ and $\{\phi_{i,j}^{\text{exp}}(f^q;\mathcal{C})\}$ based on simulations.

## 7.4 Mathematical model for the experimental outputs

We first provide a mathematical description of the nominal geometry at rest. With this in mind, we introduce the disjoint domains $\Omega_1, \Omega_2, \Omega_3 \subset \Omega$, $\overline{\Omega}_1 \cup \overline{\Omega}_2 \cup \overline{\Omega}_3 = \overline{\Omega}$. The subdomain $\Omega_2$ is associated with the region of block $(1,4)$ subject to potential damage; similarly, the subdomain $\Omega_3$ is associated with the region of block $(4,4)$, while $\Omega_1$ denotes the remainder of the microtruss. We then recall the geometric parameters $s_L, s_R \in [1,2]$ in (7.2.1) such that $(s_L - 1)\, V_{\text{nom}}$ and $(s_R - 1)\, V_{\text{nom}}$ correspond to the volume of the added masses on top

[1] Amplitudes and phases are estimated using the Matlab function `fit` ([150]), which relies on Levenberg-Marquardt algorithm.

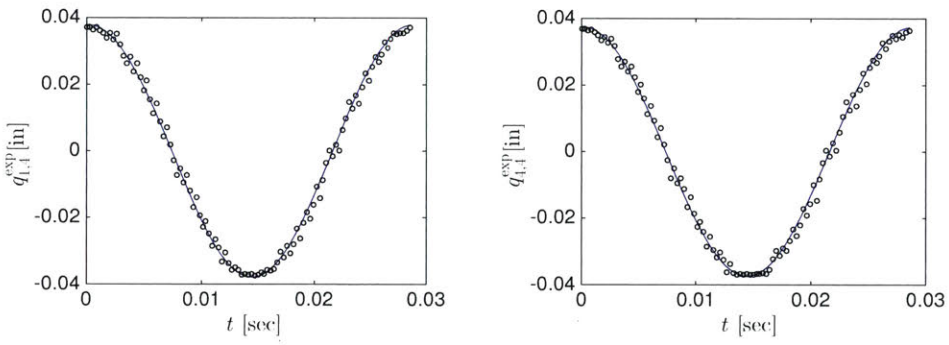


**(a)** **(b)**

**Figure 7-2:** Microtruss experiment. Time-harmonic $x_2$-displacement of blocks $(1,4)$ and $(4,4)$ in absence of added masses. The shaker input is displacement: $A^{\dim}\cos(2\pi ft)\mathbf{e}_2$, $A^{\dim} = 0.02$[in], $f = 35$ [Hz].

of blocks $(1,4)$ and $(4,4)$, respectively. Assuming that the depth of the blocks is uniformly equal to $d_{\text{mtruss}}$ and the width of the block is uniformly equal to $\ell_{\text{block}}$, then we have that $(s_L - 1)\,h$ and $(s_R - 1)\,h$ equal the thickness of the added masses on top of $(1,4)$ and $(4,4)$, respectively. Figure 7-3 shows blocks $(1,4)$ and $(4,4)$ and provides a graphical depiction of the previous definitions. In what follows, we introduce $s := (s_L, s_R)$ and we denote by $\Omega_s$ the domain $\Omega_s = \Omega_1 \cup \Omega_2(s_L) \cup \Omega_3(s_R)$.

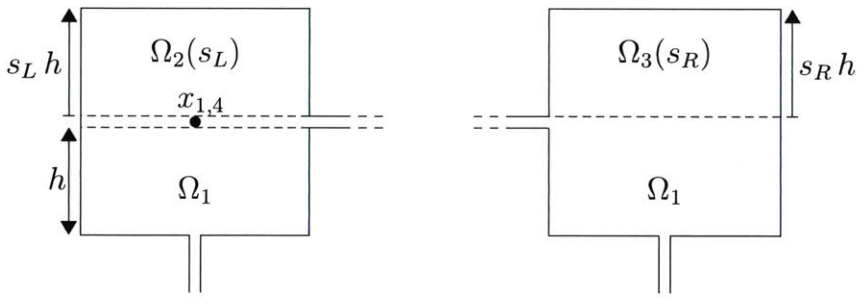


**(a)** block $(1,4)$ **(b)** block $(4,4)$

**Figure 7-3:** Microtruss experiment. Parametrization of blocks $(1,4)$ and $(4,4)$.

We can now introduce the mathematical model of the displacement field in strong form. With this in mind, we introduce the Young's modulus $E$[Pa], the Poisson's ratio $\nu$, the density $\rho$[kg/m$^3$], and the non-dimensional Rayleigh-damping coefficients $\alpha, \beta$. For acrylic, density and Poisson's ratio are well-characterized in the literature[2]: we therefore set

$$\rho = 1180\,[\text{kg/m}^3], \qquad \nu = 0.35.$$

[2]See, e.g., [102, Chapter 3.6.2] for the Poisson's ratio and the webpage `pubchem.ncbi.nlm.nih.gov` for the density.

On the other hand, we consider $\alpha, \beta, E$ as uncertain parameters. We assume that the (non-dimensional) displacement field associated with the microtruss system is of the form $U^{\text{bk}}(x,t) = \Re\{u^{\text{bk}}(x)\, e^{i\omega_f t}\}$ where $\omega_f = 2\pi f$ and $u^{\text{bk}} : \Omega_s \to \mathbb{C}^2$ satisfies (in a distributional sense) the following linear two-dimensional (plane strain) elastodynamics model with Rayleigh damping:

$$\begin{cases} -\rho L_{\text{joint}}^2\, \omega_f^2\, u^{\text{bk}} + i\omega_f\, \mathcal{C}^{\text{damp}}\left(u^{\text{bk}}\right) + \mathcal{L}\left(u^{\text{bk}}\right) = 0 & \text{in } \Omega_s, \\ u^{\text{bk}} = u^{\text{dir}} & \text{on } \Gamma^{\text{dir}}, \\ \sigma(u^{\text{bk}}) \cdot \mathbf{n} = 0 & \text{on } \partial\Omega_s \setminus \Gamma^{\text{dir}}, \end{cases} \tag{7.4.1a}$$

where $\Gamma^{\text{dir}}$ refers to the shaker attachment, $\sigma(u^{\text{bk}})$ is the stress tensor, and $\mathbf{n}$ is the outward normal. Here, the Dirichlet data is

$$u^{\text{dir}} = c^{\text{dir}} \begin{bmatrix} 0 \\ 1 \end{bmatrix}, \tag{7.4.1b}$$

the damping operator is

$$\mathcal{C}^{\text{damp}}(v) = \alpha\rho L_{\text{joint}}^2\, v + \beta\, \mathcal{L}(v), \tag{7.4.1c}$$

and finally the elasticity operator $\mathcal{L}(v) = \text{div}(\sigma(v))$ is

$$\mathcal{L}(v) = \text{div}\left(\frac{E}{1+\nu}\text{sym}\,(\nabla v) + \frac{E\nu}{(1+\nu)(1-2\nu)}\,\text{div}(v)\mathbb{I}\right), \tag{7.4.1d}$$

where $\mathbb{I}$ is the 2 by 2 identity matrix. Recalling the definition of the experimental outputs in (7.3.2), it is easy to verify that the constant $c^{\text{dir}}$ does not influence the outputs. For this reason, we arbitrarily set $c^{\text{dir}} = 1$.

We now introduce the anticipated configuration $\mu$ as

$$\mu = [\alpha, \beta, E, s_L, s_R] \in \mathcal{P}^{\text{bk}} \subset \mathbb{R}^5. \tag{7.4.2}$$

We observe that the solution $u^{\text{bk}}$ to (7.4.1) depends on the input frequency $f$ and on $\mu$, which we shall emphasize in the notation $u^{\text{bk}} = u^{\text{bk}}(f;\mu)$. We further observe that the

pair $(s_L, s_R)$ is directly related to the definition of damage in (7.6.1), while the triplet $(\alpha, \beta, E)$ collects material properties that are difficult to estimate exactly. We thus refer to $\alpha, \beta, E$ as "nuisance variables". It is important to identify an appropriate domain for these variables: too restricted a domain may confuse normal variations in the nuisance variables as distinctions between different states, too expansive a domain may artificially conflate classes and thus degrade classifier performance. We postpone the definition of the configuration set $\mathcal{P}^{\text{bk}}$ to the end of this section.

We observe that our mathematical model does not include some factors that may affect the experimental outputs. More in detail, we do not take into account potential inaccuracies in the manufacturing process, which lead to extremely high-dimensional geometric uncertainties, or to inhomogeneities in the material properties. Furthermore, we do not prescribe a stochastic model for experimental noise. In anticipation of the development of a rigorous mathematical formulation of the inference problem, we introduce an additional set of parameters $\xi \in \mathcal{V} \subset \mathbb{R}^D$, here referred to as *hidden*, such that the pair $(\mu, \xi)$ completely identifies a system configuration:

$$\mathcal{C} := (\mu, \xi) \in \mathcal{P}^{\text{exp}} := \mathcal{P}^{\text{bk}} \times \mathcal{V}. \tag{7.4.3}$$

Our bk model corresponds to $\xi = 0$.

Given the anticipated configuration $\mu \in \mathcal{P}^{\text{bk}}$, we define the bk representation of the experimental outputs $A_{i,j}^{\text{exp}}$ and $\phi_{i,j}^{\text{exp}}$ as follows:

$$A_{i,j}^{\text{bk}}(f;\mu) := \frac{A_{\text{nom}}}{|u_2^{\text{bk}}(x_{2,1};f;\mu)|}\,|u_2^{\text{bk}}(x_{i,j};f;\mu)|, \qquad A_{\text{nom}} = 0.25, \tag{7.4.4}$$

and

$$\phi_{i,j}^{\text{bk}}(f;\mu) := \arg\left(u_2^{\text{bk}}(x_{i,j};f;\mu)\right) - \arg\left(u_2^{\text{bk}}(x_{2,1};f;\mu)\right), \tag{7.4.5}$$

where $x_{i,j}$ denotes the center of the mass $(i,j)$ and $\arg(c)$ denotes the phase of the complex number $c$. As stated before, the bk outputs considered do not depend on the value of $c^{\text{dir}}$ in (7.4.1b). Provided that the linear model (7.4.1) captures accurately the physical

phenomenon and the influence of the hidden parameter $\xi$ is limited, we expect that

$$A_{i,j}^{\text{exp}}(f;\mu,\xi) \simeq A_{i,j}^{\text{bk}}(f;\mu), \quad \phi_{i,j}^{\text{exp}}(f;\mu,\xi) \simeq \phi_{i,j}^{\text{bk}}(f;\mu),$$

for all $f \in \mathcal{I}_f$, $\mu \in \mathcal{P}^{\text{bk}}$ and $i,j = 1,\ldots,4$.

### 7.4.1 Finite Element model

We resort to a FE discretization to estimate the bk outputs. In all our numerical simulations, we appeal to a P4 FE discretization with $n_{\text{e}} = 528$ elements, and 14670 degrees of freedom. We observe that experimental outputs involve pointwise evaluations of the displacement field. We do not implement any adaptive strategy to control pointwise error in the finite element solution; we refer to the literature (see, e.g., [178]) for actionable methods to estimate and control pointwise errors in FE approximations of elliptic problems

The use of high-order elements prevents the onset of shear-locking effects. It is indeed well-known that P1 (and even P2) elements might fail to appropriately represent the correct solution due to the poor approximation properties of linear (or quadratic) basis functions. We refer to the Finite Element literature for a thorough discussion about this issue (see [113] and [10, 9, 133]). Figure 7-4 empirically demonstrates this issue. We consider two FE triangulations with $n_{\text{e}} = 528$ and $n_{\text{e}} = 1296$ triangular elements, and we consider different FE discretizations of order one to five. Figures 7-4(a) and (c) show the behavior of $A_{1,1}^{\text{bk}}(\cdot,\mu)$ as a function of the frequency $f$ for $\mu = [5\cdot 10^{-4}, 10^{-4}, 2.8\cdot 10^{9}, 1, 1]$; similarly, Figures 7-4(b) and (d) show the behavior of $\phi_{1,1}^{\text{bk}}(\cdot,\mu)$ as a function of the frequency $f$ for the same value of $\mu$. We observe that the P1 discretization fails to capture the resonance, while the P2 discretization significantly overestimates the resonance frequency, especially for the coarser grid. On the other hand, for the P4 discretization, the FE error is negligible. For this reason, we base our results on the latter discretization.

### 7.4.2 Choice of the anticipated configuration set $\mathcal{P}^{\text{bk}}$

Recalling the interpretation of the parameters, we set upper bounds for $s_L, s_R$ based on the maximum added mass to be detected, while we choose a confidence region for $\alpha, \beta, E$ based on textbook values and on a single preliminary experiment for the undamaged case (i.e., $s_L = s_R = 1$). To take into account experimental noise, we perform three independent

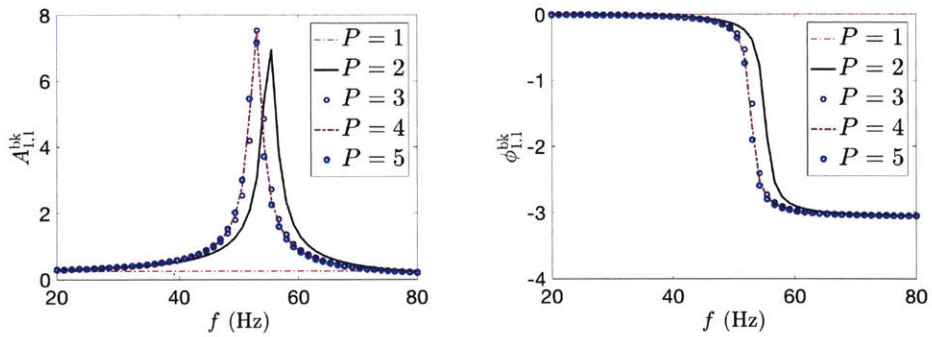


**(a)** $n_{\mathrm{e}} = 528$




**(b)** $n_{\mathrm{e}} = 528$

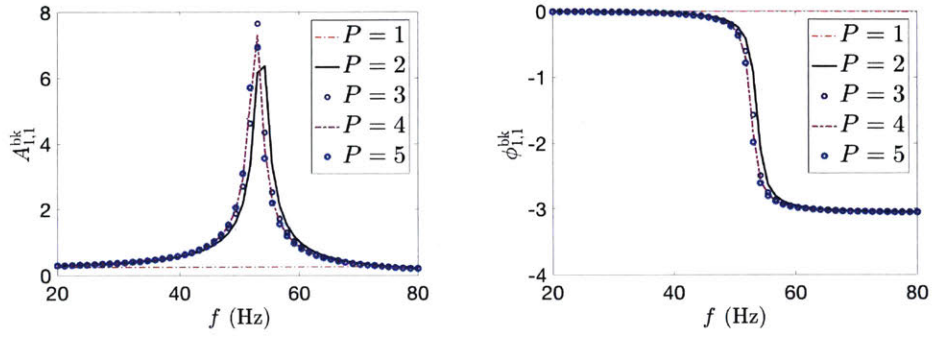


**(c)** $n_{\mathrm{e}} = 1296$




**(d)** $n_{\mathrm{e}} = 1296$

**Figure 7-4:** Microtruss experiment: comparison of different FE discretizations for output evaluations ($\mu = [5 \cdot 10^{-4}, 10^{-4}, 2.8 \cdot 10^{9}, 1, 1]$).

trials of the experiment. In more detail, we choose $\mathcal{P}^{\mathrm{bk}}$ such that for all frequencies and all realizations we obtain

$$\min_{\mu \in \Xi_{100}} A^{\mathrm{bk}}_{i,j}(f^q; \mu) < A^{\mathrm{exp}}_{i,j}(f^q; \mu^{\mathrm{exp}}, \xi^{\mathrm{exp}}) < \max_{\mu \in \Xi_{100}} A^{\mathrm{bk}}_{i,j}(f^q; \mu), \tag{7.4.6a}$$

and

$$\min_{\mu \in \Xi_{100}} \phi^{\mathrm{bk}}_{i,j}(f^q; \mu) < \phi^{\mathrm{exp}}_{i,j}(f^q; \mu^{\mathrm{exp}}, \xi^{\mathrm{exp}}) < \max_{\mu \in \Xi_{100}} \phi^{\mathrm{bk}}_{i,j}(f^q; \mu), \tag{7.4.6b}$$

where $\Xi_{100} = \{(\alpha^m, \beta^m, E^m, 1, 1)\}_{m=1}^{M} \subset \mathcal{P}^{\mathrm{bk}}$ is based on uniform random samples. Following this criterion, we choose

$$\mathcal{P}^{\mathrm{bk}} := [0.25 \cdot 10^{-3}, 0.8 \cdot 10^{-3}] \times [0.05 \cdot 10^{-3}, 0.2 \cdot 10^{-3}] \times [2.65 \cdot 10^{9}, 2.85 \cdot 10^{9}] \times [1, 2]^2. \tag{7.4.7}$$

Figure 7-5 shows a comparison between experimental and synthetic displacement amplitudes of block $(1, 1)$ for this single system configuration with no added masses. In Figure 7-

5(a), we report $\min_{\mu\in\Xi_{100}} A^{\text{bk}}_{1,1}(f^q;\mu)$, $\max_{\mu\in\Xi_{100}} A^{\text{bk}}_{1,1}(f^q;\mu)$, and the amplitude measured experimentally for each of the three trials. Similarly, in Figure 7-5(b), we report $\min_{\mu\in\Xi_{100}} \phi^{\text{bk}}_{1,1}(f^q;\mu)$, $\max_{\mu\in\Xi_{100}} \phi^{\text{bk}}_{1,1}(f^q;\mu)$ and the phase measured experimentally for each trial. We observe that our choice (7.4.7) satisfies the constraints (7.4.6).

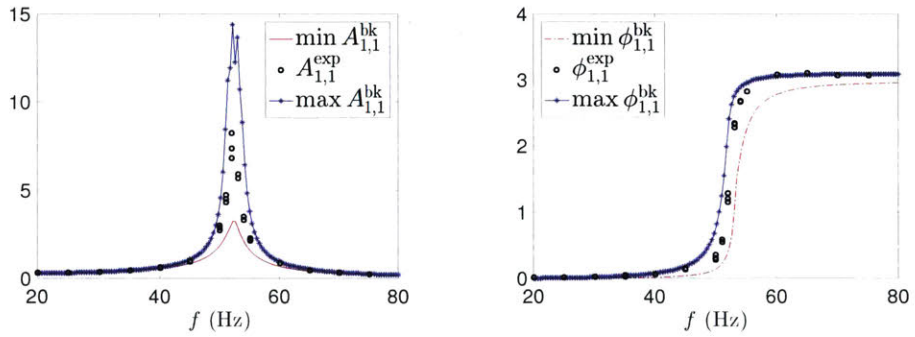


**(a)** **(b)**

**Figure 7-5:** Microtruss experiment; choice of the parameter space. Comparison between experimental results and synthetic results in absence of added masses.

## 7.5 The problem of feature extraction

### 7.5.1 Problem definition

We formalize the problem of feature extraction for the microtruss system: given the experimental outputs $\{A^{\text{exp}}_{i,j}(f^q;\mu,\xi)\}_{i,j,q}$ and $\{\phi^{\text{exp}}_{i,j}(f^q;\mu,\xi)\}_{i,j,q}$, determine the set of $Q$ features $\mathbf{z}^{\text{exp}}$ such that

$$\mathbf{z}^{\text{exp}}(\mu,\xi) = \mathcal{F}\left(\{A^{\text{exp}}_{i,j}(f^q;\mu,\xi)\}_{i,j,q}, \{\phi^{\text{exp}}_{i,j}(f^q;\mu,\xi)\}_{i,j,q}\right), \tag{7.5.1}$$

where $\mathcal{F} : \mathbb{R}^{32Q_f} \to \mathbb{R}^Q$. We observe that, by construction, experimental features depend on the system configuration $\mathcal{C} = (\mu,\xi)$. Appropriate features should be sensitive to the expected damage, and insensitive to noise. In the next section, we propose a particular choice of $\mathcal{F}$ motivated by a physical reasoning for our system and damage classes. We defer automated identification of features from experimental outputs to a subsequent work.

Exploiting the bk representations of the experimental outputs provided in section 7.4, we can define the bk features as

$$\mathbf{z}^{\text{bk}}(\mu) = \mathcal{F}\left(\{A^{\text{bk}}_{i,j}(f^q;\mu)\}_{i,j,q}, \{\phi^{\text{bk}}_{i,j}(f^q;\mu)\}_{i,j,q}\right). \tag{7.5.2}$$

We observe that, without loss of generality, we can rewrite the experimental features as

$$\mathbf{z}^{\text{exp}}(\mu,\xi) = \mathbf{z}^{\text{bk}}(\mu) + \delta\mathbf{z}(\mu,\xi), \qquad \forall\,(\mu,\xi) \in \mathcal{P}^{\text{exp}}; \tag{7.5.3}$$

we can then interpret $\mathbf{z}^{\text{bk}}(\mu)$ as *nominal features* associated with the configuration $\mathcal{C} = (\mu,\xi)$, and $\delta\mathbf{z}(\mu,\xi)$ as a perturbation. The norm $\|\delta\mathbf{z}(\mu,\xi)\|_2$ reflects the magnitude of the model error for a given configuration. We anticipate that (7.5.3) will help us draw a connection between our formulation and Robust Optimization (RO) statements for classification.

### 7.5.2 Choice of the features for the microtruss problem

Given the frequencies $\{f^q\}_{q=1}^{Q_f}$, we introduce the set of features

$$\mathbf{z}_1^{\text{bk}}(\mu) = \left[z_1^{\text{bk}}(f^1;\mu),\ldots,z_1^{\text{bk}}(f^{Q_f};\mu)\right], \quad z_1^{\text{bk}}(f;\mu) = \frac{A_{1,4}^{\text{bk}}(f;\mu)}{A_{4,4}^{\text{bk}}(f;\mu)}. \tag{7.5.4}$$

Feature $z_1^{\text{bk}}(\cdot;\mu)$ measures the asymmetry of the structure between left and right corners. From symmetry arguments it is easy to verify that

$$z_1^{\text{bk}}(f;\alpha,\beta,E,s_L,s_R) = \frac{1}{z_1^{\text{bk}}(f;\alpha,\beta,E,s_R,s_L)},$$

which implies that by exploiting this feature we should be able to discriminate between the three classes $\kappa = \{1,4\}$, $\kappa = \{2\}$, $\kappa = \{3\}$. We here use the term "class" to refer to any subset of the states of damage, $\kappa \subset \{1,\ldots,4\}$.

We then introduce the set of features

$$\mathbf{z}_2^{\text{bk}}(\mu) = \left[z_2^{\text{bk}}(f^1;\mu),\ldots,z_2^{\text{bk}}(f^{Q_f};\mu)\right], \; z_2^{\text{bk}}(f;\mu) = \frac{A_{2,4}^{\text{bk}}(f;\mu) + A_{3,4}^{\text{bk}}(f;\mu)}{A_{1,1}^{\text{bk}}(f;\mu) + A_{4,1}^{\text{bk}}(f;\mu)}. \tag{7.5.5}$$

It is easy to verify that the amplitudes $\{A_{i,j}^{\text{bk}}\}_{i,j}$ are monotically decreasing in $\alpha,\beta$ (i.e., increases in damping reduce the amplitude of the masses' displacements) and also in $s_L, s_R$ (i.e., increases in the total mass reduce the amplitude). However, while variations in $\alpha,\beta$ affect all masses, variations in $s_L, s_R$ should be mostly confined to the left and right masses (i.e., masses $(1,j)$ and $(4,j)$ for $j = 1,\ldots,4$). Therefore, the ratio $z_2^{\text{bk}}(\cdot;\mu)$ should reduce the effect of damping on our feature without affecting the effect of $s_L, s_R$, thereby improving discrimination between $\kappa = \{1\}$ and $\kappa = \{4\}$.

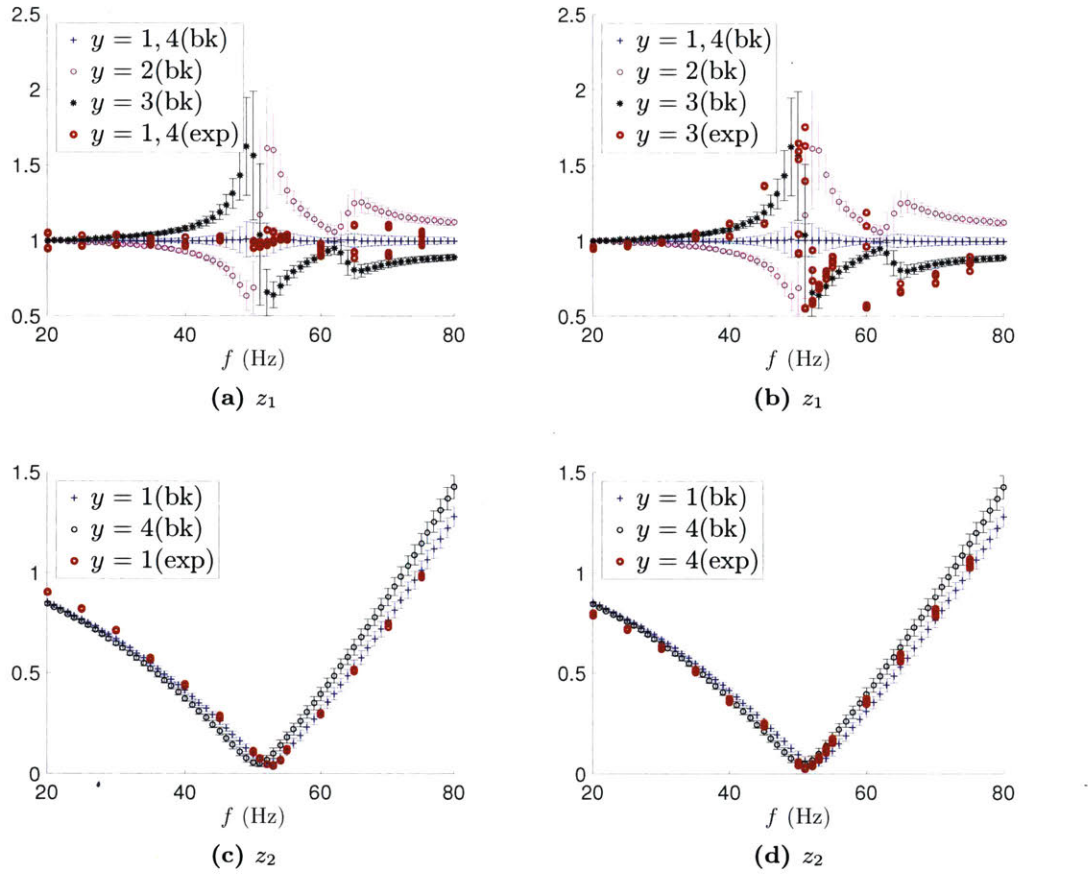


**Figure 7-6:** Microtruss experiment; discrimination capabilities of the features. Figures (a) and (b): behavior of $\{m_q^{1,\mathrm{bk}}(\kappa)\}_q$ and $\{std_q^{1,\mathrm{bk}}(\kappa)\}_q$ for the three classes $\kappa = \{1,4\}$, $\kappa = \{2\}$, $\kappa = \{3\}$, and comparison with the experimental data. Figures (c) and (d): behavior of $\{m_q^{2,\mathrm{bk}}(\kappa)\}_q$ and $\{std_q^{2,\mathrm{bk}}(\kappa)\}_q$ for the two classes $\kappa = \{1\}$ and $\kappa = \{4\}$, and comparison with the experimental data. For each experimental configuration, we report results of three independent realizations.

We now demonstrate the effectiveness of our choice of the features for the problem at hand. With this in mind, we introduce a finite-dimensional discretization $\mathcal{P}^{\mathrm{bk}}_{\mathrm{train}}$ of $\mathcal{P}^{\mathrm{bk}}$ of cardinality $|\mathcal{P}^{\mathrm{bk}}_{\mathrm{train}}| = n_{\mathrm{train}} = 10^4$. Given the frequencies $f^1, \ldots, f^{Q_f}$, $Q_f = 16$, we define the in-class mean and standard deviations:

$$m_q^{\ell,\mathrm{bk}}(\kappa) = \frac{1}{|\mathcal{P}^{\mathrm{bk}}_{\mathrm{train}}(\kappa)|} \sum_{\mu \in \mathcal{P}^{\mathrm{bk}}_{\mathrm{train}}(\kappa)} z_\ell^{\mathrm{bk}}(f^q;\mu), \tag{7.5.6a}$$

and

$$std_q^{\ell,\mathrm{bk}}(\kappa) = \frac{1}{|\mathcal{P}^{\mathrm{bk}}_{\mathrm{train}}(\kappa)| - 1} \sum_{\mu \in \mathcal{P}^{\mathrm{bk}}_{\mathrm{train}}(\kappa)} \left( z_\ell^{\mathrm{bk}}(f^q;\mu) - m_q^{\ell,\mathrm{bk}}(\kappa) \right)^2, \tag{7.5.6b}$$

where $\ell = 1, 2$, and $\mathcal{P}^{\text{bk}}_{\text{train}}(\kappa) = \{\mu \in \mathcal{P}^{\text{bk}}_{\text{train}} : f^{\text{dam}}(\mu) \in \kappa\}$, and $\kappa \subset \{1, 2, 3, 4\}$. We further consider experimentally the five different nominal system configurations corresponding to (i) $s_L = s_R = 1$, (ii) $s_L = 1$, $s_R = 2.06$, (iii) $s_L = 1$, $s_R = 1.53$, (iv) $s_L = s_R = 2.06$, and (v) $s_L = s_R = 1.53$. For each configuration, we perform three independent trials for a total of 15 experimental datapoints. Figures 7-6 show the behavior of $\{m_q^{\ell,\text{bk}}(\kappa)\}_q$ for $\ell = 1, 2$. For $\ell = 1$, we consider classes $\kappa = \{1, 4\}$, $\kappa = \{2\}$ and $\kappa = \{3\}$; for $\ell = 2$, we only consider $\kappa = \{1\}$ and $\kappa = \{4\}$. To take into account the variability of the features due to changes in $\mu$, we report error bars corresponding to twice the in-class standard deviation $std_q^{\ell,\text{bk}}(\kappa)$. We further report experimental observations from the appropriate class to show the agreement between bk and experimental features.

## 7.6 Inference stage

We summarise key quantities introduced in the previous sections. We first define the anticipated configuration set $\mathcal{P}^{\text{bk}} \subset \mathbb{R}^P$, and we denote by $\mu$ a generic element of the set. The parameter $\mu$ encodes our bk representation of a system configuration and the space $\mathcal{P}^{\text{bk}}$ contains the bk anticipation of each system configuration that can occur during the operations (online stage). We further introduce the hidden parameter $\xi \in \mathcal{V} \subset \mathbb{R}^D$ such that the pair $\mathcal{C} = (\mu, \xi) \in \mathcal{P}^{\text{exp}} := \mathcal{P}^{\text{bk}} \times \mathcal{V}$ uniquely identifies the observed experimental outputs during the online stage. Then, we introduce the damage function $f^{\text{dam}} : \mathcal{P}^{\text{bk}} \to \{1, \ldots, K\}$ such that

$$f^{\text{dam}}(\mu = [\alpha, \beta, E, s_L, s_R]) = \bar{f}^{\text{dam}}(s_L, s_R), \tag{7.6.1}$$

where $\bar{f}^{\text{dam}}$ is defined in (7.2.2). As already mentioned in section 7.4, the actual value of the model parameters $\alpha, \beta, E$ does not influence the state of damage. We further introduce the bk and experimental features $\mathbf{z}^{\text{bk}} : \mathcal{P}^{\text{bk}} \to \mathbb{R}^Q$ and $\mathbf{z}^{\text{exp}} : \mathcal{P}^{\text{exp}} \to \mathbb{R}^Q$, respectively.

In view of the classification statement, we introduce the (unknown) probability density function (pdf) over $\mathcal{V}$, $p_\xi : \mathcal{V} \to \mathbb{R}_+$, such that

$$P(\xi \in A) = \int_{\mathcal{V}} \mathbb{1}_A(\xi')\, p_\xi(\xi')\, d\xi', \quad A \subset \mathcal{V}, \tag{7.6.2}$$

where $\mathbb{1}_A$ is the indicator function associated to the set $A$. We use notation $\mathbb{E}_{\xi \sim p_\xi}[\cdot]$ to

indicate expected values with respect to the measure induced by $p_\xi$. We further denote by $\mathcal{L}^{(0,1)}$ the 0-1 loss:

$$\mathcal{L}^{(0,1)}(y,t) = \begin{cases} 0 & y = t, \\ 1 & y \neq t. \end{cases} \tag{7.6.3}$$

Finally, we define the weight $w^{\text{bk}}$, $w^{\text{bk}} : \mathcal{P}^{\text{bk}} \to \mathbb{R}_+$, such that

$$\int_{\mathcal{P}^{\text{bk}}} w^{\text{bk}}(\mu)\, d\mu = 1. \tag{7.6.4}$$

We postpone interpretation and actionable definition of the weight $w^{\text{bk}}$ until the end of this section.

We now introduce two classification problem statements.

**Monitoring problem:** given the damage function $f^{\text{dam}} : \mathcal{P}^{\text{bk}} \to \{1, \dots, K\}$, and the experimental features $\mathbf{z}^{\text{exp}} : \mathcal{P}^{\text{exp}} \to \mathbb{R}^Q$, find the classifier $g^{\text{opt}} : \mathbb{R}^Q \to \{1, \dots, K\}$ that minimizes the *experimental risk*:

$$\begin{aligned} \inf_{g \text{ measurable}} R^{\text{exp}}(g) &= \int_{\mathcal{P}^{\text{bk}}} \mathbb{E}_{\xi \sim p_\xi} \left[ \mathcal{L}^{(0,1)}(g(\mathbf{z}^{\text{exp}}(\mu,\xi)),\ f^{\text{dam}}(\mu)) \right] w^{\text{bk}}(\mu)\, d\mu \\ &= \int_{\mathcal{P}^{\text{exp}}} \mathcal{L}^{(0,1)}(g(\mathbf{z}^{\text{exp}}(\mu,\xi)),\ f^{\text{dam}}(\mu))\, w^{\text{bk}}(\mu)\, p_\xi(\xi)\, d\mu\, d\xi, \end{aligned} \tag{7.6.5}$$

where $p_\xi : \mathcal{V} \to \mathbb{R}_+$ is defined in (7.6.2), $\mathcal{L}^{(0,1)}$ in (7.6.3), and $w^{\text{bk}} : \mathcal{P}^{\text{bk}} \to \mathbb{R}_+$ in (7.6.4).

**Bk monitoring problem:** given the damage function $f^{\text{dam}} : \mathcal{P}^{\text{bk}} \to \{1, \dots, K\}$, and the bk features $\mathbf{z}^{\text{bk}} : \mathcal{P}^{\text{bk}} \to \mathbb{R}^Q$, find the classifier $g^{\text{opt,bk}} : \mathbb{R}^Q \to \{1, \dots, K\}$ that minimizes the *bk risk*:

$$\inf_{g \text{ measurable}} R^{\text{bk}}(g) = \int_{\mathcal{P}^{\text{bk}}} \mathcal{L}^{(0,1)}(g(\mathbf{z}^{\text{bk}}(\mu)),\ f^{\text{dam}}(\mu))\, w^{\text{bk}}(\mu)\, d\mu. \tag{7.6.6}$$

where $\mathcal{L}^{(0,1)}$ is defined in (7.6.3), and $w^{\text{bk}} : \mathcal{P}^{\text{bk}} \to \mathbb{R}_+$ (7.6.4).

We interpret the bk monitoring problem as a surrogate for the (actual, physical) monitoring problem. We observe that while the monitoring statement relies on experimental observations and depends on unknown quantities (the hidden parameter $\xi$ and the corresponding pdf $p_\xi$), the bk statement is entirely synthetic (except of course implicitly through the definition of $\mathcal{P}^{\text{bk}}$ as described in the previous section) and thus can be tackled even in

the absence of experimental observations. At this stage of the discussion, we have not yet discussed how the solution to (7.6.6) is related to the optimal solution to (7.6.5). This clearly depends on the magnitude of the perturbations $\delta\mathbf{z}$ in (7.5.3). In Chapter 8, we illustrate the connection between these two problems, and we also discuss the well-posedness of the mathematical statements.

We now interpret the function $w^{\text{bk}}$ in (7.6.5) and (7.6.6). In our framework, the weight $w^{\text{bk}}$ reflects the importance (assigned by the user) of classifying correctly a given configuration and is not related to the (unknown) likelihood that the bk configuration $\mu$ is observed during the online stage. This observation implies that the bk risk $R^{\text{bk}}(g)$ should be interpreted as a user-defined measure of the misclassification error rather than an expected loss.

We introduce our choice of the weight $w^{\text{bk}}$ for the microtruss problem. We consider the weight

$$w^{\text{bk}}(\mu) = w_1^{\text{bk}}(\alpha)\, w_2^{\text{bk}}(\beta)\, w_3^{\text{bk}}(E)\, w_{4,5}^{\text{bk}}(s_L, s_R), \tag{7.6.7a}$$

where $w_1^{\text{bk}}, w_2^{\text{bk}}, w_3^{\text{bk}}$ correspond to constant weights and

$$w_{4,5}^{\text{bk}}(s_L, s_R) = \begin{cases} 100 & (s_L, s_R) \in S_1 := [1, 1.05]^2; \\ 10 & (s_L, s_R) \in S_2 := [1.5, 2] \times [1, 1.05]; \\ 10 & (s_L, s_R) \in S_3 := [1, 1.05] \times [1.5, 2]; \\ 1 & (s_L, s_R) \in S_4 := [1.5, 2]^2. \end{cases} \tag{7.6.7b}$$

We choose constants such that $\int_{\mathcal{P}^{\text{bk}}} w^{\text{bk}}(\mu)\, d\mu = 1$. We observe that each of $S_1, \ldots, S_4$ are assigned equal weight.

Some comments are in order. Our choice of $w_{4,5}^{\text{bk}}$ in (7.6.7b) implies that we target our SHM classifier to detect added masses in the range $[1.5, 2]h$, and to avoid "false damaged" predictions if $s_L, s_R < 1.05$. In view of the probabilistic interpretation of the problem statement and of the numerical procedure, we observe that our choices of $w_1^{\text{bk}}, w_2^{\text{bk}}, w_3^{\text{bk}}$ correspond to the assumption that $\alpha, \beta, E$ are independent uniformly-distributed random

variables such that

$$\begin{aligned}
&\alpha \sim \text{Uniform}([0.25 \cdot 10^{-3}, 0.8 \cdot 10^{-3}]),\\
&\beta \sim \text{Uniform}([0.05 \cdot 10^{-3}, 0.2 \cdot 10^{-3}]),\\
&E \sim \text{Uniform}([2.65 \cdot 10^{9}, 2.85 \cdot 10^{9}]).
\end{aligned} \tag{7.6.8a}$$

On the other hand, our choice of $w^{\text{bk}}_{4,5}$ corresponds to assume that the random pair $(s_L, s_R)$ can be written as a mixture of independent uniform distributions over $S_1, \ldots, S_4$:

$$(s_L, s_R) = \sum_{k=1}^{4} \left(1 - \mathcal{L}^{(0,1)}(S, k)\right) E_k, \quad E_k \sim \text{Uniform}(S_k), \quad S \sim \text{Uniform}(\{1, 2, 3, 4\}). \tag{7.6.8b}$$

We shall later formally identify $w^{\text{bk}}$ with a probability density. Table 7.1 summarizes the definitions and provides links to their instantiations for the microtruss problem.

**Table 7.1:** Simulation-Based Classification: main definitions

| symbol | name | microtruss definition |
|---|---|---|
| $\mu \in \mathcal{P}^{\text{bk}}$ | anticipated configuration (set) | (7.4.2) – (7.4.7) |
| $(\mu, \xi) \in \mathcal{P}^{\text{exp}}$ | configuration (set) | (7.4.3) |
| $f^{\text{dam}} : \mathcal{P}^{\text{bk}} \to \{1, \ldots, K\}$ | damage function | (7.6.1) |
| $\mathbf{z}^{\text{exp}} : \mathcal{P}^{\text{exp}} \to \mathbb{R}^Q$ | experimental features | (7.5.1) |
| $\mathbf{z}^{\text{bk}} : \mathcal{P}^{\text{bk}} \to \mathbb{R}^Q$ | bk features | (7.5.2) |
| $w^{\text{bk}} : \mathcal{P}^{\text{bk}} \to \mathbb{R}_+$ | bk weight | (7.6.7) |

Before concluding, we state another definition, and an important remark.

**Definition 7.6.1.** *Let us define the partition of the configuration set* $\{\mathcal{P}^{\text{bk}}(k)\}_{k=1}^{K}$ *as*

$$\mathcal{P}^{\text{bk}}(k) := \{\mu \in \mathcal{P}^{\text{bk}} : \ f^{\text{dam}}(\mu) = k\}, \quad k = 1, \ldots, K.$$

*Then, we define the type-k error of a classifier* $g$ *as*

$$R^{\text{exp}}(g; k) := \int_{\mathcal{P}^{\text{bk}}(k) \times \mathcal{V}} \mathbb{E}_{\xi \sim p_\xi} \left[\mathcal{L}^{(0,1)}(g(\mathbf{z}^{\text{exp}}(\mu, \xi)), \ k)\right] w^{\text{bk}}(\mu)\, d\mu; \tag{7.6.9}$$

*similarly, we can define the bk-type-k error as*

$$R^{\mathrm{bk}}(g;k) := \int_{\mathcal{P}^{\mathrm{bk}}(k)} \mathcal{L}^{(0,1)}(g(\mathbf{z}^{\mathrm{bk}}(\mu)),\ k)\, w^{\mathrm{bk}}(\mu)\, d\mu. \tag{7.6.10}$$

*If $K = 2$, provided that $y = 1$ is the null hypothesis, our definition of type-k error coincides with the standard type I and type II errors in Hypothesis Testing.*

It is straightforward to verify that

$$R^{\mathrm{bk}}(g) = \sum_{k=1}^{K} R^{\mathrm{bk}}(g;k), \qquad R^{\mathrm{exp}}(g) = \sum_{k=1}^{K} R^{\mathrm{exp}}(g;k).$$

We observe that if we define the bk confusion matrix $\mathbb{C}^{\mathrm{bk}}(g) \in \mathbb{R}^{K,K}$ associated with the classifier $g$ such that

$$\mathbb{C}^{\mathrm{bk}}_{k,k'}(g) = \int_{\mathcal{P}^{\mathrm{bk}}(k)} \mathcal{L}^{(0,1)}(g(\mathbf{z}^{\mathrm{bk}}(\mu)),\ k')\, w^{\mathrm{bk}}(\mu)\, d\mu,$$

then, the bk type-$k$ error is the sum of the off-diagonal terms of $\mathbb{C}^{\mathrm{bk}}(g)$:

$$R^{\mathrm{bk}}(g,k) = \sum_{k' \neq k} \mathbb{C}^{\mathrm{bk}}_{k,k'}(g).$$

An analogous discussion applies to the type-$k$ error. We further observe that the choice of $w^{\mathrm{bk}}$ regulates the importance of the different types of error. More specifically, for each $k$, we can interpret the quantity

$$P^{\mathrm{bk}}_k := \int_{\mathcal{P}^{\mathrm{bk}}(k)} w^{\mathrm{bk}}(\mu)\, d\mu \tag{7.6.11}$$

as a measure of the importance of classifying correctly configurations of class $k$. For the microtruss problem, we have

$$P^{\mathrm{bk}}_1 = \ldots = P^{\mathrm{bk}}_4 = \frac{1}{4}.$$

This implies that it is equally important to classify correctly configurations of all four classes.

**Remark 7.6.1.** ***(The perspective of Robust Optimization)*** *Adopting the interpretation of bk and experimental features provided after equation* (7.5.3)*, we can view* (7.6.6) *as the* nominal problem*, and* (7.6.5) *as the* perturbed problem*. This discussion shows the connec-*

*tion between our formulation and Robust Optimization (RO) statements for classification. To stress this, we observe that we can restate the experimental risk in* (7.6.5) *as follows:*

$$R^{\text{exp}}(g) = \int_{\mathcal{P}^{\text{bk}}} \mathbb{E}_{\delta\mathbf{z}\sim P_{\delta\mathbf{z},\mu}} \left[ \mathcal{L}^{(0,1)} \left( g(\mathbf{z}^{\text{bk}}(\mu) + \delta\mathbf{z}),\, f^{\text{dam}}(\mu) \right) \right] w^{\text{bk}}(\mu)\, d\mu, \tag{7.6.12}$$

*where the probability distribution* $P_{\delta\mathbf{z},\mu}$ *is given by*

$$P_{\delta\mathbf{z},\mu}(A) = \int_{\mathcal{V}} \mathbb{1}_A(\delta\mathbf{z}(\mu,\xi))\, p_\xi(\xi)\, d\xi, \tag{7.6.13}$$

*and is defined over (a suitable* $\sigma$*-algebra of)* $\mathbb{R}^Q$*. We rigorously show* (7.6.12) *in Chapter 8.2.*

## 7.7 Conclusions

In this chapter, we introduced a mathematical framework for the problem of damage identification. This provides the foundations for the development of our computational procedure. For purposes of clarity, we introduced our formulation through the vehicle of a particular example, a microtruss; in parallel we provided the abstraction applicable to a broad range of problems.

The microtruss problem corresponds to a four-way classification problem. We defined the presence of added masses as the damage to be detected, and we identified two potential locations where damage may occur. We thus argue that this problem, despite its simplicity, exemplifies a typical SHM Level 2 task (i.e. detection and localisation); for this reason, in the next chapters we consider this problem to validate our numerical approach.

The discussion for the microtruss problem also showed that the quantity of interest only depends on a subset of the full parameter vector $\mu$, namely the parameters $s_L, s_R$. The presence of "nuisance variables" in the model complicates the classification task, and motivates the development of feature-extraction techniques to limit their effect. In Chapter 9, we demonstrate that the choice of the features in section 7.5.2 is well-suited to limit the effect of nuisance variables.

# Chapter 8

# Simulation-Based Classification: methodology and analysis

In this chapter, we introduce Simulation-Based Classification (SBC). The approach is designed to tackle inverse problems for discrete-valued quantities of interest associated with systems governed by (parametrized) PDEs. We first present the computational procedure, and we clarify the role of model reduction (section 8.1); then we study the existence and uniqueness of the solution to the bk monitoring problem (7.6.6), and we comment on the consistency of our numerical procedure (section 8.2). Finally, we propose an error bound that clarifies the influence of model error on classification performance (section 8.3).

## 8.1 Computational approach

### 8.1.1 Simulation-based classification

In view of the development of the computational approach, we define the probability measure on $\mathcal{P}^{\text{bk}}$ $P_{w^{\text{bk}}}$ such that

$$P_{w^{\text{bk}}}(A) = \int_{\mathcal{P}^{\text{bk}}} \mathbb{1}_A(\mu')\, w^{\text{bk}}(\mu')\, d\mu', \quad A \subset \mathcal{P}^{\text{bk}}. \tag{8.1.1}$$

Then, we denote by $\mu$ a random vector distributed according to $P_{w^{\text{bk}}}$, $\mu \sim P_{w^{\text{bk}}}$.

We formalize our strategy to generate the classifier $g$. We generate $M$ independent samples $\mu^1, \ldots, \mu^M$ from $P_{w^{\text{bk}}}$, and we generate the dataset $\mathcal{D}_M^{\text{bk}} := \{(\mathbf{z}^{\text{bk,m}}, y^m)\}_{m=1}^M$ where $\mathbf{z}^{\text{bk,m}} = \mathbf{z}^{\text{bk}}(\mu^m)$, $y^m = f^{\text{dam}}(\mu^m)$. Then, we employ a supervised learning algorithm that

takes as input the dataset $\mathcal{D}_M^{\text{bk}}$ and returns the classifier $g_M^\star$.

Several techniques are available to generate independent samples from an arbitrary probability density function $w^{\text{bk}}$. We refer to [189, Chapter 2] and to [81, Chapter 3] for further details. Here, we resort to identities (7.6.8) to generate samples of the configuration $\mu$.

A supervised learning (SL) algorithm for classification can be interpreted as a procedure that takes as input a dataset $\mathcal{D}_M^{\text{bk}} \subset \mathbb{R}^Q \times \{1, \dots, K\}$ and returns a classifier $g_M^\star : \mathbb{R}^Q \to \{1, \dots, K\}$:

$$[g_M^\star] = \texttt{SL-algorithm}\left(\mathcal{D}_M^{\text{bk}}\right). \tag{8.1.2}$$

Several different algorithms of the form (8.1.2) have been proposed in the literature; we refer to [104, 120, 157] for a thorough introduction to supervised learning algorithms for regression and classification. In our numerical examples, we apply five different state-of-the-art techniques to the classification problem considered in this work.

Algorithm 8.1.1 summarizes the computational procedure to approximate the solution to the bk monitoring problem: both the Offline stage described above, and the Online stage in which, given experimental features, we wish to classify our system.

**Algorithm 8.1.1** Simulation-Based Classification for SHM.

**Offline stage**

1: Generate $\mathcal{P}_M^{\text{bk}} := \{\mu^1, \dots, \mu^M\} \subset \mathcal{P}^{\text{bk}}$, $\mu^m \overset{iid}{\sim} P_{w^{\text{bk}}}$

2: Generate the dataset $\mathcal{D}_M^{\text{bk}} := \{(\mathbf{z}^{\text{bk,m}}, y^m)\}_{m=1}^M$ where $\mathbf{z}^{\text{bk,m}} = \mathbf{z}^{\text{bk}}(\mu^m)$, $y^m = f^{\text{dam}}(\mu^m)$.

3: Employ the learning algorithm (8.1.2) to generate the classifier $g_M^\star$.

**Online stage**

1: Collect the experimental measurements and extract the features $\mathbf{z}^{\text{exp}}$.

2: Return the label $g_M^\star(\mathbf{z}^{\text{exp}})$.

We observe that, unlike in model-based approaches, our procedure directly addresses the task of interest — the estimation of the state of damage — and does not — either implicitly or explicitly — provide estimates for the actual value of $\mu$. We claim that the estimation problem for $\mu$ is (unnecessarily) much more general than the original classification problem of interest, and in particular the former will typically be ill-posed. For instance, the

application of model-based approaches to the microtruss problem requires the estimate of the full vector $\mu$, which includes both quantities related to damage (the geometric parameters $s_L, s_R$) but also nuisance variables (the material properties $\alpha, \beta, E$) of no direct interest to the engineering task at hand. For more realistic problems with many more parameters the nuisance variables can easily number in the hundreds and often without any evident correlations.

Another distinguishing feature of Simulation-Based Classification is related to the possibility of incorporating information related to model error without the need for fully characterizing the configuration $\mathcal{C} = (\mu, \xi)$. We can indeed include estimates of the perturbation $\delta\mathbf{z}$ to inform the learning procedure. The process of including data uncertainties at training stage is usually referred to as *robustification*. We shall consider this in future work.

### 8.1.2 Application of pMOR

As already mentioned in Chapter 1.4.2, classification performances strongly depend on the size $M$ of the dataset. Since each datapoint involves the solution to several PDEs (in our case $Q_f$, one for each frequency), the offline computational burden is extremely large. This explains the importance of model order reduction.

We briefly discuss the application of pMOR in the context of Simulation-Based Classification. During a preprocessing stage (typically denoted the offline stage), we generate a Reduced Order Model (ROM) $\tilde{u}^{\text{bk}}(f;\mu) \approx u^{\text{bk}}(f;\mu)$ such that we may form $\tilde{\mathbf{z}}^{\text{bk}}(\mu) \approx \mathbf{z}^{\text{bk}}(\mu)$ for all $\mu \in \mathcal{P}^{\text{bk}}$. Then, for each parameter $\mu^1, \ldots, \mu^M$, we estimate $\mathbf{z}^{\text{bk}}(\mu^m)$ using the ROM $\tilde{\mathbf{z}}^{\text{bk}}(\mu^m)$. We observe that if $M$ is sufficiently large and computing $\tilde{\mathbf{z}}^{\text{bk}}(\mu^m)$ is significantly less expensive than computing $\mathbf{z}^{\text{bk}}(\mu^m)$, then we can amortize and indeed neglect the cost of the preprocessing stage.

Algorithm 8.1.2 summarizes the computational procedure. Note that both the offline stage and the online stage of the pMOR procedure are effected in the offline stage of the classification algorithm. In Chapter 9, we discuss the application of the particular pMOR technique, the Reduced Basis method, adopted in this work to tackle the microtruss problem.

**Algorithm 8.1.2** Simulation-Based Classification for SHM with pMOR.

**Offline stage**

1: Generate $\mathcal{P}_M^{\text{bk}} := \{\mu^1, \ldots, \mu^M\} \subset \mathcal{P}^{\text{bk}}$, $\mu^m \overset{iid}{\sim} P_{w^{\text{bk}}}$

2: a. MOR: construct the Reduced Order Model;

b. MOR: use the ROM to generate the dataset $\mathcal{D}_M^{\text{bk}} := \{(\tilde{\mathbf{z}}^{\text{bk}}(\mu^m), f^{\text{dam}}(\mu^m))\}_{m=1}^M$

3: Employ the learning algorithm (8.1.2) to generate the classifier $g_M^\star$.

**Online stage**

1: Collect the experimental measurements and extract the features $\mathbf{z}^{\text{exp}}$.

2: Return the label $g_M^\star(\mathbf{z}^{\text{exp}})$.

## 8.2 Mathematical analysis

### 8.2.1 Probabilistic interpretation of the monitoring problems

We shall now introduce a probabilistic interpretation of the monitoring problems. This will help us develop and analyze our computational approach. With this in mind, we first recall the definition of $P_{w^{\text{bk}}}$ in (8.1.1),

$$P_{w^{\text{bk}}}(A) = \int_{\mathcal{P}^{\text{bk}}} \mathbb{1}_A(\mu')\, w^{\text{bk}}(\mu')\, d\mu', \quad A \subset \mathcal{P}^{\text{bk}},$$

and we define the probability measure on $\mathcal{P}^{\text{exp}}$, $P_{(\mu,\xi)}^{\text{exp}}$, such that

$$P_{(\mu,\xi)}^{\text{exp}}(A \times B) = \int_{\mathcal{P}^{\text{bk}} \times \mathcal{V}} \mathbb{1}_A(\mu)\, \mathbb{1}_B(\xi)\, w^{\text{bk}}(\mu')\, p_\xi(\xi')\, d\mu' d\xi', \quad A \subset \mathcal{P}^{\text{bk}},\ B \subset \mathcal{V}. \tag{8.2.1}$$

Recalling (7.6.4) and (7.6.2), it is easy to verify that $P_{w^{\text{bk}}}$ is a probability measure over $\mathcal{P}^{\text{bk}}$, and $P_{(\mu,\xi)}^{\text{exp}}$ is a probability measure over $\mathcal{P}^{\text{exp}}$. As in section 8.1, we denote here by $\mu$ a random vector distributed according to $P_{w^{\text{bk}}}$, $\mu \sim P_{w^{\text{bk}}}$; similarly, we denote by $(\mu, \xi)$ a random pair distributed according to $P_{(\mu,\xi)}^{\text{exp}}$.

Recalling the definitions of the bk features $\mathbf{z}^{\text{bk}} : \mathcal{P}^{\text{bk}} \to \mathbb{R}^Q$ and of the damage function $f^{\text{dam}} : \mathcal{P}^{\text{bk}} \to \{1, \ldots, K\}$, we define the random pair

$$(Z^{\text{bk}}, Y) := (\mathbf{z}^{\text{bk}}(\mu), f^{\text{dam}}(\mu)), \qquad \mu \sim P_{w^{\text{bk}}}.$$

We further denote by $P_{(Z^{\text{bk}},Y)}$ the corresponding image probability distribution defined over $\mathbb{R}^Q \times \{1,\ldots,K\}$:

$$P_{(Z^{\text{bk}},Y)}(A \times \{k\}) = \int_{(\mathbf{z}^{\text{bk}},f^{\text{dam}})^{-1}(A\times\{k\})} w^{\text{bk}}(\mu)\, d\mu,$$

where $(\mathbf{z}^{\text{bk}}, f^{\text{dam}})^{-1}(A \times \{k\}) := \{\mu \in \mathcal{P}^{\text{bk}} : (\mathbf{z}^{\text{bk}}(\mu), f^{\text{dam}}(\mu)) \in A \times \{k\}\}$ is the pre-image of $A\times\{k\}$. We observe that $P_{(Z^{\text{bk}},Y)}$ is uniquely identified by the weight $w^{\text{bk}}$, the bk features $\mathbf{z}^{\text{bk}}$ and by the damage function $f^{\text{dam}}$. Similarly, we can define the random pair

$$(Z^{\text{exp}}, Y) := (\mathbf{z}^{\text{exp}}(\mu,\xi), f^{\text{dam}}(\mu)), \qquad (\mu,\xi) \sim P^{\text{exp}}_{(\mu,\xi)},$$

and the corresponding image probability distribution $P_{(Z^{\text{exp}},Y)}$.

Recalling the change of variable formula, we can restate the two problem statements proposed in Chapter 7.6. In more detail, the monitoring problem (7.6.5) can be restated as follows

$$g^{\text{opt}} = \arg \inf_{g \text{ measurable}} R^{\text{exp}}(g) = \mathbb{E}_{(Z^{\text{exp}},Y)\sim P_{(Z^{\text{exp}},Y)}} \left[\mathcal{L}^{(0,1)}\left(g(Z^{\text{exp}}), Y\right)\right], \tag{8.2.2}$$

while the bk monitoring problem can be restated as follows:

$$g^{\text{opt,bk}} = \arg \inf_{g \text{ measurable}} R^{\text{bk}}(g) = \mathbb{E}_{(Z^{\text{bk}},Y)\sim P_{(Z^{\text{bk}},Y)}} \left[\mathcal{L}^{(0,1)}\Big(g(Z^{\text{bk}}), Y\Big)\right]. \tag{8.2.3}$$

Problem statements (8.2.2) and (8.2.3) are well-suited for the analysis. We can indeed rigorously address the following questions.

**Existence and uniqueness of the solutions to** (8.2.2) **and** (8.2.3): we can determine sufficient conditions under which the solutions to (8.2.2) and (8.2.3) (and thus to (7.6.5) and (7.6.6)) exist and are unique. We present a formal result in the next section.

**Unified statistical interpretation of model error:** from the learning perspective, random experimental error and systematic error due to model inadequacy introduce a shift of the statistical properties of the predictors (features). This shows the connection with the notion of *concept drift* ([232, 218]) and *dataset shift* ([153]) studied in machine learning. It is possible to show that this shift can be completely characterized by the probability distribution of $\delta\mathbf{z}$. We present the precise result in the next section.

**Consistency of SBC:** if $\mu^1, \ldots, \mu^M$ are independent identically distributed (iid) samples from $P_{w^{\mathrm{bk}}}$, $\mu \overset{iid}{\sim} P_{w^{\mathrm{bk}}}$, then the dataset $\mathcal{D}_M^{\mathrm{bk}}$ consists of $M$ independent samples from the joint distribution $P_{(Z^{\mathrm{bk}},Y)}$. This has two important implications. First, for a wide class of classifiers (e.g., kernel methods, [210] ), we can exploit standard results in learning theory to study the consistency of the classifier $g_M^\star$ for the best-knowledge monitoring problem, that is (see, e.g., [220])

$$p \lim_{M\to\infty} R^{\mathrm{bk}}(g_M^\star) = \inf_{g \,\text{measurable}} R^{\mathrm{bk}}(g),$$

where $p\lim$ denotes the limit in probability. Second, we can formalize questions related to the Design Of Experiment (DOE) such as frequency selection and sensor placement in a rigorous mathematical fashion, as (grouped-) variable selection problems. In this work, we do not address the connection between DOE and variable selection, which is the topic of ongoing research.

### 8.2.2 Technical results

We present two technical results that complete the discussion started in section 8.2.1. First, we discuss existence and uniqueness of solutions to the monitoring problems and indeed we develop an explicit — through not readily evaluated — expression for $g^{\mathrm{opt,bk}}$. Second, we clarify the relationship between the probability measures $P_{(Z^{\mathrm{exp}},Y)}$ and $P_{(Z^{\mathrm{bk}},Y)}$. For the sake of clarity, we recap the definition of $P_{w^{\mathrm{bk}}}$ in (8.1.1),

$$P_{w^{\mathrm{bk}}}(A) = \int_{\mathcal{P}^{\mathrm{bk}}} \mathbb{1}_A(\mu')\, w^{\mathrm{bk}}(\mu')\, d\mu', \quad A \subset \mathcal{P}^{\mathrm{bk}},$$

and of $P^{\mathrm{exp}}_{(\mu,\xi)}$ in (8.2.1),

$$P^{\mathrm{exp}}_{(\mu,\xi)}(A \times B) = \int_{\mathcal{P}^{\mathrm{bk}}\times\mathcal{V}} \mathbb{1}_A(\mu)\, \mathbb{1}_B(\xi)\, w^{\mathrm{bk}}(\mu')\, p_\xi(\xi')\, d\mu'\, d\xi', \quad A \subset \mathcal{P}^{\mathrm{bk}},\ B \subset \mathcal{V}.$$

We assume here that $P_{w^{\mathrm{bk}}}$ and $P^{\mathrm{exp}}_{(\mu,\xi)}$ are Borel-measurable, that is they are defined on all open sets of $\mathcal{P}^{\mathrm{bk}}$ and $\mathcal{P}^{\mathrm{exp}}$, respectively. A sufficient condition for which $P_{w^{\mathrm{bk}}}$ and $P^{\mathrm{exp}}_{(\mu,\xi)}$ are Borel-measurable is that $w^{\mathrm{bk}} \in L^1(\mathcal{P}^{\mathrm{bk}})$ and $p_\xi \in L^1(\mathcal{V})$. We further recall the random pair

$$(Z^{\mathrm{bk}}, Y) := (\mathbf{z}^{\mathrm{bk}}(\mu), f^{\mathrm{dam}}(\mu)), \qquad \mu \sim P_{w^{\mathrm{bk}}},$$

with probability distribution $P_{(Z^{\text{bk}},Y)}$, and

$$(Z^{\text{exp}}, Y) := (\mathbf{z}^{\text{exp}}(\mu, \xi), f^{\text{dam}}(\mu)), \qquad (\mu, \xi) \sim P^{\text{exp}}_{(\mu,\xi)},$$

with probability distribution $P_{(Z^{\text{exp}},Y)}$.

Next Lemma shows that if $\mathbf{z}^{\text{bk}}$ and $\mathbf{z}^{\text{exp}}$ are continuous, $f^{\text{dam}}$ is Borel-measurable, and $P_{w^{\text{bk}}}$ and $P^{\text{exp}}_{(\mu,\xi)}$ are Borel-measurable, then $P_{(Z^{\text{bk}},Y)}$ and $P_{(Z^{\text{exp}},Y)}$ are also Borel-measurable.

**Lemma 8.2.1.** *Suppose that*

1. *the probability measures $P_{w^{\text{bk}}}$ in (8.1.1) and $P^{\text{exp}}_{(\mu,\xi)}$ in (8.2.1) are Borel-measurable;*
2. *the bk features $\mathbf{z}^{\text{bk}} : \mathcal{P}^{\text{bk}} \to \mathbb{R}^Q$ and the experimental features $\mathbf{z}^{\text{exp}} : \mathcal{P}^{\text{exp}} \to \mathbb{R}^Q$ are continuous;*
3. *the discrete function $f^{\text{dam}} : \mathcal{P}^{\text{bk}} \to \{1, \ldots, K\}$ is Borel-measurable.*

*Then, the probability measures $P_{(Z^{\text{bk}},Y)}$ and $P_{(Z^{\text{exp}},Y)}$ are Borel-measurable on $\mathbb{R}^Q \times \{1, \ldots, K\}$.*

*Proof.* We only prove that $P_{(Z^{\text{bk}},Y)}$ is Borel-measurable. The proof of the measurability of $P_{(Z^{\text{exp}},Y)}$ is analogous. Let $A \subset \mathbb{R}^Q$ be an open set and let $k \in \{1, \ldots, K\}$. We must show that $P_{(Z^{\text{bk}},Y)}(A \times \{k\})$ is well-defined. By construction, we have that

$$P_{(Z^{\text{bk}},Y)}(A \times \{k\}) = \int_{(Z^{\text{bk}},Y)^{-1}(A\times\{k\})} w^{\text{bk}}(\mu)\, d\mu.$$

As a result, we must show that

$$\begin{aligned}(Z^{\text{bk}}, Y)^{-1}(A \times \{k\}) &= \{\mu \in \mathcal{P}^{\text{bk}} : \mathbf{z}^{\text{bk}}(\mu) \in A,\ f^{\text{dam}}(\mu) = k\} \\ &= \left(\mathbf{z}^{\text{bk}}\right)^{-1}(A) \cap \left(f^{\text{dam}}\right)^{-1}(k)\end{aligned}$$

is a Borel set. Since $\mathbf{z}^{\text{bk}}$ is continuous and $A$ is open, $\left(\mathbf{z}^{\text{bk}}\right)^{-1}(A)$ is also open. On the other hand, by assumption, $\left(f^{\text{dam}}\right)^{-1}(k)$ is Borel. Thesis follows by recalling that the intersection of Borel sets is also Borel. □

Next Proposition addresses the problem of existence and uniqueness of the solution to (7.6.6). An analogous discussion applies also to the monitoring problem (7.6.5).

**Proposition 8.2.1.** *The optimal solution* $g^{\text{opt,bk}}$ *to* (7.6.6) *is given by*

$$g^{\text{opt,bk}}(\mathbf{z}) = \arg \max_{k=1,\dots,K} P_{(Z^{\text{bk}},Y)}(Y = k|Z^{\text{bk}} = \mathbf{z}). \tag{8.2.4}$$

*Here,* $P_{(Z^{\text{bk}},Y)}(Y = k|\, Z^{\text{bk}} = \mathbf{z})$ *denotes the conditional probability of the event* $\{Y = k\}$ *given* $\{Z^{\text{bk}} = \mathbf{z}\}$.

*Furthermore, if there exists* $\epsilon > 0$ *such that*

$$P_{Z^{\text{bk}}}\left(P_{(Z^{\text{bk}},Y)}(Y = g^{\text{opt,bk}}(\mathbf{z})|Z^{\text{bk}} = \mathbf{z}) \geq \max_{k \neq g^{\text{opt,bk}}(\mathbf{z})} P_{(Z^{\text{bk}},Y)}(Y = k|Z^{\text{bk}} = \mathbf{z}) + \epsilon\right) = 1, \tag{8.2.5}$$

*then any solution* $g$ *to* (7.6.6) *satisfies* $g^{\text{opt,bk}}(\mathbf{z}) = g(\mathbf{z})$ *for* $P_{Z^{\text{bk}}}$*-almost every* $\mathbf{z} \in \mathbb{R}^Q$.

*Proof.* We first show that (8.2.4) is measurable. Recalling [67, Theorem A.24 page 586], since $P_{(Z^{\text{bk}},Y)}$ is Borel-measurable, if we denote by $P_{Z^{\text{bk}}}$ the corresponding marginal distribution, there exists for $P_{Z^{\text{bk}}}$- almost-every $\mathbf{z} \in \mathbb{R}^Q$ and for $k = 1, \dots, K$ a measurable function $\xi_k^{\text{bk}} : \mathbb{R}^Q \to \mathbb{R}$ such that $\xi_k^{\text{bk}}(\mathbf{z}) = P_{(Z^{\text{bk}},Y)}(Y = k|Z^{\text{bk}} = \mathbf{z})$. Recalling that the pointwise maximum of measurable functions is also measurable, this implies that, under the hypotheses of Lemma 8.2.1, the function $g^{\text{opt,bk}}$ in (8.2.4) is measurable.

We now observe that

$$\begin{aligned} R^{\text{bk}}(g) = & \int_{\mathbb{R}^Q \times \{1,\dots,K\}} \mathcal{L}^{(0,1)}(g(\mathbf{z}), y)\, dP_{(Z^{\text{bk}},Y)}(\mathbf{z}), y) = \int_{\mathbb{R}^Q} \sum_{k \neq g(\mathbf{z})} P_{(Z^{\text{bk}},Y)}(Y = k|Z^{\text{bk}} = \mathbf{z}))\, dP_{Z^{\text{bk}}}(\mathbf{z}) \\ = & \ 1 - \int_{\mathbb{R}^Q} P_{(Z^{\text{bk}},Y)}(Y = g(\mathbf{z})|Z^{\text{bk}} = \mathbf{z}))\, dP_{Z^{\text{bk}}}(\mathbf{z}) \\ \geq & \ 1 - \int_{\mathbb{R}^Q} \max_k P_{(Z^{\text{bk}},Y)}(Y = k|Z^{\text{bk}} = \mathbf{z}))\, dP_{Z^{\text{bk}}}(\mathbf{z}) = R^{\text{bk}}(g^{\text{opt,bk}}). \end{aligned}$$

Since $g^{\text{opt,bk}}$ is measurable, this implies that $g^{\text{opt,bk}}$ is a solution to (7.6.6).

Let $g$ be a classifier such that $R^{\text{bk}}(g^{\text{opt,bk}}) = R^{\text{bk}}(g)$. Using the same reasoning as before, it is possible to verify that

$$R^{\text{bk}}(g) = R^{\text{bk}}(g^{\text{opt,bk}}) + \int_{\mathbb{R}^Q} \left(P_{(Z^{\text{bk}},Y)}(Y = g^{\text{opt,bk}}(\mathbf{z})|Z^{\text{bk}} = \mathbf{z}) - P_{(Z^{\text{bk}},Y)}(Y = g(\mathbf{z})|Z^{\text{bk}} = \mathbf{z})\right) dP_{Z^{\text{bk}}}(\mathbf{z}).$$

Recalling (8.2.5), we find

$$R^{\mathrm{bk}}(g) \geq R^{\mathrm{bk}}(g^{\mathrm{opt,bk}}) + \epsilon \int_{\mathbb{R}^Q} \mathcal{L}^{(0,1)}(g(\mathbf{z}), g^{\mathrm{opt,bk}}(\mathbf{z}))\, d\, P_{Z^{\mathrm{bk}}}(\mathbf{z}).$$

Then, we must have

$$\int_{\mathbb{R}^Q} \mathcal{L}^{(0,1)}(g(\mathbf{z}), g^{\mathrm{opt,bk}}(\mathbf{z}))\, d\, P_{Z^{\mathrm{bk}}}(\mathbf{z}) = 0,$$

which implies that $g(\mathbf{z}) = g^{\mathrm{opt,bk}}(\mathbf{z})$ for $P_{Z^{\mathrm{bk}}}$-almost every $\mathbf{z} \in \mathbb{R}^Q$. □

In view of the proof of a formula that relates the probability measures $P_{(Z^{\mathrm{exp}},Y)}$ and $P_{(Z^{\mathrm{bk}},Y)}$, we recall the probability distribution $P_{\delta\mathbf{z},\mu}$ defined in (7.6.13):

$$P_{\delta\mathbf{z},\mu}(A) = \int_{\mathcal{V}} \mathbb{1}_A(\delta\mathbf{z}(\mu,\xi))\, p_\xi(\xi)\, d\xi.$$

We observe that since $p_\xi \in L^1(\mathcal{V})$ and $\delta\mathbf{z}(\mu,\cdot)$ is continuous $P_{\delta\mathbf{z},\mu}$ is a Borel measure (cf. Lemma 8.2.1). We further introduce notation

$$A - \mathbf{v} := \{\mathbf{w} - \mathbf{v} : \mathbf{w} \in A\}, \quad \forall\, A \subset \mathbb{R}^Q, \ \ \mathbf{v} \in \mathbb{R}^D.$$

Next Proposition contains the key result.

**Proposition 8.2.2.** *Given the Borel set $A \subset \mathbb{R}^Q$ and $k \in \{1, \ldots, K\}$, the following identity holds:*

$$P_{(Z^{\mathrm{exp}},Y)}(A \times \{k\}) = \int_{\mathcal{P}^{\mathrm{bk}}(k)} P_{\delta\mathbf{z},\mu}(A - \mathbf{z}^{\mathrm{bk}}(\mu))\, w^{\mathrm{bk}}(\mu)\, d\mu, \tag{8.2.6}$$

*where $\mathcal{P}^{\mathrm{bk}}(k)$ is defined in Definition 7.6.1, $w^{\mathrm{bk}}$ is defined in* (7.6.4)*, and $P_{\delta\mathbf{z},\mu}$ is defined in* (7.6.13).

*Proof.* Exploiting (7.6.13), we find

$$\begin{aligned} P_{(Z^{\mathrm{exp}},Y)}(A \times \{k\}) &= \int_{\mathcal{P}^{\mathrm{bk}} \times \mathcal{V}} \mathbb{1}_A(\mathbf{z}^{\mathrm{bk}}(\mu) + \delta\mathbf{z}(\mu,\xi))\, \mathbb{1}_{\{k\}}(f^{\mathrm{dam}}(\mu))\, w^{\mathrm{bk}}(\mu)\, p_\xi(\xi)\, d\mu\, d\xi \\ &= \int_{\mathcal{P}^{\mathrm{bk}}(k)} \left( \int_{\mathcal{V}} \mathbb{1}_{A - \mathbf{z}^{\mathrm{bk}}(\mu)}(\delta\mathbf{z}(\mu,\xi))\, p_\xi(\xi)\, d\xi \right) w^{\mathrm{bk}}(\mu)\, d\mu \\ &= \int_{\mathcal{P}^{\mathrm{bk}}(k)} P_{\delta\mathbf{z},\mu}(A - \mathbf{z}^{\mathrm{bk}}(\mu))\, w^{\mathrm{bk}}(\mu)\, d\mu. \end{aligned}$$

□

Before concluding, we derive (7.6.12). Assuming that $p_\xi \in L^1(\mathcal{V})$ and $\delta\mathbf{z} : \mathcal{P}^{\text{exp}} \to \mathbb{R}^Q$ is continuous, we find

$$\begin{aligned} R^{\text{exp}}(g) = & \int_{\mathcal{P}^{\text{bk}}} \left( \int_{\mathcal{V}} \mathcal{L}^{(0,1)}(g(\mathbf{z}^{\text{bk}}(\mu) + \delta\mathbf{z}(\mu,\xi)),\, f^{\text{dam}}(\mu)) p_\xi(\xi)\, d\xi \right) w^{\text{bk}}(\mu)\, d\mu \\ = & \int_{\mathcal{P}^{\text{bk}}} \mathbb{E}_{\xi\sim p_\xi} \left[ \mathcal{L}^{(0,1)}(g(\mathbf{z}^{\text{bk}}(\mu) + \delta\mathbf{z}(\mu,\xi)),\, f^{\text{dam}}(\mu)) \right] w^{\text{bk}}(\mu), d\mu \\ = & \int_{\mathcal{P}^{\text{bk}}} \mathbb{E}_{\delta\mathbf{z}\sim P_{\delta\mathbf{z},\mu}} \left[ \mathcal{L}^{(0,1)}(g(\mathbf{z}^{\text{bk}}(\mu) + \delta\mathbf{z}),\, f^{\text{dam}}(\mu)) \right] w^{\text{bk}}(\mu), d\mu, \end{aligned}$$

which is (7.6.12). Here, in the first equality we employed the definition of expectation with respect to a probability measure, while in the second step we employed the change of variable formula.

## 8.3 Error analysis

### 8.3.1 Main result

We first present two definitions.

**Definition 8.3.1.** *Given the classifier $g : \mathbb{R}^Q \to \{1, \dots, K\}$, we define the k-acceptance region*

$$\mathcal{Z}(g,k) := \{\mathbf{z} \in \mathbb{R}^Q : g(\mathbf{z}) = k\}, \tag{8.3.1}$$

*where $k = 1, \dots, K$.*

**Definition 8.3.2.** *Given the classifier $g : \mathbb{R}^Q \to \{0,1\}$ and the constant $\epsilon > 0$, we define the $\epsilon$-uncertainty indicator $E^{\text{bk}}$ as*

$$E^{\text{bk}}(g,\epsilon,\mu) := \begin{cases} 0 & \text{if } \mathcal{B}_\epsilon(\mathbf{z}^{\text{bk}}(\mu)) \subset\subset \mathcal{Z}(g,k), \qquad \text{for some (unique) } k \in \{1,\dots,K\}; \\ 1 & \text{otherwise;} \end{cases} \tag{8.3.2}$$

*where $\mathcal{B}_\epsilon(\mathbf{z})$ is the $Q$-dimensional ball of radius $\epsilon$ centered in $\mathbf{z} \in \mathbb{R}^Q$, and $\mathcal{Z}(g,k)$ is defined in* (8.3.1).

The $\epsilon$-uncertainty indicator $E^{\text{bk}}$ is equal to zero if $\mathbf{z}^{\text{bk}}(\mu)$ is sufficiently far from the

separating hyper-planes associated with the classifier $g$. Furthermore, $E^{\text{bk}}$ is monotonic increasing in $\epsilon$, and $E^{\text{bk}}(g, \epsilon = 0, \mu) = 0$ unless $\mathbf{z}^{\text{bk}}(\mu)$ lies on a separating hyper-plane. Therefore, it can be interpreted as a measure of local robustness to data uncertainties. We further observe that $E^{\text{bk}}(g, \epsilon, \mu) = 0$ if and only if

$$g(\mathbf{z}^{\text{bk}}(\mu)) = g(\mathbf{z}^{\text{bk}}(\mu) + \delta\mathbf{z}) \quad \forall\, \delta\mathbf{z} \in \mathcal{B}_\epsilon(\mathbf{0}).$$

Recalling the definition of $0-1$ loss, we thus find

$$\mathcal{L}^{(0,1)}\left(g(\mathbf{z}^{\text{bk}}(\mu)),\, g(\mathbf{z}^{\text{bk}}(\mu) + \delta\mathbf{z})\right) \leq E^{\text{bk}}(g, \epsilon, \mu) \quad \forall\, \delta\mathbf{z} \in \mathcal{B}_\epsilon(\mathbf{0}). \tag{8.3.3}$$

We formally relate the $\epsilon$-uncertainty indicator (8.3.2) to other measures of local robustness that have been proposed in the literature. Given the parameter $\mu \in \mathcal{P}^{\text{bk}}$ and the classifier $g$, we define

$$r^{\text{bk}}(\mu, g) := \inf_{\mathbf{z} \in \mathcal{Z}^\star(g, g(\mathbf{z}^{\text{bk}}(\mu)))} \|\mathbf{z} - \mathbf{z}^{\text{bk}}(\mu)\|_2, \tag{8.3.4}$$

where $\mathcal{Z}^\star(g, k) = \bigcup_{k' \neq k} \mathcal{Z}(g, k')$ and $\mathcal{Z}(g, k')$ is defined in (8.3.1). It is possible to show that we can rewrite the $\epsilon$-uncertainty indicator $E^{\text{bk}}$ as

$$E^{\text{bk}}(g, \epsilon, \mu) = \begin{cases} 0 & \text{if } r^{\text{bk}}(\mu, g) > \epsilon; \\ \\ 1 & \text{otherwise.} \end{cases}$$

The quantity $r^{\text{bk}}(\mu, g)$ in (8.3.4) is known as *stability radius*, and it is widely used in control theory ([109]), and optimization ([244]) as measure of local robustness. It can be shown (see [205]) that the stability radius is also an instance of Wald's maximin model ([227]), which is employed in statistics and decision theory.

We now present the main result of this section.

**Proposition 8.3.1.** *Let the classifier $g : \mathbb{R}^Q \to \{1, \ldots, K\}$ and the damage function $f^{\text{dam}} : \mathcal{P}^{\text{bk}} \to \{1, \ldots, K\}$ be measurable functions. Let us further define $\epsilon^{\text{bk}} > 0$ as*

$$\epsilon^{\text{bk}} := \|\delta\mathbf{z}\|_{L^\infty(\mathcal{P}^{\text{exp}}; \mathbb{R}^Q)}, \quad \delta\mathbf{z}(\mu, \xi) = \mathbf{z}^{\text{exp}}(\mu, \xi) - \mathbf{z}^{\text{bk}}(\mu). \tag{8.3.5}$$

*Then, the following hold:*

$$R^{\exp}(g) \leq R^{\mathrm{bk}}(g) + \int_{\mathcal{P}^{\mathrm{bk}}} E^{\mathrm{bk}}(g, \epsilon^{\mathrm{bk}}, \mu)\, w^{\mathrm{bk}}(\mu)\, d\mu =: R^{\exp}_{\mathrm{UB}}(g, \epsilon^{\mathrm{bk}}), \tag{8.3.6}$$

*and*

$$R^{\exp}(g;k) \leq R^{\mathrm{bk}}(g;k) + \int_{\mathcal{P}^{\mathrm{bk}}(k)} E^{\mathrm{bk}}(g, \epsilon^{\mathrm{bk}}, \mu)\, w^{\mathrm{bk}}(\mu)\, d\mu =: R^{\exp}_{\mathrm{UB}}(g, \epsilon^{\mathrm{bk}}, k), \tag{8.3.7}$$

*for $k = 1, \ldots, K$ and for any choice of $p_\xi : \mathcal{V} \to \mathbb{R}_+$ in* (7.6.5).

*Proof.* We show only (8.3.6), as the proof of (8.3.7) is analogous. Applying the triangle inequality, we find

$$\begin{aligned} R^{\exp}(g) \leq\ & \underbrace{\int_{\mathcal{P}^{\exp}} \mathcal{L}^{(0,1)}(g(\mathbf{z}^{\mathrm{bk}}(\mu)),\, f^{\mathrm{dam}}(\mu))\, w^{\mathrm{bk}}(\mu)\, p_\xi(\xi)\, d\mu\, d\xi}_{=(I)} \\ & + \underbrace{\int_{\mathcal{P}^{\exp}} \mathcal{L}^{(0,1)}(g(\mathbf{z}^{\mathrm{bk}}(\mu)),\, g(\mathbf{z}^{\exp}(\mu,\xi))\, w^{\mathrm{bk}}(\mu)\, p_\xi(\xi)\, d\mu\, d\xi}_{=(II)} \end{aligned}$$

Then, recalling the definition of $w^{\mathrm{bk}}$ in (7.6.4), we observe that

$$(I) = \int_{\mathcal{P}^{\mathrm{bk}}} \mathcal{L}^{(0,1)}(g(\mathbf{z}^{\mathrm{bk}}(\mu)),\, f^{\mathrm{dam}}(\mu))\, w^{\mathrm{bk}}(\mu) \underbrace{\int_{\mathcal{V}} p_\xi(\xi)\, d\xi}_{=1}\, d\mu = R^{\mathrm{bk}}(g).$$

On the other hand, recalling (8.3.3), we find

$$(II) \leq \int_{\mathcal{P}^{\mathrm{bk}}} E^{\mathrm{bk}}(g, \epsilon^{\mathrm{bk}}, \mu)\, w^{\mathrm{bk}}(\mu) \underbrace{\int_{\mathcal{V}} p_\xi(\xi)\, d\xi}_{=1}\, d\mu = \int_{\mathcal{P}^{\mathrm{bk}}} E^{\mathrm{bk}}(g, \epsilon^{\mathrm{bk}}, \mu)\, w^{\mathrm{bk}}(\mu)\, d\mu.$$

Thesis follows. □

Our error analysis clarifies that the online performance of a classifier $g$ depend on two distinct factors: (i) the bk risk $R^{\mathrm{bk}}(g)$, and (ii) the integral involving the $\epsilon$-uncertainty indicator $E^{\mathrm{bk}}$. The bk risk $R^{\mathrm{bk}}(g)$ accounts for the nominal performance of the classifier; the integral involving $E^{\mathrm{bk}}$ accounts for the robustness of $g$ to data uncertainties and depends on the roughness of the separating hyperplane(s). As observed in section 8.2, traditional machine learning algorithms aim to minimise the nominal risk (here $R^{\mathrm{bk}}(g)$). If model error

is moderate, estimate (8.3.6) shows that minimising the nominal risk leads to accurate online performance. On the other hand, if model error is sufficiently large, then this choice does not necessarily lead to accurate decision rules for the online stage.

Before concluding this section, we state a remark.

**Remark 8.3.1.** *(**The separable case**) We discuss the special case in which configuration classes are separable and the classifier $g$ separates them over $\mathcal{P}^{\text{bk}}$, that is*

$$R^{\text{bk}}(g) = 0.$$

*In this case, provided that the model error is sufficiently small, we can guarantee perfect separation even in presence of model error. Let us define the quantity*

$$\delta_k = \inf_{\mu \in \mathcal{P}^{\text{bk}}:\, g(\mathbf{z}^{\text{bk}}(\mu))=k} \; \inf_{\mathbf{z} \in \mathcal{Z}^\star(g,k)} \|\mathbf{z}^{\text{bk}}(\mu) - \mathbf{z}\|_2.$$

*where $\mathcal{Z}^\star(g,k) = \bigcup_{k' \neq k} \mathcal{Z}(g,k')$ and $\mathcal{Z}(g,k')$ is defined in* (8.3.1)*. Then, if $\epsilon^{\text{bk}} < \min_k \delta_k$, we find that*

$$E^{\text{bk}}(g, \epsilon^{\text{bk}}, \mu) \equiv 0, \quad \forall\, \mu \in \mathcal{P}^{\text{bk}}$$

*and exploiting Proposition 8.3.1 we find that*

$$R^{\text{exp}}(g) = 0;$$

*this implies that the classifier $g$ is a solution to problem* (7.6.5)*.*

### 8.3.2 Model bias and experimental risk

We now wish to relate model bias to classification performance for a special case. This will provide insights about the connection between the modelling stage and the inference stage. Let us assume that experimental features can be written as[1]

$$\mathbf{z}^{\text{exp}}(\mu, \xi) = \widehat{\mathcal{F}}\left(u^{\text{exp}}(\mu, \xi)\right),$$

where $u^{\text{exp}}(\mu, \xi) \in \mathcal{U}$ is the system state associated with $(\mu, \xi)$, $\mathcal{U} = \mathcal{U}(\Omega)$ is a suitable Hilbert space defined over a domain $\Omega \subset \mathbb{R}^d$, and $\widehat{\mathcal{F}}$ is a linear continuous functional over $\mathcal{U}$,

[1] We consider here the case of static data to not deal with the dependence on frequency.

$\widehat{\mathcal{F}} \in \mathcal{U}'$, with continuity constant $C_F$. Let us further assume that the bk features are given by

$$\mathbf{z}^{\text{bk}}(\mu) = \widehat{\mathcal{F}}(u^{\text{bk}}(\mu)),$$

where $u^{\text{bk}}(\mu)$ is the solution to the variational problem

$$G^{\text{bk}}(u^{\text{bk}}(\mu); \mu) = \ell(\mu), \quad \text{in } \mathcal{U}'.$$

Here, we assume that $G^{\text{bk}}(\cdot; \mu)$ is an inf-sup stable linear operator with stability constant $\beta^{\text{bk}}(\mu)$ and $\ell(\mu) \in \mathcal{U}'$ for any $\mu \in \mathcal{P}^{\text{bk}}$. If we define the *model bias* $f^{\text{bias}} : \mathcal{P}^{\text{exp}} \to \mathcal{U}'$ as

$$f^{\text{bias}}(\mu, \xi) := G^{\text{bk}}(u^{\text{exp}}(\mu, \xi); \mu) - \ell(\mu), \qquad \forall\, (\mu, \xi) \in \mathcal{P}^{\text{exp}},$$

we obtain

$$\|\delta\mathbf{z}(\mu, \xi)\|_2 = \|\widehat{\mathcal{F}}(u^{\text{exp}}(\mu, \xi) - u^{\text{bk}}(\mu))\|_2 \leq \frac{C_F}{\beta^{\text{bk}}(\mu)} \|f^{\text{bias}}(\mu, \xi)\|_{\mathcal{U}'},$$

which implies that

$$\epsilon^{\text{bk}} = \sup_{(\mu,\xi)\in\mathcal{P}^{\text{exp}}} \|\delta\mathbf{z}(\mu, \xi)\|_2 \leq \sup_{(\mu,\xi)\in\mathcal{P}^{\text{exp}}} \frac{C_F}{\beta^{\text{bk}}(\mu)} \|f^{\text{bias}}(\mu, \xi)\|_{\mathcal{U}'}. \tag{8.3.8}$$

Combining estimates (8.3.8) with (8.3.6), we obtain that the performance of our monitoring system depends on four distinct factors: (i) the nominal performance through the bk risk $R^{\text{bk}}(g)$, (ii) the robustness of $g$ to data uncertainties throught the $\epsilon$-uncertainty indicator $E^{\text{bk}}$, (iii) the stability of the PDE through the stability constant $\beta^{\text{bk}}(\mu)$, and (iv) the uncertainty in the model through the bias $f^{\text{bias}}$. We observe that a direct consequence of estimates (8.3.6) and (8.3.8) is the accomodation of the inevitable, even if small, departure of the physical system from our idealization. However, we observe that (8.3.8) is not fully actionable since $\|f^{\text{bias}}(\mu, \xi)\|_{\mathcal{U}'}$ is typically unknown.

## 8.4 Conclusions

We presented a Simulation-Based Classification approach for Structural Health Monitoring; the approach takes advantage of recent advances in parametrized Model Order Reduction to

inexpensively form quasi-exhaustive synthetic training datasets based on a bk parametrized mathematical model. We further presented a mathematical analysis, which motivates the problem formulation introduced in Chapter 7 and shows that, for proper choices of the supervised-learning procedure for classification, the classification rule obtained based on SBC approaches the optimal bk risk in the limit $M \to \infty$. Finally, we presented an *a priori* error analysis that links nominal performance (associated with the bk risk $R^{\text{bk}}(\cdot)$), to experimental performance (associated with the experimental risk $R^{\text{exp}}(\cdot)$). We observed that, if estimates for the error in feature evaluations are available at training stage, we can exploit our error analysis to inform the machine-learning procedure.

# Chapter 9

# Application to the microtruss problem

We discuss the application of the Simulation-Based approach presented in Chapter 8 to the microtruss problem. We first present the strategy used to generate the classifier (section 9.1), we describe the application of the RB method to speed up the calculations (section 9.2), and we present the classification results (section 9.3). Finally, in section 9.4, we compare our technique with two model-based approaches.

## 9.1 Computation of the classifier

Exploiting the reasoning of Chapter 7.5.2, we now introduce the classifier used in the numerical tests: given the set of features $\mathbf{z}_1^{\text{exp}}$ and $\mathbf{z}_2^{\text{exp}}$,

- **Level 1:** distinguish between $\{1,4\}$, $\{2\}$ and $\{3\}$ based on $\mathbf{z}_1^{\text{exp}}$;
- **Level 2:** if Level 1 returns $\{1,4\}$, distinguish between $\{1\}$ and $\{4\}$ based on $\mathbf{z}_2^{\text{exp}}$.

We observe that the first layer corresponds to a threeway classification problem, while the second layer corresponds to a binary problem. From a practical perspective, our proposal requires the training of two classifiers: a threeway classifier for the first level and a binary classifier for the second level. We can thus interpret a classifier $g$ as the pair $g = (g_1, g_2)$ where $g_1 : \mathbb{R}^{Q_f} \to \{0,2,3\}$, $g_2 : \mathbb{R}^{Q_f} \to \{1,4\}$, and 0 is the label associated to $\{1,4\}$ for the first level.

In view of the presentation of the numerical results, we define the level-1 and level-2 bk risks:

$$R^{\text{bk,level 1}}(g) = \int_{\mathcal{P}^{\text{bk}}} \mathcal{L}^{(0,1)}(g_1(\mathbf{z}_1^{\text{bk}}(\mu)), f_1^{\text{dam}}(\mu))\, w^{\text{bk}}(\mu)\, d\mu, \tag{9.1.1a}$$

and

$$R^{\text{bk,level 2}}(g) = \frac{1}{P_1^{\text{bk}} + P_4^{\text{bk}}} \int_{\mathcal{P}^{\text{bk}}(1)\cup\mathcal{P}^{\text{bk}}(4)} \mathcal{L}^{(0,1)}(g_2(\mathbf{z}_2^{\text{bk}}(\mu)), f^{\text{dam}}(\mu))\, w^{\text{bk}}(\mu)\, d\mu, \tag{9.1.1b}$$

where $P_1^{\text{bk}}, \ldots, P_4^{\text{bk}}$ are defined in (7.6.11), and

$$f_1^{\text{dam}}(\mu) = \begin{cases} 0 & \text{if } f^{\text{dam}}(\mu) \in \{1, 4\}, \\ 2 & \text{if } f^{\text{dam}}(\mu) = 2, \\ 3 & \text{if } f^{\text{dam}}(\mu) = 3. \end{cases} \tag{9.1.1c}$$

We observe that $0 \leq R^{\text{bk,level 1}}(g), R^{\text{bk,level 2}}(g) \leq 1$. Similar definitions can be given for level-1 and level-2 experimental risks $R^{\text{exp,level 2}}(g)$ and $R^{\text{exp,level 2}}(g)$.

## 9.2 Reduced-Basis Approximation

In this section, we discuss how we reduce the computational burden associated with the construction of the dataset $\mathcal{D}_M^{\text{bk}}$ for the microtruss system. More specifically, we wish to speed up computations of the map

$$(f, \mu) \mapsto A_{i,j}^{\text{bk}}(f; \mu)$$

in the limit of many queries using the Reduced Basis (RB) method. With this in mind, we first present the weak formulation of the bk model (section 9.2.1), then we present the RB approximation (section 9.2.2), and finally we provide numerical results to demonstrate the effectiveness of the RB approach (section 9.2.3).

### 9.2.1 Parametrized microtruss model

We first introduce the weak statement associated with the time-harmonic asymptotic solution to (7.4.1) in the configuration-dependent domain $\Omega_s$: given the frequency $f$, and the

bk configuration $\mu = [\alpha, \beta, E, s_L, s_R]$, find $u^{\text{bk}}(f;\mu) \in \mathcal{U}_s := H^1(\Omega_s;\mathbb{C}^2)$ such that

$$\begin{cases} (1 + i\omega_f\beta)\, E\, b_{\Omega_s}(u^{\text{bk}}(f;\mu), v) \,+\, (-\omega_f^2 + i\omega_f\alpha)\, \rho L^2 m_{\Omega_s}(u^{\text{bk}}(f;\mu), v) = 0. \\ u^{\text{bk}}(f;\mu)|_{\Gamma^{\text{dir}}} = u^{\text{dir}} \end{cases} \tag{9.2.1a}$$

for all $v \in \mathcal{U}_{s,0} = H^1_{0,\Gamma^{\text{dir}}}(\Omega_s;\mathbb{C}^2)$, where $\omega_f = 2\pi f$,

$$m_{\Omega_s}(u,v) = \int_{\Omega_s} u \cdot \bar{v}\, dx, \tag{9.2.1b}$$

and

$$b_{\Omega_s}(u,v) = \int_{\Omega_s} \frac{1}{1+\nu}\, \text{sym}(\nabla u) \,:\, \overline{\text{sym}(\nabla v)} + \frac{1}{(1+\nu)(1-2\nu)}\, \text{div}(u)\, \overline{\text{div}(v)}\, dx. \tag{9.2.1c}$$

Here, $\bar{\cdot}$ refers to the complex conjugate.

We then introduce a geometric mapping between a parameter-independent domain $\Omega^{\text{ref}}$ and the configuration-dependent domain $\Omega_s$. With this in mind, we introduce the reference domain $\Omega^{\text{ref}} := \Omega_1^{\text{ref}} \cup \Omega_2^{\text{ref}} \cup \Omega_3^{\text{ref}}$ such that $\Omega_1^{\text{ref}} = \Omega_1$, $\Omega_2^{\text{ref}} = \Omega_2(s_L = 1)$, $\Omega_3^{\text{ref}} = \Omega_3(s_R = 1)$, and we define the affine map

$$\mathcal{T} : \Omega^{\text{ref}} \times [1,2]^2 \to \Omega_s, \qquad \mathcal{T}(x, s_L, s_R) = \begin{cases} x & \text{if } x \in \Omega_1^{\text{ref}}, \\ x_1\mathbf{e}_1 + s_L x_2 \mathbf{e}_2 & \text{if } x \in \Omega_2^{\text{ref}}, \\ x_1\mathbf{e}_1 + s_R x_2 \mathbf{e}_2 & \text{if } x \in \Omega_3^{\text{ref}}, \end{cases} \tag{9.2.2}$$

where $\{\mathbf{e}_1, \mathbf{e}_2\}$ is the canonical basis. By tedious but straightforward calculations, we find that, for any $u, v \in H^1(\Omega_s;\mathbb{C}^2)$,

$$(1 + i\omega_f\beta)\, E\, b_{\Omega_s}(u,v) \,+\, (-\omega_f^2 + i\omega_f\alpha) m_{\Omega_s}(u,v) = \sum_{q=1}^{10} \Theta_q(f;\mu)\, a^q(\hat{u}, \hat{v}) \tag{9.2.3}$$

where $\hat{u}(x) = u(\mathcal{T}(x,s))$, $\hat{v}(x) = v(\mathcal{T}(x,s))$, and the parameter-dependent coefficients $\{\Theta_q\}_{q=1}^{10}$ and the parameter-independent bilinear forms $\{a^q\}_{q=1}^{10}$ are reported in Appendix D. Then, we introduce the lift $u^{\text{lift}} \in H^1(\Omega^{\text{ref}};\mathbb{C}^2)$ such that $u^{\text{lift}} \equiv 0$ outside $\Omega_1$, $u^{\text{lift}}(x_{i,j}) = 0$ for all $i,j = 1,\ldots,4$, and $u^{\text{lift}}|_{\Gamma^{\text{dir}}} = u^{\text{dir}}$; we observe that $u^{\text{lift}}(\mathcal{T}^{-1}(x, s_L, s_R))$ does not depend on the values of $s_L$ and $s_R$.

We can now introduce the parametrized best-knowledge model for the lifted field in

the reference configuration and we relate the solution to the experimental measurements. Given a frequency $f$ and bk configuration $\mu$ in $\mathcal{P}_f^{\rm bk}$, we seek the solution $\mathring{u}^{\rm bk}(f;\mu) := u^{\rm bk}(\mathcal{T}(\cdot,s),f;\mu) - u^{\rm lift} \in \mathcal{U}_0 = H^1_{0,\Gamma^{\rm dir}}(\Omega^{\rm ref};\mathbb{C}^2)$ to the following variational problem

$$a(\mathring{u}^{\rm bk}(f;\mu),v;f,\mu) = \ell(v;f,\mu), \qquad \forall\, v \in \mathcal{U}_0, \tag{9.2.4a}$$

where

$$a(w,v;f,\mu) = \sum_{q=1}^{10} \Theta_q(f,\mu)\, a^q(w,v), \qquad \ell(v;f,\mu) = -\sum_{q=1}^{10} \Theta_q(f,\mu)\, a^q(u^{\rm lift},v), \tag{9.2.4b}$$

and

$$(f,\mu) \in \mathcal{P}_f^{\rm bk} := \mathcal{I}_f \times \mathcal{P}^{\rm bk}. \tag{9.2.4c}$$

Recalling the definition of the map $\mathcal{T}$ (such that $\mathcal{T}^{-1}(x_{i,j},s_L,s_R) = x_{i,j}$ for all $s_L, s_R$), and the definition of $u^{\rm lift}$, we finally find

$$A_{i,j}^{\rm bk}(f;\mu) = \frac{A_{\rm nom}}{|\mathring{u}_2^{\rm bk}(x_{2,1};f,\mu)|}\, |\mathring{u}_2^{\rm bk}(x_{i,j};f,\mu)|, \tag{9.2.5}$$

where $i,j = 1,\ldots,4$, and $(f,\mu) \in \mathcal{P}_f^{\rm bk}$. Since $u_2^{\rm bk}(x_{i,j};f,\mu) = \mathring{u}_2^{\rm bk}(x_{i,j};f,\mu) + u^{\rm lift}(x_{i,j}) = \mathring{u}_2^{\rm bk}(x_{i,j};f,\mu)$, (9.2.4)-(9.2.5) is equivalent to (7.4.4).

In view of the application of the RB method, we define the norm for $\mathcal{U}_0$

$$\|u\| := \sqrt{E^{\rm ref} b_{\Omega^{\rm ref}}(u,u) + \rho L^2 m_{\Omega^{\rm ref}}(u,u)}, \tag{9.2.6}$$

where $E^{\rm ref} = 2.8 \cdot 10^9$[Pa], and $m_{\Omega^{\rm ref}}(\cdot,\cdot)$ and $b_{\Omega^{\rm ref}}(\cdot,\cdot)$ are defined in (9.2.1b) and (9.2.1c), respectively. We further define the dual norm of the residual

$$R(u;f,\mu) := \sup_{v\in\mathcal{U}_0} \frac{|a(u,v;f,\mu) - \ell(v;f,\mu)|}{\|v\|}. \tag{9.2.7}$$

Finally, we introduce the FE discretization $\mathcal{U}_0^{\mathcal{N}}$ of the space $\mathcal{U}_0$ based on P4 polynomials and $\mathcal{N} = 14670$ degrees of freedom (cf. Chapter 7.4.1). We denote by $\mathring{u}_{\mathcal{N}}^{\rm bk}(f;\mu) \in \mathcal{U}_0^{\mathcal{N}}$ the FE approximation of the solution to (9.2.4).

### 9.2.2 Application of the Reduced Basis (RB) method

The key idea of RB is to restrict trial and test spaces in (9.2.4) to a low-dimensional space $W_N \subset \mathcal{U}_0^{\mathcal{N}}$ with $N \ll \mathcal{N}$. For a given pair $(f, \mu)$, we define the RB approximation $\mathring{u}_{N,\mathcal{N}}^{\text{bk}}(f;\mu) \in W_N$ of $\mathring{u}_{\mathcal{N}}^{\text{bk}}(f;\mu)$ as the solution to the $N$-dimensional variational problem:

$$a(\mathring{u}_{N,\mathcal{N}}^{\text{bk}}(f;\mu), v; f, \mu) = \ell(v; f, \mu), \qquad \forall v \in W_N. \tag{9.2.8a}$$

The RB outputs are then evaluated as

$$\widetilde{A}_{i,j}^{\text{bk}}(f;\mu) = \frac{A_{\text{nom}}}{|\left(\mathring{u}_{N,\mathcal{N}}^{\text{bk}}(x_{2,1}; f, \mu)\right)_2|} |\left(\mathring{u}_{N,\mathcal{N}}^{\text{bk}}(x_{i,j}; f, \mu)\right)_2|, \tag{9.2.8b}$$

$i, j = 1, \ldots, 4$, $(f, \mu) \in \mathcal{P}_f^{\text{bk}}$, which yields features (see (7.5.4) and (7.5.5)):

$$\widetilde{\mathbf{z}}_1^{\text{bk}}(\mu) = \left[\tilde{z}_1^{\text{bk}}(f^1;\mu), \ldots, \tilde{z}_1^{\text{bk}}(f^{Q_f};\mu)\right], \quad \tilde{z}_1^{\text{bk}}(f;\mu) = \frac{\widetilde{A}_{1,4}^{\text{bk}}(f;\mu)}{\widetilde{A}_{4,4}^{\text{bk}}(f;\mu)}, \tag{9.2.8c}$$

and

$$\widetilde{\mathbf{z}}_2^{\text{bk}}(\mu) = \left[\tilde{z}_2^{\text{bk}}(f^1;\mu), \ldots, \tilde{z}_2^{\text{bk}}(f^{Q_f};\mu)\right], \quad \tilde{z}_2^{\text{bk}}(f;\mu) = \frac{\widetilde{A}_{2,4}^{\text{bk}}(f;\mu) + \widetilde{A}_{3,4}^{\text{bk}}(f;\mu)}{\widetilde{A}_{1,1}^{\text{bk}}(f;\mu) + \widetilde{A}_{4,1}^{\text{bk}}(f;\mu)}. \tag{9.2.8d}$$

We generate the space $W_N$ based on snapshots from the bk manifold $\mathcal{M}_{\mathcal{N}}^{\text{bk}} = \{\mathring{u}_{\mathcal{N}}^{\text{bk}}(f;\mu) : (f,\mu) \in \mathcal{P}_f^{\text{bk}}\}$. More precisely, we consider a Lagrange ([175]) approximation space $W_N$ as the span of $N$ snapshots $\{\mathring{u}_{\mathcal{N}}^{\text{bk}}(f^n;\mu^n)\}_{n=1}^N$, where $\{(f^n,\mu^n)\}_{n=1}^N$ are selected based on the residual-based weak-Greedy algorithm (cf. Algorithm 2.1.1): given $\{(f^n,\mu^n)\}_{n=1}^{N-1}$, set $(f^N,\mu^N)$ equal to

$$(f^N,\mu^N) := \arg \max_{(f,\mu)\in\mathcal{P}_{f,\text{train}}^{\text{bk}}} \Delta_{N-1}^{\text{bk}}(f,\mu) := R(\mathring{u}_{N-1,\mathcal{N}}^{\text{bk}}(f;\mu); f, \mu),$$

where $\mathcal{P}_{f,\text{train}}^{\text{bk}}$ is a suitably finite-dimensional discretization of $\mathcal{P}_f^{\text{bk}}$ of cardinality $|\mathcal{P}_{f,\text{train}}^{\text{bk}}| = n_{\text{train}}$. We recall that this procedure allows us to identify quasi-optimal reduced spaces $W_N$ relative to the Kolmogorov gold standard (see [32] and [56, section 8]).

To reduce the computational cost in the limit of many queries, we pursue an offline/online strategy. During the offline stage (step 2.a in Algorithm 8.1.2), we construct the space

$W_N$, and we assemble and store suitable parameter-independent quantities related to the construction of the linear system (9.2.8) in terms of the offline expansion (9.2.4b). Then, during the online stage (step 2.b in Algorithm 8.1.2), we compute the coefficients of the RB solution associated with a suitable basis of $W_N$, and we evaluate the outputs of interest and subsequently features; the operation count (for a given $(f, \mu)$) depends only on $N$. The offline stage is performed once and is parameter-independent, while the online stage is repeated for each value of $(f, \mu)$: since the cost of a single online evaluation is significantly less expensive than the corresponding FE evaluation, we can easily amortize the offline computational cost in the limit of many queries.

### 9.2.3 Numerical results

Figure 9-1(a) shows the convergence of $\Delta^{\text{bk}}_{N-1}(f^N, \mu^N)$ of the weak-Greedy algorithm ($n_{\text{train}} = 10^3$). We observe that convergence is not monotonic with $N$: this is to be expected since the problem is not coercive and we consider only Galerkin projection; monotonicity could be guaranteed by appealing to the minimum residual formulation ([144]). We further observe that for $N \gtrsim 15$ the residual stagnates: this is due to round-off errors in residual evaluation; potential strategies to address this issue are proposed in [45, 42]. Nevertheless, we observe that for $N \gtrsim 15$ we already obtain a sufficient $10^6$ reduction in the residual value. Furthermore, Figures 9-1(b)-(c) show that for $N = 20$ the RB error prediction in feature evaluation is negligible if compared with intra-class differences. In what follows, we may thus effectively equate $\mathring{u}^{\text{bk}}_{\mathcal{N}}$ and $\mathring{u}^{\text{bk}}_{N=20,\mathcal{N}}$.

Finally, we comment on the computational cost. We consider here a P4 FE discretization ($\mathcal{N} = 14670$) and a RB reduced model based on $N = 20$ snapshots. Simulations are performed on a Mac OS-X Intel Core i7 2.8GHz, RAM 16GB. The RB offline cost is roughly $24s$, while the cost of a single input-output evaluation is roughly

$$0.18s \quad \text{for FE}, \quad 4.4 \cdot 10^{-3}s \quad \text{for RB}.$$

Assuming that each datapoint $\mathbf{z}^{\text{bk}}(\mu)$ is based on $Q_f$ frequencies, our RB approach is computationally advantageous if $24s + 4.4 \cdot 10^{-3}s \times MQ_f < 0.18s \times MQ_f$, or

$$MQ_f \gtrsim 180.$$

Since we consider $M \approx 10^4$, $Q_f \approx 10$, the cost of the offline stage is negligible. We also observe that in three space dimensions the RB advantage will further increase.

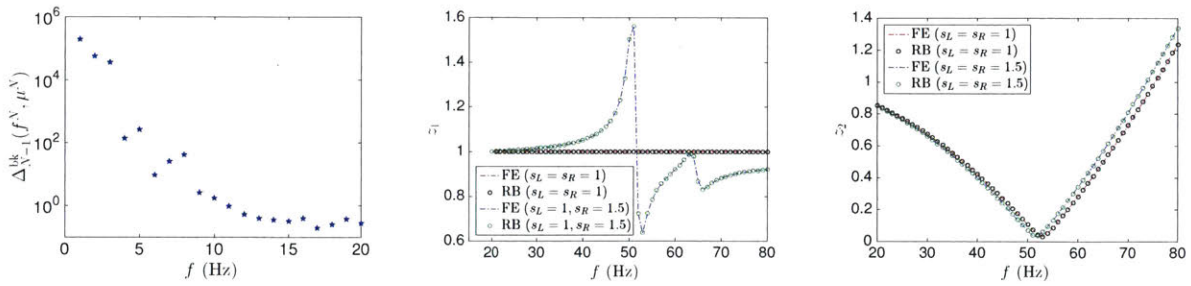


**(a)** **(b)** **(c)**

**Figure 9-1:** Microtruss experiment: RB Approximation. Figure (a): convergence of the weak-Greedy. Figures (b) and (c): comparison between FE and RB feature predictions for $\alpha = 5 \cdot 10^{-4}$, $\beta = 10^{-4}$, $E = 2.8 \cdot 10^9$ and three different choices of the geometric parameters.

## 9.3 Classification results

We consider five distinct classifiers for both levels : one-vs-all Support Vector Machine with Gaussian kernels (ova-SVM,[184, 61, 58]), decision trees ([38]), $\kappa$ = 5-nearest neighbor (kNN, [104, Chapter 13]), artificial neural network with 10 hidden layers (ANN, [34]), and nearest-mean classifier (NMC). We recall that NMC assigns to observations the label of the class of training samples whose centroid $\mathbf{m}(k)$ is closest to observations in a suitable norm. Two standard NMC procedures, which correspond to two different choices of the norm, are

$$g(\mathbf{z}) := \arg \min_{k \in \{1,\dots,K\}} \sum_{q=1}^{Q} (z_q - m_q^{\text{bk}}(k))^2, \tag{9.3.1}$$

and

$$g(\mathbf{z}) := \arg \min_{k \in \{1,\dots,K\}} \sum_{q=1}^{Q} \frac{(z_q - m_q^{\text{bk}}(k))^2}{std_q^{\text{bk}}(k)}, \tag{9.3.2}$$

where $m_q^{\text{bk}}(k)$, $std_q^{\text{bk}}(k)$ are sample mean and sample standard deviations of the training samples of the class $\kappa = \{k\}$ as defined in (7.5.6a) and (7.5.6b). We standardize data[1] for the second level, whereas we do not standardize data for the first level: due to the small

[1] We recall that standardization of data implies that we train the classifier based on the modified features $\hat{z}_q = \frac{z_q - m_q^{\text{bk}}}{std_q^{\text{bk}}}$ where $m_q^{\text{bk}}$, $std_q^{\text{bk}}$ are respectively the sample mean and the sample standard deviation of the training set for all classes.

variations of $z_1$ far from resonance, standardization of $z_1$ increases sensitivity to model error. For NMC, we apply (9.3.1) for the first level and (9.3.2) for the second level.

We appeal to off-the-shelf Matlab implementations ([150]) of ova-SVM, decision trees, kNN and ANN. More precisely, we rely on `fitcsvm` for binary SVM, `fitctree` for decision trees, `fitknn` for kNN and `train` for ANN. We refer to the Matlab documentation and to the above-mentioned references for further details.

In order to assess performance on experimental data, we consider experimentally the five different nominal system configurations introduced in section 7.5.2. For each configuration, we consider three independent trials for a total of 15 experimental datapoints. We remark that these experimental datapoints do not include the datapoint employed to estimate $\mathcal{P}^{\text{bk}}$.

We first study performance on synthetic data. More specifically, we study the dependence of the bk risk on the number $M$ of training points. We generate a dataset with $N_{\text{train}} = 10^4$ datapoints corresponding to the following 9 frequencies:

$$\{f^q\}_{q=1}^{Q_f} = \{20.1, 25.1, 30.1, 35.1, 40.1, 45.1, 65.1, 70.1, 75.1\}.$$

We choose to not consider frequencies close to resonance since the noise is higher. Then, we consider $M$ datapoints for training and $N_{\text{train}} - M$ datapoints for estimating the bk risk. In order to account for the effects of partition, we average results over 100 random splits of the dataset.

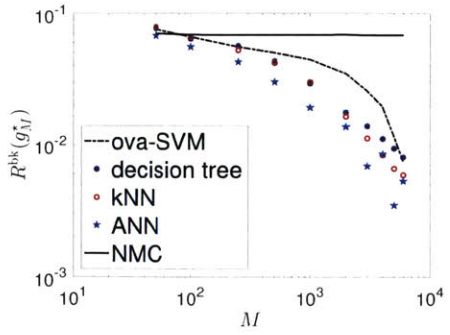


**(a)**

**Figure 9-2:** Microtruss experiment: behavior of the overall (both levels) bk risk $R^{\text{bk}}(g_M^\star)$ with $M$ for five different Machine Learning algorithms.

Figure 9-2 shows the behavior of the bk risk $R^{\text{bk}}(g_M^\star)$ with $M$ for the above mentioned classifiers. We observe that performance strongly depends on the amount of training data;

this demonstrates empirically the importance of pMOR in the generation of sufficiently large datasets. We further observe that, unlike the other classifiers, performance of NMC does not improve as $M$ increases; this is to be expected since NMC is not in general consistent.

We now study performance for real experimental data. Towards this end, we consider a dataset $\mathcal{D}^{\text{bk}}_{N_{\text{train}}}$ with $N_{\text{train}} = 10^4$ datapoints based on the same 9 frequencies considered for the previous test. We reserve $M = 7 \cdot 10^3$ datapoints for training and validation, and $3 \cdot 10^3$ for testing. As for the previous test, we average results over 100 random splits of the dataset. For this test, we report estimates of the synthetic and experimental risks separately for first and second level (see (9.1.1)).

**Table 9.1:** Classification performances, $R^{\cdot,\text{level1}}(g)$ and $R^{\cdot,\text{level2}}(g)$, for different learning algorithms for 100 random permutations of learning and test synthetic datasets

| | Level 1 | |
|---|---|---|
| | bk-risk $R^{\text{bk,level 1}}(g)$ | exp risk ($5 \times 3$) $R^{\text{exp,level 1}}(g)$ |
| ova-SVM | 0.0012 | 0.0107 |
| decision tree | 0.0007 | 0.0533 |
| kNN ($k = 5$) | 0.0013 | 0 |
| ANN (10 layers) | 0.0006 | 0.5773 |
| NMC | 0.0161 | 0 |

| | Level 2 | |
|---|---|---|
| | bk-risk $R^{\text{bk,level 2}}(g)$ | exp risk ($3 \times 3$) $R^{\text{exp,level 2}}(g)$ |
| ova-SVM | 0.0096 | 0.3333 |
| decision tree | 0.0013 | 0.6667 |
| kNN ($k = 5$) | 0.0079 | 0 |
| ANN (10 layers) | 0.0017 | 0.5773 |
| NMC | 0.1044 | 0 |

Table 9.1 shows results for both levels and for both synthetic and real data. We observe that kNN and NMC succeed in classifying all the experimental data, while decision trees and Neural Networks perform extremely poorly on experimental data. This demonstrates empirically that SVM, ANN and decision trees are more sensitive to data uncertainty than kNN and NMC. We further observe that, among the choices considered in this work, kNN is the only option that guarantees accurate synthetic and experimental performances.

Before concluding, we apply the five classification algorithms considered in the previous test to the four-way classification task based on the outputs $\{A^{\cdot}_{i,j}(f^q)\}_{i,j,q}$ (i.e., $Q = 144$ predictors, single-level classification). For this test, we reserve $M = 7 \cdot 10^3$ datapoints for learning, and $3 \cdot 10^3$ datapoints for testing; furthermore, we average results over 40 random

splits of the datasets. Table 9.2 shows the results for both standardized and unstandardized data. We observe that classifiers built on the full dataset of outputs $\{A_{i,j}^{\cdot}(f^q)\}_{i,j,q}$ are significantly more sensitive to data perturbations. This explains the poor performance on real data.

**Table 9.2:** Classification performances for four-way classification based on the bk (or experimental) outputs $\{A_{i,j}^{\cdot}(f^q)\}_{i,j,q}$. Bk and exp risks, $R^{\text{bk}}(g)$ and $R^{\text{exp}}(g)$ for different learning algorithms for 40 random permutations of learning and test synthetic datasets.

**(a)** with standardization

| | bk-risk $R^{\text{bk}}(g)$ | exp risk $(5 \times 3)$ $R^{\text{exp}}(g)$ |
|---|---|---|
| ova-SVM | 0 | 0.6000 |
| decision tree | 0.0018 | 0.6422 |
| kNN ($k = 5$) | 0.0003 | 0.8000 |
| ANN (10 layers) | 0.0003 | 0.8000 |
| NMC | 0.0921 | 0.6000 |

**(b)** no standardization

| | bk-risk $R^{\text{bk}}(g)$ | exp risk $(5 \times 3)$ $R^{\text{exp}}(g)$ |
|---|---|---|
| ova-SVM | 0.0213 | 0.2000 |
| decision tree | 0.0016 | 0.6400 |
| kNN ($k = 5$) | 0.0141 | 0.0133 |
| ANN (10 layers) | 0 | 0.4889 |
| NMC | 0.2453 | 0.5978 |

## 9.4 Two model-based approaches for the microtruss problem

### 9.4.1 Formulation of the inverse problem

As explained in the introduction, in the model-based approach we first must solve an inverse problem for the full parameter vector $\mu$, and then return the label $\hat{y} = f^{\text{dam}}(\mu^\star)$ where $\mu^\star$ is the estimate of the anticipated configuration. In this section, we appeal to a deterministic approach to tackle the inverse problem. Given the features $\mathbf{z}_1^\star, \mathbf{z}_2^\star \in \mathbb{R}^{Q_f}$, we consider two different minimization statements:

$$\mu^{\star,1} = \arg \min_{\mu \in \mathcal{P}^{\text{bk}}} \|\mathbf{z}_1^\star - \mathbf{z}_1^{\text{bk}}(\mu)\|_2^2 + \|\mathbf{z}_2^\star - \mathbf{z}_2^{\text{bk}}(\mu)\|_2^2, \tag{9.4.1}$$

and

$$\mu^{\star,2} = \arg \min_{\mu \in \bigcup_{k=1}^{4} \widetilde{S}_k} \|\mathbf{z}_1^\star - \mathbf{z}_1^{\mathrm{bk}}(\mu)\|_2^2 + \|\mathbf{z}_2^\star - \mathbf{z}_2^{\mathrm{bk}}(\mu)\|_2^2, \tag{9.4.2}$$

where $\widetilde{S}_k = \{\mu = [\alpha, \beta, E, s_L, s_R] \in \mathcal{P}^{\mathrm{bk}} : (s_L, s_R) \in S_k\}$, and $S_1, \ldots, S_4$ are the regions defined in (7.6.7). We remark that in both approaches we estimate both the quantities directly related to our definition of damage (the geometric quantities $s_L, s_R$), and the nuisance variables (the material properties $E, \alpha, \beta$).

We resort to an off-the-shelf Matlab optimizer to solve (9.4.1) and (9.4.2). In more detail, we resort to `fmincon`, and we consider both on an interior-point algorithm (see, e.g., [43]), and a sequential quadratic programming (SQP, see e.g. [35]) method for non-convex optimization. The gradient of the objective function is estimated through finite difference. We appeal to the RB approximation described in this chapter to reduce the computational burden. For (9.4.1), we consider four different initial conditions — one for each region $\widetilde{S}_1, \ldots, \widetilde{S}_4$. On the other hand, we decompose (9.4.2) into the four distinct problems

$$\mu^{\star,2,k} = \arg \min_{\mu \in \widetilde{S}_k} \|\mathbf{z}_1^\star - \mathbf{z}_1^{\mathrm{bk}}(\mu)\|_2^2 + \|\mathbf{z}_2^\star - \mathbf{z}_2^{\mathrm{bk}}(\mu)\|_2^2, \qquad k = 1, \ldots, 4,$$

and then we define $\mu^{\star,2}$ as follows:

$$\mu^{\star,2} = \arg \min_{\mu \in \{\mu^{\star,2,k}\}_{k=1}^{4}} \|\mathbf{z}_1^\star - \mathbf{z}_1^{\mathrm{bk}}(\mu)\|_2^2 + \|\mathbf{z}_2^\star - \mathbf{z}_2^{\mathrm{bk}}(\mu)\|_2^2.$$

### 9.4.2 Numerical results

Table 9.3 shows the unnormalized confusion matrices for synthetic ($M = 40$) and experimental ($M = 5 \cdot 3$) data. We observe that both approaches classify correctly all synthetic datapoints, but they fail to discriminate between the states $y = 1$ and $y = 4$ for real data. The reason is the presence of non-parametric error in the mathematical model. As observed in Chapter 8.1, this should not be surprising: the estimate of the full vector $\mu$ is a much more general problem than the estimate of the state of damage $f^{\mathrm{dam}}(\mu)$, and thus is more likely to be ill-posed (see [220, Chapter 1.9]). We observe that it could be reasonably contended that the inability to discriminate $y = 1$ and $y = 4$ is due to the lack of any regularization relative to $\mu$ (apart from the constraint $\mu \in \mathcal{P}^{\mathrm{bk}}$). However, although we could certainly

include a prior relative to the anticipated physical problems, we cannot in good faith include any prior information on the geometric parameters directly related to damage.

As regards the computational cost, a typical solve for a single initial condition requires roughly $100 - 150$ iterations and $800 - 1000$ evaluations of the objective ($7200 - 9000$ PDE solves) for the interior-point algorithm, and $30 - 50$ iterations and $300 - 500$ evaluations of the objective for SQP. For more challenging problems with several parameters the required number of iterations and also the number of required restarts would be much larger. For this reason, despite more advanced model reduction techniques as well as more careful implementations might speed up calculations, we envision that the approach is not well-suited for real-time calculations.

**Table 9.3:** Confusion matrices for the model-based approaches (9.4.1) and (9.4.2) for synthetic and real data. Results reported are based on the interior-point algorithm.

**(a)** Strategy (9.4.1)

| | Synthetic data | | | |
|---|---|---|---|---|
| | $y=1$ | $y=2$ | $y=3$ | $y=4$ |
| $\hat{y}=1$ | 11 | 0 | 0 | 0 |
| $\hat{y}=2$ | 0 | 9 | 0 | 0 |
| $\hat{y}=3$ | 0 | 0 | 11 | 0 |
| $\hat{y}=4$ | 0 | 0 | 0 | 9 |

**(b)** Strategy (9.4.2)

| | Synthetic data | | | |
|---|---|---|---|---|
| | $y=1$ | $y=2$ | $y=3$ | $y=4$ |
| $\hat{y}=1$ | 11 | 0 | 0 | 0 |
| $\hat{y}=2$ | 0 | 9 | 0 | 0 |
| $\hat{y}=3$ | 0 | 0 | 11 | 0 |
| $\hat{y}=4$ | 0 | 0 | 0 | 9 |

**(c)** Strategy (9.4.1)

| | Real data | | | |
|---|---|---|---|---|
| | $y=1$ | $y=2$ | $y=3$ | $y=4$ |
| $\hat{y}=1$ | 0 | 2 | 0 | 1 |
| $\hat{y}=2$ | 0 | 0 | 0 | 0 |
| $\hat{y}=3$ | 0 | 0 | 6 | 0 |
| $\hat{y}=4$ | 0 | 0 | 0 | 6 |

**(d)** Strategy (9.4.2)

| | Real data | | | |
|---|---|---|---|---|
| | $y=1$ | $y=2$ | $y=3$ | $y=4$ |
| $\hat{y}=1$ | 3 | 0 | 0 | 0 |
| $\hat{y}=2$ | 0 | 0 | 0 | 0 |
| $\hat{y}=3$ | 0 | 0 | 6 | 0 |
| $\hat{y}=4$ | 6 | 0 | 0 | 0 |

## 9.5 Conclusions

We applied the Simulation-Based approach presented in Chapter 8 to the microtruss problem. We introduced physically-informed features, which are tailored to the particular states of damage we wish to detect, and a Reduced Basis approximation, which dramatically reduces the offline computational cost. We applied five different machine learning algorithms, at least one of which performs very well on both synthetic and real (experimental) data.

We further discussed the application of two model-based approaches to the same classification problem. Numerical results show that, although both model-based approaches are

accurate for synthetic data, they are not able to discriminate between the state $y = 1$ and the state $y = 4$ for experimental data. This empirically shows that both these model-based approaches are more sensitive to model error than the simulation-based technique discussed in this thesis. Furthermore, they are not well-suited for the real-time framework due to the large amount of PDE solves required online.

# Chapter 10

# Conclusions

## 10.1 Summary and conclusions

This thesis presents work toward the development of efficient model reduction strategies for Data Assimilation (DA) for systems modeled by PDEs. We specifically focused on two DA tasks: state estimation for stationary problems, and damage identification for SHM applications.

In **Part I** of the present thesis, we developed and analysed the Parametrized-Background Data-Weak (PBDW) approach to the problem of steady-state variational data assimilation (state estimation). The approach was originally proposed by Maday et al. in [142] for perfect measurements and is characterized by the following characteristics.

- *Projection-by-data:* in PBDW the mathematical model is only used to generate the background space $\mathcal{Z}_N$. This feature simplifies the implementation, and provides flexibility regarding the choice of the domain of interest $\Omega$ and the choice of the ambient space $\mathcal{U}$.

- *Variational formulation:* PBDW relies on a variational formulation. This feature provides a suitable framework for the analysis, and also for properly addressing tasks related to the design of experiments (e.g. sensor placement).

- *Background and update spaces:* PBDW state estimate is the sum of two components: the former, the deduced background $z^\star$, is informed by the experimental observations, through the background space $\mathcal{Z}_N$, and addresses the uncertainty in the parameters of the model; the latter, the update $\eta^\star$, is informed by the experimental observations,

through the space of Riesz representers $\mathcal{U}_M$, and addresses the deficiencies of the bk model.

In this work, we provided three contributions to the original PBDW formulation.

- *A posteriori error analysis* (Chapter 4): we proposed an experimental procedure based on Monte Carlo sampling of observation functionals that provides confidence intervals for the $L^2$ error in state and the error in $L^2$ outputs. Although the error estimation procedure was primarily designed to certify the accuracy of a given state estimate, it can also be applied to other DA assimilation tasks: (i) the prediction of $L^2$ outputs, (ii) the data-driven empirical enrichment of the PBDW background space $\mathcal{Z}_N$ based on unmodeled physics identified through a set of preliminary (offline) DA results, and (iii) the adaptive selection of the PBDW tunable parameters.

- *Localised state estimation* (Chapter 5): we proposed a model reduction approach for the construction of local approximation spaces over a domain $\Omega$ strictly contained in the domain $\Omega^{\text{bk}}$ in which the PDE model (and thus the corresponding solution manifold) is properly defined. We presented a thorough mathematical analysis to prove the optimality (in the sense of Kolmogorov) of our construction, and we also presented several numerical results to show its effectiveness.

- *State estimation based on pointwise noisy measurements* (Chapter 6): we extended the PBDW formulation to pointwise noisy measurements. By exploiting the theory of RKHS, we considered spaces $\mathcal{U}$ for which the Riesz representers $\{K_{x_m}\}_m$ associated with the observation functionals $\{\delta_{x_m}\}_m$ are explicitly known. We demonstrated that explicit expressions for the representers greatly improve the flexibility of the approach, and also guarantee faster convergence with respect to the number of measurements $M$ than in the approach presented in [142, 143]. The extension relies on an adaptive procedure — guided by the error estimator developed in Chapter 4 — that takes into account the noise, model accuracy, and the characteristic length-scale of the difference $u^{\text{true}} - z^\star_\xi$. In particular, adaptation in the value of $\xi$ allows us to properly weight the trust in the bk model with respect to the trust in the experimental measurements. We presented *a priori* error estimates to motivate the approach from a theoretical standpoint, and several numerical examples to illustrate the different elements of the methodology.

In **Part II**, we proposed a Simulation-Based approach for classification, and we discussed its application to a Structural Health Monitoring problem, the microtruss problem. Simulation-Based approaches exploit (i) synthetic results obtained by repeated solution of a parametrized mathematical model for different values of the parameters (corresponding to different configurations), and (ii) supervised-learning algorithms to generate a classifier that monitors the damage state of the system. In this thesis, we exploited recent advances in parametric Model Order Reduction to reduce the computational burden associated with the construction of the offline training dataset, we proposed a mathematical formulation which integrates the PDE model within the classification framework, and we derived an error bound which clarifies the influence of model error on classification performance. We finally applied our technique to the microtruss problem: for certain choices of the classifiers we were able to predict the correct state of damage associated with experimental configurations.

## 10.2 Future work

During the course of this work, we have identified several areas of future research. For purposes of presentation, we shall distinguish between state estimation and damage identification.

### 10.2.1 State estimation

#### Generalization of the PBDW formulation

In section 2.1.1, we found that we can rewrite the partial-spline model for a rank-$N$ background, $u_N^{\text{bk}}(x;\mu) = \sum_{n=1}^N \phi_n(\mu)\zeta_n(x)$, as (cf. (2.1.4)):

$$(\mu_\xi^\star, \eta_\xi^\star) := \arg \min_{(\mu,\eta)\in\mathcal{P}^{\text{bk}}\times\mathcal{U}} \xi\|\eta\|^2 + \frac{1}{M}\sum_{m=1}^M \left(\ell_m^o\left(\sum_{n=1}^N \phi_n(\mu)\zeta_n\right) + \ell_m^o(\eta) - \ell_m^{\text{obs}}\right)^2,$$

and we can then define the corresponding state estimate $u_\xi^\star = \sum_{n=1}^N \phi_n(\mu_\xi^\star)\zeta_n + \eta_\xi^\star$. It is straightforward to verify that the state estimate $u_\xi^\star$ equals $\hat{u}_\xi^\star = \sum_{n=1}^N \widehat{\phi}_{\xi,n}\,\zeta_n + \hat{\eta}_\xi^\star$, where

$$(\widehat{\phi}_\xi^\star, \hat{\eta}_\xi^\star) = \arg \min_{(\phi,\eta)\in\Phi_N\times\mathcal{U}} \xi\|\eta\|^2 + \frac{1}{M}\sum_{m=1}^M \left(\ell_m^o\left(\sum_{n=1}^N \phi_n\,\zeta_n\right) + \ell_m^o(\eta) - \ell_m^{\text{obs}}\right)^2,$$

and $\Phi_N = \{[\phi_1(\mu), \ldots, \phi_N(\mu)] : \mu \in \mathcal{P}^{\text{bk}}\}$.

In this thesis, we substituted $\Phi_N$ with the full space $\mathbb{R}^N$ to obtain the PBDW formulation (2.1.5). Although this greatly simplifies the implementation, and also the analysis, it might lead to an excessive loss of information, especially when $N \approx M$. If we denote by $\bar{\mu} \in \mathcal{P}^{\text{bk}}$ the centroid of $\mathcal{P}^{\text{bk}}$ and we normalize the basis $\zeta_1, \ldots, \zeta_N$, we typically observe

$$\max_{\mu \in \mathcal{P}^{\text{bk}}} |\phi_1(\mu) - \phi_1(\bar{\mu})| \gg \max_{\mu \in \mathcal{P}^{\text{bk}}} |\phi_2(\mu) - \phi_2(\bar{\mu})| \gg \ldots$$

By considering $\Phi_N = \mathbb{R}^N$, we completely discard this information.

Based on the previous discussion, we might consider more stringent relaxations $\widetilde{\Phi}_N \subsetneq \mathbb{R}^N$. Clearly, the choice of $\widetilde{\Phi}_N$ should be a compromise between (i) proximity of $\widetilde{\Phi}_N$ to $\Phi_N$, and (ii) computational complexity associated with the corresponding optimization problem to solve. In this respect, in [33], the authors proposed a generalization of the PBDW in this direction, which corresponds to the solution to a suitable recovery problem of the form described in Chapter 2.2.2.

### Localised state estimation with nonlinear models

In Chapter 5, we presented a computational approach to construct local approximation spaces associated with potentially high-dimensional solution manifolds. The procedure — based on the solution to a transfer eigenproblem — and the analysis relied on the assumption that the underlined PDE model was linear. Extending the computational procedure and, even more ambitiously, the analysis to nonlinear problems would increase significantly the range of applications to which the technique can be applied.

### Selection of the observation centers for pointwise measurements

In Chapter 3, we presented a strategy (cf. Algorithm 3.2.1) for the selection of transducers' locations for the noise-free PBDW formulation based on the maximization of the inf-sup constant $\beta_{N,M}$. Numerical results demonstrated the importance of properly chosing the observation centers for $N \simeq M$. In Chapter 6, we observed that if we rely on explicit kernels we cannot in general compute the inf-sup constant $\beta_{N,M}$; as a result, we cannot apply Algorithm 3.2.1 for the selection of the observation centers.

For this reason, we aim to design strategies for the selection of the observation centers

that address both stability and approximation that do not involve the calculation of the inf-sup constant $\beta_{N,M}$. In this respect, we wish to combine the Greedy procedure presented in Algorithm 3.2.1 with techniques developed in the kernel methods' literature for collocation methods for PDEs ([111, 198]) and scattered data approximation ([156, section 3.1.1], [237]).

### 10.2.2 Damage identification

#### High-dimensional damage description: PR-scRBE

A prerequisite for good classifier performance is a sufficiently rich description of undamaged and damaged states. Absent such a complete description (i) a classifier will certainly not be able to discriminate between different states of damage (not represented in the offline training dataset), and (ii) we may not be able to identify features which can discriminate between undamaged and damaged states.

For practical engineering systems — such as airframes, shiploaders, bridges, offshore platforms — accurate parametrizations should take into account variations in material properties, geometry, boundary conditions, and also topology; this clearly leads to very high-dimensional parameter domains. The dimensionality of the parameter domain precludes application of the classical Reduced Basis approach employed in this thesis: we are confronted with the well-known curse of dimensionality. However, we might appeal to a more ambitious parametrized Model Order Reduction approach: the Port-Reduced static-condensation Reduced-Basis-Element (PR-scRBE, [171, 72, 203]) method. PR-scRBE combines Component Model Synthesis (CMS) technique [116, 11]— as regards components and ports — and the Reduced Basis (RB) method — as regards bubbles and in particular parametric treatment.

The PR-scRBE method, like the simpler classical RB approach, consists of two stages: a pMOR offline stage, and a pMOR online stage. During the offline stage, we construct a library of parametrized and interoperable archetype components. Each archetype component represents a specific geometric form, for instance a beam or a fin, and may feature various ports of different types; in addition, all components of a library share the same parametrized mathematical component (e.g., Helmholtz acoustics, Helmholtz elasto-dynamics, heat-transfer). During the online stage, we synthesize any parametrized bk model, for given bk model parameter $\mu \in \mathcal{P}^{\text{bk}}$, as an assembly of instantiated archetype compo-

nents. We then appeal to the RB method to reduce the degrees of freedom in the interior of each component, and we appeal to port-reduction approaches to reduce the degrees of freedom at the interfaces (ports) between components. The combination of these two reduction techniques leads to a dramatic decrease of the total number of degrees of freedom compared to the high-fidelity model, and thus leads to dramatic computational speed-ups.

For many engineering systems of interest for SHM applications, the description of damaged and undamaged system configurations in terms of components is particularly favorable. We have indeed that many of the systems described above are naturally described by an assembly of, possibly parametrized, building blocks; in addition, damage generation is a local phenomenon, and thus can be effectively described at the component-level. For this reason, we envision that the use of PR-scRBE might enable us to tackle more realistic engineering problems.

### Automatic feature identification

As shown in the numerical results of Chapter 9, appropriate choice of features is absolutely crucial for classification. In particular, features which are sensitive to the anticipated damage but relatively insensitive to nuisance variables and measurement noise greatly simplify the classification task and ultimately improve the robustness and hence performance of the deployed classifier. Furthermore, we may view feature identification, or "extraction" — which includes both sensor placement and frequency selection, and perhaps also actuator considerations — within the broader context of Design of Experiment (DOE).

In this thesis, given the experimental outputs $\{A^{\text{exp}}_{i,j}(f^q)\}_{i,j,q}$, we proposed the features $\mathbf{z}_1(\cdot) = [z_1(f^1;\cdot)]_{q=1}^{Q_1}$, $\mathbf{z}_2(\cdot) = [z_2(f^1;\cdot)]_{q=1}^{Q_1}$ defined in (7.5.4) - (7.5.5). Numerical results demonstrate that our choices are well-suited to discriminate between the undamaged state and damaged states. The relations (7.5.4) - (7.5.5) are identified by inspection of bk model predictions, preliminary experimental studies (prior to the offline stage of the classification procedure), and physical arguments informed by the classical disciplines of elasticity and dynamics.

As future work, we wish to develop computational techniques for automatic, or at least semi-automatic, feature extraction. These methods promise not only more effective classifiers but also more effective deployment; for example, in the microtruss context, we may be able to reduce the number of sensors as well as the number of shaker excitation frequencies.

We envision that automatic feature extraction techniques can greatly benefit from recent advances in Robust Optimization (RO, [20, 30]) and Mixed Integer Optimization (MIO, [31]). Since RO and MIO techniques are directly informed by the target risk $R^{\text{bk}}(\cdot)$, we might design feature that are "optimal" with respect to our stated objectives as reflected in $w^{\text{bk}}$. We might also consider feature extraction by (grouped-)variable selection techniques developed in the DOE literature (see [121], [36, Section 7.5], [179]) for regression analysis.

### Impulsive and ambient loading

We have until this point largely taken the source and nature of excitation as given. We can expand our choices to perhaps better discriminate and to more effectively deploy.

For our microtruss problem, we resort to a shaker to apply a known displacement at prescribed frequencies. Shakers provide a high signal-to-noise ratio and furthermore can excite a broad range of modal frequencies. However, shakers are cumbersome and expensive to install and particularly difficult to apply *in situ*. Furthermore, shakers are not practicable if we wish to continually monitor structures in the field.

Impact hammers represent an important alternative to shakers for SHM actuation in particular as regards installation and operation. From a mathematical standpoint hammer excitation can be interpreted as an impulse in the time domain; the Laplace transform connects the frequency and time domain. An example of impulsive SHM is Acoustic Pulse Reflectometry (APR, [4, 200]): a microphone measures the reflections of an acoustic pulse in a pipeline to deduce damage "scatterers" such as holes or obstructions; similar concepts may be applied more generally within the elastodynamics context. Quite apart from practical considerations, these impulsive — effectively, time-of-flight — protocols would appear to offer very good sensitivity to damage; "feature extraction" concepts can then be applied to optimize sensor and actuator location and also sampling strategies.

It is also of interest to consider not just *active* systems in which we provide forced and controlled (say, hammer) input excitations, but also *passive* systems — "output-only" methods — which rely on ambient loading as naturally arises in operation of the deployed system ([79, Chapter 4.11],[65]). The latter are of course ideal as regards installation and maintenance in real structures in the field. The SHM literature proposes a variety of approaches for passive systems: in particular we cite Operational Modal Analysis (OMA, [6]) which identifies modal properties of structures from ambient vibration data; representative examples

of OMA techniques include peak-picking ([146]), Frequency Domain Decomposition (FDD, [39]), and Time Domain Decomposition (TDD, [125]).

Integration of our pMOR Simulation Based Classification approach to SHM with time-domain analysis and impulsive excitation, and ambient or operational load conditions represents a very promising area of future research.

# Appendix A

# *A posteriori* error estimation: analysis of the finite-$\nu$ error

In this Appendix, we present a thorough analysis of the finite-$\nu$ error in both $L^2$ functionals and $L^2$ error. In more detail, we rigorously demonstrate that finite-$\nu$ error is a balance between transducer resolution and regularity of the spatial field. In section A.1, we present a number of definitions, and an useful lemma. Then, in section A.2, we present the proofs of the two main results presented in Chapter 4.

## A.1 Preliminaries

We first introduce the convolutional kernel

$$\omega_{d,\nu}(r) = \frac{C(d)}{\nu^d}\omega\left(\frac{r}{\nu}\right), \tag{A.1.1a}$$

where $C(d)$ is a normalization constant such that

$$\int_{\mathbb{R}^d} \omega_{d,\nu}(|x-y|)\,dx = 1, \qquad \forall\, x, y \in \mathbb{R}^d, \tag{A.1.1b}$$

and $\omega : \mathbb{R}_+ \to \mathbb{R}_+$ is a positive function such that

$$\omega(\rho) = 0, \quad \forall\, \rho \geq 1. \tag{A.1.1c}$$

Given $\omega_{d,\nu}$, we can introduce the function $g_d : \mathbb{R}_+ \to \mathbb{R}_+$ such that

$$g_d(r) := \frac{C(d)}{r^{d-1}} \int_0^{1/r} \frac{1}{s^{d+1}} \omega\left(\frac{1}{s}\right) ds, \tag{A.1.2}$$

and the constant

$$C_\omega(p,d) = \left(\mathcal{A}(d) \int_0^\infty (g_d(r))^p r^{d-1}\, dr\right)^{1/p}, \tag{A.1.3}$$

where $\mathcal{A}(1) = 2$, $\mathcal{A}(2) = 2\pi$, $\mathcal{A}(3) = 4\pi$ is related to the dimension.

Next Lemma shows that $C_\omega(p,d)$ is finite if $p < \frac{d}{d-1}$ and $\omega(r) \sim r^{-\alpha}$ as $r \to 0^+$ for some $\alpha < d$.

**Lemma A.1.1.** *Let $p < \frac{d}{d-1}$ and let $\omega_{d,\nu}$ be the kernel defined in* (A.1.1). *Then, if $\omega(r) \sim r^{-\alpha}$ as $r \to 0^+$ for some $\alpha < d$, the constant $C_\omega(p,d)$ in* (A.1.3) *is finite.*

*Proof.* Let us consider the function

$$\hat{g}_d(r) := \int_0^{1/r} \frac{1}{s^{d+1}} \omega\left(\frac{1}{s}\right) ds.$$

Applying change-of-variables formula, and recalling (A.1.1c), we find

$$\hat{g}_d(r) = \begin{cases} \displaystyle\int_r^1 s^{d-1}\omega(s)\, ds & \text{if } s \le 1; \\ 0 & \text{otherwise.} \end{cases}$$

Since $\omega(r) \sim r^{-\alpha}$ as $r \to 0^+$ for $\alpha < d$, $\hat{g}_d$ is bounded for any $r \ge 0$.

We now consider the integral

$$(C_\omega(p,d))^p = \mathcal{A}(d) \int_0^\infty (g_d(r))^p\, r^{d-1}\, dr \;=\; \mathcal{A}(d) \int_0^1 [\hat{g}_d(r)]^p\; r^{(d-1)(1-p)}\, dr.$$

Since $\hat{g}_d$ is finite for $r \to 0^+$, $C_\omega(p,d)$ is finite if and only if $(d-1)(1-p) > -1$, which implies $p < \frac{d}{d-1}$. Thesis follows. □

Previous definitions are motivated by Lemma A.1.2.

**Lemma A.1.2.** *Let $\xi \in W^{1,q}(\Omega^{\text{obs}})$, where $\Omega^{\text{obs}} \subset \mathbb{R}^d$ and $q \in (d, \infty]$, and let $\omega_{d,\nu}$ be a convolutational kernel. Let us further recall the definition of $\nu$-neighborhood of $\Omega$ $\Omega_\nu = \{x \in \mathbb{R}^d : dist(\Omega, x) < \nu\}$.*

*Then, if $\Omega_\nu \subset\subset \Omega^{\text{obs}}$, the following estimate holds:*

$$\|\mathcal{F}_\nu(\xi) - \xi\|_{L^\infty(\Omega)} \leq C_\omega(p,d)\nu^{1-d/q}\|\nabla\xi\|_{L^q(\Omega_\nu)}, \tag{A.1.4}$$

*where $C_\omega(p,d)$ is defined in (A.1.3) and $\mathcal{F}_\nu(\xi)(x) = \int_{\Omega^{\text{obs}}} \omega_{d,\nu}(|x-y|)\,\xi(y)\,dy$.*

*Proof.* Since $\xi \in C(\Omega^{\text{obs}})$ (see, e.g., [181, Theorem 1.3.5]), we must show that $|\mathcal{F}_\nu(\xi)(x) - \xi(x)| \leq C_\omega(p,d)\nu^{1-d/q}\|\nabla\xi\|_{L^q(\Omega^{\text{obs}})}$ for all $x \in \Omega$. With no loss of generality, we assume $\xi \in C^1(\Omega^{\text{obs}})$; the generalization to $\xi \in W^{1,q}$ can be performed using a density argument. We omit this passage.

Let us take $\bar{x} \in \Omega$. Since $\Omega_\nu \subset\subset \Omega^{\text{obs}}$, we have that $\bar{x} + \mathcal{B}_\nu(0) \subset \Omega^{\text{obs}}$. Then, referring to the Fubini theorem and the Cauchy-Schwartz and Hölder inequalities, we can estimate $\mathcal{F}_\nu(\xi)(\bar{x}) - \xi(\bar{x})$ as

$$\begin{aligned}
\mathcal{F}_\nu(\xi)(\bar{x}) - \xi(\bar{x}) &= \int_{\Omega^{\text{obs}}} \omega_{d,\nu}(|x-\bar{x}|)\,\xi(x)\,dx - \xi(\bar{x}), \\
&\doteq \int_{\Omega^{\text{obs}}} \omega_{d,\nu}(|x-\bar{x}|)\,(\xi(x) - \xi(\bar{x}))\,dx && \text{(A.1.1b)}, \\
&= \int_{\Omega^{\text{obs}}} \frac{C(d)}{\nu^d}\,\omega(|x-\bar{x}|/\nu)\left(\int_0^1 \nabla\xi(\bar{x} + t(x-\bar{x}))\cdot(x-\bar{x})\,dt\right)dx, \\
&= \int_0^1 \left(\int_{\mathcal{B}_\nu(\bar{x})} \frac{C(d)}{\nu^d}\,\omega(|x-\bar{x}|/\nu)\,\nabla\xi(\bar{x} + t(x-\bar{x}))\cdot(x-\bar{x})\,dx\right)dt && \text{(Fubini theorem)}, \\
&= \int_0^1 \left(\int_{\mathcal{B}_{t\nu}(0)} \frac{C(d)}{\nu^d t^{d+1}}\,\omega(|y|/t\nu)\,\nabla\xi(\bar{x}+y)\cdot y\,dy\right)dt && (t(x-\bar{x}) = y,\ t^d dx = dy), \\
&= \int_0^1 \left(\int_{\mathcal{B}_\nu(0)} \frac{C(d)}{\nu^d t^{d+1}}\,\omega(|y|/t\nu)\,\nabla\xi(\bar{x}+y)\cdot y\,dy\right)dt && (\omega(\rho) = 0,\ \forall\,\rho \geq 1), \\
&= \int_{\mathcal{B}_\nu(0)} \nabla\xi(\bar{x}+y)\cdot y\left(\int_0^1 \frac{C(d)}{\nu^d t^{d+1}}\,\omega(|y|/t\nu)\,dt\right)dy, && \text{(Fubini theorem)} \\
&= \int_{\mathcal{B}_\nu(\bar{x})} \nabla\xi(\bar{x}+y)\cdot y\,\frac{1}{|y|^d}\left(\int_0^{\nu/|y|} \frac{C(d)}{s^{d+1}}\,\omega(1/s)\,ds\right)dy, && (t\nu/|y| = s) \\
&= \int_{\mathcal{B}_\nu(\bar{x})} \nabla\xi(\bar{x}+y)\cdot\frac{y}{|y|}\,\frac{1}{\nu^{d-1}}\,g_d(|y|/\nu)\,dy
\end{aligned}$$

$$\mathcal{F}_\nu(\xi)(\bar{x}) - \xi(\bar{x}) \leq \|\frac{1}{\nu^{d-1}} g_d(|\cdot|/\nu)\|_{L^p(\mathbb{R}^d)}\|\nabla\xi\|_{L^q(\Omega_\nu)} \quad \text{(Hölder)}.$$

We finally observe that:

$$\begin{aligned}\|\tfrac{1}{\nu^{d-1}} g_d(|\cdot|/\nu)\|_{L^p(\mathbb{R}^d)} &= \tfrac{1}{\nu^{d-1}} \left(\int_0^\infty (g_d(\rho/\nu))\, \rho^{d-1}\, d\rho\right)^{1/p} \\ &= \left(\mathcal{A}(d)\, \int_0^\infty (g_d(r))^p r^{d-1}\, dr\right)^{1/p} \nu^{d/p-d+1} = C_{\omega(p,d)}\, \nu^{d/p-d+1}.\end{aligned}$$

Thesis follows. □

## A.2 Error bounds for the finite-$\nu$ error

We now wish to apply Lemma A.1.2 to show error bounds for the finite-$\nu$ error in output functionals and in $L^2$ error. For convenience, we report the statements already presented in Chapter 4.

**Proposition A.2.1.** *Let $\omega_{d,\nu}$ be a convolutional kernel of the form* (A.1.1) *such that $\omega(r) \sim r^{-\alpha}$ for some $\alpha < d$. Then, if $\Omega_\nu \subset\subset \Omega^{\text{obs}}$, the following hold.*

- *If $e \in W^{1,q}(\Omega^{\text{obs}})$, $q \in (d, \infty]$, then*

$$|E_{\mathcal{L}} - \hat{E}^{\infty}_{\mathcal{L}}| \leq C_\omega(p,d) \nu^{1-d/q} |\Omega|^{1/2} \|\zeta\|_{L^2(\Omega)} \|\nabla e\|_{L^q(\Omega_\nu)}. \tag{A.2.1a}$$

- *If $\zeta \in W^{1,q}(\Omega)$, $q \in (d, \infty]$, $e \in L^\infty(\Omega^{\text{obs}})$, then*

$$\begin{aligned}|E_{\mathcal{L}} - \widehat{E}^{\infty}_{\mathcal{L}}| \leq\ & C_\omega(p,d)\, C_1(\Omega, \Omega^{\text{obs}}) \nu^{1-d/q} \|e\|_{L^2(\Omega)} \|\zeta\|_{W^{1,q}(\Omega)} \\ & + C_2(\Omega, \Omega^{\text{obs}}) \nu \|e\|_{L^\infty(\Omega_\nu)} \|\zeta\|_{W^{1,q}(\Omega)}.\end{aligned} \tag{A.2.1b}$$

*Proof.* Estimate (A.2.1a) follows by applying Lemma A.1.2 and the Cauchy-Schwartz inequality.

We now show (A.2.1b). Since $\Omega_\nu \subset\subset \Omega^{\text{obs}}$, recalling [1, Theorem 5.24], there exists $\zeta^{\text{ext}} \in W^{1,q}(\Omega^{\text{obs}})$ such that

$$\zeta^{\text{ext}}|_\Omega \equiv \zeta, \qquad \|\zeta^{\text{ext}}\|_{W^{1,q}(\Omega^{\text{obs}})} \leq C_1(\Omega, \Omega^{\text{obs}}) \|\zeta\|_{W^{1,q}(\Omega)}. \tag{A.2.2}$$

Then, we introduce $\widehat{\mathcal{F}}_\nu : L^2(\Omega_\nu) \mapsto L^2(\Omega_\nu)$ such that

$$\widehat{\mathcal{F}}_\nu(w) = \int_{\Omega_\nu} \omega_{d,\nu}(|x-y|) w(y)\, dy. \tag{A.2.3}$$

We observe that for all $w \in L^\infty(\Omega_\nu)$, we have

$$\widehat{\mathcal{F}}_\nu(w)(x) = \mathcal{F}_\nu(w)(x),\ \forall\, x \in \Omega; \quad |\widehat{\mathcal{F}}_\nu(w)(x)| \le \|w\|_{L^\infty(\Omega_\nu)}\ \forall\, x \in \Omega_\nu \setminus \Omega. \tag{A.2.4}$$

It follows from (A.2.3) and (A.2.4) that

$$\begin{aligned}\int_\Omega \zeta(y)\,\mathcal{F}_\nu(e)(y)\,dy = &\int_{\Omega_\nu} \zeta^{\rm ext}(y)\,\Big(\int_{\Omega_\nu} \omega_{d,\nu}(|x-y|)e(x)\,dx\Big)\,dy - \int_{\Omega_\nu\setminus\Omega} \zeta^{\rm ext}(y)\,\widehat{\mathcal{F}}_\nu(e)(y)\,dy\\ = &\int_\Omega e(x)\,\mathcal{F}_\nu(\zeta^{\rm ext})(x)\,dx + \int_{\Omega_\nu\setminus\Omega}\Big(e(y)\,\widehat{\mathcal{F}}_\nu(\zeta^{\rm ext})(y) - \widehat{\mathcal{F}}_\nu(e)(y)\,\zeta^{\rm ext}(y)\Big)\,dy.\end{aligned}$$

Then,

$$E_{\mathcal{L}} - \widehat{E}^\infty_{\mathcal{L}} = \underbrace{\int_\Omega e(x)\,\big(\zeta(x) - \mathcal{F}_\nu(\zeta^{\rm ext})(x)\big)\,dx}_{(I)} + \underbrace{\int_{\Omega_\nu\setminus\Omega}\Big(e(y)\,\widehat{\mathcal{F}}_\nu(\zeta^{\rm ext})(y) - \widehat{\mathcal{F}}_\nu(e)(y)\,\zeta^{\rm ext}(y)\Big)\,dy}_{(II)}.$$

Applying Lemma A.1.2 to $\zeta^{\rm ext}$, recalling (A.2.2) and using the Cauchy-Schwartz inequality, we obtain

$$|(I)| \le C_\omega(p,d)\,C_1(\Omega,\Omega^{\rm obs})\nu^{1-d/q}\|e\|_{L^2(\Omega)}\|\zeta\|_{W^{1,q}(\Omega)}.$$

On the other hand, observing that for every $\xi \in L^\infty(\Omega^{\rm obs})$ we have that

$$\Big|\int_{\Omega_\nu\setminus\Omega} \xi(x)\,dx\Big| \le C(\Omega)\nu\|\xi\|_{L^\infty(\Omega^{\rm obs})},$$

we find that

$$\big|(II)\big| \le 2C(\Omega)\nu\|e\,\zeta^{\rm ext}\|_{L^\infty(\Omega_\nu)} \le C_2(\Omega,\Omega^{\rm obs})\nu\|e\|_{L^\infty(\Omega_\nu)}\|\zeta\|_{W^{1,q}(\Omega)}.$$

Thesis follows. □

**Proposition A.2.2.** *Let $e \in W^{1,q}(\Omega^{\rm obs})$, where $\Omega^{\rm obs} \subset \mathbb{R}^d$ and $q \in (d,\infty]$. Let $\omega_{d,\nu}$ be a convolutional kernel of the form* (A.1.1) *such that $\omega(r) \sim r^{-\alpha}$ for some $\alpha < d$. Then, if $\Omega_\nu \subset\subset \Omega^{\rm obs}$, the following estimate holds:*

$$\Delta^\nu(\nu) \le C_\omega(p,d)\sqrt{|\Omega|}\,\nu^{1-d/q}\,\|\nabla e\|_{L^q(\Omega_\nu)}. \tag{A.2.5}$$

*Proof.* Using the inverse triangle inequality, and (A.1.4), we find

$$\begin{aligned} |\widehat{E}^{\infty}(\nu) - E| = & \; |\|e\|_{L^2(\Omega)} - \|\mathcal{F}_\nu(e)\|_{L^2(\Omega)}| \leq \|e - \mathcal{F}_\nu(e)\|_{L^2(\Omega)}, \\ \leq & \; \sqrt{|\Omega|}\|e - \mathcal{F}_\nu(e)\|_{L^\infty(\Omega)} \leq C_\omega(p,d)\sqrt{|\Omega|}\,\nu^{1-d/q}\,\|\nabla e\|_{L^q(\Omega_\nu)}. \end{aligned}$$

□

# Appendix B

# *A posteriori* error estimation: extension to heteroscedastic noise

## B.1 Main result

We study the extension of the discussion of Chapter 4 to the case of heteroscedastic random noise. Specifically, we consider the following set of assumptions.

- **H1** $\{X_j\}_{j=1}^J$ is a sequence of $J$ i.i.d. random variables such that $X_j \sim \text{Uniform}(\Omega)$.
- **H2** $\{\varepsilon_j\}_{j=1}^J$ is a sequence of independent random variables such that $\mathbb{E}[\varepsilon_j] = 0$, $\mathbb{V}[\varepsilon_j] = \sigma_j^2 \in [\sigma_{LB}^2, \sigma_{UB}^2]$, and

$$\sup_j \mathbb{E}[|\varepsilon_j|^3] < \infty, \qquad \sup_j \mathbb{E}[|\varepsilon_j|^4] < \infty.$$

- **H3** $X_i$ and $\varepsilon_j$ are independent of each other $i, j = 1, \ldots, J$.

We observe that the extension to heteroscedastic noise does not affect our discussion about the finite-$\nu$ error; thus, in what follows, we only focus on finite-$J$ and finite-noise error. For simplicity, we only consider the case of $L^2(\Omega)$ functionals; the same ideas can also be applied to the estimation of the $L^2(\Omega)$ error.

We state the main result of this appendix.

**Theorem B.1.1.** *Let $\{F_j\}_{j=1}^\infty$ and $\{G_j\}_{j=1}^\infty$ be two random sequences such that*

1. *$F_1, F_2, \ldots$ are i.i.d. random variables such that $\mathbb{E}[F_j] = \mu_F$, $\mathbb{V}[F_j] = \sigma_F^2$, $\mathbb{E}[|F_j|^3] < \infty$;*

2. $G_1, G_2, \ldots$ *are independent random variables such that* $\mathbb{E}[G_j] = 0$, $\mathbb{V}[G_j] = \sigma_j^2 \in [\sigma^2_{\min}, \sigma^2_{\max}]$, $\sup_j \mathbb{E}[|G_j|^3] < \infty$ *and* $\sup_j \mathbb{E}[|G_j|^4] < \infty$;

3. $\mathbb{E}[F_{j'} G_j] = 0$, $\sup_j \mathbb{E}[|F_j| G_j^2] < \infty$, $\sup_j \mathbb{E}[F_j^2 |G_j|] < \infty$ *for* $j, j' = 1, 2, \ldots$.

*Then, if we define* $Y_j = F_j + G_j$ *and the sample mean and variance*

$$\bar{Y}_J := \frac{1}{J} \sum_{j=1}^{\infty} Y_j, \qquad \widehat{se}^2_{Y,J} := \frac{1}{J} \sum_{j=1}^{\infty} (Y_j - \bar{Y}_J)^2, \tag{B.1.1}$$

*the confidence region*

$$\widehat{C}_J(\alpha) = \left[ \bar{Y}_J - \frac{z_{1-\alpha/2}}{\sqrt{J}} \sqrt{\widehat{se}^2_{Y,J} + \sigma^2_{\max} - \sigma^2_{\min} + \delta}, \quad \bar{Y}_J + \frac{z_{1-\alpha/2}}{\sqrt{J}} \sqrt{\widehat{se}^2_{Y,J} + \sigma^2_{\max} - \sigma^2_{\min} + \delta} \right] \tag{B.1.2}$$

*satisfies* $\liminf_J P\left(\mu_F \in \widehat{C}_J(\alpha)\right) \geq 1 - \alpha$, *for any* $\delta > 0$.

Theorem B.1.1 can be applied to the estimation of $\widehat{E}^{\infty}_{\mathcal{L}}(\nu)$ by considering

$$F_j = \mathcal{F}_\nu(e)(X_j)\, \zeta(X_j)\, |\Omega|, \quad G_j = \varepsilon_j\, \zeta(X_j)\, |\Omega|$$

and assuming that $\{X_j\}_{j=1}^J$ and $\{\varepsilon_j\}_{j=1}^J$ satisfy H1, H2, H3. We observe that the random variables $Y_j$ are observable – realizations of $\{Y_j\}_j$ are $\{\ell_j^{\text{err}}\}_j$; while we have that $\sigma^2_{\max} = E^2_\zeta \sigma^2_{UB}$ and $\sigma^2_{\min} = E^2_\zeta \sigma^2_{LB}$ with $E^2_\zeta = |\Omega|^2\, \mathbb{E}[\zeta(X_1)^2]$.

The remainder of this Appendix is organized as follows. In section B.2, we present four preliminary results. Then, in section B.3, we present the proof of Theorem B.1.1.

## B.2 Preliminaries

**Definition B.2.1.** *We say that the random sequence* $\{Z_j\}_j$ *converges in probability towards the random variable* $Z$ *if for all* $\delta > 0$*:*

$$\lim_{j \to \infty} P(|Z_j - Z| > \delta) = 0. \tag{B.2.1}$$

*We denote convergence in probability by* $p\lim_j Z_j = Z$.

**Lemma B.2.1.** *Let $\{Z_j\}_j$ be a sequence of random variables such that $\sup_j \mathbb{E}[Z_j^2] < \infty$, and $\mathbb{E}[Z_i\, Z_j] = 0$ if $i \neq j$. Then,*

$$p\lim_J \frac{1}{J}\sum_{j=1}^{J} Z_j = 0. \tag{B.2.2}$$

Lemma B.2.1 is a consequence of Chebyshev's inequality (see, e.g., [119, Chapter 5,Corollary 5.2]). We refer to Ref. [119, Exercise 20.1] for a guided proof.

**Lemma B.2.2.** *Let $\{Z_j\}_j$ be a random sequence of independent random variables such that $\mathbb{E}[Z_j] = \mu_j$, $\mathbb{V}[Z_j] = \sigma_j^2$, with $\mu_{\min} \leq \mu_j \leq \mu_{\max}$ and $\sigma_j^2 \leq \bar{\sigma}^2 < \infty$. Then, for every $\delta > 0$*

$$\lim_{J\to\infty} P\left(\mu_{\min} - \delta \leq \frac{1}{J}\sum_{j=1}^{J} Z_j \leq \mu_{\max} + \delta\right) = 1. \tag{B.2.3}$$

*Proof.* We observe that

$$\frac{1}{J}\sum_{j=1}^{J} Z_j \leq \frac{1}{J}\sum_{j=1}^{J}(Z_j - \mu_j + \mu_{\max}) = \frac{1}{J}\sum_{j=1}^{J} Z_j^o + \mu_{\max}; \tag{B.2.4a}$$

and

$$\frac{1}{J}\sum_{j=1}^{J} Z_j \geq \frac{1}{J}\sum_{j=1}^{J}(Z_j - \mu_j + \mu_{\min}) = \frac{1}{J}\sum_{j=1}^{J} Z_j^o + \mu_{\min}; \tag{B.2.4b}$$

where $Z_j^o = Z_j - \mu_j$.

We observe that the random sequence $\{Z_j^o\}_j$ satisfies the hypotheses of Lemma B.2.1. Then, thesis follows from (B.2.2). □

**Lemma B.2.3.** *Let $\{\Phi_j\}_j$, $\{\Psi_j\}_j$ be two random sequences such that*

*i* $p\lim_j \Phi_j - \Psi_j = 0$;

*ii there exists $\alpha, \beta > 0$ such that for all $\delta > 0$, $\lim_j P(\alpha - \delta \leq \Psi_j \leq \beta + \delta) = 1$.*

*Then, for every $\delta > 0$,*

$$\lim_j P(\alpha - \delta \leq \Phi_j \leq \beta + \delta) = 1.$$

*Proof.* Let us introduce the events

$$A_{J,\delta} := \{\omega : \ |\Phi_J(\omega) - \Psi_J(\omega)| \leq \tfrac{1}{2}\delta\},$$

$$E_{J,\delta} := \{\omega : \ \Psi_J(\omega) \in [\alpha - \delta/2, \beta + \delta/2]\},$$

where $\delta > 0$.

Using hypothesis (i), for any given $\delta' > 0$, there exists $J^\star$ such that for all $J \geq J^\star$:

$$\delta' \geq P(|\Phi_J(\omega) - \Psi_J(\omega)| \geq \delta/2) = 1 - P(|\Phi_J(\omega) - \Psi_J(\omega)| \leq \delta/2) = 1 - P(A_{J,\delta}).$$

Using the total probability theorem, we find

$$P(A_{J,\delta}) = P(A_{J,\delta} \cap E_{J,\delta}) + P(A_{J,\delta} \cap E^c_{J,\delta}).$$

We observe that

$$\begin{aligned} P(A_{J,\delta} \cap E_{J,\delta}) = \ & P\left((\Psi_J - \delta/2 \leq \Phi_J \leq \Psi_J + \delta/2) \ \cap \ (\alpha - \delta/2 \leq \Psi_J \leq \beta + \delta/2)\right) \\ \leq \ & P(\alpha - \delta \leq \Phi_J \leq \beta + \delta). \end{aligned}$$

On the other hand, we have that $P(A_{J,\delta} \cap E^c_{J,\delta}) \leq P(E^c_{J,\delta})$, and then

$$\delta' \geq 1 - P(\alpha - \delta \leq \Phi_J \leq \beta + \delta) - P(E^c_{J,\delta}).$$

Recalling hypothesis (ii), we have that $P(E^c_{J,\delta}) \to 0$ as $J \to \infty$ for every $\delta > 0$. This implies that there exists $J^{\star\star}$ such that for all $J \geq J^{\star\star}$ $P(E^c_{J,\delta}) \leq \delta'$; as a result, for $J \geq \max(J^\star, J^{\star\star})$, we obtain

$$P(\alpha - \delta \leq \Phi_J \leq \beta + \delta) \geq 1 - 2\delta'.$$

Since $\delta'$ can be chosen arbitrary small, thesis follows. □

We now exploit the previous lemmas to prove an important limit in probability.

**Proposition B.2.1.** *Let $\{F_j\}_j$ and $\{G_j\}_j$ satisfy the hypotheses of Theorem B.1.1, and let $\widehat{se}_{Y,J}$ be defined in* (B.1.1). *Then, for any $\delta > 0$, we have that*

$$\lim_J \ P\left(-\sigma^2_{\max} + \widehat{se}^2_{Y,J} - \delta \leq \sigma^2_F \ \leq \ -\sigma^2_{\min} + \widehat{se}^2_{Y,J} + \delta\right) \ = 1. \tag{B.2.5}$$

*Proof.* Let us define

$$\Phi_J = \sigma_F^2 - \widehat{se}_{Y,J}^2, \quad \Psi_J = \sigma_F^2 - \widehat{se}_{F,J}^2 + \frac{1}{J}\sum_{j=1}^{J} G_j^2$$

where $\widehat{se}_{F,J}^2 = \frac{1}{J}\sum_{j=1}^{J}(F_j - \overline{F}_J)^2$, $\overline{F}_J = \frac{1}{J}\sum_{j=1}^{J} F_j$. Recalling that $p\lim_J \widehat{se}_{F,J}^2 = \sigma_F^2$ and then applying Lemma B.2.2, it is straightforward to verify that

$$\lim_J P\left(\sigma_{\min}^2 - \delta \leq \Psi_J \leq \sigma_{\max}^2 + \delta\right) = \lim_J P\left(\sigma_{\min}^2 - \delta \leq \frac{1}{J}\sum_{j=1}^{J} G_j^2 \leq \sigma_{\max}^2 + \delta\right) = 1$$

for any $\delta > 0$. On the other hand, we observe that

$$\Phi_J - \Psi_J = \underbrace{-\frac{2}{J}\sum_{j=1}^{J} F_j\, G_j}_{=(I)} + \underbrace{\left(\overline{G}_J\right)^2}_{=(II)} - \underbrace{\overline{F}_J\,\overline{G}_J}_{=(III)},$$

where $\overline{G}_J = \frac{1}{J}\sum_{j=1}^{J} G_j$.

We study the limits of $(I)$, $(II)$ and $(III)$ separately. Since the random variables $Z_j = F_j\, G_j$ are independent and $Z_j$ satisfy the hypotheses of Lemma B.2.1, we find that

$$p\lim_J (I) = 0,$$

Furthermore, applying [119, Theorem 17.5] and exploiting the fact that $p\lim_J \overline{G}_J = 0$ (consequence of Lemma B.2.1), we find that

$$p\lim_J (II) = \left(\overline{G}_J\right)^2 = 0.$$

Finally, we observe that we can write $(III)$ as follows: $(III) = \frac{1}{J}\sum_{j=1}^{J} Z_j$ with $Z_j = \overline{F}_J\, G_j$. Recalling the third hypothesis of Theorem B.1.1, we observe that

$$\mathbb{E}[Z_j] = \mathbb{E}[\overline{F}_J\, G_j] = \frac{1}{J}\sum_{j'=1}^{J} \mathbb{E}[F_{j'}\, G_j] = 0$$

and also $\sup_j \mathbb{E}[Z_j^2] < \infty$. Then, applying again Lemma B.2.1, we conclude that

$$p\lim_J (III) = 0.$$

By combining the three different pieces, we obtain

$$p\lim_J (\Phi_J - \Psi_J) = p\lim_J (I) + p\lim_J (II) + p\lim_J (III) = 0.$$

Thesis then follows by applying Lemma B.2.3. □

## B.3 Application of Lyapunov Central Limit Theorem

We first verify that the random sequence $\{Y_j := F_j + G_j\}_{j=1}^{\infty}$ satisfies the hypotheses of Lyapunov Central Limit Theorem (see, e.g., [119, Theorem 21.2]). We have indeed that

$$\mathbb{E}[Y_j] = \mathbb{E}[F_j] + \mathbb{E}[G_j] = \mu_F; \tag{B.3.1a}$$

$$\mathbb{E}[Y_j^2] = \mathbb{E}[F_j^2] + \mathbb{E}[G_j^2] + 2\mathbb{E}[F_j G_j] = \sigma_F^2 + \mu_F^2 + \sigma_j^2 < \infty; \tag{B.3.1b}$$

$$\mathbb{E}[|Y_j|^3] \leq \mathbb{E}[|F_j|^3] + \mathbb{E}[|G_j|^3] + 3\mathbb{E}[|F_j|^2|G_j|] + 3\mathbb{E}[|F_j||G_j|^2] < \infty. \tag{B.3.1c}$$

Applying Lyapunov Central Limit Theorem to the random sequence $\{Y_j\}_j$, we obtain

$$C_J^{\text{th}}(\alpha) = \left[\overline{Y}_J - \frac{1}{\sqrt{J}} S_J^{\text{th}}\, z_{1-\alpha/2},\ \overline{Y}_J + \frac{1}{\sqrt{J}} S_J^{\text{th}}\, z_{1-\alpha/2}\right],$$

where $(S_J^{\text{th}})^2 = \frac{1}{J}\sum_{j=1}^J \mathbb{V}[Y_j] = \frac{1}{J}\sum_{j=1}^J \sigma_j^2 + \sigma_F^2$, is a $(1-\alpha)$ asymptotic confidence interval for $\mu_F$. Exploiting Proposition B.2.1, we find

$$\lim_J P\left((S_J^{\text{th}})^2 \leq \widehat{se}_{Y,J}^2 + \sigma_{\max}^2 - \sigma_{\min}^2 + \delta\right) = 1,$$

and thus $\lim_J P(C_J^{\text{th}}(\alpha) \subset C_J(\alpha)) = 1$. As a result, we obtain that

$$\liminf_J P\left(\mu_F \in C_J(\alpha)\right) \geq \liminf_J P\left(\mu_F \in C_J^{\text{th}}(\alpha)\right) = \lim_J P\left(\mu_F \in C_J^{\text{th}}(\alpha)\right) = 1 - \alpha.$$

Thesis follows.

# Appendix C

# Caccioppoli inequalities for some elliptic PDEs

In this appendix, we prove Caccioppoli inequalities for the solution to a number of elliptic problems. Caccioppoli inequalities represent the basic tool to prove regularity results for elliptic boundary value problems. We refer to the book of Giaquinta and Martinazzi [93] for further details.

This appendix is organized as follows. In section C.1, we introduce some preliminaries. Then, in section C.2, we first consider the case of harmonic equations (Laplace's equation) and we observe that the same strategy can be easily extended to advection-diffusion-reaction, Helmholtz's equations and to linear elastodynamics. Finally, in section C.3, we study the problem of Stokes.

## C.1 Preliminaries

We first present some definitions and general hypotheses. We denote by $u_g^{\text{bk}} \in \mathcal{V}^{\text{bk}} = H^1(\Omega^{\text{bk}})$ the solution to the variational problem:

$$G(u_g^{\text{bk}}, v) = 0 \qquad \forall v \in \mathcal{V}_0^{\text{bk}}, \qquad u_g^{\text{bk}}|_{\Gamma^{\text{in}}} = g,$$

where $\mathcal{V}_0^{\text{bk}} := \{v \in \mathcal{V}^{\text{bk}} : v|_{\Gamma^{\text{in}}} = 0\}$, $g \in \mathcal{T} = H^{1/2}(\Gamma^{\text{in}})$. In what follows, we assume that $\Gamma^{\text{in}}$ is an open subset of $\partial\Omega^{\text{bk}}$ and that $\Omega^{\text{bk}}$ is a Lipschitz domain. We further introduce $\Omega \subset \Omega^{\text{bk}} \subset \mathbb{R}^d$ such that $\delta := dist(\overline{\Omega}, \overline{\Gamma}^{\text{in}}) > 0$.

The objective of this appendix is to show that

$$\|\nabla u_g^{\text{bk}}\|_{L^2(\Omega)} \leq \|u_g^{\text{bk}}\|_{L^2(\Omega^{\text{bk}})}, \qquad \forall g \in \mathcal{T}. \tag{C.1.1}$$

We recall that (C.1.1) guarantees that the space generated by the transfer eigenmodes is optimal in the sense of Kolmogorov (see Chapter 5).

We further introduce quantities that will be used to prove estimates of the form (C.1.1). First, we introduce the $t$-neighborhood of $\Omega$ in $\Omega^{\text{bk}}$:

$$\Omega_t := \{x \in \Omega^{\text{bk}} : \, dist(x, \overline{\Omega}) < t\}. \tag{C.1.2}$$

We observe that $\Omega_t \subset \Omega_{t'}$ if $t < t'$. Then, we introduce $\eta_{t,s} \in C^1(\mathbb{R}^d)$ such that

$$0 \leq \eta_{t,s}(x) \leq 1, \qquad \eta_{t,s}(x) = \begin{cases} 1 & \text{in } \Omega_t, \\ 0 & \text{in } \Omega^{\text{bk}} \setminus \Omega_s, \end{cases} \tag{C.1.3}$$

where $t < s$. We observe that we can choose $\eta_{t,s}$ such that

$$\|\nabla \eta_{t,s}(x)\|_2 \leq \frac{C}{s-t}, \tag{C.1.4}$$

where $C$ might depend on $\Omega$. We further observe that if $s < \delta$, $\eta_{t,s}|_{\Gamma^{\text{in}}} \equiv 0$.

Before concluding, we comment on the notation adopted. In this appendix, we employ bold letters to indicate vector-valued functions. Furthermore, we denote by $\|\cdot\|_2$ the Euclidean norm in $\mathbb{C}^d$ with the understanding that if $\mathbf{v}$ is complex $\|\mathbf{v}\|_2 = \sqrt{\mathbf{v} \cdot \bar{\mathbf{v}}}$. Similarly, we denote by $\|\cdot\|_F$ the Frobenius norm in $\mathbb{C}^{d,d}$. We state upfront that, in what follows, we denote by $C$ a positive constant that uniquely depends on $\Omega, \Omega^{\text{bk}}$.

## C.2 Laplace's equation and simple extensions

We first study the Laplace's equation. Next theorem coincides with [93, Theorem 4.1].

**Proposition C.2.1.** *Let $u_g^{\text{bk}} \in \mathcal{V}^{\text{bk}}$ be the solution to*

$$\int_{\Omega^{\text{bk}}} \nabla u_g^{\text{bk}} \cdot \nabla v \, dx = 0, \qquad \forall v \in \mathcal{V}_0^{\text{bk}}, \quad u_g^{\text{bk}}|_{\Gamma^{\text{in}}} = g, \tag{C.2.1}$$

*where $g \in \mathcal{T}$. Then, given the Lipschitz domain $\Omega \subset \Omega^{\text{bk}}$, $\delta := dist(\overline{\Omega}, \overline{\Gamma}^{\text{in}}) > 0$, we find*

$$\int_\Omega \|\nabla u_g^{\text{bk}}\|_2^2 \, dx \leq \frac{C(\Omega)}{\delta^2} \int_{\Omega^{\text{bk}}} (u_g^{\text{bk}})^2 \, dx. \tag{C.2.2}$$

*Proof.* Let us consider $v = u_g^{\text{bk}} \eta_{t,s}^2$ with $0 \leq t < s \leq \delta$. By substituting in (C.2.1), we find

$$\int_{\Omega^{\text{bk}}} \|\nabla u_g^{\text{bk}}\|_2^2 \eta_{t,s}^2 \, dx = -2 \int_{\Omega^{\text{bk}}} \left(\eta_{t,s} \nabla u_g^{\text{bk}}\right) \left(u_g^{\text{bk}} \nabla \eta_{t,s}\right).$$

Then, applying Cauchy-Schwartz inequality,

$$\int_{\Omega^{\text{bk}}} \|\nabla u_g^{\text{bk}}\|_2^2 \eta_{t,s}^2 \, dx \leq 2 \left(\int_{\Omega^{\text{bk}}} \|\nabla u_g^{\text{bk}}\|_2^2 \eta_{t,s}^2 \, dx\right)^{1/2} \left(\int_{\Omega^{\text{bk}}} \|\nabla \eta_{t,s}\|_2^2 (u_g^{\text{bk}})^2 \, dx\right)^{1/2}.$$

By dividing both sides by $\left(\int_{\Omega^{\text{bk}}} \|\nabla u_g^{\text{bk}}\|_2^2 \eta_{t,s}^2 \, dx\right)^{1/2}$ and then squaring both sides of the equation, we find

$$\int_{\Omega^{\text{bk}}} \|\nabla u_g^{\text{bk}}\|_2^2 \eta_{t,s}^2 \, dx \leq 4 \int_{\Omega^{\text{bk}}} (u_g^{\text{bk}})^2 \|\nabla \eta_{t,s}\|_2^2 \, dx.$$

Finally, if we set $t = 0$ and $s = \delta$, recalling (C.1.3)-(C.1.4), we find that $\eta_{t,s} \equiv 1$ in $\Omega$ and $\|\nabla \eta_{t,s}(x)\|_2 \leq \frac{C}{\delta}$ for all $x \in \Omega^{\text{bk}}$. As a result, we find

$$\int_\Omega \|\nabla u_g^{\text{bk}}\|_2^2 \, dx \leq \int_{\Omega^{\text{bk}}} \|\nabla u_g^{\text{bk}}\|_2^2 \eta_{t,s}^2 \, dx \leq 4 \int_{\Omega^{\text{bk}}} (u_g^{\text{bk}})^2 \|\nabla \eta_{t,s}\|_2^2 \, dx \leq \frac{4C}{\delta^2} \int_{\Omega^{\text{bk}}} (u_g^{\text{bk}})^2 \, dx.$$

Thesis follows. □

Some comments are in order. First, we observe that with the same proof we can generalize the result as

$$\int_\Omega \|\nabla u_g^{\text{bk}}\|_2^2 \, dx \leq \frac{C(\Omega)}{\delta^2} \int_{\Omega^{\text{bk}}} (u_g^{\text{bk}} - \lambda)^2 \, dx, \qquad \lambda \in \mathbb{R}.$$

Second, we observe that we do not require that $\Omega \subset\subset \Omega^{\text{bk}}$, but only that $\delta > 0$, that is, we require that $\Gamma^{\text{in}}$ is well-separated from $\Omega$.

We now extend the result to a wider class of PDEs.

**Proposition C.2.2.** *Let $u_g^{\text{bk}} \in \mathcal{V}^{\text{bk}}$ be the solution to*

$$\int_{\Omega^{\text{bk}}} \nu \nabla u_g^{\text{bk}} \cdot \nabla v + \left(\mathbf{b} \cdot \nabla u_g^{\text{bk}}\right) v + c u_g^{\text{bk}} v \, dx = 0 \qquad \forall v \in \mathcal{V}_0^{\text{bk}}, \qquad u_g^{\text{bk}}|_\Gamma = g, \tag{C.2.3}$$

*where* $\nu, \mathbf{b}, c \in L^\infty(\Omega^{\text{bk}})$. *We assume that* $\nu(x) \geq \nu_{\min} > 0$ *and that* $\mathbf{b}, c$ *guarantees the existence and uniqueness of the solution* $u_g^{\text{bk}}$ *for any choice of* $g \in \mathcal{T}$.

*Then, the following holds:*

$$\int_\Omega \|\nabla u_g^{\text{bk}}\|_2^2 \, dx \leq \frac{1}{\nu_{\min}} \left( \|c\|_{L^\infty(\Omega^{\text{bk}})} + \frac{\|\mathbf{b}\|^2_{L^\infty(\Omega^{\text{bk}})} C(\Omega)}{\delta^2} \right) \|u_g^{\text{bk}}\|_{L^2(\Omega^{\text{bk}})}. \tag{C.2.4}$$

We observe that Proposition C.2.2 includes advection-diffusion-reaction and Helmholtz's equations as special cases. We also observe that with analogous proof we can consider more general boundary conditions on open subsets of $\partial\Omega^{\text{bk}} \setminus \Gamma^{\text{in}}$ that are well-separated from $\Omega$. For example, if we consider the problem

$$\begin{cases} \int_{\Omega^{\text{bk}}} \nu \nabla u_g^{\text{bk}} \cdot \nabla v + \left(\mathbf{b} \cdot \nabla u_g^{\text{bk}}\right) v + c u_g^{\text{bk}} v \, dx + \int_{\Gamma'} h u_g^{\text{bk}} v \, d\sigma = \int_{\Gamma'} h u_g^{\text{bk}} v \, d\sigma \quad \forall v \in \mathcal{V}_0^{\text{bk}}, \\ u_g^{\text{bk}}|_\Gamma = g, \end{cases}$$

estimate (C.2.4) still holds provided that we substitute $\delta$ with

$$\hat{\delta} = \min\left( dist(\overline{\Omega}, \overline{\Gamma}^{\text{in}}), \, dist(\overline{\Omega}, \overline{\Gamma}') \right).$$

We now consider the case of linear elastodynamics. Although the proof follows the exact same ideas of the proof of Proposition C.2.1, we report the proof.

**Proposition C.2.3.** *Let* $\mathbf{u}_g^{\text{bk}} \in \mathcal{V}^{\text{bk}}$ *be the solution to*

$$\begin{cases} \int_{\Omega^{\text{bk}}} 2\mu \text{sym}(\nabla \mathbf{u}_g^{\text{bk}}) : \overline{\text{sym}(\nabla \mathbf{v})} + \lambda \, \text{div}\,(\mathbf{u}_g^{\text{bk}}) \, \overline{\text{div}\,(\mathbf{u}_g^{\text{bk}})} \, dx - A(\omega) \int_{\Omega^{\text{bk}}} \mathbf{u}_g^{\text{bk}} \cdot \overline{\mathbf{v}} \, dx = 0 \ \forall \mathbf{v} \in \mathcal{V}_0^{\text{bk}}, \\ \mathbf{u}_g^{\text{bk}}|_{\Gamma^{\text{in}}} = \mathbf{g} \end{cases} \tag{C.2.5}$$

*where* $\mathbf{g} \in \mathcal{T}$ *and* $A(\omega) = \frac{-\omega^2 - i\omega\alpha}{1 + i\omega\beta}$, $(\mu, \lambda)$ *are the Lamé elastic moduli and* $(\alpha, \beta)$ *are the Rayleigh-damping coefficients. Then, we have*

$$\|\nabla \mathbf{u}_g^{\text{bk}}\|_{L^2(\Omega)} \leq \frac{1}{C_\Omega^{\text{korn}}} \left( 2|A(\omega)| + \frac{C}{2\delta^2}(\mu + \lambda) \right) \|\mathbf{u}_g^{\text{bk}}\|_{L^2(\Omega)} \tag{C.2.6a}$$

*where* $C_\Omega^{\text{korn}} > 0$ *is defined as*

$$C_\Omega^{\text{korn}} = \min_{\mathbf{w}\in H^1(\Omega)} \frac{\int_\Omega 2\mu\|\text{sym}(\nabla\mathbf{w})\|_F^2 + \lambda\,|\text{div}\,(\mathbf{w})|^2\,dx}{\|\nabla\mathbf{w}\|^2_{L^2(\Omega)}} \tag{C.2.6b}$$

*and*

$$\|\nabla\mathbf{w}\|_{L^2(\Omega)} = \int_\Omega \|\nabla\mathbf{w})\|_F^2\,dx.. \tag{C.2.6c}$$

*Proof.* We define $\eta = \eta_{0,\delta}$. Then, we introduce

$$B(\mathbf{u}_g^{\text{bk}},\eta) := \int_{\Omega^{\text{bk}}} \left(2\mu\,\|\text{sym}(\nabla\mathbf{u}_g^{\text{bk}})\|_F^2 + \lambda|\text{div}(\mathbf{u}_g^{\text{bk}})|^2\right)\eta^2\,dx.$$

We observe that

$$B(\mathbf{u}_g^{\text{bk}},\eta) \geq \int_\Omega \left(2\mu\,\|\text{sym}(\nabla\mathbf{u}_g^{\text{bk}})\|_F^2 + \lambda|\text{div}(\mathbf{u}_g^{\text{bk}})|^2\right)dx \geq C_\Omega^{\text{korn}}\,\|\nabla\,\mathbf{u}_g^{\text{bk}}\|^2_{L^2(\Omega)}, \tag{C.2.7}$$

and $C_\Omega^{\text{korn}} > 0$ due to Korn's inequality (see, e.g., [112]).

By substituting $\mathbf{v} = \mathbf{u}_g^{\text{bk}}\eta^2$ in (C.2.5), we find

$$\begin{aligned} B(\mathbf{u}_g^{\text{bk}},\eta) = \;& A(\omega)\int_{\Omega^{\text{bk}}}\|\mathbf{u}_g^{\text{bk}}\|_2^2\eta^2\,dx + \int_{\Omega^{\text{bk}}}\left(\sqrt{2\mu}\text{sym}(\nabla\mathbf{u}_g^{\text{bk}})\eta\right) : \left(2\sqrt{2\mu}\nabla\eta\otimes\overline{\mathbf{u}_g^{\text{bk}}}\right)dx \\ & + \int_{\Omega^{\text{bk}}}\left(\sqrt{2\lambda}\eta\text{div}(\mathbf{u}_g^{\text{bk}})\right)\left(\sqrt{2\lambda}\nabla\eta\cdot\overline{\mathbf{u}_g^{\text{bk}}}\right)dx. \end{aligned}$$

Applying Cauchy-Schwartz and Young's inequality at the right hand side, we find

$$B(\mathbf{u}_g^{\text{bk}},\eta) \leq |A(\omega)|\|\mathbf{u}_g^{\text{bk}}\|^2_{L^2(\Omega^{\text{bk}})} + \frac{C\epsilon}{2\delta}B(\mathbf{u}_g^{\text{bk}},\eta) + \frac{C}{2\epsilon\delta}(\mu+\lambda)\,\|\mathbf{u}_g^{\text{bk}}\|^2_{L^2(\Omega^{\text{bk}})}.$$

Substituting $\epsilon = \frac{\delta}{C}$, we find

$$B(\mathbf{u}_g^{\text{bk}},\eta) \leq 2\left(|A(\omega)| + \frac{C}{\delta^2}(\mu+\lambda)\right)\|\mathbf{u}_g^{\text{bk}}\|^2_{L^2(\Omega^{\text{bk}})}. \tag{C.2.8}$$

Thesis follows by combining (C.2.7) and (C.2.8). □

## C.3 Stokes' problem

We now study the extension to Stokes problem: find $(\mathbf{u}_g^{\text{bk}}, p) \in \mathcal{V}^{\text{bk}} \times L_0^2(\Omega^{\text{bk}})$ such that

$$\begin{cases} \int_{\Omega^{\text{bk}}} \nabla \mathbf{u}_g^{\text{bk}} : \nabla \mathbf{v} - p(\text{div}(\mathbf{v})\, dx = 0 & \forall \mathbf{v} \in \mathcal{V}_0^{\text{bk}} \\ \int_\Omega q\, (\text{div}(\mathbf{u}_g^{\text{bk}})\, dx = 0 & \forall q \in L^2(\Omega) \\ \mathbf{u}_g^{\text{bk}}|_{\Gamma^{\text{in}}} = \mathbf{g} \end{cases} \tag{C.3.1}$$

The proof here reported follows the same argument of Kang in [124].

We first present two lemmas.

**Lemma C.3.1.** *([89, Theorem III.3.1, page 171]) Let $\Omega'$ be a Lipschitz domain. Let $f \in L^2(\Omega')$ such that $\int_{\Omega'} f\, dx = 0$. Then, there exists $\mathbf{w} \in H_0^1(\Omega')$ such that*

$$\text{div}(\mathbf{w}) = f, \qquad \|\nabla \mathbf{w}\|_{L^2(\Omega)} \leq C \|f\|_{L^2(\Omega)},$$

*where $C$ depends on $\Omega'$, but does not depend on $f$.*

**Lemma C.3.2.** *([92, Lemma 3.1, page 161]) Let $f : (\tau_0, \tau_1) \mapsto \mathbb{R}_+$, $f \in L^\infty(\tau_0, \tau_1)$, $\tau_0 > 0$. Suppose that*

$$f(t) \leq \left(A(s-t)^{-\alpha} + B\right) + \theta f(s)$$

*for all $\tau_0 \leq t < s \leq \tau_1$ and for $A, B, \alpha, \theta \geq 0$, $\theta < 1$.*

*Then, we have*

$$f(t) \leq C\left(A(s-t)^{-\alpha} + B\right),$$

*for all $\tau_0 \leq t < s \leq \tau_1$, and $C = C(\alpha, \theta) > 0$.*

We now present an interesting estimate for the pressure.

**Proposition C.3.1.** *Let $\Omega, \Omega^{\text{bk}}$ be Lipschitz domains. Let $p \in L_0^2(\Omega^{\text{bk}})$ be the solution to* (C.3.1). *Then, for every $0 \leq r < s < \delta$, the following estimate holds:*

$$\int_{\Omega_r} p^2\, dx \leq \frac{C}{(s-r)^2} \int_{\Omega_t} \|\mathbf{u}_g^{\text{bk}}\|_2^2\, dx. \tag{C.3.2}$$

*Proof.* If we substitute $\mathbf{v} = \mathbf{u}_g^{\text{bk}}\eta_{t,s}$ in $(\text{C.3.1})_1$, we find

$$\int_{\Omega^{\text{bk}}} \|\nabla \mathbf{u}_g^{\text{bk}}\|_F^2 \, \eta_{t,s}^2 \, dx = -\int_{\Omega^{\text{bk}}} \eta_{t,s} \nabla \mathbf{u}_g^{\text{bk}} \, : \, (\mathbf{u}_g^{\text{bk}} \otimes \nabla \eta_{t,s}) \, dx \, + \int_{\Omega^{\text{bk}}} p \, \eta_{t,s} (\nabla \eta_{t,s} \cdot \mathbf{u}_g^{\text{bk}}) \, dx.$$

We observe that

$$\eta_{t,s} \nabla \mathbf{u}_g^{\text{bk}} \, : \, (\mathbf{u}_g^{\text{bk}} \otimes \nabla \eta_{t,s}) \leq \frac{1}{2} \eta_{t,s}^2 \|\nabla \mathbf{u}_g^{\text{bk}}\|_F^2 \, + \frac{C}{2} \|\mathbf{u}_g^{\text{bk}}\|_2^2 \, \|\nabla \eta_{t,s}\|_2^2,$$

where $C > 0$ depends only on the dimension $d$. Then, observing that $\|\nabla \eta_{t,s}\|_2^2 > 0$ only in $\Omega_s \setminus \Omega_t$ and exploiting Cauchy-Schwartz inequality, we obtain

$$\int_{\Omega^{\text{bk}}} \eta_{t,s}^2 \|\nabla \mathbf{u}_g^{\text{bk}}\|_F^2 \, dx \, \leq C \int_{\Omega_s} \|\mathbf{u}_g^{\text{bk}}\|_2^2 \, \|\nabla \eta_{t,s}\|_2^2 \, dx \, + \int_{\Omega_s \setminus \Omega_t} (p \eta_{t,s})^2 \, dx. \tag{C.3.3}$$

We now introduce $\eta_{r,t}$, $r < t < s$. Recalling Lemma C.3.1 we further introduce $\mathbf{w} \in H_0^1(\Omega_t)$ such that

$$\text{div}(\mathbf{w}) = p\eta_{r,t}^2 - \overline{p\eta_{r,t}^2}, \qquad \|\nabla \mathbf{w}\|_{L^2(\Omega_t)} \leq C \|p\eta_{r,t}^2\|_{L^2(\Omega_t)},$$

where $\overline{p\eta_{r,t}^2}$ denotes the mean of $p\eta_{r,t}^2$ over $\Omega_t$. We observe that $\mathbf{w} \in \mathcal{V}_0^{\text{bk}}$. Then, recalling that $p \in L_0^2(\Omega^{\text{bk}})$ and exploiting $(\text{C.3.1})_1$, we find

$$\int_{\Omega^{\text{bk}}} p(p\eta_{r,t}^2) \, dx \, = \int_{\Omega^{\text{bk}}} p(p\eta_{r,t}^2 - \overline{p\eta_{r,t}^2}) \, dx \, = \int_{\Omega_t} p \, \text{div}(\mathbf{w}) \, dx = \int_{\Omega_t} \nabla \mathbf{u}_g^{\text{bk}} \, : \, \nabla \mathbf{w} \, dx$$

Then, applying Cauchy Schwartz inequality and recalling that $\|\nabla \mathbf{w}\|_{L^2(\Omega_t)} \leq C \|p\eta_{r,t}^2\|_{L^2(\Omega_t)}$, we find

$$\int_{\Omega^{\text{bk}}} p^2 \, \eta_{r,t}^2 \, dx \, = \frac{1}{4\epsilon} \int_{\Omega_t} \|\nabla \mathbf{u}_g^{\text{bk}}\|_F^2 \, dx + C\epsilon \int_{\Omega_t} p^2 \, \eta_{r,t}^4 \, dx \leq \frac{1}{4\epsilon} \int_{\Omega_t} \|\nabla \mathbf{u}_g^{\text{bk}}\|_F^2 \, dx + C\epsilon \int_{\Omega_t} p^2 \, \eta_{r,t}^2 \, dx,$$

where in the second identity we used the fact that $\eta_{r,t} \leq 1$. By choosing $\epsilon = \frac{1}{2C}$, we find

$$\int_{\Omega_r} p^2 \, dx \leq \int_{\Omega_t} p^2 \, \eta_{r,t}^2 \, dx \, \leq C \int_{\Omega_t} \|\nabla \mathbf{u}_g^{\text{bk}}\|_F^2 \, dx. \tag{C.3.4}$$

Combining (C.3.3) and (C.3.4), we find

$$\begin{aligned}\int_{\Omega_r} p^2\,dx \leq\ & C\int_{\Omega_t}\|\nabla \mathbf{u}_g^{\mathrm{bk}}\|_F^2\,dx \underbrace{\leq}_{\text{(C.3.3)}} \tfrac{C}{(s-t)^2}\int_{\Omega_s}\|\mathbf{u}_g^{\mathrm{bk}}\|_2^2\,dx + C\int_{\Omega_s\setminus\Omega_t} p^2\,dx \\ \leq\ & \tfrac{C}{(s-r)^2}\int_{\Omega_s}\|\mathbf{u}_g^{\mathrm{bk}}\|_2^2\,dx + C\int_{\Omega_s\setminus\Omega_t} p^2\,dx\end{aligned}$$

If we sum $C\int_{\Omega_r} p^2\,dx$ on both sides, we find

$$\int_{\Omega_r} p^2\,dx \leq \frac{C'}{(s-r)^2}\int_{\Omega_s}\|\mathbf{u}_g^{\mathrm{bk}}\|_2^2\,dx + \frac{C}{C+1}\int_{\Omega_s} p^2\,dx.$$

Applying Lemma C.3.2 with $f(\tau) = \int_{\Omega_\tau} p^2\,dx$, we finally obtain (C.3.2). □

We can now show Caccioppoli inequality.

**Proposition C.3.2.** *Let $\Omega, \Omega^{\mathrm{bk}}$ be Lipschitz domains. Then, for any $g \in \mathcal{T}$, we have that*

$$\int_{\Omega}\|\nabla \mathbf{u}_g^{\mathrm{bk}}\|_F^2\,dx \leq \frac{C}{\delta^2}\int_{\Omega^{\mathrm{bk}}}\|\mathbf{u}_g^{\mathrm{bk}}\|_2^2\,dx. \tag{C.3.5}$$

*Proof.* Let $\eta = \eta_{0,\delta/2}$. Then, by substituting in (C.3.3),

$$\int_{\Omega}\|\nabla\,\mathbf{u}_g^{\mathrm{bk}}\|_F^2\,dx \leq C\int_{\Omega_{\delta/2}}\|\mathbf{u}_g^{\mathrm{bk}}\|_2^2\underbrace{\|\nabla\eta_{t,s}\|_2^2}_{\leq (C/\delta)^2}\,dx + \int_{\Omega_{\delta/2}}(p\eta_{t,s})^2\,dx.$$

If now we apply Proposition C.3.1 with $r = \delta/2$ and $s = \delta$, we find

$$\int_{\Omega}\|\nabla\,\mathbf{u}_g^{\mathrm{bk}}\|_F^2\,dx \leq \frac{C}{\delta^2}\int_{\Omega_{\delta/2}}\|\mathbf{u}_g^{\mathrm{bk}}\|_2^2\,dx + \frac{C}{\delta^2}\int_{\Omega_{\delta/2}}\|\mathbf{u}_g^{\mathrm{bk}}\|_2^2\,dx.$$

Thesis follows. □

# Appendix D

# Parametric-affine expansion for the microtruss problem

Below, we report the parameter-dependent coefficients $\{\Theta_q\}_{q=1}^{10}$ and the parameter-independent bilinear forms $\{a^q\}_{q=1}^{10}$ associated with the microtruss problem considered in this work.

$$\Theta_q(f,\mu=[\alpha,\beta,E,s_L,s_R]) = \begin{cases} (1+i\omega_f\beta)E & q=1, \\ (-\omega_f^2+i\omega_f\alpha)\rho L^2 & q=2, \\ (1+i\omega_f\beta)s_L\,E & q=3, \\ (1+i\omega_f\beta)E & q=4, \\ (1+i\omega_f\beta)s_L^{-1}\,E & q=5, \end{cases} \quad \begin{cases} (-\omega_f^2+i\omega_f\alpha)\rho L^2 s_L & q=6, \\ (1+i\omega_f\beta)s_R\,E & q=7, \\ (1+i\omega_f\beta)\,E & q=8, \\ (1+i\omega_f\beta)s_R^{-1}\,E & q=9, \\ (-\omega_f^2+i\omega_f\alpha)\rho L^2 s_R & q=10, \end{cases} \tag{D.0.1a}$$

and

$$a^q(u,v) = \begin{cases} b_{\Omega_1^{\text{ref}}}(u,v) & q=1 \\ m_{\Omega_1^{\text{ref}}}(u,v) & q=2, \\ \displaystyle\int_{\Omega_2^{\text{ref}}} \frac{1-\nu}{(1+\nu)(1-2\nu)}\frac{\partial u_1}{\partial x_1}\frac{\partial v_1}{\partial x_1} + \frac{1}{2(1+\nu)}\frac{\partial u_2}{\partial x_1}\frac{\partial v_2}{\partial x_1}\,dx & q=3, \end{cases} \tag{D.0.1b}$$

$$a^q(u,v) = \begin{cases} \displaystyle\int_{\Omega_2^{\text{ref}}} \frac{\nu}{(1+\nu)(1-2\nu)} \left( \frac{\partial u_1}{\partial x_1}\frac{\partial v_2}{\partial x_2} + \frac{\partial u_2}{\partial x_2}\frac{\partial v_1}{\partial x_1} \right) + \frac{1}{2(1+\nu)} \left( \frac{\partial u_1}{\partial x_2}\frac{\partial v_2}{\partial x_1} + \frac{\partial u_2}{\partial x_1}\frac{\partial v_1}{\partial x_2} \right) dx & q = 4, \\ \displaystyle\int_{\Omega_2^{\text{ref}}} \frac{1-\nu}{(1+\nu)(1-2\nu)} \frac{\partial u_2}{\partial x_2}\frac{\partial v_2}{\partial x_2} + \frac{1}{2(1+\nu)} \frac{\partial u_1}{\partial x_2}\frac{\partial v_1}{\partial x_2} dx & q = 5, \\ m_{\Omega_2^{\text{ref}}}(u,v) & q = 6, \\ \displaystyle\int_{\Omega_3^{\text{ref}}} \frac{1-\nu}{2(1+\nu)(1-2\nu)} \frac{\partial u_1}{\partial x_1}\frac{\partial v_1}{\partial x_1} + \frac{1}{2(1+\nu)} \frac{\partial u_2}{\partial x_1}\frac{\partial v_2}{\partial x_1} dx & q = 7, \\ \displaystyle\int_{\Omega_3^{\text{ref}}} \frac{\nu}{(1+\nu)(1-2\nu)} \left( \frac{\partial u_1}{\partial x_1}\frac{\partial v_2}{\partial x_2} + \frac{\partial u_2}{\partial x_2}\frac{\partial v_1}{\partial x_1} \right) + \frac{1}{2(1+\nu)} \left( \frac{\partial u_1}{\partial x_2}\frac{\partial v_2}{\partial x_1} + \frac{\partial u_2}{\partial x_1}\frac{\partial v_1}{\partial x_2} \right) dx & q = 8, \\ \displaystyle\int_{\Omega_3^{\text{ref}}} \frac{1-\nu}{(1+\nu)(1-2\nu)} \frac{\partial u_2}{\partial x_2}\frac{\partial v_2}{\partial x_2} + \frac{1}{2(1+\nu)} \frac{\partial u_1}{\partial x_2}\frac{\partial v_1}{\partial x_2} dx & q = 9, \\ m_{\Omega_3^{\text{ref}}}(u,v) & q = 10, \end{cases} \tag{D.0.1c}$$

# Bibliography


[1] R A Adams and J JF Fournier. *Sobolev spaces*, volume 140. Academic press, 2003.

[2] F Albrecht, B Haasdonk, S Kaulmann, and M Ohlberger. The localized reduced basis multiscale method. In *Proceedings of the Conference Algoritmy*, pages 393–403, 2015.

[3] BO Almroth, P Stern, and FA Brogan. Automatic choice of global shape functions in structural analysis. *AIAA Journal*, 16(5):525–528, 1978.

[4] N Amir, O Barzelay, A Yefet, and T Pechter. Condenser tube examination using acoustic pulse reflectometry. *Journal of Engineering for Gas Turbines and Power*, 132(1):014501, 2010.

[5] N Aronszajn. Theory of reproducing kernels. *Transactions of the American mathematical society*, pages 337–404, 1950.

[6] S K Au, F-L Zhang, and Y-C Ni. Bayesian operational modal analysis: theory, computation, practice. *Computers & Structures*, 126:3–14, 2013.

[7] I Babuška, U Banerjee, and J E Osborn. Generalized finite element methods — main ideas, results and perspective. *International Journal of Computational Methods*, 1(01):67–103, 2004.

[8] I Babuška and R Lipton. Optimal local approximation spaces for generalized finite element methods with application to multiscale problems. *Multiscale Modeling & Simulation*, 9(1):373–406, 2011.

[9] I Babuška and M Suri. Locking effects in the finite element approximation of elasticity problems. *Numerische Mathematik*, 62(1):439–463, 1992.

[10] I Babuška and M Suri. On locking and robustness in the finite element method. *SIAM Journal on Numerical Analysis*, 29(5):1261–1293, 1992.

[11] M CC Bampton and R R Craig, Jr. Coupling of substructures for dynamic analyses. *AIAA Journal*, 6(7):1313–1319, 1968.

[12] M Barrault, Y Maday, N C Nguyen, and A T Patera. An empirical interpolation method: application to efficient reduced-basis discretization of partial differential equations. *Comptes Rendus Mathematique*, 339(9):667–672, 2004.

[13] A Barth, C Schwab, and N Zollinger. Multi-level monte carlo finite element method for elliptic pdes with stochastic coefficients. *Numerische Mathematik*, 119(1):123–161, 2011.

[14] A Basudhar and S Missoum. Adaptive explicit decision functions for probabilistic design and optimization using support vector machines. *Computers & Structures*, 86(19):1904–1917, 2008.

[15] A Basudhar and S Missoum. A sampling-based approach for probabilistic design with random fields. *Computer Methods in Applied Mechanics and Engineering*, 198(47):3647–3655, 2009.

[16] A Basudhar and S Missoum. An improved adaptive sampling scheme for the construction of explicit boundaries. *Structural and Multidisciplinary Optimization*, 42(4):517–529, 2010.

[17] A Basudhar, S Missoum, and A H Sanchez. Limit state function identification using support vector machines for discontinuous responses and disjoint failure domains. *Probabilistic Engineering Mechanics*, 23(1):1–11, 2008.

[18] K. J. Bathe. *Finite element procedures.* Prentice Hall, 1996.

[19] T Belytschko, Y Krongauz, D Organ, M Fleming, and P Krysl. Meshless methods: an overview and recent developments. *Computer methods in applied mechanics and engineering*, 139(1):3–47, 1996.

[20] A Ben-Tal, L El Ghaoui, and A Nemirovski. *Robust optimization.* Princeton University Press, 2009.

[21] O Benedettini, TS Baines, HW Lightfoot, and RM Greenough. State-of-the-art in integrated vehicle health management. *Proceedings of the Institution of Mechanical Engineers, Part G: Journal of Aerospace Engineering*, 223(2):157–170, 2009.

[22] L Bengtsson, M Ghil, and E Källén. *Dynamic meteorology: data assimilation methods*, volume 36. Springer, 1981.

[23] P Benner, S Gugercin, and K Willcox. A survey of projection-based model reduction methods for parametric dynamical systems. *SIAM review*, 57(4):483–531, 2015.

[24] A F Bennett. *Inverse modeling of the ocean and atmosphere.* Cambridge University Press, 2002.

[25] AF Bennett. Array design by inverse methods. *Progress in oceanography*, 15(2):129–156, 1985.

[26] AF Bennett and PC McIntosh. Open ocean modeling as an inverse problem: tidal theory. *Journal of Physical Oceanography*, 12(10):1004–1018, 1982.

[27] M Benzi, G H Golub, and J Liesen. Numerical solution of saddle point problems. *Acta numerica*, 14(1):1–137, 2005.

[28] G Berkooz, P Holmes, and J L Lumley. The proper orthogonal decomposition in the analysis of turbulent flows. *Annual review of fluid mechanics*, 25(1):539–575, 1993.

[29] A Berlinet and C Thomas-Agnan. *Reproducing kernel Hilbert spaces in probability and statistics*, volume 3. Kluwer Academic Boston, 2004.

[30] D Bertsimas, D B Brown, and C Caramanis. Theory and applications of robust optimization. *SIAM review*, 53(3):464–501, 2011.

[31] D Bertsimas and R Weismantel. *Optimization over integers*, volume 13. Dynamic Ideas Belmont, 2005.

[32] P Binev, A Cohen, W Dahmen, R DeVore, G Petrova, and P Wojtaszczyk. Convergence rates for greedy algorithms in reduced basis methods. *SIAM Journal on Mathematical Analysis*, 43(3):1457–1472, 2011.

[33] P Binev, A Cohen, W Dahmen, R DeVore, G Petrova, and P Wojtaszczyk. Data assimilation in reduced modeling. *arXiv preprint arXiv:1506.04770*, 2015.

[34] C M Bishop. *Neural networks for pattern recognition*. Oxford university press, 1995.

[35] P T Boggs and J W Tolle. Sequential quadratic programming. *Acta numerica*, 4:1–51, 1995.

[36] S Boyd and L Vandenberghe. *Convex optimization*. Cambridge university press, 2004.

[37] A M Bratseth. Statistical interpolation by means of successive corrections. *Tellus A*, 38(5):439–447, 1986.

[38] L Breiman, J Friedman, C J Stone, and R A Olshen. *Classification and regression trees*. CRC press, 1984.

[39] R Brincker, L Zhang, and P Andersen. Modal identification from ambient responses using frequency domain decomposition. In *Proc. of the 18th International Modal Analysis Conference (IMAC), San Antonio, Texas*, 2000.

[40] A Buffa, Y Maday, A T Patera, C Prud homme, and G Turinici. A priori convergence of the greedy algorithm for the parametrized reduced basis method. *ESAIM: Mathematical Modelling and Numerical Analysis*, 46(03):595–603, 2012.

[41] M D Buhmann. Radial basis functions. *Acta Numerica 2000*, 9:1–38, 2000.

[42] A Buhr, C Engwer, M Ohlberger, and S Rave. A numerically stable a posteriori error estimator for reduced basis approximations of elliptic equations. *arXiv preprint arXiv:1407.8005*, 2014.

[43] R H Byrd, M E Hribar, and J Nocedal. An interior point algorithm for large-scale nonlinear programming. *SIAM Journal on Optimization*, 9(4):877–900, 1999.

[44] Y Cao, J Zhu, I M Navon, and Z Luo. A reduced-order approach to four-dimensional variational data assimilation using proper orthogonal decomposition. *International Journal for Numerical Methods in Fluids*, 53(10):1571–1583, 2007.

[45] F Casenave, A Ern, and T Lelièvre. Accurate and online-efficient evaluation of the a posteriori error bound in the reduced basis method. *ESAIM: Mathematical Modelling and Numerical Analysis*, 48(01):207–229, 2014.

[46] P Cawley and RD Adams. The location of defects in structures from measurements of natural frequencies. *The Journal of Strain Analysis for Engineering Design*, 14(2):49–57, 1979.

[47] G Chardon, A Cohen, and L Daudet. Sampling and reconstruction of solutions to the helmholtz equation. *arXiv preprint arXiv:1301.0237*, 2013.

[48] S Chaturantabut and D C Sorensen. Nonlinear model reduction via discrete empirical interpolation. *SIAM Journal on Scientific Computing*, 32(5):2737–2764, 2010.

[49] W Chen, Y Xiong, K-L Tsui, and S Wang. A design-driven validation approach using bayesian prediction models. *Journal of Mechanical Design*, 130(2):021101, 2008.

[50] S H Cheung, T A Oliver, E E Prudencio, S Prudhomme, and R D Moser. Bayesian uncertainty analysis with applications to turbulence modeling. *Reliability Engineering & System Safety*, 96(9):1137–1149, 2011.

[51] V. Chew. Confidence, prediction, and tolerance regions for the multivariate normal distribution. *Journal of the American Statistical Association*, 61(315):605–617, 1966.

[52] F Chinesta and E Cueto. *PGD-based modeling of materials, structures and processes.* Springer, 2014.

[53] F Chinesta, A Huerta, G Rozza, and K Willcox. Model order reduction: a survey. 2016.

[54] F Chinesta, P Ladeveze, and E Cueto. A short review on model order reduction based on proper generalized decomposition. *Archives of Computational Methods in Engineering*, 18(4):395–404, 2011.

[55] O A Chkrebtii, D A Campbell, M A Girolami, and B Calderhead. Bayesian uncertainty quantification for differential equations. *arXiv preprint arXiv:1306.2365*, 2013.

[56] A Cohen and R DeVore. Approximation of high-dimensional parametric pdes. *Acta Numerica*, 24:1–159, 2015.

[57] AIAA Standards Committee et al. Aiaa guide for the verification and validation of computational fluid dynamics simuations (g-077-1998), 1998.

[58] C Cortes and V N Vapnik. Support-vector networks. *Machine learning*, 20(3):273–297, 1995.

[59] P Courtier, J-N Thépaut, and A Hollingsworth. A strategy for operational implementation of 4d-var, using an incremental approach. *Quarterly Journal of the Royal Meteorological Society*, 120(519):1367–1387, 1994.

[60] G P Cressman. An operational objective analysis system. *Monthly Weather Review*, 87(10):367–374, 1959.

[61] N Cristianini and J Shawe-Taylor. *An introduction to support vector machines and other kernel-based learning methods.* Cambridge university press, 2000.

[62] N N Cuong. *Reduced-basis approximations and a posteriori error bounds for nonaffine and nonlinear partial differential equations: Application to inverse analysis.* PhD thesis, Citeseer, 2005.

[63] R Daley. *Atmospheric data analysis.* Number 2. Cambridge university press, 1993.

[64] B Dawson. Vibration condition monitoring techniques for rotating machinery. *The shock and vibration digest*, 8(12):3, 1976.

[65] A Deraemaeker, E Reynders, G De Roeck, and J Kullaa. Vibration-based structural health monitoring using output-only measurements under changing environment. *Mechanical systems and signal processing*, 22(1):34–56, 2008.

[66] R DeVore, G Petrova, and P Wojtaszczyk. Greedy algorithms for reduced bases in banach spaces. *Constructive Approximation*, 37(3):455–466, 2013.

[67] L Devroye, L Györfi, and G Lugosi. *A probabilistic theory of pattern recognition*, volume 31. Springer Science & Business Media, 2013.

[68] S S Dhillon and K Chakrabarty. Sensor placement for effective coverage and surveillance in distributed sensor networks. In *Wireless Communications and Networking, 2003. WCNC 2003. 2003 IEEE*, volume 3, pages 1609–1614. IEEE, 2003.

[69] T J DiCiccio and B Efron. Bootstrap confidence intervals. *Statistical science*, pages 189–212, 1996.

[70] F Dimet and O Talagrand. Variational algorithms for analysis and assimilation of meteorological observations: theoretical aspects. *Tellus A*, 38(2):97–110, 1986.

[71] B Efron. Better bootstrap confidence intervals. *Journal of the American statistical Association*, 82(397):171–185, 1987.

[72] J L Eftang and A T Patera. Port reduction in parametrized component static condensation: approximation and a posteriori error estimation. *International Journal for Numerical Methods in Engineering*, 96(5):269–302, 2013.

[73] A Eliassen. Provisional report on calculation of spatial covariance and autocorrelation of the pressure field. Technical report, 1954. Report no 5.

[74] L.C. Evans. *Partial Differential Equations*. Graduate studies in mathematics. American Mathematical Society, 1998.

[75] R Everson and L Sirovich. Karhunen–loeve procedure for gappy data. *JOSA A*, 12(8):1657–1664, 1995.

[76] T Evgeniou, M Pontil, and T Poggio. Regularization networks and support vector machines. *Advances in computational mathematics*, 13(1):1–50, 2000.

[77] W Fan and P Qiao. Vibration-based damage identification methods: a review and comparative study. *Structural Health Monitoring*, 10(1):83–111, 2011.

[78] C R Farrar, S W Doebling, and D A Nix. Vibration–based structural damage identification. *Philosophical Transactions of the Royal Society of London A: Mathematical, Physical and Engineering Sciences*, 359(1778):131–149, 2001.

[79] C R Farrar and K Worden. *Structural health monitoring: a machine learning perspective*. John Wiley & Sons, 2012.

[80] JP Fink and WC Rheinboldt. On the error behavior of the reduced basis technique for nonlinear finite element approximations. *ZAMM-Journal of Applied Mathematics and Mechanics/Zeitschrift für Angewandte Mathematik und Mechanik*, 63(1):21–28, 1983.

[81] George Fishman. *Monte Carlo: concepts, algorithms, and applications.* Springer Science & Business Media, 2013.

[82] RL Fox and H Miura. An approximate analysis technique for design calculations. *AIAA Journal*, 9(1):177–179, 1971.

[83] G Franceschini and S Macchietto. Model-based design of experiments for parameter precision: State of the art. *Chemical Engineering Science*, 63(19):4846–4872, 2008.

[84] M Frangos, Y Marzouk, K Willcox, and B van Bloemen Waanders. Surrogate and reduced-order modeling: A comparison of approaches for large-scale statistical inverse problems. *Large-Scale Inverse Problems and Quantification of Uncertainty*, 123149, 2010.

[85] M Friswell and J E Mottershead. *Finite element model updating in structural dynamics*, volume 38. Springer Science & Business Media, 1995.

[86] M I Friswell. Damage identification using inverse methods. *Philosophical Transactions of the Royal Society of London A: Mathematical, Physical and Engineering Sciences*, 365(1851):393–410, 2007.

[87] M I Friswell, J E Mottershead, and H Ahmadian. Finite–element model updating using experimental test data: parametrization and regularization. *Philosophical Transactions of the Royal Society of London A: Mathematical, Physical and Engineering Sciences*, 359(1778):169–186, 2001.

[88] D Galbally, K Fidkowski, K Willcox, and O Ghattas. Nonlinear model reduction for uncertainty quantification in large-scale inverse problems. 2009.

[89] G P Galdi. *An introduction to the mathematical theory of the Navier-Stokes equations: Steady-state problems.* Springer Science & Business Media, 2011.

[90] L. S. Gandin. Objective analysis of meteorological fields. *Israel Program for Scientific Translations*, page 242, 1965.

[91] T Gasser and H G Müller. Kernel estimation of regression functions. In *Smoothing techniques for curve estimation*, pages 23–68. Springer, 1979.

[92] M Giaquinta. *Multiple integrals in the calculus of variations and nonlinear elliptic systems.* Number 105. Princeton University Press, 1983.

[93] M Giaquinta and L Martinazzi. *An introduction to the regularity theory for elliptic systems, harmonic maps and minimal graphs.* Springer Science & Business Media, 2013.

[94] M B Giles. Multilevel monte carlo path simulation. *Operations Research*, 56(3):607–617, 2008.

[95] M B Giles. Multilevel monte carlo methods. *Acta Numerica*, 24:259, 2015.

[96] C I Goldstein. A finite element method for solving helmholtz type equations in waveguides and other unbounded domains. *Mathematics of Computation*, 39(160):309–324, 1982.

[97] M A Grepl, Y Maday, N C Nguyen, and A T Patera. Efficient reduced-basis treatment of nonaffine and nonlinear partial differential equations. *ESAIM: Mathematical Modelling and Numerical Analysis*, 41(3):575–605, 2007.

[98] M D Gunzburger. *Finite element methods for viscous incompressible flows: a guide to theory, practice, and algorithms.* Academic Press, San Diego, 1989.

[99] L Györfi, M Kohler, A Krzyzak, and H Walk. *A distribution-free theory of nonparametric regression.* Springer Science & Business Media, 2006.

[100] B Haasdonk. Convergence rates of the pod–greedy method. *ESAIM: Mathematical Modelling and Numerical Analysis*, 47(03):859–873, 2013.

[101] B Haasdonk and M Ohlberger. Reduced basis method for finite volume approximations of parametrized linear evolution equations. *ESAIM: Mathematical Modelling and Numerical Analysis-Modélisation Mathématique et Analyse Numérique*, 42(2):277–302, 2008.

[102] H G Harris and G Sabnis. *Structural modeling and experimental techniques.* CRC press, 1999.

[103] EE Hart, SJ Cox, K Djidjeli, and VO Kubytskyi. Solving an eigenvalue problem with a periodic domain using radial basis functions. *Engineering analysis with boundary elements*, 33(2):258–262, 2009.

[104] T. Hastie, R. Tibshirani, and J. Friedman. *The elements of statistical learning*, volume 2. Springer, 2009.

[105] J C Helton. Uncertainty and sensitivity analysis techniques for use in performance assessment for radioactive waste disposal. *Reliability Engineering & System Safety*, 42(2):327–367, 1993.

[106] J S Hesthaven, G Rozza, and B Stamm. Certified reduced basis methods for parametrized partial differential equations. *SpringerBriefs in Mathematics*, 2015.

[107] J S Hesthaven and T Warburton. Nodal high-order methods on unstructured grids: I. time-domain solution of maxwell's equations. *Journal of Computational Physics*, 181(1):186–221, 2002.

[108] C Himpe, T Leibner, and Rave S. Hierarchical approximate proper orthogonal decomposition. *arXiv preprint arXiv:160705210*, 2016.

[109] D Hinrichsen and A J Pritchard. Stability radii of linear systems. *Systems & Control Letters*, 7(1):1–10, 1986.

[110] K C Hoang, BC Khoo, GR Liu, N C Nguyen, and A T Patera. Rapid identification of material properties of the interface tissue in dental implant systems using reduced basis method. *Inverse Problems in Science and Engineering*, 21(8):1310–1334, 2013.

[111] YC Hon, R Schaback, and X Zhou. An adaptive greedy algorithm for solving large rbf collocation problems. *Numerical Algorithms*, 32(1):13–25, 2003.

[112] C O Horgan. Korn's inequalities and their applications in continuum mechanics. *SIAM review*, 37(4):491–511, 1995.

[113] T JR Hughes. *The finite element method: linear static and dynamic finite element analysis*. Courier Corporation, 2012.

[114] J E Hurtado. An examination of methods for approximating implicit limit state functions from the viewpoint of statistical learning theory. *Structural Safety*, 26(3):271–293, 2004.

[115] J E Hurtado and D A Alvarez. Classification approach for reliability analysis with stochastic finite-element modeling. *Journal of Structural Engineering*, 129(8):1141–1149, 2003.

[116] W C Hurty. Dynamic analysis of structural systems using component modes. *AIAA journal*, 3(4):678–685, 1965.

[117] L Iapichino, A Quarteroni, and G Rozza. A reduced basis hybrid method for the coupling of parametrized domains represented by fluidic networks. *Computer Methods in Applied Mechanics and Engineering*, 221:63–82, 2012.

[118] K Ito and SS Ravindran. A reduced-order method for simulation and control of fluid flows. *Journal of computational physics*, 143(2):403–425, 1998.

[119] J. Jacod and P. E Protter. *Probability essentials*. Springer, 2003.

[120] G James, D Witten, T Hastie, and R Tibshirani. *An introduction to statistical learning*. Springer, 2013.

[121] S Joshi and S Boyd. Sensor selection via convex optimization. *Signal Processing, IEEE Transactions on*, 57(2):451–462, 2009.

[122] M Kahlbacher and S Volkwein. Galerkin proper orthogonal decomposition methods for parameter dependent elliptic systems. *Discussiones Mathematicae, Differential Inclusions, Control and Optimization*, 27(1):95–117, 2007.

[123] R E Kalman. A new approach to linear filtering and prediction problems. *Journal of Fluids Engineering*, 82(1):35–45, 1960.

[124] K Kang. On regularity of stationary stokes and navier-stokes equations near boundary. *Journal of Mathematical Fluid Mechanics*, 6(1):78–101, 2004.

[125] V M Karbhari and F Ansari. *Structural health monitoring of civil infrastructure systems*. Elsevier, 2009.

[126] S Kaulmann, M Ohlberger, and B Haasdonk. A new local reduced basis discontinuous galerkin approach for heterogeneous multiscale problems. *Comptes Rendus Mathematique*, 349(23):1233–1238, 2011.

[127] G Kimeldorf and G Wahba. Some results on tchebycheffian spline functions. *Journal of mathematical analysis and applications*, 33(1):82–95, 1971.

[128] R Kohavi et al. A study of cross-validation and bootstrap for accuracy estimation and model selection. In *Ijcai*, volume 14, pages 1137–1145, 1995.

[129] J Krebs, AK Louis, and H Wendland. Sobolev error estimates and a priori parameter selection for semi-discrete tikhonov regularization. *Journal of Inverse and Ill-Posed Problems*, 17(9):845–869, 2009.

[130] K Kunisch and S Volkwein. Galerkin proper orthogonal decomposition methods for a general equation in fluid dynamics. *SIAM Journal on Numerical analysis*, 40(2):492–515, 2002.

[131] T Lassila, A Manzoni, A Quarteroni, and G Rozza. A reduced computational and geometrical framework for inverse problems in hemodynamics. *International journal for numerical methods in biomedical engineering*, 29(7):741–776, 2013.

[132] M Lecerf, D Allaire, and K Willcox. Methodology for dynamic data-driven online flight capability estimation. *AIAA Journal*, 53(10):3073–3087, 2015.

[133] L Li. Discretization of the timoshenko beam problem by thep and theh-p versions of the finite element method. *Numerische Mathematik*, 57(1):413–420, 1990.

[134] Z Li and IM Navon. Optimality of variational data assimilation and its relationship with the kalman filter and smoother. *Quarterly Journal of the Royal Meteorological Society*, 127(572):661–683, 2001.

[135] C Lieberman, K Willcox, and O Ghattas. Parameter and state model reduction for large-scale statistical inverse problems. *SIAM Journal on Scientific Computing*, 32(5):2523–2542, 2010.

[136] J. S. Lim. *Two-dimensional signal and image processing.* Prentice Hall, 1990.

[137] GR Liu, Khin Zaw, and YY Wang. Rapid inverse parameter estimation using reduced-basis approximation with asymptotic error estimation. *Computer Methods in Applied Mechanics and Engineering*, 197(45):3898–3910, 2008.

[138] A C Lorenc. Analysis methods for numerical weather prediction. *Royal Meteorological Society, Quarterly Journal*, 112:1177–1194, 1986.

[139] AC Lorenc. A global three-dimensional multivariate statistical interpolation scheme. *Monthly Weather Review*, 109(4):701–721, 1981.

[140] Y Maday and O Mula. A generalized empirical interpolation method: Application of reduced basis techniques to data assimilation. In *Analysis and Numerics of Partial Differential Equations*, pages 221–235. Springer, 2013.

[141] Y Maday, O Mula, AT Patera, and M Yano. The generalized empirical interpolation method: stability theory on hilbert spaces with an application to the stokes equation. *Computer Methods in Applied Mechanics and Engineering*, 287:310–334, 2015.

[142] Y Maday, A T Patera, J D Penn, and M Yano. A parameterized-background data-weak approach to variational data assimilation: formulation, analysis, and application to acoustics. *International Journal for Numerical Methods in Engineering*, 2014.

[143] Y Maday, A T Patera, J D Penn, and M Yano. PBDW state estimation: Noisy observations; configuration-adaptive background spaces; physical interpretations. *ESAIM: Proceedings and Surveys*, 50:144–168, 2015.

[144] Y Maday, A T Patera, and D V Rovas. A blackbox reduced-basis output bound method for noncoercive linear problems. *in Studies in Mathematics and its Applications, D. Cioranescu and J. L. Lions, eds., Elsevier Science B. V*, pages 533–569, 2001.

[145] Y Maday and E M Rønquist. A reduced-basis element method. *Journal of scientific computing*, 17(1-4):447–459, 2002.

[146] N M M Maia and J M M e Silva. *Theoretical and experimental modal analysis*. Research Studies Press, 1997.

[147] L Mainini and K Willcox. Surrogate modeling approach to support real-time structural assessment and decision making. *AIAA Journal*, 53(6):1612–1626, 2015.

[148] S C Malik and S Arora. *Mathematical analysis*. New Age International, 1992.

[149] G Matheron. Principles of geostatistics. *Economic geology*, 58(8):1246–1266, 1963.

[150] MATLAB. *version 8.5 (R2015a)*. The MathWorks Inc., Natick, Massachusetts, 2015.

[151] J M Melenk and I Babuška. The partition of unity finite element method: basic theory and applications. *Computer methods in applied mechanics and engineering*, 139(1):289–314, 1996.

[152] C A Micchelli and T J Rivlin. *A survey of optimal recovery*. Springer, 1977.

[153] J G Moreno-Torres, T Raeder, R Alaiz-RodríGuez, N V Chawla, and F Herrera. A unifying view on dataset shift in classification. *Pattern Recognition*, 45(1):521–530, 2012.

[154] J E Mottershead, M Link, and M I Friswell. The sensitivity method in finite element model updating: a tutorial. *Mechanical systems and signal processing*, 25(7):2275–2296, 2011.

[155] Z P Mourelatos, R Kuczera, and M Latcha. An efficient monte carlo reliability analysis using global and local metamodels. In *Proceedings of 11th AIAA/ISSMO multidisciplinary analysis and optimization conference, September, Portsmouth, VA*, 2006.

[156] S Müller. *Complexity and stability of kernel-based reconstructions*. PhD thesis, Dissertation, Georg-August-Universitttingen, Institut fr Numerische und Angewandte Mathematik, Lotzestrasse 16-18, D-37083 Gttingen, 2009.

[157] K P Murphy. *Machine learning: a probabilistic perspective*. MIT press, 2012.

[158] F Naets, J Croes, and W Desmet. An online coupled state/input/parameter estimation approach for structural dynamics. *Computer Methods in Applied Mechanics and Engineering*, 283:1167–1188, 2015.

[159] D A Nagy. Modal representation of geometrically nonlinear behavior by the finite element method. *Computers & Structures*, 10(4):683–688, 1979.

[160] F J Narcowich and J D Ward. Norms of inverses and condition numbers for matrices associated with scattered data. *Journal of Approximation Theory*, 64(1):69–94, 1991.

[161] L. W. T. Ng and K. E. Wilcox. Multifidelity approaches for optimization under uncertainty. *International Journal for Numerical Methods Engineering*, 100:746–772, 2014.

[162] A K Noor and J M Peters. Reduced basis technique for nonlinear analysis of structures. *Aiaa journal*, 18(4):455–462, 1980.

[163] W L Oberkampf and T G Trucano. Verification and validation in computational fluid dynamics. *Progress in Aerospace Sciences*, 38(3):209–272, 2002.

[164] T A Oliver, N Malaya, R Ulerich, and R D Moser. Estimating uncertainties in statistics computed from direct numerical simulation. *Physics of Fluids (1994-present)*, 26(3):035101, 2014.

[165] T A Oliver and R D Moser. Bayesian uncertainty quantification applied to rans turbulence models. In *Journal of Physics: Conference Series*, volume 318, page 042032. IOP Publishing, 2011.

[166] E M Ortiz, G J Clark, A Babbar, J L Vian, V L Syrmos, and M M Arita. Multi source data integration for aircraft health management. In *Aerospace Conference, 2008 IEEE*, pages 1–12. IEEE, 2008.

[167] S H Owen and M S Daskin. Strategic facility location: A review. *European Journal of Operational Research*, 111(3):423–447, 1998.

[168] A T Patera and G Rozza. Reduced basis approximation and a posteriori error estimation for parametrized partial differential equations, 2007.

[169] A Paul-Dubois-Taine and D Amsallem. An adaptive and efficient greedy procedure for the optimal training of parametric reduced-order models. *International Journal for Numerical Methods in Engineering*, 102(5):1262–1292, 2015.

[170] J S Peterson. The reduced basis method for incompressible viscous flow calculations. *SIAM Journal on Scientific and Statistical Computing*, 10(4):777–786, 1989.

[171] D B Phuong Huynh, D J Knezevic, and A T Patera. A static condensation reduced basis element method: approximation and a posteriori error estimation. *ESAIM: Mathematical Modelling and Numerical Analysis*, 47(01):213–251, 2013.

[172] A Pinkus. *N-widths in Approximation Theory*. Springer Science & Business Media, 1985.

[173] R Pinnau. Model reduction via proper orthogonal decomposition. In *Model Order Reduction: Theory, Research Aspects and Applications*, pages 95–109. Springer, 2008.

[174] T Poggio and CR Shelton. On the mathematical foundations of learning. *American Mathematical Society*, 39(1):1–49, 2002.

[175] TA Porsching. Estimation of the error in the reduced basis method solution of nonlinear equations. *Mathematics of Computation*, 45(172):487–496, 1985.

[176] C Prud'homme, D V Rovas, K Veroy, L Machiels, Y Maday, A T Patera, and G Turinici. Reliable real-time solution of parametrized partial differential equations: Reduced-basis output bound methods. *Journal of Fluids Engineering*, 124(1):70–80, 2002.

[177] C Prud'homme, D V Rovas, K Veroy, and A T Patera. A mathematical and computational framework for reliable real-time solution of parametrized partial differential equations. *ESAIM: Mathematical Modelling and Numerical Analysis*, 36(05):747–771, 2002.

[178] S Prudhomme and J T Oden. On goal-oriented error estimation for elliptic problems: application to the control of pointwise errors. *Computer Methods in Applied Mechanics and Engineering*, 176(1):313–331, 1999.

[179] F Pukelsheim. *Optimal design of experiments*, volume 50. siam, 1993.

[180] A Quarteroni, A Manzoni, and F Negri. *Reduced Basis Methods for Partial Differential Equations: An Introduction*, volume 92. Springer, 2015.

[181] A Quarteroni and A Valli. *Numerical approximation of partial differential equations*, volume 23. Springer Science & Business Media, 2008.

[182] C E Rasmussen. Gaussian processes for machine learning. 2006.

[183] J Rice. *Mathematical statistics and data analysis*. Nelson Education, 2006.

[184] R Rifkin and A Klautau. In defense of one-vs-all classification. *The Journal of Machine Learning Research*, 5:101–141, 2004.

[185] J. W.M. Rogers and C. Plett. *Radio frequency integrated circuit design*. Artech House, 2010.

[186] D J Rosenkrantz, R E Stearns, and P M Lewis, II. An analysis of several heuristics for the traveling salesman problem. *SIAM journal on computing*, 6(3):563–581, 1977.

[187] H Rowaihy, S Eswaran, M Johnson, D Verma, A Bar-Noy, T Brown, and T La Porta. A survey of sensor selection schemes in wireless sensor networks. In *Defense and Security Symposium*, pages 65621A–65621A. International Society for Optics and Photonics, 2007.

[188] G Rozza, DB P Huynh, and A T Patera. Reduced basis approximation and a posteriori error estimation for affinely parametrized elliptic coercive partial differential equations. *Archives of Computational Methods in Engineering*, 15(3):229–275, 2008.

[189] R Y Rubinstein and D P Kroese. *Simulation and the Monte Carlo method*, volume 707. John Wiley & Sons, 2007.

[190] A Rytter. *Vibration Based Inspection of Civil Engineering Structures*. PhD thesis, Ph. D. dissertation, 1993.

[191] OS Salawu. Detection of structural damage through changes in frequency: a review. *Engineering structures*, 19(9):718–723, 1997.

[192] S Salsa. *Partial differential equations in action: from modelling to theory.* Springer Science & Business Media, 2008.

[193] M Sanayei and O Onipede. Damage assessment of structures using static test data. *AIAA journal*, 29(7):1174–1179, 1991.

[194] M Sanayei and M J Saletnik. Parameter estimation of structures from static strain measurements. i: Formulation. *Journal of Structural Engineering*, 122(5):555–562, 1996.

[195] M Sanayei and M J Saletnik. Parameter estimation of structures from static strain measurements. ii: Error sensitivity analysis. *Journal of structural Engineering*, 122(5):563–572, 1996.

[196] R G Sargent. Verification and validation of simulation models. In *Proceedings of the 37th conference on Winter simulation*, pages 130–143. winter simulation conference, 2005.

[197] R Schaback. Error estimates and condition numbers for radial basis function interpolation. *Advances in Computational Mathematics*, 3(3):251–264, 1995.

[198] R Schaback and H Wendland. Adaptive greedy techniques for approximate solution of large rbf systems. *Numerical Algorithms*, 24(3):239–254, 2000.

[199] B Schölkopf and A J Smola. *Learning with kernels: support vector machines, regularization, optimization, and beyond.* MIT press, 2002.

[200] DB Sharp and DM Campbell. Leak detection in pipes using acoustic pulse reflectometry. *Acta Acustica united with Acustica*, 83(3):560–566, 1997.

[201] J Shawe-Taylor and N Cristianini. *Kernel methods for pattern analysis.* Cambridge university press, 2004.

[202] L Sirovich. Turbulence and the dynamics of coherent structures. part i: Coherent structures. *Quarterly of applied mathematics*, 45(3):561–571, 1987.

[203] K Smetana. A new certification framework for the port reduced static condensation reduced basis element method. *Computer Methods in Applied Mechanics and Engineering*, 283:352–383, 2015.

[204] K Smetana and A T Patera. Optimal local approximation spaces for component-based static condensation procedures. Technical report, MIT, 2015. submitted to SIAM Journal on Scientific Computing.

[205] M Sniedovich. A bird's view of info-gap decision theory. *The Journal of Risk Finance*, 11(3):268–283, 2010.

[206] W Staszewski, C Boller, and G R Tomlinson. *Health monitoring of aerospace structures: smart sensor technologies and signal processing.* John Wiley & Sons, 2004.

[207] R Ştefănescu and I M Navon. Pod/deim nonlinear model order reduction of an adi implicit shallow water equations model. *Journal of Computational Physics*, 237:95–114, 2013.

[208] R Ştefănescu, A Sandu, and I M Navon. Pod/deim reduced-order strategies for efficient four dimensional variational data assimilation. *Journal of Computational Physics*, 295:569–595, 2015.

[209] M L Stein. *Interpolation of spatial data: some theory for kriging.* Springer Science & Business Media, 2012.

[210] I Steinwart. Consistency of support vector machines and other regularized kernel classifiers. *Information Theory, IEEE Transactions on*, 51(1):128–142, 2005.

[211] A M Stuart. Inverse problems: a bayesian perspective. *Acta Numerica*, 19:451–559, 2010.

[212] T Taddei. An adaptive parametrized-background data-weak approach to variational data assimilation. Technical report, MIT, 2016. submitted to Mathematical Modeling and Numerical Analysis (March 2016).

[213] T Taddei, J D Penn, and Patera A T. Experimental a posteriori error estimation by monte carlo sampling of observation functionals. Technical report, MIT, 2016. submitted to International Journal for Numerical Methods in Engineering (August 2016).

[214] T Taddei, J D Penn, M Yano, and A T Patera. Simulation-based classification; a model-order-reduction approach for structural health monitoring. *Archives of Computational Methods in Engineering*, pages 1–23, 2016.

[215] T Taddei, S Perotto, and A Quarteroni. Reduced basis techniques for nonlinear conservation laws. *ESAIM: Mathematical Modelling and Numerical Analysis*, 49(3):787–814, 2015.

[216] O Talagrand. Assimilation of observations, an introduction. *Journal meteorological society of Japan Series 2*, 75:81–99, 1997.

[217] H J Thiébaux and MA Pedder. Spatial objective analysis with applications in atmospheric science. *London: Academic Press, 1987*, 1, 1987.

[218] A Tsymbal. The problem of concept drift: definitions and related work. *Computer Science Department, Trinity College Dublin*, 106, 2004.

[219] K Urban and A T Patera. A new error bound for reduced basis approximation of parabolic partial differential equations. *Comptes Rendus Mathematique*, 350(3):203–207, 2012.

[220] V N Vapnik. *Statistical learning theory*, volume 1. Wiley New York, 1998.

[221] V N Vapnik. *The nature of statistical learning theory.* Springer Science & Business Media, 2013.

[222] PTM Vermeulen and AW Heemink. Model-reduced variational data assimilation. *Monthly weather review*, 134(10):2888–2899, 2006.

[223] K Veroy, C Prud'homme, D V Rovas, and A T Patera. A posteriori error bounds for reduced-basis approximation of parametrized noncoercive and nonlinear elliptic partial differential equations. In *Proceedings of the 16th AIAA computational fluid dynamics conference*, volume 3847, pages 23–26, 2003.

[224] F Vidal-Codina, N C Nguyen, M B Giles, and J Peraire. A model and variance reduction method for computing statistical outputs of stochastic elliptic partial differential equations. *Journal of Computational Physics*, 297:700–720, 2015.

[225] G Wahba. Improper priors, spline smoothing and the problem of guarding against model errors in regression. *Journal of the Royal Statistical Society. Series B (Methodological)*, pages 364–372, 1978.

[226] G Wahba. *Spline models for observational data*, volume 59. Siam, 1990.

[227] A Wald. Statistical decision functions which minimize the maximum risk. *Annals of Mathematics*, pages 265–280, 1945.

[228] L Wasserman. *All of statistics: a concise course in statistical inference*. Springer Science & Business Media, 2013.

[229] H Wendland. Piecewise polynomial, positive definite and compactly supported radial functions of minimal degree. *Advances in computational Mathematics*, 4(1):389–396, 1995.

[230] H Wendland. *Scattered data approximation*, volume 17. Cambridge university press, 2004.

[231] H Wenzel. *Health monitoring of bridges*. John Wiley & Sons, 2008.

[232] G Widmer and M Kubat. Learning in the presence of concept drift and hidden contexts. *Machine learning*, 23(1):69–101, 1996.

[233] C R K Wikle and L M Berliner. A bayesian tutorial for data assimilation. *Physica D: Nonlinear Phenomena*, 230(1):1–16, 2007.

[234] K Willcox. Unsteady flow sensing and estimation via the gappy proper orthogonal decomposition. *Computers & fluids*, 35(2):208–226, 2006.

[235] E G Williams. *Fourier acoustics: sound radiation and nearfield acoustical holography*. Academic press, 1999.

[236] S Willis. Olm: A hands-on approach. In *ICAF 2009, Bridging the Gap between Theory and Operational Practice*, pages 1199–1214. Springer, 2009.

[237] D Wirtz and B Haasdonk. A vectorial kernel orthogonal greedy algorithm. *Proceedings of DWCAA12*, 6:83–100, 2013.

[238] K Worden and JM Dulieu-Barton. Damage identification in systems and structures. *Int. J. Struct. Health Monit*, 3:85–98, 2004.

[239] D Xiao, F Fang, A G Buchan, C C Pain, I M Navon, J Du, and G Hu. Non-linear model reduction for the navier–stokes equations using residual deim method. *Journal of Computational Physics*, 263:1–18, 2014.

[240] M Yano. A space-time petrov–galerkin certified reduced basis method: Application to the boussinesq equations. *SIAM Journal on Scientific Computing*, 36(1):A232–A266, 2014.

[241] M Yano. Private communication. June 2015.

[242] W C Young and R G Budynas. *Roark's formulas for stress and strain*, volume 7. McGraw-Hill New York, 2002.

[243] C Zang and M Imregun. Structural damage detection using artificial neural networks and measured frf data reduced via principal component projection. *Journal of Sound and Vibration*, 242(5):813–827, 2001.

[244] S Zlobec. Characterizing optimality in mathematical programming models. *Acta Applicandae Mathematica*, 12(2):113–180, 1988.